National Library of Canada

Acquisitions and Bibliographic Services Branch

395 Wellington Street
Ottawa, Ontario
K1A 0N4

Bibliothèque nationale du Canada

Direction des acquisitions et des services bibliographiques

395, rue Wellington
Ottawa (Ontario)
K1A 0N4

Your file Votre référence

Our file Notre référence

NOTICE

The quality of this microform is heavily dependent upon the quality of the original thesis submitted for microfilming. Every effort has been made to ensure the highest quality of reproduction possible.

If pages are missing, contact the university which granted the degree.

Some pages may have indistinct print especially if the original pages were typed with a poor typewriter ribbon or if the university sent us an inferior photocopy.

Reproduction in full or in part of this microform is governed by the Canadian Copyright Act, R.S.C. 1970, c. C-30, and subsequent amendments.

AVIS

La qualité de cette microforme dépend grandement de la qualité de la thèse soumise au microfilmage. Nous avons tout fait pour assurer une qualité supérieure de reproduction.

S'il manque des pages, veuillez communiquer avec l'université qui a conféré le grade.

La qualité d'impression de certaines pages peut laisser à désirer, surtout si les pages originales ont été dactylographiées à l'aide d'un ruban usé ou si l'université nous a fait parvenir une photocopie de qualité inférieure.

La reproduction, même partielle, de cette microforme est soumise à la Loi canadienne sur le droit d'auteur, SRC 1970, c. C-30, et ses amendements subséquents.

Canada

UNIVERSITY OF ALBERTA

THE CREVICE CORROSION OF STAINLESS STEEL

By

© **Shuisheng Wang**

A thesis submitted to the Faculty of Graduate Studies and Research in partial fulfillment of the requirements for the degree of **DOCTOR OF PHILOSOPHY**

IN

METALLURGICAL ENGINEERING

DEPARTMENT OF **MINING, METALLURGICAL AND PETROLEUM ENGINEERING**

EDMONTON, ALBERTA

FALL 1994

National Library
of Canada

Acquisitions and
Bibliographic Services Branch

395 Wellington Street
Ottawa, Ontario
K1A 0N4

Bibliothèque nationale
du Canada

Direction des acquisitions et
des services bibliographiques

395, rue Wellington
Ottawa (Ontario)
K1A 0N4

Your file Votre référence

Our file Notre référence

The author has granted an irrevocable non-exclusive licence allowing the National Library of Canada to reproduce, loan, distribute or sell copies of his/her thesis by any means and in any form or format, making this thesis available to interested persons.

L'auteur a accordé une licence irrévocable et non exclusive permettant à la Bibliothèque nationale du Canada de reproduire, prêter, distribuer ou vendre des copies de sa thèse de quelque manière et sous quelque forme que ce soit pour mettre des exemplaires de cette thèse à la disposition des personnes intéressées.

The author retains ownership of the copyright in his/her thesis. Neither the thesis nor substantial extracts from it may be printed or otherwise reproduced without his/her permission.

L'auteur conserve la propriété du droit d'auteur qui protège sa thèse. Ni la thèse ni des extraits substantiels de celle-ci ne doivent être imprimés ou autrement reproduits sans son autorisation.

ISBN 0-315-95280-6

Canada

Name SHUISHENG WANG

Dissertation Abstracts International is arranged by broad, general subject categories. Please select the one subject which most nearly describes the content of your dissertation. Enter the corresponding four-digit code in the spaces provided.

Crevice Corrosion
SUBJECT TERM

0743
SUBJECT CODE

U·M·I

Subject Categories

THE HUMANITIES AND SOCIAL SCIENCES

COMMUNICATIONS AND THE ARTS
Architecture 0729
Art History 0377
Cinema 0900
Dance 0378
Fine Arts 0357
Information Science 0723
Journalism 0391
Library Science 0399
Mass Communications 0708
Music 0413
Speech Communication 0459
Theater 0465

EDUCATION
General 0515
Administration 0514
Adult and Continuing 0516
Agricultural 0517
Art 0273
Bilingual and Multicultural 0282
Business 0688
Community College 0275
Curriculum and Instruction 0727
Early Childhood 0518
Elementary 0524
Finance 0277
Guidance and Counseling 0519
Health 0680
Higher 0745
History of 0520
Home Economics 0278
Industrial 0521
Language and Literature 0279
Mathematics 0280
Music 0522
Philosophy of 0998
Physical 0523
Psychology 0525
Reading 0535
Religious 0527
Sciences 0714
Secondary 0533
Social Sciences 0534
Sociology of 0340
Special 0529
Teacher Training 0530
Technology 0710
Tests and Measurements 0288
Vocational 0747

LANGUAGE, LITERATURE AND LINGUISTICS
Language
- General 0679
- Ancient 0289
- Linguistics 0290
- Modern 0291

Literature
- General 0401
- Classical 0294
- Comparative 0295
- Medieval 0297
- Modern 0298
- African 0316
- American 0591
- Asian 0305
- Canadian (English) 0352
- Canadian (French) 0355
- English 0593
- Germanic 0311
- Latin American 0312
- Middle Eastern 0315
- Romance 0313
- Slavic and East European 0314

PHILOSOPHY, RELIGION AND THEOLOGY
Philosophy 0422
Religion
- General 0318
- Biblical Studies 0321
- Clergy 0319
- History of 0320
- Philosophy of 0322

Theology 0469

SOCIAL SCIENCES
American Studies 0323
Anthropology
- Archaeology 0324
- Cultural 0326
- Physical 0327

Business Administration
- General 0310
- Accounting 0272
- Banking 0770
- Management 0454
- Marketing 0338

Canadian Studies 0385
Economics
- General 0501
- Agricultural 0503
- Commerce-Business 0505
- Finance 0508
- History 0509
- Labor 0510
- Theory 0511

Folklore 0358
Geography 0366
Gerontology 0351
History
- General 0578
- Ancient 0579
- Medieval 0581
- Modern 0582
- Black 0328
- African 0331
- Asia, Australia and Oceania 0332
- Canadian 0334
- European 0335
- Latin American 0336
- Middle Eastern 0333
- United States 0337

History of Science 0585
Law 0398
Political Science
- General 0615
- International Law and Relations 0616
- Public Administration 0617

Recreation 0814
Social Work 0452
Sociology
- General 0626
- Criminology and Penology 0627
- Demography 0938
- Ethnic and Racial Studies 0631
- Individual and Family Studies 0628
- Industrial and Labor Relations 0629
- Public and Social Welfare 0630
- Social Structure and Development 0700
- Theory and Methods 0344

Transportation 0709
Urban and Regional Planning 0999
Women's Studies 0453

THE SCIENCES AND ENGINEERING

BIOLOGICAL SCIENCES
Agriculture
- General 0473
- Agronomy 0285
- Animal Culture and Nutrition 0475
- Animal Pathology 0476
- Food Science and Technology 0359
- Forestry and Wildlife 0478
- Plant Culture 0479
- Plant Pathology 0480
- Plant Physiology 0817
- Range Management 0777
- Wood Technology 0746

Biology
- General 0306
- Anatomy 0287
- Biostatistics 0308
- Botany 0309
- Cell 0379
- Ecology 0329
- Entomology 0353
- Genetics 0369
- Limnology 0793
- Microbiology 0410
- Molecular 0307
- Neuroscience 0317
- Oceanography 0416
- Physiology 0433
- Radiation 0821
- Veterinary Science 0778
- Zoology 0472

Biophysics
- General 0786
- Medical 0760

EARTH SCIENCES
Biogeochemistry 0425
Geochemistry 0996
Geodesy 0370
Geology 0372
Geophysics 0373
Hydrology 0388
Mineralogy 0411
Paleobotany 0345
Paleoecology 0426
Paleontology 0418
Paleozoology 0985
Palynology 0427
Physical Geography 0368
Physical Oceanography 0415

HEALTH AND ENVIRONMENTAL SCIENCES
Environmental Sciences 0768
Health Sciences
- General 0566
- Audiology 0300
- Chemotherapy 0992
- Dentistry 0567
- Education 0350
- Hospital Management 0769
- Human Development 0758
- Immunology 0982
- Medicine and Surgery 0564
- Mental Health 0347
- Nursing 0569
- Nutrition 0570
- Obstetrics and Gynecology 0380
- Occupational Health and Therapy 0354
- Ophthalmology 0381
- Pathology 0571
- Pharmacology 0419
- Pharmacy 0572
- Physical Therapy 0382
- Public Health 0573
- Radiology 0574
- Recreation 0575
- Speech Pathology 0460
- Toxicology 0383

Home Economics 0386

PHYSICAL SCIENCES
Pure Sciences
Chemistry
- General 0485
- Agricultural 0749
- Analytical 0486
- Biochemistry 0487
- Inorganic 0488
- Nuclear 0738
- Organic 0490
- Pharmaceutical 0491
- Physical 0494
- Polymer 0495
- Radiation 0754

Mathematics 0405
Physics
- General 0605
- Acoustics 0986
- Astronomy and Astrophysics 0606
- Atmospheric Science 0608
- Atomic 0748
- Electronics and Electricity 0607
- Elementary Particles and High Energy 0798
- Fluid and Plasma 0759
- Molecular 0609
- Nuclear 0610
- Optics 0752
- Radiation 0756
- Solid State 0611

Statistics 0463

Applied Sciences
Applied Mechanics 0346
Computer Science 0984
Engineering
- General 0537
- Aerospace 0538
- Agricultural 0539
- Automotive 0540
- Biomedical 0541
- Chemical 0542
- Civil 0543
- Electronics and Electrical 0544
- Heat and Thermodynamics 0348
- Hydraulic 0545
- Industrial 0546
- Marine 0547
- Materials Science 0794
- Mechanical 0548
- Metallurgy 0743
- Mining 0551
- Nuclear 0552
- Packaging 0549
- Petroleum 0765
- Sanitary and Municipal 0554
- System Science 0790

Geotechnology 0428
Operations Research 0796
Plastics Technology 0795
Textile Technology 0994

PSYCHOLOGY
General 0621
Behavioral 0384
Clinical 0622
Developmental 0620
Experimental 0623
Industrial 0624
Personality 0625
Physiological 0989
Psychobiology 0349
Psychometrics 0632
Social 0451

UNIVERSITY OF ALBERTA

RELEASE FORM

NAME OF AUTHOR: **Shuisheng Wang**

TITLE OF THESIS: **The Crevice Corrosion of Stainless Steel**

DEGREE: **Doctor of Philosophy**

YEAR THIS DEGREE GRANTED: **Fall 1994**

Permission is hereby granted to the University of Alberta Library to reproduce single copies of this thesis, and to lend or sell such copies for private, scholarly or scientific research purposes only.

The author reserves all other publication and other rights in association with the copyright in the thesis, and except as hereinbefore provided neither the thesis nor any substantial portion thereof may be printed or otherwise reported in any material form whatever without the author's prior written permission.

Shuisheng Wang

Shuisheng Wang

606 Chemical/Mineral Engineering Building
116 Street - 92 Avenue
Edmonton, Alberta T6G 2G6

Date: Sept 29, 1994

UNIVERSITY OF ALBERTA

FACULTY OF GRADUATE STUDIES AND RESEARCH

The undersigned certify that they have read, recommend to the Faculty of Graduate Studies and Research for acceptance, a thesis entitled **THE CREVICE CORROSION OF STAINLESS STEEL** submitted by **Shuisheng Wang** in partial fulfillment of the requirement for the degree of **DOCTOR OF PHILOSOPHY** in **METALLURGICAL ENGINEERING**.

Dr. S.A. Bradford
Supervisor

Dr. B.M. Patchett

Dr. D.G. Ivey

Dr. J.A. Plambeck

Dr. H. Henein

Dr. Scott X. Mao

Date: Sept 28/94

ABSTRACT

The measurement of cyclic polarization curves is one of the most important methods used to study the features of crevice corrosion. However, usually a reference electrode is placed outside a crevice to control the potential during the measurement. In that case, the applied potential controls the potential of the sample surface outside a crevice instead of the crevice potential of the sample. In this study, a novel experimental setup was constructed to measure the cyclic anodic potentiodynamic polarization curves of AISI 303, 304 and 316 stainless steels by controlling the potential inside a crevice. The new method of controlling the potential inside a crevice is compared with the common method of controlling the potential outside a crevice. The significant difference between placing a reference electrode inside and outside a crevice indicates that the reference electrode inside a crevice much better controls the potential to simulate electrochemical characteristics of crevice corrosion. The pH variation within the crevice is recorded during the scan. The pH first increases slightly, and then gradually decreases in the passive region and at the beginning of the transpassive region. From the transpassive region, and past the reversal of the scan, the pH begins to decrease rapidly. In the final stage, the pH increases slightly.

The susceptibility to crevice corrosion of different stainless steels has been evaluated by the method. The effects of temperature and chloride ion concentration on the cyclic polarization curve have also been studied. Based on the charge passed during the scan, a mathematical model was developed to calculate the pH value along the cyclic anodic potentiodynamic polarization curve. The pH values in the theoretical calculation are reasonably close to the values obtained in the experiment and the trend of the pH change in the theoretical calculation is the same as that in the experiment. Both the experimental and theoretical results for the pH change show that when the passive film is broken down, the pH value is much higher than the critical pH value for the initiation of crevice corrosion during the accelerated crevice corrosion process. A modified mechanism of crevice corrosion is proposed.

ACKNOWLEDGEMENTS

I wish to express my sincere gratitude to Dr. S.A. Bradford, my supervisor, for his excellent supervision and suggestions throughout the course of the study.

I am very grateful to Drs. B.M. Patchett, R.L. Eadie, J.A. Plambeck and H. Henein for valuable suggestions and discussions. I am also very obliged to Dr. D.G. Bellow, Department of Mechanical Engineering for providing the potentiostat for me to use.

Very special thanks to Ms. Tina Barker, Mr. Bob Smith, Mr. Bob Konzuk, Mr. Shiraz Merali, Mr. John Czuroski, Mr. Jacques Gibeau and Mr. Doug Booth for their help during the research.

Finally, I would like to thank my wife, Lihua Shi, for her selfless support and encouragement during my study at the University of Alberta.

Table of Symbols

A_c	Bare electrode area
A_a	Covered electrode area
A(j)	The molar fraction of metal j in the alloy
B(j)	The charge of metal j dissolved in the solution
C	The capacitance
C_h	The charge
$C_h(j)$	The charge used to produce ions of the metal j in the alloy
C_o	The molar concentration of oxygen dissolved in solution
C_u	The capacitance of the uncovered area
C_f	The capacitance of the passive film area
D	Diaphragm
D_o	Diffusion constant
d	Crevice width
E	Potential
E_c	Corrosion potential
E_{corr}	The potential at natural corrosion
E_{cp}	The critical potential for the initiation of pitting or crevice corrosion
$E_{crev.}$	Potential inside crevice
E_{Fl}	Flade potential
$E_{Fl,0}$	Flade potential at pH 0
E_{lim}	The potential below which no crevice corrosion occurs
E_{np}	The pit nucleation potential (another expression for critical pitting potential E_{cp})
E_o	Potential at standard conditions
E_{out}	Potential outside crevice
E_{pass}	Passivation potential

E_{prot}	The critical potential for protection
E_{pzc}	The potential of zero charge
$E_{surface}$	The potential at the metal surface
E^{scr}	The scratching potential
$\triangle E$	Potential difference
e	The charge of electron
F	Faraday constant
f	The percentage of current used to produce metal j in total current
G	The molar concentration of $[Cr^{3+}]$ at equilibrium
G_1	The molar concentration of $[Fe^{3+}]$ at equilibrium
H	The molar concentration of $[Cr(OH)^{2+}]$ at equilibrium
H_1	The molar concentration of $[Fe(OH)^{2+}]$ at equilibrium
I	Current
I_a	Anodic current
$(I_a)_{crev.}$	Anodic current inside crevice
$(I_a)_{out}$	Anodic current outside crevice
I_c	Cathodic current
$(I_c)_{crev.}$	Cathodic current inside crevice
$(I_c)_{out}$	Cathodic current outside crevice
I(j)	Current used to produce metal j
I_{max}	The maximum anodic current at the active and passive region in polarization curve
IR	Potential drop in the solution
IR*	The difference between the potential $E_{surface}$ and E_{pass}
i	Current density
J	The molar concentration of $[Cr(OH)_2+]$ at equilibrium
J_1	The molar concentration of $[Fe(OH)_2+]$ at equilibrium
L	The molar concentration of $[Cr(OH)_3]$ at equilibrium
L_1	The molar concentration of $[Fe(OH)_3]$ at equilibrium
M	Molar concentration

M_t	Metal
N	Normal concentration
O	The molar concentration of $[Ni^{2+}]$ at equilibrium
P	The molar concentration of $[Ni(OH)^{+}]$ at equilibrium
Po_2	Pressure of oxygen
pH_{adj}	pH value after considering the effect of Cl^- in the reaction volume
$pH_{calculated}$	The calculated pH value in the reaction volume
pH_{Ecal}	The pH value obtained from the experiment at the calculated point
pH_{ori}	The pH value at the first point on the polarization curve
pH_f	The pH value at the last point on the polarization curve
Q	The molar concentration of $[Ni(OH)_2]$ at equilibrium
q_m	The surface charge density
R	Resistance
R_f	The passive film resistance
R_g	Gas constant
R_{ori}	The mole ratio of Cr/Fe in the stainless steel
R_s	The solution resistance
R_u	The charge transfer resistance of the uncovered area
S	The molar concentration of $[H^+]$ at equilibrium when the $[Cr^{3+}]_T$ is greater than $[OH^-]_T$
S_1	The molar concentration of $[H^+]$ at equilibrium when considering iron in the form of Fe^{3+}
T	Absolute temperature
t	time
t_s	The scan time from the beginning of the scan to the potential at which the cathodic reduction of oxygen stops
U	The molar concentration of $[Fe^{2+}]$ at equilibrium
V	The molar concentration of $[Ni(OH)^{+}]$ at equilibrium
V_r	The reaction volume

V(t)	The total volume of solution for the produced ions within the crevice in time t when the crevice width is equal to or less than 0.0018 cm.
V(t1)	The total volume of solution for the produced ions within the crevice in time t when the crevice width is equal to 0.0033 cm
W	The molar concentration of $[Fe(OH)_2]$ at equilibrium
$W(O_2)$	The moles of oxygen diffused into the reaction volume from t_1 to t_2
$W(OH^-)$	The moles of OH^- produced in the reaction volume
W(j)	The moles of metal j ions produced in the reaction volume
X	The molar concentration of $[H^+]$ at equilibrium when the $[Cr^{3+}]_T$ is equal to or less than $[OH^-]_T$
Y	The remaining percentage of the charge to produce the OH^- ion in the reaction volume
Z	The ionic charge
[x]	Molar Concentration of x
$[H^+]_f$	The final molar concentration of H^+ produced within the crevice
$[OH^-]_f$	The final molar concentration of OH^- produced within the crevice
$[OH^-]_T$	The total molar concentration of OH^- produced in the reaction volume
$[OH^-]_r$	The remaining concentration of $[OH^-]$ in the reaction volume after all the chromium ions in the reaction volume form chromium hydroxide
$[Fe^{2+}]_T$	The total concentration of Fe^{2+} produced in the reaction volume
$[Ni^{2+}]_T$	The total concentration of Ni^{2+} produced in the reaction volume
γ	The surface tension

γ_{max}	The maximum surface tension at $q_m=0$
ϵ	The dielectric constant of the material
δ_d	Diffusion distance
δ_{dv}	Diffusion distance in the vertical direction

Table of Abbreviations

AC	Alternating current
A/D	Alternating current/direct current
AISI	American Iron and Steel Institute
CCR	Crevice corrosion resistance
CCT	Critical crevice corrosion temperature
CRT	Cathode ray tube
dc	Direct current
div	Division
FC	Fully-creviced electrode
FFT	Fast Fourier Transform
Fig.	Figure, Figures
I/O	Input/output
NC	Non-creviced test electrode
PC	Partially-creviced electrode
PTFE	Polytetrafluoroethylene
psd	Power spectral density
r.m.s.	Root-mean-square
Sat.	Saturated
SCE	Saturated calomel electrode
SEM	Scanning electron microscopy
SHE	Standard hydrogen electrode
Sol.	Solution
SW	Seawater
ZIAM	Zero impedance ammeter
ZRA	Zero resistance ammeter

Table of Contents

Chapters		Pages
1. Introduction	----------	1
2. Literature Review	----------	5
2.1 Mechanisms of Crevice Corrosion	----------	5
2.2 Experimental Methods in Crevice Corrosion	----------	15
2.2.1 Electrochemical Methods for Investigating the Electrochemical Conditions in the Crevice	----------	16
2.2.1.1 Direct, In Situ, Measurement	----------	16
2.2.1.2 Semi-direct Method	----------	17
2.2.1.3 Artificial Crevices	----------	17
2.2.1.4 Simulation of the Chemistry of Localized Corrosion	----------	18
2.2.2 Experimental Methods for Investigating the Initiation of Crevice Corrosion	----------	18
2.2.2.1 Electrochemical Noise Measurement	----------	18
2.2.2.2 AC Impedance Methods	----------	21
2.2.2.3 Polarization Curve Measurements	----------	22
2.2.2.4 Indication of Initiation Time by Corrosion Potential and Current Measurement	----------	25
2.2.2.4.1 Potential Measurement	----------	25
2.2.2.4.2 Current Measurement	----------	25
2.3 Effect of Various Factors on Crevice Corrosion	----------	27
2.3.1 Effect of Chloride Ion Concentration	----------	27
2.3.2 Effect of pH	----------	28
2.3.3 Effect of Temperature	----------	29

2.3.4 Effect of Anodic Current Density ---------- 29
2.3.5 Effect of Composition of Alloys ---------- 30
2.3.6 Effect of Crevice Geometry ---------- 32
2.3.7 Effect of Inclusions and Other Metal Defects ---------- 33

3. Statements of Problems and Objectives ---------- 36

4. Experimental Materials, Equipment, Set-up and Procedures ---------- 38
4.1 Experimental Materials ---------- 38
4.2 Experimental Equipment ---------- 38
4.3 Experimental Set-up ---------- 39
4.4 Experimental Procedures ---------- 40
4.4.1 Preparation of the Specimen ---------- 40
4.4.2 Preparation of the Testing Solutions ---------- 41
4.4.3 Galvanostatic Tests ---------- 41
4.4.4 Cyclic Potentiodynamic Tests ---------- 41
4.4.5 Potentiodynamic Tests Studying the Initiation of Crevice Corrosion ---------- 42

5. Experimental Results and Discussion ---------- 43
5.1 Comparison of the Method of Controlling Potential Inside a Crevice with the Method of Controlling Potential Outside a Crevice ---------- 43
5.2 Effect of Crevice Width on AISI 304, 303 and 316 Stainless Steels ---------- 44
5.3 Effect of Different Stainless Steels on Crevice Corrosion ---------- 51
5.4 Effect of Temperature on AISI 304 Stainless Steel ---------- 52
5.5 Effect of NaCl Concentration on AISI 304 Stainless Steel ---------- 55
5.6 The Initiation of Crevice Corrosion by Controlling Potential Inside a Crevice ---------- 57

5.7 The Modified Mechanism of Crevice Corrosion under Applied Anodic Potential ---------- 59
5.8 Implication of the Experimental Results to Industrial Application ---------- 60
6. A Mathematical Model for Calculation of pH Values along the Polarization Curve ---------- 62
6.1 Introduction ---------- 62
6.2 Assumptions Used in the Model ---------- 62
6.2.1 Metal Dissolution within a Crevice ---------- 62
6.2.2 Mass Transport in and outside a Crevice ---------- 63
6.3.3 Reaction Equilibria ---------- 64
6.2.4 Depletion of Oxygen within a Crevice ---------- 67
6.2.5 Correction of pH for Presence of Chloride Ions ---------- 69
6.3 The Calculation of pH Value along the Polarization Curve ---------- 70
6.3.1 The Calculation of the Concentration of OH^- in the Reaction Volume ---------- 70
6.3.2 The Calculation of the Concentration of Metal Ions in the Reaction Volume ---------- 73
6.3.3 The Calculation of pH along the Polarization Curve ---------- 74
6.4 Comparison of Simulation Results with Experimental Values ---------- 79
6.5 A Sensitivity Analysis of the Assumption about Uniform Dissolution ---------- 82
6.6 Discussion of Other Factors Affecting the pH Values within the Crevice ---------- 83
6.6.1 Effect of Chromium Ions within a Crevice on the pH Value ---------- 83
6.6.2 Effect of Iron Ions within a Crevice on the pH Value ---------- 87

6.6.3 Effect of Diffusion of Hydrogen Ions on the pH Value ---------- 88

6.7 Implication of the Mathematical Model to Crevice Corrosion ---------- 89

7. Conclusions ---------- 91

8. Suggestions for Further Work ---------- 93

Tables ---------- 94

Figures ---------- 107

References ---------- 188

Appendix ---------- 198

List of Tables

Tables		Pages
1. Critical pH Value and Corrosion Rates in Crevices for Various Stainless Steels Exposed in Natural Seawater for Two Years	----------	94
2. Crevice Corrosion of Various Metals in Contact with Red Medical Rubber	----------	94
3. Chemical Composition of the Test Stainless Steels	----------	95
4. The Critical Potentials E_{cp} and E_{prot} for AISI 304 Stainless Steel at Different Crevice Widths in 10% NaCl Solution at a Temperature of 20°C and Scan Rate of 0.5 mV/s	----------	95
5. The Critical Potentials E_{cp} and E_{prot} for AISI 303 Stainless Steel at Different Crevice Widths in 10% NaCl Solution at a Temperature of 20°C and Scan Rate of 0.5 mV/s	----------	95
6. The Critical Potentials E_{cp} and E_{prot} for AISI 316 Stainless Steel at Different Crevice Widths in 10% NaCl Solution at a Temperature of 20°C and Scan Rate of 0.5 mV/s	----------	96
7. The Critical Potentials E_{cp} and E_{prot} for Different Stainless Steels at Crevice Width of 12 μm in 10% NaCl Solution at a Temperature of 20°C and Scan Rate of 0.5 mV/s	----------	96
8. The Critical Potentials E_{cp} and E_{prot} for Different Stainless Steels at Crevice Width of 40 μm in 10% NaCl Solution at a Temperature of 20°C and Scan Rate of 0.5 mV/s	----------	96
9. The Critical Potentials E_{cp} and E_{prot} for Different Stainless Steels at Crevice Width of 96 μm in 10% NaCl Solution at a Temperature of 20°C and Scan Rate of 0.5 mV/s	----------	97

10. The Critical Potentials E_{cp} and E_{prot} for Different Stainless Steels at Crevice Width of 180 μm in 10% NaCl Solution at a Temperature of 20°C and Scan Rate of 0.5 mV/s ---------- 97
11. Effect of Seawater Temperature on the Probability of Crevice Corrosion Initiation, Multiple Crevice Test, 30 Day Exposure ---------- 98
12. The Critical Potentials E_{cp} and E_{prot} for AISI 304 Stainless Steel at Different Temperatures (°C) for a Crevice Width of 12 μm in 10% NaCl Solution at a Scan Rate of 0.5 mV/s ---------- 98
13. The Critical Potentials E_{cp} and E_{prot} for AISI 304 Stainless Steel at Different Temperatures (°C) for a Crevice Width of 12 μm in 10% NaCl Solution at a Scan Rate of 0.2 mV/s ---------- 99
14. The Critical Potentials E_{cp} and E_{prot} for AISI 304 Stainless Steel at Different NaCl Concentrations for a Crevice Width of 12 μm at a Temperature of 20°C and Scan Rate of 0.5 mV/s ---------- 99
15. The Critical Potentials E_{cp} and E_{prot} for AISI 304 Stainless Steel at Different NaCl Concentrations for a Crevice Width of 12 μm at a Temperature of 20°C and Scan Rate of 0.2 mV/s ---------- 100
16. Diffusion Coefficients of Ions ---------- 100
17. Hydrolysis Equilibria ---------- 101
18. pH Values from Experiment and Theoretical Calculation Obtained by Controlling Potential inside a 12 μm Crevice at a Scan Rate of 0.5 mV/s in 10% NaCl Solution of pH about 7.25 at a Temperature of 20°C ---------- 102
19. pH Values from Experiment and Theoretical Calculation Obtained by Controlling Potential inside a 40 μm Crevice

at a Scan Rate of 0.5 mV/s in 10% NaCl Solution of pH about 7.15 at a Temperature of 20°C ---------- 103

20. pH Values from Experiment and Theoretical Calculation Obtained by Controlling Potential inside a 96 μm Crevice at a Scan Rate of 0.5 mV/s in 10% NaCl Solution of pH about 6.89 at a Temperature of 20°C ---------- 104

21. pH Values from Experiment and Theoretical Calculation Obtained by Controlling Potential inside a 180 μm Crevice at a Scan Rate of 0.5 mV/s in 10% NaCl Solution of pH about 7.05 at a Temperature of 20°C ---------- 105

22. pH Values from Experiment and Theoretical Calculation Obtained by Controlling Potential inside a 330 μm Crevice at a Scan Rate of 0.5 mV/s in 10% NaCl Solution of pH about 7.00 at a Temperature of 20°C ---------- 106

23. Comparison of the Theoretical pH Values When Iron Dissolves as Fe^{2+} with the Theoretical pH Values When Iron dissolves as Fe^{3+} for the Last Point of the Polarization Curves ---------- 106

List of Figures

Figures		Pages
1.	Potential and pH change for Steel A (13% Cr) and potential change for Steel B (17% Cr) during crevice corrosion. Width of crevice = 0.15 mm. $E_{crev.}$ = potential of specimen within crevice. $E_{out.}$ = potential of outer surface. ----------	107
2.	Mechanism of crevice corrosion initiation stage. I_c and I_a denote cathodic and anodic current on polarization curves. The subscripts crev and out refer to crevice and outer surface respectively. Diagram e shows propagation stage. R = internal (electrolyte) resistance in crevice corrosion cell. E_{Fl} = Flade potential. ----------	108
3.	Schematic representation of the four stages which can be distinguished in the mechanism of the crevice corrosion process on stainless steel. A. Start: general corrosion; B. Differential aeration: local current, migration of ions; C. Increasing concentration of ions, including H^+; D. Depassivation, active/passive cell, propagation. ----------	109
4.	Schematic polarization curve of the electrolyte within a pit, crevice or crack for the potential shift mechanism. ----------	109
5.	Schematic illustrating the relation between the local cell site in the crevice and the polarization curve of the crevice solution for a sample polarized to potential A in the passive region. ----------	110
6.	Schematic illustrating a decrease in IR* resulting from development and enlargement of the active region by	

change in concentration of the cavity solution. (a) no active region appearing for the solution composition in the cavity; (b) acidification and/or aggressive ion buildup decreasing IR*. ---------- 110

7. Schematic representation of $\gamma=\gamma max-2\pi dq_m^2/\epsilon$ with nominal values of E and q_m for illustrative purposes. ---------- 111

8. Model of initial (dashed) and final potential gradients and surface charge densities of parallel metallic plates forming a crevice in which the mirror double layer interacts strongly. ---------- 111

9. Crevice set-up. ---------- 111

10. The metal-Perspex artificial crevice assembly. ---------- 112

11. The variation of potential along the artificial crevice of type 304 stainless steel with time in free corrosion. ---------- 112

12. The variation of potential with distance from crevice mouth measured on the stainless steel. ---------- 113

13a. General arrangement of the artificial crevice. ---------- 113

13b. Detailed construction of the resin fibre potential probe. ---------- 114

14. Crevice corrosion apparatus of two compartment cell. ---------- 114

15. Time record for mild steel electrode in 0.5 N H_2SO_4 20 min after immersion (sampling rate = 10 s). ---------- 114

16. Time record from Fig. 15 after dc tread removal. ---------- 115

17. FFT spectrum for time record shown in Fig. 15. ---------- 115

18. Memory alloy (Ti-Ni) in 0.3 M HCl. Electrochemical noise amplitude spectrum showing effects of crevice attack. ---------- 116

19. Schematic diagram of the apparatus for the measurement of corrosion potential fluctuations. ---------- 116

20. Typical wave forms of the corrosion potential fluctuations obtained when micropits were formed and when crevice corrosion was proceeding: (a) 4M NaCl + 0.1M NaClO

(pH=11.2), with micropits; (b) 1M NaCl + 0.1M NaClO (pH=11.6), with crevice corrosion. ---------- 117

21. Power spectral density (psd) of the corrosion potential fluctuation shown in Fig. 20. ---------- 117

22. Electrical setup for simultaneous potential and current noise measurements. ---------- 118

23. Potential-time plot for typical galvanic couple. ---------- 118

24. Potential and current records showing potential and current transients typical of stage 2 of potential evolution (linear treads not removed) Sampling interval 8 s and the ratio of bare electrode area (A_c) to covered electrode area (A_a), A_c/A_a= 13.8, A_a=1450 mm^2. ---------- 119

25. Variation of potential and current with time for long term experiment (values obtained as in Fig. 23): A_c/A_a= 13.8, A_a=1450 mm^2. ---------- 120

26. Variation of standard deviation of potential and current records with time for data in Fig. 25. ---------- 121

27. Hypothetical equivalent circuit for breakdown or repair of air-passivated AA6061 in aqueous chloride solutions. R_u is the charge transfer resistance of the uncovered area; R_f is the passive film resistance; R_s is the solution resistance; C_u is the capacitance of the uncovered area; C_f is the capacitance of the passive film area. ---------- 121

28. (a, top left) Corrosion potential as a function of time for AA6061 in air-sparged 0.05N sodium chloride solution and solutions acidified to pH 5.8, 4.8, 3.8 and 2.8. (b, above) Charge transfer resistance as a function of time. (c, left) Double layer capacitance as a function of time. ---------- 122

29. Polarization diagram obtained with cyclic anodic polarization of stainless steel in chloride solution,

showing open-circuit critical pitting potential (E_{cp}) and protection potential (E_{prot}). ---------- 123

30. Assembly used for measurements of the critical potential for crevice corrosion. A-Plexiglas rod; B-specimen; C-specimen lead; D,E-specimen holder; F,G-support; L-Luggin capillary; I-perforated Plexiglas tube; K-lead to the cathode. ---------- 123

31. Correlation of the potential difference E_{cp}-E_{prot} and corrosion weight loss of stainless steels exposed to seawater for 4.25 years. ---------- 124

32. Electrode assembly fabricated from Plexiglas block for crevice studies. Orifice dimensions: 0.75 cm by 6.25 cm. Internal probe openings spaced at 1.25 cm intervals. ---------- 124

33. Crevice potential variation of CF-8 stainless steel together with anodic polarization curve and calculated current distribution. Hydrogen-saturated N H_2SO_4 at 25°C. Crevice width: 0.0225 cm. ---------- 125

34. Crevice potential variation at a depth of 0.625 cm as a function of crevice width. Material: CF-8; control potential: 0.20 V(vs. SCE); N H_2SO_4 at 25°C. ---------- 126

35. E_{corr} vs. time: Type 316 crevice with approximately 10 μm gap in 1M NaCl, pH 6, crevice area ratio 1:1. ---------- 126

36. Schematic composite E_{corr}/time curve showing the development of corrosion in Type 316 crevices. ---------- 126

37. Schematic representation of different types of experimental possibilities for electrochemical cells to be used in crevice corrosion testing; NC Non-creviced test electrode, PC Partially-creviced electrode, FC Fully-creviced electrode, D Diaphragm. ---------- 127

38. Schematic of test loop utilized for remote crevice evaluation. ---------- 127
39. Current (logarithmic) to remote crevices as a function of time for type 304 stainless steel during a 28-day exposure in seawater at 10, 25 and 50°C. ---------- 128
40. Typical current (logarithmic) and potential values versus time for type 304 stainless steel in seawater at 25°C. Specimen was polarized at -0.2 V(Ag/AgCl) between days 0 and 30 and between days 35 and 40. Specimen was freely corroding between days 30 and 35. ---------- 129
41. Relationship between pH and chromium ion concentration in the crevice solution. ---------- 130
42. Influence of anodic current density on change in pH (0.5N NaCl), volume 5 cm^3. Time of polarization, 24 hours. ---------- 130
43. Relationship between scratch pitting potential and composition of Fe-Cr-Mo alloys by scratch method in deaerated synthetic seawater at 90°C, pH 7.2 $\pm$ 0.2, and their resistance to crevice corrosion after 6 days of exposure to aerated 10% $FeCl_3$ at 21 $\pm$ 1°C. ---------- 131
44. Effect of crevice width on corrosion rate (1) and distance into the crevice where attack occurs (2) for 13% Cr stainless steel exposed to 5M NaCl solution for 52 days. ---------- 132
45. Effect of cathode to anode area ratio on crevice corrosion in 3% NaCl, 50°C. Crevice was made between a Bakelite bolt and nut and stainless steel plate. ---------- 132
46. Alloy rankings for experimental high-purity equivalents of alloy 316 with various Mn and S levels. ---------- 133
47. Potential-pH diagram for MnS-H_2O-Cl^- system calculated on the basis of 0.1 M for SO_4^{2-}, Cl^- and Mn^{2+}. ---------- 134

48. Conditions under which 304 stainless steel remains active or becomes active during dissolution at 25 $\mu A/cm^2$ in deaerated sodium chloride/sodium thiosulfate electrolytes. ---------- 135
49. Sample holder and sample. ---------- 136
50. Crevice assembly. ---------- 136
51. Experimental set-up for controlling the potential inside a crevice. ---------- 137
52. Variation of potential inside the crevice with time at constant current density in 10 wt.% NaCl solution. ---------- 138
53. Variation of potential outside the crevice with time at constant current density in 10 wt.% NaCl solution. ---------- 138
54. Variation of potential difference with time for potential inside a crevice and potential outside a crevice at constant current density in 10 wt.% NaCl solution. ---------- 139
55. Effect of current density on potential difference between potential inside a crevice and potential outside a crevice at 30 minutes. ---------- 139
56. The cyclic potentiodynamic polarization curve for 304 stainless steel in 3.5% NaCl solution, pH 7.00 and 20°C, obtained by controlling potential inside a 12 μm crevice. Scan rate was 0.5 mV/s. Measured pH values within the crevice are shown on the curve. ---------- 140
57. The cyclic potentiodynamic polarization curve for 304 stainless steel in 3.5% NaCl solution, pH 7.00 and 20°C, obtained by controlling potential outside a 12 μm crevice. Scan rate was 0.5 mV/s. Measured pH values within the crevice are shown on the curve. ---------- 141
58. The cyclic potentiodynamic polarization curve for 304 stainless steel in 10% NaCl solution, pH 7.25 and 20°C, obtained by controlling potential inside a 12 μm crevice.

Scan rate was 0.5 mV/s. Measured pH values within the crevice are shown on the curve. ---------- 142

59. The cyclic potentiodynamic polarization curve for 304 stainless steel in 10% NaCl solution, pH 7.15 and 20°C, obtained by controlling potential inside a 40 μm crevice. Scan rate was 0.5 mV/s. Measured pH values within the crevice are shown on the curve. ---------- 143

60. The cyclic potentiodynamic polarization curve for 304 stainless steel in 10% NaCl solution, pH 6.89 and 20°C, obtained by controlling potential inside a 96 μm crevice. Scan rate was 0.5 mV/s. Measured pH values within the crevice are shown on the curve. ---------- 144

61. The cyclic potentiodynamic polarization curve for 304 stainless steel in 10% NaCl solution, pH 7.05 and 20°C, obtained by controlling potential inside a 180 μm crevice. Scan rate was 0.5 mV/s. Measured pH values within the crevice are shown on the curve. ---------- 145

62. The cyclic potentiodynamic polarization curve for 304 stainless steel in 10% NaCl solution, pH 7.00 and 20°C, obtained by controlling potential inside a 330 μm crevice. Scan rate was 0.5 mV/s. Measured pH values within the crevice are shown on the curve. ---------- 146

63. The cyclic potentiodynamic polarization curve for 303 stainless steel in 10% NaCl solution, pH 7.25 and 20°C, obtained by controlling potential inside a 12 μm crevice. Scan rate was 0.5 mV/s. Measured pH values within the crevice are shown on the curve. ---------- 147

64. The cyclic potentiodynamic polarization curve for 303 stainless steel in 10% NaCl solution, pH 7.25 and 20°C, obtained by controlling potential inside a 40 μm crevice.

Scan rate was 0.5 mV/s. Measured pH values within the crevice are shown on the curve. ---------- 148

65. The cyclic potentiodynamic polarization curve for 303 stainless steel in 10% NaCl solution, pH 7.00 and 20°C, obtained by controlling potential inside a 96 μm crevice. Scan rate was 0.5 mV/s. Measured pH values within the crevice are shown on the curve. ---------- 149

66. The cyclic potentiodynamic polarization curve for 303 stainless steel in 10% NaCl solution, pH 7.00 and 20°C, obtained by controlling potential inside a 180 μm crevice. Scan rate was 0.5 mV/s. Measured pH values within the crevice are shown on the curve. ---------- 150

67. The cyclic potentiodynamic polarization curve for 316 stainless steel in 10% NaCl solution, pH 7.13 and 20°C, obtained by controlling potential inside a 12 μm crevice. Scan rate was 0.5 mV/s. Measured pH values within the crevice are shown on the curve. ---------- 151

68. The cyclic potentiodynamic polarization curve for 316 stainless steel in 10% NaCl solution, pH 7.20 and 20°C, obtained by controlling potential inside a 40 μm crevice. Scan rate was 0.5 mV/s. Measured pH values within the crevice are shown on the curve. ---------- 152

69. The cyclic potentiodynamic polarization curve for 316 stainless steel in 10% NaCl solution, pH 7.25 and 20°C, obtained by controlling potential inside a 96 μm crevice. Scan rate was 0.5 mV/s. Measured pH values within the crevice are shown on the curve. ---------- 153

70. The cyclic potentiodynamic polarization curve for 316 stainless steel in 10% NaCl solution, pH 7.15 and 20°C, obtained by controlling potential inside a 180 μm crevice.

Scan rate was 0.5 mV/s. Measured pH values within the crevice are shown on the curve. ---------- 154

71. The cyclic potentiodynamic polarization curve for 303 stainless steel in 10% NaCl solution, pH 7.50 and 20°C, obtained by controlling potential inside a 330 μm crevice. Scan rate was 0.5 mV/s. Measured pH values within the crevice are shown on the curve. ---------- 155

72. The cyclic potentiodynamic polarization curve for 316 stainless steel in 10% NaCl solution, pH 7.00 and 20°C, obtained by controlling potential inside a 330 μm crevice. Scan rate was 0.5 mV/s. Measured pH values within the crevice are shown on the curve. ---------- 156

73. The cyclic potentiodynamic polarization curve for 304 stainless steel in 10% NaCl solution, pH 7.25 and 10°C, obtained by controlling potential inside a 12 μm crevice. Scan rate was 0.5 mV/s. Measured pH values within the crevice are shown on the curve. ---------- 157

74. The cyclic potentiodynamic polarization curve for 304 stainless steel in 10% NaCl solution, pH 7.25 and 25°C, obtained by controlling potential inside a 12 μm crevice. Scan rate was 0.5 mV/s. Measured pH values within the crevice are shown on the curve. ---------- 158

75. The cyclic potentiodynamic polarization curve for 304 stainless steel in 10% NaCl solution, pH 7.00 and 35°C, obtained by controlling potential inside a 12 μm crevice. Scan rate was 0.5 mV/s. Measured pH values within the crevice are shown on the curve. ---------- 159

76. Pit nucleation potential vs. rate of potential change for 19Cr-9Ni stainless steel. ---------- 160

77. The cyclic potentiodynamic polarization curve for 304 stainless steel in 10% NaCl solution, pH 7.00 and 10°C, obtained by controlling potential inside a 12 μm crevice. Scan rate was 0.2 mV/s. Measured pH values within the crevice are shown on the curve. ---------- 161

78. The cyclic potentiodynamic polarization curve for 304 stainless steel in 10% NaCl solution, pH 6.80 and 20°C, obtained by controlling potential inside a 12 μm crevice. Scan rate was 0.2 mV/s. Measured pH values within the crevice are shown on the curve. ---------- 162

79. The cyclic potentiodynamic polarization curve for 304 stainless steel in 10% NaCl solution, pH 7.19 and 25°C, obtained by controlling potential inside a 12 μm crevice. Scan rate was 0.2 mV/s. Measured pH values within the crevice are shown on the curve. ---------- 163

80. The cyclic potentiodynamic polarization curve for 304 stainless steel in 10% NaCl solution, pH 6.91 and 35°C, obtained by controlling potential inside a 12 μm crevice. Scan rate was 0.2 mV/s. Measured pH values within the crevice are shown on the curve. ---------- 164

81. The cyclic potentiodynamic polarization curve for 304 stainless steel in 3.5% NaCl solution, pH 7.25 and 20°C, obtained by controlling potential inside a 12 μm crevice. Scan rate was 0.5 mV/s. Measured pH values within the crevice are shown on the curve. ---------- 165

82. The cyclic potentiodynamic polarization curve for 304 stainless steel in 15% NaCl solution, pH 7.50 and 20°C, obtained by controlling potential inside a 12 μm crevice. Scan rate was 0.5 mV/s. Measured pH values within the crevice are shown on the curve. ---------- 166

83. The cyclic potentiodynamic polarization curve for 304 stainless steel in 3.5% NaCl solution, pH 7.53 and 20°C, obtained by controlling potential inside a 12 μm crevice. Scan rate was 0.2 mV/s. Measured pH values within the crevice are shown on the curve. ---------- 167

84. The cyclic potentiodynamic polarization curve for 304 stainless steel in 10% NaCl solution, pH 6.80 and 20°C, obtained by controlling potential inside a 12 μm crevice. Scan rate was 0.2 mV/s. Measured pH values within the crevice are shown on the curve. ---------- 168

85. The cyclic potentiodynamic polarization curve for 304 stainless steel in 15% NaCl solution, pH 7.37 and 20°C, obtained by controlling potential inside a 12 μm crevice. Scan rate was 0.2 mV/s. Measured pH values within the crevice are shown on the curve. ---------- 169

86. SEM micrograph of a polished surface of AISI 304 stainless steel without corrosion (1800X). ---------- 170

87. X-ray analysis of small inclusion in SEM on the polished surface of AISI 304 stainless steel without corrosion in Fig. 86. ---------- 171

88. X-ray analysis of large inclusion in SEM on the polished surface of AISI 304 stainless steel without corrosion in Fig. 86. ---------- 172

89. Corroded surface of AISI 304 stainless steel in optical microscopy at a current density of 20 $\mu A/cm^2$ during potentiodynamic polarization at a scan rate of 0.2 mV/s in 10% NaCl solution at temperature of 20°C (6.4X). ---------- 173

90. The corroded spot in Fig. 89 under optical microscopy (320X). ---------- 173

91. The corroded spot in Fig. 89 under optical microscopy (320X). ---------- 174
92. SEM micrograph of the corroded spot in Fig. 89 (260X). ---------- 174
93. SEM micrograph of part of the corroded spot in Fig. 89 (1500X). ---------- 175
94. SEM micrograph of part of the corroded spot in Fig. 89 (1800X). ---------- 175
95. X-ray analysis of small inclusion in SEM on the corroded spot of AISI 304 stainless steel in Fig. 93 at i=20 $\mu A/cm^2$ during potentiodynamic polarization at a scan rate of 0.2 mV/s in 10% NaCl solution at a temperature of 20°C. ---------- 176
96. X-ray analysis of large inclusion in SEM on the corroded spot of AISI 304 stainless steel in Fig. 93 at i=20 $\mu A/cm^2$ during potentiodynamic polarization at a scan rate of 0.2 mV/s in 10% NaCl solution at a temperature of 20°C. ---------- 177
97. Corroded surface of AISI 304 stainless steel in optical microscopy at a current density of 50 $\mu A/cm^2$ during potentiodynamic polarization at a scan rate of 0.2 mV/s in 10% NaCl solution at temperature of 20°C (6.4X). ---------- 178
98. SEM micrograph of part of the corroded spot in Fig. 89 (700X). ---------- 178
99. Corroded surface of AISI 304 stainless steel in optical microscopy at a current density of 100 $\mu A/cm^2$ during potentiodynamic polarization at a scan rate of 0.2 mV/s in 10% NaCl solution at temperature of 20°C (6.4X). ---------- 179
100. Corroded surface of AISI 304 stainless steel in optical microscopy at a current density of 200 $\mu A/cm^2$ during potentiodynamic polarization at a scan rate of

0.2 mV/s in 10% NaCl solution at temperature of 20°C (6.4X). ---------- 179

101. Corroded surface of AISI 304 stainless steel in optical microscopy at a current density of 500 $\mu A/cm^2$ during potentiodynamic polarization at a scan rate of 0.2 mV/s in 10% NaCl solution at temperature of 20°C (6.4X). ---------- 180

102. Corroded surface of AISI 304 stainless steel in optical microscopy after the scanning direction was reversed at 500 $\mu A/cm^2$ to finish the cycle during cyclic potentiodynamic polarization at a scan rate of 0.2 mV/s in 10% NaCl solution at temperature of 20°C (6.4X). ---------- 180

103. Reaction volume inside a crevice. ---------- 181

104. Diffusion direction of ions in the reaction volume when the crevice width is equal to or less than 0.018 cm. ---------- 181

105. Diffusion direction of ions in the reaction volume when the crevice width is greater than 0.018 cm. ---------- 182

106 The cyclic potentiodynamic polarization curve for 304 stainless steel in 10% NaCl solution, pH 7.25 and 20°C, obtained by controlling potential inside a 12 μm crevice. Scan rate was 0.5 mV/s. Calculated pH values within the crevice are shown on the curve. ---------- 183

107. The cyclic potentiodynamic polarization curve for 304 stainless steel in 10% NaCl solution, pH 7.15 and 20°C, obtained by controlling potential inside a 40 μm crevice. Scan rate was 0.5 mV/s. Calculated pH values within the crevice are shown on the curve. ---------- 184

108. The cyclic potentiodynamic polarization curve for 304 stainless steel in 10% NaCl solution, pH 6.89 and 20°C, obtained by controlling potential inside a 96 μm crevice.

Scan rate was 0.5 mV/s. Calculated pH values within the crevice are shown on the curve. ---------- 185

109. The cyclic potentiodynamic polarization curve for 304 stainless steel in 10% NaCl solution, pH 7.05 and 20°C, obtained by controlling potential inside a 180 μm crevice. Scan rate was 0.5 mV/s. Calculated pH values within the crevice are shown on the curve. ---------- 186

110. The cyclic potentiodynamic polarization curve for 304 stainless steel in 10% NaCl solution, pH 7.00 and 20°C, obtained by controlling potential inside a 330 μm crevice. Scan rate was 0.5 mV/s. Calculated pH values within the crevice are shown on the curve. ---------- 187

1. INTRODUCTION

Among the different forms of localized corrosion, it is a common occurrence in practice that crevice corrosion causes serious damage to metal construction and chemical equipment. Generally speaking, almost all metals may suffer from crevice corrosion. Of all the metals, passivating corrosion-resistant metals such as stainless steel, aluminum, and titanium corrode most easily by crevice corrosion, especially in media containing chloride ions.

As crevice corrosion is very similar to pitting corrosion in many ways, it is very useful to compare the similarities and dissimilarities between these two kinds of localized corrosion. In comparing initiation modes, pitting can initiate at different vulnerable points on a metallic surface where the surrounding corrosive medium has free access. The corrosive medium must contain some active anions, such as Cl^- or I^-. Crevice corrosion, in contrast, only attack a portion of the metallic surface, which forms a narrow gap with metal or non-metallic materials. The stagnant solution must be present in the gap and aggressive medium may penetrate into the gap. The active anions are not a necessary condition to initiate crevice corrosion. Pitting can initiate at heterogeneities on the metal surface such as nonmetallic inclusions, grain boundaries, etc. According to many investigators, crevice corrosion can also be initiated by nonmetallic inclusions, defects, etc.

In comparing morphology, pits in pitting are deep and narrow. The pits in crevice corrosion, in contrast, are often large and shallow. Because of immobility of the solution in the crevice, an exchange between the crevice solution and the bulk solution is difficult. Therefore, the changes in the composition of crevice solution occur much more rapidly than in the case of uncovered pits. In most cases, crevice corrosion occurs more rapidly and over a wider range of corrosive conditions than pitting. For this reason, the general consensus is that crevice corrosion is more detrimental than pitting in practice.

As crevice corrosion is widespread and detrimental in practice, it has engaged the attention of many investigators (1-8). The first particular recognition was accorded to the

concept of differential aeration, advanced by R.B. Mears and U.R. Evans (4), to explain the reason for crevice corrosion. Since then, further investigations indicate that the mechanism of crevice corrosion is more complex than just differential aeration. It includes the following aspects:

- crevice type
- crevice geometry
- total geometry; ratio of metal area inside to area outside crevice
- the solution outside the crevice (bulk solution, environment)
- the solution inside the crevice
- differences developing between the inside and outside solutions
- transport mechanism (outside, towards and inside the crevice)
- electrochemical reactions
- secondary chemical reactions
- IR drop in the crevice solution
- alloy composition and microstructure
- surface conditions

Although the processes of crevice corrosion are very complicated, many investigations have been performed by scientists all over the world to determine what conditions lead to crevice corrosion, how the basic mechanisms of crevice corrosion work and to develop effective methods for protection. Many mechanisms have been proposed to account for the initiation and propagation of crevice corrosion. Several criteria have been developed to characterize susceptibility of a given metal or alloy to crevice corrosion. These include (1) the critical potential for the initiation of crevice corrosion (E_{cp}); (2) the difference between the critical potential for the initiation of crevice corrosion E_{cp} and the protection potential for crevice corrosion E_{prot} obtained during cyclic polarization of a specimen; (3) critical pH; (4) critical crevice temperature; and (5) critical anodic current density for passivation. Meanwhile, a number of novel experimental methods for the investigation of crevice corrosion have been developed to establish general principles and to obtain new results which can reveal the true

mechanisms involved in crevice corrosion and the effects of external and internal variables on crevice corrosion.

Several ways have been developed to prevent crevice corrosion. These include (1) elimination of crevice: use of nonabsorbent gaskets, such as Teflon; (2) keeping the metal clean: removing the deposits; avoiding the corners in which the stagnant solution may form, etc.

Despite the progress made in understanding the mechanism of crevice corrosion and the influence of both external (environment composition, temperature, electrode potential) and internal parameters (alloy composition, surface preparation etc.) on crevice corrosion, many questions remain unanswered and even contradictory conclusions are obtained. The reason for this is that the exact same experimental conditions are impossible to repeat during the study of crevice corrosion and also different experimental methods are used during the study of crevice corrosion.

The purpose of this thesis is to study the crevice corrosion of stainless steel in order to better understand the mechanism of crevice corrosion and to develop some criteria for evaluating the susceptibility of different stainless steels.

The second chapter of this thesis is the review of some basic mechanisms of crevice corrosion, experimental methods and the effects of external and internal variables on crevice corrosion. The third chapter of this thesis states the present problems in the study of crevice corrosion and the objectives of the thesis. In the fourth chapter, a new experimental method is described for the study of crevice corrosion of stainless steel. The new experimental method is used to measure the cyclic potentiodynamic polarization curve of stainless steel in NaCl solution by controlling the potential inside a crevice in order to study crevice corrosion. During the experiment, the pH values within the crevice are also recorded. In the fifth chapter, the new experimental method is compared with the conventional experimental method by controlling potential outside a crevice. The results show that the new experimental method is better. The results obtained by this new method are also discussed and a modified four stage mechanism of crevice corrosion is proposed. In the sixth chapter, a mathematical model for the calculation of pH values along the cyclic anodic polarization curve is developed based on the thermodynamical

equilibrium, experimental set-up and experimental data. Theoretical results are in close agreement with the experimental ones.

2. Literature Review

2.1 Mechanisms of Crevice Corrosion

Many papers have dealt with the crevice corrosion mechanism of metals, especially stainless steels (9-36). Vermilyea and Tedmon (11) have proposed a theory for the concentration and potential variations inside a crevice. A consequence of the theory, confirmed by experiments, is that a small potential difference in a crevice can cause a large concentration change and a corresponding large increase in the corrosion current at a given potential. Bombara (12) gave a theoretical treatment of a possible mechanism for crevice corrosion as well as stress corrosion cracking for a localized model in terms of active-passive cells. Isaacs (13) also studied the dissolution of stainless steel in artificial crevices as a function of potential and chloride ion activity. Impedance measurements have shown the presence of a resistive layer on the steel which limits the rate of electrode reaction in the localized corrosion of stainless steel. The potential across the layer, equal to the product of the direct current and layer resistance, varies linearly with the electrode potential indicating ohmic ionic conduction across the layer. The solubility of the metal ions and the current depend markedly on the chloride concentration and the complex chemistry within the cavity.

Crolet and Defranoux et al. (14-16) calculated incubation times for crevice corrosion of stainless steels theoretically. They found that the pH and buffer power of the corrosion medium are of little practical influence and, conversely, thickness of crevices and the depassivating pH of stainless steels are very effective factors.

Karlberg and Wranglen (18) explained the mechanism of crevice corrosion, taking into account the acidification effect in the crevice and the resulting change in the Flade potential, E_{Fl}, as well as an IR drop in the crevice solution. The Flade potential is the lowest equilibrium potential at which electrochemical production of a protective oxide film is thermodynamically possible. It is very close to the passivation potential and

sometime is considered as the passivation potential. They measured potential and pH change for both a 13% Cr steel (steel A) and a 17% Cr steel (steel B) during crevice corrosion. The result is shown in Fig. 1. In the initiation period, the potential difference (P.D.) $\Delta E = E_{out} - E_{crev}$ between the outer surface and the crevice was small and then both potentials rose to a maximum and fell, the E_{crev} falling more rapidly than E_{out}. After a few hours, both potentials attained an almost constant value. When crevice attack starts, both potentials fall. Whereas the potential of the anode (crevice) surface is lowered due to activation, the potential of the cathode (outer) surface is lowered due to cathodic polarization. During the propagation of a crevice attack, a certain P.D. developed between anode and cathode; the P.D. magnitude is a measure of the rate of attack in accordance with ohmic law. As the active surface within the crevice increases, the corrosion current increases and so does the ohmic potential drop and the cathodic polarization of the outer surface. That the pH of the crevice solution increases rapidly immediately after filling the cell with electrolyte is obvious due to the fact that initially O_2 is consumed and OH^- is produced within the crevice according to the cathode reaction:

$$O_2 + 2H_2O + 4e^- \rightarrow 4OH^- \qquad (1)$$

After all O_2 within the crevice is consumed, the cathode reaction (1) occurs entirely on the outer surface whereas on the crevice surface mainly the anode reactions occur:

$$Fe \rightarrow Fe^{2+} + 2e^- \qquad (2)$$

$$Cr \rightarrow Cr^{3+} + 3e^- \qquad (3)$$

When the Fe^{2+} and Cr^{3+} concentrations reach certain values, hydrolysis takes place:

$$Cr^{3+} + 3H_2O \rightarrow Cr(OH)_3 + 3H^+ \qquad (4)$$

$$Fe^{2+} + 2H_2O \rightarrow Fe(OH)_2 + 2H^+ \qquad (5)$$

These reactions generate H^+, which means the pH is lowered again after having passed

a maximum value.

The mechanism of crevice corrosion of stainless steels in neutral aerated Cl^- solutions is illustrated by the schematic polarization diagrams for crevice and outer surface shown in Fig. 2.

(a) Initially, the polarization diagrams for the crevice and outer surface are identical. The entire steel surface is passive; the air-formed oxide film allows a fairly high anodic current density, however. The redox potential for the cathode reaction (1) above is given by

$$E=E_o+(R_gT/ZF)\ln[Po_2/(OH^-)^4] \qquad (6)$$

which shows that a change of pH causes a potential change four times that caused by a corresponding change of O_2 pressure. Although both a lowering of O_2 content and a rise of pH are factors which cause a lowering of the potential, the measured potentials are initially changed in the positive direction, apparently due to a strengthening of the air-formed oxide film.

(b) The anode curves are moved towards lower current, both in the crevice and on the outer surface, due to a thickening of the oxide film, corresponding to more noble values of measured potentials. From the crevice towards the outer surface there flows in the solution a small current of the size $(I_a)_{crev.}-(I_c)_{crev.}=(I_c)_{out.}-(I_a)_{out.}$, which means that there is an ohmic potential drop in the same direction. This is so small, however, that crevice and outer surface still have practically the same potential.

(c) The difference in O_2 content and cathodic P.D. between crevice and outer surface is now large. In the crevice, the anode reaction dominates the cathodic reaction, which means that the amount of OH^- formed in the crevice is negligible in comparison with that of the Fe^{2+} generated. At all times we have the relation

$$(I_a)_{crev.}+(I_a)_{out.} = (I_c)_{crev.}+(I_c)_{out.} \qquad (7)$$

(d) Hydrolysis of Fe^{2+} and Cr^{3+} results in a lowering of the pH of the crevice solution.

With the successively increasing cell current, Cl^- migrates into the crevice. The result is an acid solution of Fe^{2+} and Cr^{3+} chlorides. Both H^+ and Cl^- increase the rate of the anode reaction, H^+ by dissolving the oxide film, Cl^- by peptizing it. The acidification of the crevice solution raises E_{Fl} according to the following equation (25)

$$E_{Fl} = E_{Fl,o} - 0.059pH \qquad (8)$$

(e) E_{Fl} of the crevice surface has now been raised so much that the crevice surface is active whereas the outer surface is still passive. The propagation stage of the crevice attack has been reached. The corrosion current and hence also the P.D.(ΔE) between crevice and outer surface is increased. ΔE reaches a steady state value. In the slot (crevice mouth) $Fe(OH)_3$ accumulates. It is formed with O_2 consumption and also renders O_2 diffusion into the crevice more difficult. Crevice corrosion is self-propagating (autocatalytic) in the same way as pitting.

A similar mechanism of crevice corrosion was proposed by Matsushima et al. (24). They also gave an explanation of the initiation of crevice corrosion in terms of polarization curves.

Oldfield and Sutton (19, 20) summarized the opinions of many authors and developed a detailed mathematical model in which the various stages of crevice corrosion can be simulated, taking account of many factors involved. In this model four stages can be distinguished during crevice attack, namely: (A) deoxygenation, (B) increase of the salt and acid concentrations, (C) depassivation, and (D) propagation, as shown in Fig. 3.

(A) At the start of the first stage the composition of the solutions inside and outside the crevice is the same. The alloy surface is covered with a passive film, allowing the passage of a small anodic current (the passive current) which transfers metal ions into solution. The anodic current is balanced by cathodic reduction of oxygen taking place all over the alloy surface; namely the following reactions will occur:

Anodic: $M_t \rightarrow M_t^{2+} + 2e^-$ (9)

Cathodic: $H_2O + 1/2O_2 + 2e^- \rightarrow 2OH^-$ (10)

Overall: $M_t + H_2O + 1/2O_2 \rightarrow M_t(OH)_2$ (11)

Although the current densities involved are generally very low, the rate of consumption of oxygen within the crevice may easily exceed the rate of replenishment by oxygen diffusing from the outside solution due to the restricted mass transfer, and the system begins to operate as a differential aeration cell. Metal inside the crevice acts as an anode, while the remaining metal surface in contact with the bulk electrolyte acts as a cathode. Considering the determining factors, such as crevice geometry, passive current density, solubility and diffusion constant of oxygen, temperature and agitation, the length of time to deplete oxygen in the crevice and the distance covered by the diffusion of oxygen during the first stage can be calculated.

(B) During the second stage of the process further differences may develop between the composition of the bulk solution and the crevice solution. The passive film is still intact and allows an anodic current to pass into the solution. This current transfers metal ions into the solution in the same ratio as the alloy composition. However, the balancing oxygen reduction reaction is restricted to the metal surface outside the crevice with current flowing from the inside to the outside. The slow anodic dissolution of metal in the crevice leads to local accumulation of M^{2+}. To maintain charge neutrality, anions (primarily Cl^-) migrate from the bulk electrolyte into the crevice. Hydrolysis of the dissolution products of metal occurs, which increases acidity in the crevice electrolyte.

$$M_tCl_2 + H_2O \rightarrow M_t(OH)_2 + 2HCl \quad (12)$$

Apart from originating from hydrolysis, protons will also be produced directly by anodic oxidation, for instance:

$$Fe + H_2O \rightarrow Fe(OH)^+ + H^+ + 2e^- \quad (13)$$

The combined effect of increasing concentrations of chloride ions and decreasing pH in the inner solution creates a crevice solution which becomes steadily more aggressive toward the passive layer. The critical pH, at which the passive film breaks down, and the time necessary to reduce pH to the critical value in the crevice, can also be obtained through tedious calculation from ion migration and diffusion during this time, with an empirical correction for the effect on the pH of Cl^- ions in the crevice.

(C) During the third stage of the process the passivity of the alloy surface within the crevice is destroyed by the aggressive inner solution when the local acidity attains a critical value. The interior surface of the crevice consequently becomes activated at some vulnerable sites. Pitting occurs and activation later is extended to the entire crevice surface, so that propagation of crevice corrosion will start. The resistance of the passive layer to the aggressive solution, containing metal ions, chloride ions and hydrogen ions in fairly high concentrations, determines the time which is necessary to create such an aggressive inner solution where general attack proceeds. The time lapse required for the first three stages is generally called the incubation period. Because of the shorter time necessary to reach the critical acidity leading to passivity breakdown, the initiation of crevice corrosion is faster than that of pitting.

(D) After the incubation period the fourth stage of the corrosion process begins. In this stage the attack propagates, with the alloy inside the crevice dissolving rapidly. This anodic process is balanced by the reduction of oxygen outside the crevice and possibly by hydrogen ion reduction inside. In this respect the external face: crevice area ratio is very important in determining the rate of the propagation.

This model is helpful in selecting materials and permits determination of the limiting Cl^- concentration that can safely be used for an alloy with a given crevice geometry. But there are two drawbacks to the model: firstly, that mass transfer is not dealt with in a completely rigorous manner and secondly, no consideration is given to the effect of IR potential drops inside the crevice.

From the above mathematical modelling of the corrosion process and its use to predict critical parameters such as crevice geometry and crevice corrosion initiation time, Oldfield and Sutton (25) and Rowlands (26) developed a critical parameter, the crevice

corrosion resistance (CCR) value to predict the performance of stainless steels with respect to crevice corrosion. The crevice corrosion resistance (CCR) value is nominally the exposure time required for corrosion to commence in a metal to non-metal crevice 5 mm deep with a gap of 0.5 μm. The input parameters to the computer model to determine the CCR value are the alloy composition, the pH of critical crevice solution with appropriate chlorinity dictated by the alloy composition, and the passivation current which flows during the incubation period prior to the breakdown of the passive film in the crevice. The critical crevice solution pH and passivation current are fairly easily determined using electrochemical techniques in the laboratory. From the CCR values, a simple ranking of the resistance of various materials to crevice corrosion can be obtained.

Pickering and coworkers (27-31) proposed a potential-shift mechanism based on the active/passive transition. They emphasized the great importance of the value of the electrode potential in the cavity. In particular, the deciding factor may be the relationship between the electrode potential and the passivation potential of the cavity electrode. The acidification in the crevice is not a necessary condition for the initiation of crevice corrosion (32).

The role of the cavity electrode potential is easily understood with the help of the polarization plot shown in Fig. 4 (31, 34). When the polarization curve of the crevice electrolyte contains an active/passive transition, i.e. a passivation potential (E_{pass}), a stable localized corrosion process occurs when the electrode potential in the crevice is less than the passivation potential. Then, metal dissolution in the crevice occurs at high rates in the active region of the polarization curve, while the outer surface is in the passive region and dissolves at a low passive rate. Thus, the IR drop or the electrode-potential variation between the crevice and the outer surface is the important parameter. The importance of IR drop in crevice corrosion initiation was also stressed by Shaw et al. (35).

Since the crevice electrode potential must be below the passivation potential (E_{pass}) for a stable local cell to exist, the IR drop must be greater than a specific value IR*, where IR* is the difference between the potential at the outer surface and the E_{pass}. Therefore, the condition for the stability of a local cell is that IR > IR*. The changing

solution composition inside the crevice can influence the magnitude of the IR drop that is needed to shift the potential into the active region; e.g., acidification does this by increasing the passivation potential. Thus, when the crevice electrode potential is decreased to below the passivation potential (E_{pass}) by sufficient IR drop, that part of the cavity will become active and dissolve at a high rate while the rest of the surface is passive. This idea is illustrated in Fig. 5. As shown in Fig. 5, the corrosion (or applied) potential at the outer surface (point A) is in the passive region. With an increase of the distance into the crevice, the electrode potential shifts to more negative values, and at the boundary of the corroded region, IR=IR*, i.e., at the active/passive boundary, $E=E_{pass}$. As one moves further into the crevice, the potential becomes even lower as IR increases. From the E vs. I behavior of the active region of the polarization curve, the metal dissolution rate decreases. Therefore, the site of maximum metal dissolution is restricted to a region of the crevice walls that is a certain distance into the crevice from the crevice opening. At shorter distances from the crevice opening, corrosion is not observed, and deep within the crevice corrosive attack decreases until it stops. On the other hand, if E_{pass} is far below the applied potential or, in the limit, the active region is not seen for the solution composition in the crevice, as shown in Fig. 6 (a), the condition IR > IR* is not met. Therefore, modification of the solution composition such as gas bubble accumulation on the crevice surface, acidification, or Cl^- ion buildup is needed for localized corrosion to occur by the potential-shift mechanism. For example, the acidification and/or aggressive ion buildup in the crevice solution decreases IR* [Fig. 6 (b)] and increases IR by an increase in passive current. The IR drop can also be increased by gas or solid on the surface that forms a microcrevice (36-39). The consequence of decreasing IR* or of increasing IR is that the condition (IR > IR*) can be met easily. The I_{max} may also be increased, consistent with the known effects of acidification and/or aggressive ion buildup on increasing the rate of local cell processes, where IR* and I_{max} are defined in Fig. 5. The strong effects of H^+ and Cl^- on the magnitudes of E_{pass} and passive current for corrosion-resistant alloys are well known in the corrosion literature (40,41).

Xu and Pickering (42) have also developed a computational model to calculate the

potential and current distribution in the electrolyte phase and on the electrode surface for a system in which a part of the anode is passivated while the rest remains in the active dissolution state. In the case of a crevice, a critical distance into the crevice exists beyond which active corrosion takes place; that is, the critical distance is the location of the active/passive transient potential E_{pass} on the polarization curve in crevice electrolyte. In addition to the active/passive behavior of the material, solution conductivity, applied potential at the sample's outer surface, crevice gap and depth dimension and passivation current density affect this critical distance to different degrees.

Brigham (43) has also developed another approach based on thermodynamic arguments to address the initiation step leading to accessibility to the hydrogen reaction on an anodically polarized metal surface.

From the thermodynamics of the planar metal/electrolyte interface, an equation can be derived:

$$\gamma = \gamma_{max} - 2\pi d q_m^2/\epsilon \qquad (14)$$

where γ_{max} is the integration constant obtained by setting $q_m=0$, q_m is the surface charge density, γ the surface tension, d the distance between the sheets of charge and ϵ the dielectric constant of the material between the sheets. These relationships are shown schematically in Fig. 7. The applied potential E for which $q_m=0$ is commonly known as the potential of zero charge, E_{pzc}.

Also an equation can be obtained from thermodynamics of the crevice geometry:

$$\gamma + \text{constant} = \pi\epsilon(kT/e)^2/2l \qquad (15)$$

where e is the charge of the electron, l *is* the separation distance of the plates, k is the Planck constant and T is the absolute temperature. The $1/l$ relationship in equation (15) indicates that the interaction energy rises rapidly as $l \rightarrow 0$.

The functional relationship between q_m and l, obtained by combining equations

(14) and (15), has the form

$$q_m^2 = \text{constant} - (\epsilon kT/e)/4dl \qquad (16)$$

It is clear that as the plates are brought closer together (as $l \rightarrow 0$) the surface charge density is reduced to its limiting value ($q_m^2 \rightarrow 0$).

A simplified model of the crevice, shown in Fig. 8, can be drawn for a passive metal such as stainless steel immersed in a concentrated oxidizing electrolyte. On the outside of the plate, the steep potential gradient characteristic of a sample polarized to a high noble potential induces a large positive surface charge density on the metal. However, in the crevice, the initial mirror image potential gradients (dashed) are attenuated by their strong interaction at close approach. As a result, the net gradient is reduced and as indicated by equation (16), the surface charge density approaches zero. This condition ($q_m \rightarrow 0$) describes a metal polarized close to E_{pzc}. E_{pzc} is -0.37V (SHE) for Fe. It appears that a single metallic coupon, normally considered to be an equipotential surface when no corrosion current flows, can be polarized in one location (the exposed surface) to a very noble potential, say +0.5V (SHE) and in another (the crevice) to E_{pzc} of approximately -0.4V (SHE). Any subsequent electrochemical reaction which might occur will depend on the nature of the stainless steel coupon and the electrolyte but it is clear that at E_{pzc} in the range of -0.4V (SHE) the reaction

$$2H^+ + 2e^- \rightarrow H_2 \qquad (17)$$

is immediately accessible in acid solutions. At the same time, the charge density on the passive surface outside the crevice remains at a high positive value, typical of the strongly anodic polarization associated with passivity. Thus, Brigham (44) postulated that the stability conditions governing crevice corrosion initiation can be related to the accessibility of the hydrogen reaction in the crevice, that is, E_{pzc} must be active with respect to the hydrogen line for crevice corrosion to occur. He has also directly observed (45) the electrochemical reactions associated with a naturally growing crevice, including

hydrogen production and metal dissolution, by using a glass lens to form a crevice on stainless steel in acid chloride/sulfide solution.

A number of steady-state and transient models have been proposed for simulated crevice corrosion considering factors such as crevice geometry, transport of solution, bulk solution compositions, etc., because there are many difficulties associated with the experimental measurement of the electrochemical conditions within a crevice. Alkire et al. (46-49) have done much work on these aspects. Also some researchers (50,51) used statistical methods to study the pit initiation according to experimentally observed phenomena such as highly oscillatory and often seemingly random current transients measured from metal samples exposed to conditions suitable for localized corrosion. But both steady-state and transient models still need a lot of work in order to make great progress. Recently, Sharland (52) gave a very detailed review of the theoretical models of localized corrosion.

2.2 Experimental Methods in Crevice Corrosion

The purpose of crevice corrosion tests as described in the literature can be divided broadly into two groups:

(a) to investigate the mechanism of crevice attack;

(b) to determine the susceptibility of an alloy to crevice attack.

In both respects, the initiation as well as the propagation characteristics have to be taken into account.

There are many experimental methods that can be used to investigate crevice corrosion. Of all the methods, the electrochemical methods are the most important and widely used. They reveal many characteristic features in crevice corrosion. Roughly, the electrochemical methods can be used to study crevice corrosion in two areas:

(i) investigation of the electrochemical conditions in the crevice;

(ii) investigation of the initiation and propagation of crevice corrosion.

2.2.1 Electrochemical Methods for Investigating the Electrochemical Conditions in the Crevice

According to the general theory for crevice corrosion, the passive film is broken down inside the cavity due to a decrease in local pH value. The determination of the solution chemistry and potential within these 'occluded cells' is essential, not only for evaluating crevice corrosion susceptibility, but also for understanding the mechanisms of crevice corrosion. Therefore, many experimental methods for investigating the electrochemical conditions in the crevice have been carried out and the experimental methods employed could be loosely subdivided into the following groups (53):

(i) direct, in situ, measurement;

(ii) semi-direct methods involving (a) solution extraction and analysis or (b) a freezing technique followed by solution analysis;

(iii) the use of an artificial crevice including simulated crevice and macrocells;

(iv) simulation of the chemistry of localized corrosion.

2.2.1.1 Direct, In Situ, Measurement

The essential criterion for in situ measurement is that the test probe should cause minimum perturbation of the system under study. In situ measurements in a crevice are made by mounting the electrode in a plastic or metal block forming one half of the crevice (Fig. 9) (53-65). Relatively large probes can be used provided the crevice dimensions are correspondingly large, but again the possibility of the probe and mounting arrangement altering the local conditions must be considered.

Alavi and Cottis (66) used an artificial crevice assembly shown in Fig. 10 to determine the potential and pH in the crevice. The pH was measured with a palladium/hydrogen diffusion electrode. The results are shown in Fig. 11 and 12 which indicate that the crevice potential is more negative than the external potential and the crevice becomes acidified and corrodes actively.

Despite the small size of the probes used in the monitoring of crevice potential, they still introduce a 'dead volume' of electrolyte at the probe tip which may be an important part with respect to the rest of the crevice. To meet the demands of smaller

potential probes, Haltman and Robinson (67) have developed a novel salt bridge based on fibres of ion exchange resin. The assembly is shown in Fig. 13. Fig. 13a is the general arrangement for measuring pH and corrosion potential within the crevice. Fig. 13b shows the detailed construction of the resin fibre potential probe. The resin fibre probe has a relatively high electrical resistance but has the significant advantage that it can be produced flush with the crevice wall, thus avoiding the entrainment of additional electrolyte.

2.2.1.2 Semi-direct Methods

The solution extraction technique involves sampling solution from the crevice and analyzing for the various species of interest. This analysis may be immediate at the site of extraction, for example by the 'paper and probe' method of Smith et al. (68) in which miniature pH and reference electrodes were used to measure the pH of the solution extracted at the tip of a stress corrosion crack using lens tissue. Indicator paper has also been used to measure the pH (69,70). More commonly, micro-volumes of solutions are removed from the crevice and analyzed at a later stage (71,72). Two factors to be considered in both these tests are (a) interaction of the extracted solution with the atmosphere (e.g. oxidation of ferrous ions to ferric ions) and (b) in the case of cracks the volume of solution extracted in relation to the volume of the crack.

The freezing technique involves freezing of the solution in the crevice (73), fracturing the specimen (or extracting the frozen contents from the pit or crevice) and analyzing for pH and metal ions as the solution melts, using indicator paper.

2.2.1.3 Artificial Crevices

A variety of artificial cavities has been developed to simplify the problems of solution analysis and measurement of potential. In some cases this has involved the development of macrocells which simulate localized corrosion conditions by creating a restriction to mass transport in a fritted disc, asbestos plug, etc., between an aerated and de-aerated compartment (Fig. 14) (53,74-82). Crevices are often, in their nature, artificial and they may be formed between metal plates or for example under an O-ring

(83). When in situ measurement is difficult the crevice can be opened after completion of the test and the contents analyzed using indicator methods (84). A technique was employed to study the crevice corrosion behavior of a high strength steel (85) which illustrated that under free corrosion potentials, these crevices were not subject to acidification and attack.

In studying artificial crevices, it is important to be aware that the results can not be directly related to real crevices. Nevertheless, the contribution which these studies have made to an understanding of localized corrosion processes has been considerable.

2.2.1.4 Simulation of the Chemistry of Localized Corrosion

These studies are aimed at simulating the assumed solution chemistry in the crevice by creating appropriate conditions in a cell, then monitoring, for example, the pH and potential under these conditions. Some research (85-87) was carried out to measure the potential and pH when iron was immersed in a de-aerated solution of saturated $FeCl_2$. The results from this technique cannot be applied directly, since mass transport is not considered, but they can provide information on the pH in concentrated solution and the steady state potential of the metal under these conditions. Euvrard et al. (88) developed an experimental set-up for production of large volumes (up to 150 mL) of crevice solution for a 304L stainless steel by means of anodic dissolution in a circulating deaerated chloride neutral solution. Electrochemical and chemical analysis have confirmed good agreement of the solution produced with the real crevice solution.

2.2.2 Experimental Methods for Investigating the Initiation of Crevice Corrosion

2.2.2.1 Electrochemical Noise Measurements

Electrochemical noise is the term often used to describe spontaneous fluctuations occurring in electrochemical systems. The detection and analysis of the fluctuations in current and potential of electrodes are receiving increasing attention in electrochemistry as a means for the study of electrode processes (89-91). Recently, correlations between type of potential noise detected and the nature of localized corrosion have been found

(92-111). Dawson et al. (94,95) recorded the potential difference between two identical electrodes at open-circuit potential as a function of time, as shown in Fig. 15. The corrosion potential fluctuations are superimposed upon the dc level of either the free corrosion potential or the difference in potential between two electrodes. A least squares method was used to remove the dc component from the data. Data analysis was carried out by microprocess computer with Fast Fourier Transform (FFT). Fig. 16 shows the time record from Fig. 15 after removal of the dc trend. The FFT spectrum of the time record shown in Fig. 16 is shown in Fig. 17. From the relationship between the noise amplitude and frequency, a correlation between the nature of the corrosion attack and the low frequency fluctuations of the electrode potential has been found. The electrochemical noise output is a constant amplitude over a range of very low frequencies and decreases in amplitude at frequencies above this range. The slope of the high frequency roll-off bears a relation to the nature of the corrosion attack. A roll-off slope of -10 db/decade or less is indicative of pitting corrosion whereas -40 db/decade shows general corrosion. A sharp peak at a single frequency indicates crevice attack as indicated in Fig. 18. Further, the amplitude of the voltage noise in the form of low frequency root-mean-square (r.m.s.) amplitude or standard deviation of the time record gives a qualitative indication of the dissolution rate. There is some evidence that the standard deviation of the noise may be proportional to the dissolution rate of metals.

Magaino et al. (96) studied spectral analysis of corrosion fluctuations for localized corrosion of type 304 stainless steel by the apparatus shown in Fig. 19. They found a clear difference existed between the potential fluctuation for micropit formation and that for crevice corrosion, as shown in Fig. 20. The potential fluctuation in micropit formation shows a rapid drop followed by a slow rise and that in crevice corrosion shows a rapid rise followed by a slow drop.

The difference between the potential fluctuation of micropit formation and that for crevice corrosion was also clear in their power spectrum as shown Fig. 21. The value of power spectral density (psd) for micropit formation decreased linearly as the frequency increased in the frequency range 0.002-0.1Hz, whereas the attenuation rate of psd with frequency increased remarkably from about 0.01Hz when crevice corrosion was

proceeding.

Simes and Ferreira (97) used an electrical setup shown in Fig. 22 for simultaneous measurement of current and potential noise, in an attempt to find correlations between them and the phenomena observed on a freely corroding stainless steel surface containing a crevice. Both the potential noise and the current noise were monitored by means of a zero resistance ammeter (ZRA), a switch box and a high resolution voltmeter.

The potential evolution for one particular experiment, shown in Fig. 23, was obtained by plotting the mean values of the potential records against time of immersion of the specimens, and analysis of a number of similar plots suggests a four stage potential evolution:

(i) strong increase of the potential with few or no fluctuations;

(ii) the potential rises slowly and potential transients become obvious (Fig. 24a);

(iii) sudden potential drop;

(iv) the potential become approximately constant, showing only small, slow fluctuations.

Stages 3 and 4 are easily recognized, whereas stages 1 and 2 are often difficult to distinguish. The first is normally associated with a growth of the oxide film on the metal surface (18,20). The transients that characterize the second stage consist of a sharp decrease in the potential, followed by a much slower rise (Fig. 24a). These have been interpreted (98) as representing rapid local breakdown of the passive film, followed by its repair.

The potential drop of the third stage probably reveals the exact moment when crevice corrosion starts. While corrosion was continuing the corrosion potential ranged from -100 to -250 mV (SCE) and showed only slow fluctuations. These fluctuations are generally smaller (< 1mV) than the transients during stage 2.

The plots of the mean values of each potential or current record against time for the complete duration of the experiment also show some interesting features. In most cases a decrease in the potential corresponds to an increase in the current, while an increase in the potential is related to a current drop (Fig. 25).

The plot of the standard deviation of the same records again (Fig.26) indicates

that this parameter is sensitive to both the initiation of corrosion and the repassivation phenomena, since they show maxima at 0 hr (initiation of corrosion), ~900 hr (repassivation) and ~1200 hr (reinitiation of corrosion).

Therefore, electrochemical noise provides a reliable technique for studying crevice corrosion, since it gives information on the evolution of processes inside the crevice. In particular, it has proved to be sensitive to the onset of crevice corrosion.

2.2.2.2 AC Impedance Methods

The charge-transfer resistance (R) and double layer capacitance (C) associated with the metal-solution interface of a corroding surface can be determined by AC impedance measurements (99). The resistance to charge transfer encountered when a metal atom is converted to a metal ion in solution is related to R. The reciprocal of R is directly proportional to the corrosion rate if the corrosion process is activation controlled (100). The ability of the interface to store the charge separated in the corrosion process is related to C. Consequently, R and C are characteristic of the surface phenomena associated with the corroding metal-solution interface in which we are interested.

Reising (101) used the AC impedance method to determine whether oxygen molecules, hydrogen ions, or aluminum ions initiate crevice corrosion of aluminum alloy 6061 in aqueous chloride solutions. AC impedance measurements are expressed as functions of time in order to correlate their changes with changes in the surface properties. A frequency of 0.25 Hz and an amplitude of +10 mV were selected for these experiments. A typical complex plane is semicircular in shape, which suggests that the corrosion process is relatively simple and may be modeled by a parallel RC electrical circuit. An equivalent circuit for the breakdown of a passive film on an aluminum alloy based on these measurement is proposed in Fig. 27.

If the charge-transfer resistance (R_u) associated with those areas which are uncovered is orders of magnitude less than the resistance (R_f) associated with the passive film, a plot of R vs. t could change dramatically with the initiation of film breakdown in accordance with the rules for summing parallel resistances.

The corrosion behavior of an aluminum alloy 6061 specimen in 0.05 N NaCl solutions when oxygen is available is shown in Fig. 28a, b and c. Acidified, as well as unacidified, solutions were used to observe the effect which would result from the lower pH produced by the hydrolysis step in the crevice mechanism. Random fluctuations in the R-t plots for pH 5.8 (dots) and pH 4.8 (circles) solutions suggest that the passivity is a steady state in which breakdown and repair mechanisms are competing. The plot (squares) for the pH 3.8 solution indicates a definite increase in corrosion rate. The plot (triangles) for the pH 2.8 solution indicates a rapid breakdown of surface. Fig. 28c indicates the capacitances associated with the specimens immersed in the pH 5.8 (dots) and pH 4.8 (circles) solutions are virtually the same and change very little over the duration of these experiments. The plot (squares) for the pH 3.8 solution shows a slow increase in C with time, which suggests that the original surface is slowly breaking down in agreement with the corresponding R-t plot which indicates that a partial breakdown has occurred. The plot (triangles) for the pH 2.8 solutions indicates the surface film breaks down rapidly in the first couple of hours.

Through this method, the role of oxygen, hydrogen ions and Al ions in initiating crevice corrosion can be studied by changing the solution compositions.

Ferreira and Dawson (102) studied the crevice corrosion of 316 stainless steel, also by impedance measurements which can provide in-situ mechanistic information on the process involved. They found that crevice corrosion initiates in a similar manner to pitting corrosion, i.e., in the first phase pits are formed within the crevice because the equivalent circuit obtained from the experimental data in crevice corrosion is identical to the one used in the simulation of the complex plots obtained for the case of pit initiation (103).

2.2.2.3 Polarization Curve Measurements

Considering that the susceptibility of different steels to pitting corrosion can be characterized by the value of the critical potentials for pit nucleation (E_{cp}) and for protection (E_{prot}), the concept may be extended to the existence of a critical potential for the initiation of crevice corrosion (104). The same technique used for pitting corrosion

is applied to the study of crevice corrosion. Generally speaking the anodic current in anodic polarization increases quickly after the critical pitting potential (also called breakdown or breakthrough potential). After breakdown, when a given anodic current density has been reached, the potentiodynamic scan is reversed in the negative direction. A potential is found where the reversed current intersects the passive current. This potential is called the protection potential by Pourbaix and coworkers (Fig. 29) (105-107). The meaning given to the protection potential is that at potentials between E_{cp} and E_{prot} the existing pits are able to propagate, but no new pits nucleate, while at potentials below E_{prot}, pitting and the progress of crevice corrosion are prevented. The initiation of pitting can take place only at potentials above the critical pitting potential. Either galvanostatic or potentiostatic methods can be used. However when the metal under test shows passivity, the potentiostatic method is to be preferred.

Ulanovskii (104) employed a potentiodynamic technique in order to determine the potential necessary to break down the passivating film within the crevice. He also measured the potential of the open metal surface without a crevice, when polarized with a low cathodic current. Based on these two potentials, he discussed the susceptibility of the given steel to crevice corrosion under open circuit conditions.

Szklarska-Smialowska and Mankowski (108) used an assembly shown in Fig. 30 to measure E_{cp} for five stainless steels. The specimen was mounted facing upward in a Plexiglas holder. The boundary between the specimen and holder was isolated with Apiezon N grease. After immersion of the specimen into the solution, a vertically oriented Plexiglas rod, 5 mm in diameter, was pressed with its flat bottom against the exposed specimen surface.

The measurements were performed under potentiodynamic and galvanostatic conditions. Potentiodynamic tests were carried out starting from the open circuit potential. The potential at which there occurred a rapid and definite increase in the current corresponded to the critical potential for crevice corrosion initiation (E_{cp}). The galvanostatic tests were conducted using various constant anodic current densities. Under these conditions the potential registered at a given current density increased with time to a maximum and then decreased. The maximum potential value was taken as E_{cp}.

However, the test results indicated that the applied anodic current densities should be restricted to 2 $\mu A/cm^2$, or the E_{cp} values should be extrapolated to I=0. Each method gives reproducible results, however the surface roughness of the test specimen affects the value of E_{cp}.

A prediction regarding crevice corrosion susceptibility of stainless steel may be based on the difference between E_{cp} and E_{prot} (109). As shown in Fig. 31, a good correlation exists between the long-term corrosion behaviour of several alloys in seawater and laboratory polarization tests. However, Rowlands (110), who attempted to use the same technique for a series of alloys, observed a large scatter of experimental results, which did not permit confirmation of the above correlation to be obtained.

Up to now, there have been doubts concerning the existence of a characteristic potential of crevice corrosion nucleation. In 1971, Rozenfeld (111) emphasized the importance of more definitely ascertaining potentials at which crevice corrosion nucleates and develops. But France and Greene (62) have claimed that the critical potential for crevice corrosion cannot be determined because of its indefinite dependence on the geometry of the crevice. They used the electrode assembly shown in Fig. 32 to measure the potential distribution along the crevice length. The results are shown in Fig. 33 and 34. Considering the 0.2 V potential gradient of Fig. 33, each crevice length defines a unique potential which has a corresponding current density value on the anodic polarization curve. From the anodic polarization curve, the current distribution can be obtained. Fig. 34 shows the pronounced influence of crevice width. In this experiment, the potential at a depth of 0.625 cm was monitored at a constant external control potential of 0.20 V. Crevices less than 0.00375 cm wide remain active (i.e. below -0.3 V), while crevices wider than 0.005 cm are maintained passive to a depth of 0.625 cm. Therefore, crevice potential is not an absolute value, but depends on crevice dimensions as well as anodic polarization characteristics. The drawbacks in the experiment are that the crevice potential is controlled externally and the anodic polarization curve obtained in the bulk solution is assumed to be the same for the crevice solution.

2.2.2.4 Indication of Initiation Time by Corrosion Potential and Current Measurement

As corrosion potential and current vary with the condition of the metal surface, they are frequently measured to indicate the initiation of crevice corrosion as a function of time.

2.2.2.4.1 Potential Measurement

Oldfield and Sutton (20) obtained an indication of the initiation of crevice attack occurring between two clamped stainless steel AISI 316 specimens, by measuring the corrosion potential as a function of time, in 1M NaCl solution adjusted to pH 6. The result is shown in Fig. 35. The two curves shown represent the two extremes of the resulting family of curves and indicate the scatter of results. In the first stage of the test, an increase in the potential in the noble direction is observed, presumably resulting from the thickening or healing of the passive film. Secondly, a period is observed during which the corrosion potential remains at a fairly constant value, although at times fluctuations in the active direction characteristic of local breakdown of passivity may be observed. In the next stage activation takes place, as indicated by a relatively rapid fall of the corrosion potential from the passive region to about -300 mV (vs. SCE), depending on the composition of the stainless steel. Finally the corrosion potential remains at a low value during the propagation stage. The interpretations of potential behaviour were supported by examination of corrosion morphology at various stages of the process. The relationship of their significant features to typical E_{corr}/time is summarized in Fig. 36.

Matsushima et al. (24) observed the onset of crevice corrosion by measuring the potential inside an artificial crevice simultaneously with the anodic current, keeping the free surface of the specimen at a constant potential. A change of the crevice potential in the active direction was accompanied by an increase of the anodic current.

2.2.2.4.2 Current Measurement

One method frequently used is to measure the cell current between separated

metal surfaces, for example, one simulating an area exposed to a well-aerated bulk solution and the other one under conditions of crevice attack (for instance, an acidified solution with increased salt concentration and devoid of oxygen).

For this technique, a kind of double-compartment cell as shown in Fig. 37 (b and e) must be used. However, a combination of two test electrodes, one of which is a fully creviced condition, can also be used (Fig. 37f). The use of zero resistance ammeters is recommended for this application. Another technique is to measure the current-time behavior of a specimen when the potential is kept at a specified value, usually with a potentiostat (109). These kinds of measurements can be performed in single compartment cells on creviced as well as on uncreviced samples, or in double compartment cells. In all the cases the compartment containing the test electrode, which is maintained at a constant potential value, must also be provided with an auxiliary electrode.

Lee (112) used this kind of electrochemical approach for investigating crevice corrosion initiation and propagation. The test apparatus is schematically depicted in Fig. 38. The test technique allows measurement of time to initiation and rate of propagation of the crevice. This is achieved by electrically coupling a small test specimen (anode) through a zero impedance ammeter (ZIAM) to a large specimen (cathode). Both specimens are immersed in an electrolyte and the anode is 'sandwiched' between two nonmetallic plates. This creates a crevice. The current between the cathode and the anode is monitored as a function of time. The results are shown in Fig. 39. The time at which visual detection of crevice corrosion was evident is depicted by arrows. From the corroded surface area of each crevice specimen, corrosion rates were calculated from weight-loss data and average current measurements over the entire 28-day exposure period.

Excellent agreement between the two methods of determining corrosion rates was obtained. This indicates that the net current to the crevice specimens was primarily anodic with minimal contributing cathodic current.

Lee also used the specimen assembly to study the effect of polarization on the crevice corrosion. Fig. 40 depicts the potential and current for a remote crevice assembly with 15 crevices that was polarized at E=-0.2 V (Ag/AgCl) for 30 days, followed by a

5 day period under freely corroding conditions, and finally for 5 days again polarized to E= -0.2 V. No corrosion was evident during polarization. Upon disconnection of the potentiostat, however, an immediate increase in current to the crevice specimens was measured along with a shift in potential to more noble values. Visual evidence of corrosion was apparent within one hour, and the extent of the corrosion increased over the five days while freely corroding conditions existed.

2.3 Effects of Various Factors on Crevice Corrosion

2.3.1 Effect of Chloride Ion Concentration

The concentration of chloride ion plays an important role in crevice corrosion. Compared to pitting, crevice corrosion is more frequently encountered in Cl^--free solution, but in the presence of chloride ions, the intensity of both crevice corrosion and pitting increases with increasing Cl^- concentration (104,113,114). For example, Bambara et al. (115) found the following order of decreasing crevice corrosion susceptibility of different AISI stainless steels in Cl^--free and Cl^--containing dilute sulfuric acid, respectively: 302 > 304 > 321 and 304 > 302 > 321 > 316.

The exact role of chloride ions in crevice corrosion is unclear. Lee et al. (116) studied the changes in concentration of H^+ and Cl^- during corrosion of carbon steel in an artificial crevice. Increased concentration of Cl^- in the bulk electrolyte was found to accelerate change in pH and produce more acidic conditions in the crevice. Verink et al. (117) measured the Cl^- concentration in an artificial crevice on 12% Cr steel. A linear relationship was found between $[Cl^-]$ and $2[Fe^{2+}] + 3[Cr^{3+}]$ (in mole/L). It was concluded that Fe^{2+} and Cr^{3+} were in the form of $FeCl_2xH_2O$ and $CrCl_3yH_2O$.

From the experimental evidence on pitting, it seems likely that the Cl^- ions encourage breakdown in two ways. Firstly, they increase the conductivity of the solution surrounding the metal. This prevents excessive potential buildup without requiring diffusion of negatively charged ions from cathodic sites to anodic sites and hence enhances the dissolution process. Secondly, there is some chemical interaction between

the Cl^- ions and the film structure which leads to local thinning and sometimes eventual removal. It also occurs in crevice corrosion. Sharland (52) has given a detailed review about the role of Cl^- ion in localized corrosion.

2.3.2 Effect of pH

Ulanovskii and Korovin (118) claimed that there is a critical pH value below which the potential of steel shifts in the negative direction and this is accompanied by severe damage of the passive film. Table 1 compares these critical pH values with corrosion rates measured in natural seawater for various stainless steels in a crevice 0.05 mm wide. Kurtepov et al. (119) also compared the critical pH in 3% NaCl at 20°C and 100°C for three stainless steels. The results were as follows:

Steel type	Critical pH for stainless steel activation	
	at 20°C	at 100°C
Fe-17Cr	3.1	----
18Cr-10Ni-Ti	1.4	3
18Cr-12Ni-3Mo-Ti	0.34	2.4

Mor et al. (120) also concluded that when pH reaches a certain value, crevice corrosion occurs. Kain and Lee (121) found that crevice corrosion initiation and propagation are controlled, in part, by the pH of the crevice solution. Variation in pH can be attributed to differences in crevice geometry, alloy composition and bulk environment chemistry.

Lukomski and Bohnenkamp (122) measured the pH in artificial crevices on steel exposed to 3N KCl solution and found that the pH decreased as the chromium ion concentration increased up to 0.1 mol/L and was constant at higher chromium ion concentrations (Fig. 41). High acidities of the crevice solution have been found not only for stainless steels but also for aluminum (101,123).

2.3.3 Effect of Temperature

A critical crevice corrosion temperature (CCT) can be used as a criterion of crevice corrosion susceptibility of steel just as the pitting corrosion temperature can serve as a criterion of pitting susceptibility (124). Experimental evidence has shown that a CCT exists for the onset of crevice corrosion of stainless steel in a number of oxidizing chloride media. The respective measurements have been performed by Brigham and Tozer (125) and Brigham (126) in the same manner as for determining the critical pitting temperature, but with the specimens simulating severe crevices. It was found that the CCT was influenced predominantly by the Cr and Mo content of the alloys. Numerically, the value of CCT for wholly austenitic alloys wrapped with elastic bands and exposed to 10% $FeCl_3$ was found to be

$$CCT = -(45°C \pm 5) + 11(\%Mo) + 35(\%Cr-18) \qquad (18)$$

Yashiro et al. (127) studied the effect of temperature on crevice corrosion behavior of 304 stainless steel in deoxygenated 0.5 M NaCl solution up to 250°C with the stepwise cyclic polarization technique. They found that typical general corrosion within the crevice was observed up to 80° and at 250°C, while pitting dominated crevice corrosion between 150 and 250°C. At elevated temperatures, the repassivation potential for crevice corrosion corresponded to the highest potential below which crevice corrosion never generated.

2.3.4 Effect of Anodic Current Density

Ulanovskii (128) has shown that anodic polarization of a metal in small volumes of electrolyte leads to reduction in pH, and the higher the anodic current density, the greater the reduction in pH (Fig. 42). With the same current density, the pH drops as the time of polarization is prolonged. Therefore, many investigators presume that the occurrence and rate of crevice corrosion should depend on the behaviour of metal in its

active state. It has been suggested (19,129) that the critical passivation current (I_{max} in Fig. 5) can be used as a criterion of crevice corrosion susceptibility.

2.3.5 Effect of Composition of Alloys

Many comparative studies have been undertaken to determine the crevice corrosion susceptibility of various alloys. Some results regarding crevice corrosion of stainless steels and other metals and alloys in contact with medical rubber are listed in Table 2 (130). It is shown that under the indicated experimental conditions, Cr, Mo, Ti and Ni do not suffer crevice corrosion nor does Cr-Ni-Mo-Ti stainless steel.

Dundas (131) studied the effect of austenitic stainless steel composition on crevice corrosion resistance in 10% $FeCl_3$ solution. The results indicated that crevice corrosion resistance increased as Cr content is increased in the range from 20 to 25% and as Mo content is increased in the range from 2 to 4.6%. Large amounts of Cu have a small and yet measurable detrimental effect on the resistance of austenitic stainless steel to crevice corrosion and large amounts of Mg appear to have a detrimental effect.

Pessal and Nurminen (132) studied the pitting and crevice corrosion resistance of several ferritic stainless steels. Pitting resistance was determined by measurements of E_{cp} using a scratch method. Crevice resistance was evaluated for specimens in contact with Teflon, immersed in oxygenated 10% $FeCl_3$ at ambient temperature. The results of these experiments, shown in Fig. 43, indicate that the maximum resistance to crevice corrosion is obtained by raising both E_{cp} and the (Cr+Mo) concentration.

Crevice corrosion resistance in chloride solution was measured by Streicher (133) for the following alloys: Hastelloys C, C-276 and C-4 with compositions 16Cr-5Fe-16Mo-4W-Ni(bal.), 16Cr-5Fe-16Mo-3.5W-Ni(Bal.) and 16Cr-15Mo-67Fe, respectively. Measurements were conducted in 10% $FeCl_3$ solution of pH 1.6 at 50°C. The results have shown that heat treatment in the range of 640 to 1200°C may result in the formation of a Mo-rich intermetallic phase, mu-phase, and, for alloys with more than ~0.004% C, a Mo-rich carbide. The Mo-rich M_6C carbide impairs the crevice corrosion resistance. Alloy C-276 is resistant to crevice corrosion up to 0.01%C. Heat treated alloy C with

0.05%C suffers from crevice corrosion but it is resistant to crevice corrosion in solution-annealed conditions. Alloy C-4 with 0.06%C is subject to crevice corrosion in both the annealed and heat treated conditions. The presumed reason for the relatively high crevice corrosion susceptibility of Hastelloy C-4 is the absence of W which is present in both Hastelloy C and C-276. Asphahani (134) also studied the crevice corrosion resistance of alloys AISI 316 stainless steel, Incoloy alloy 825, Hastelloy alloy G, Haynes alloy 625 and Hastelloy alloy C-276 in 3.8% $FeCl_3$ at 70°C. The results show that the higher the Mo content in the alloy, the more positive the potential at which localized attack occurs. The excellent crevice corrosion resistance of Hastelloy C-276 is also attributed to the high Mo content and the presence of W.

According to Sharp and Laliberte (9), Mo additions to the alloy have a much smaller effect on the corrosion rate in crevice corrosion than on the initiation of crevice corrosion. Although the addition of Mo to stainless steels reduces their corrosion rate in crevice solution regardless of whether Mo salts are present in this solution, the addition of Mo salts to the solution does not inhibit corrosion to any significant extent. However, Kain (135) found that in the more concentrated environments, the austenitic stainless steels offered more resistance to crevice corrosion propagation than the ferritic grades at comparable Cr and Mo content in a 40 day test. This apparent advantage of the austenitics is supported by the improved resistance to propagation exhibited by Mo-free 304 compared with the ferritic 18Cr-2Mo alloy.

Korovin and Ulanovskii (136) have found that the addition of 1% Cu to chromium steels and Cr-Ni steels increases their crevice corrosion resistance in seawater. The effect of Cu is attributed to the following: (1) restraining of the anodic process at low pH; (2) decreasing pH at which the passive film is destroyed; and (3) shifting potential at this pH to less negative values. Pleva (137) obtained a different conclusion, however, when he studied the influence of Cu on the pitting and crevice corrosion resistance of two types of stainless steels (20Cr-25Ni-4.6Mo and 20Cr-25Ni-6Mo). Results indicated that no general and consistent effect was noted even if there were some variations in corrosion resistance. The observed precipitation of a Cu film in the active crevices on some specimens may be a factor causing fluctuations and influencing the local character of the

corrosion mechanism. The effect of Cu alloying on localized corrosion is so weak that it will be totally overshadowed by other minor variations in alloying and variations in the corrosion medium itself.

Oldfield (138) studied the influence of the minor elements N, Mn and S on crevice corrosion resistances of stainless steels ranging from AISI 316 to 6% Mo austenitic stainless steels. Generally, with an increasing content of Mn and S, the crevice corrosion resistance of the alloy is decreased. Results on the influence of N on high purity alloys indicate a negative effect of N in the range of 0.1 to 0.15%, followed by a positive effect at levels above 0.2%. The positive effect of Mo in the range of 5 to 7% was also demonstrated.

2.3.6 Effect of Crevice Geometry

Crevice geometry is a very important factor in crevice corrosion (130). The width and depth of the crevice control the access of oxygen into the crevice and affect the internal gradients of concentration, potential distribution, etc. In sufficiently wide crevices, the access of oxygen and the exchange with external solution is not significantly affected; thus, neither impoverishment in oxygen nor acidification occurs. In very narrow crevices, on the other hand, the concentration gradients are so steep that the breakdown of passivity can occur even close to the mouth of the crevice. In this case, deeper regions will be virtually free of corrosion attack.

In Fig.44 (130), the corrosion rate and the corrosion penetration depth measured after 52 days of exposure of a 13% Cr stainless steel to 5M NaCl solution are plotted vs. crevice width. A peak in corrosion intensity is observed for 0.1- to 0.2-mm wide crevices, while above 0.25 mm, crevice corrosion practically ceases. The corrosion rate measured inside the crevice increases as its width diminishes. Similarly, crevice corrosion does not occur on aluminum in crevices wider than ~0.25 mm (130).

The rate of crevice corrosion is greatly affected by the cathode to anode area ratio. As shown in Fig. 45 (24) with an increase in area ratio of cathode to anode, the corrosion rate is increased.

It is also notable that the rate of crevice corrosion initiation is affected by the type of material forming the second wall of a crevice. The effectiveness in nucleating crevice corrosion on stainless steel has been found (139) to decrease in the following order from the most to least effective systems: elastic > > glass (or Teflon) > metal > nylon (or wood).

2.3.7 Effect of Inclusions and Other Metal Defects

In a study on crevice corrosion of different stainless steels (108), some traces of localized attack were observed by microscopic examination just after attainment of E_{cp}. Initially, only the boundaries of the steel surface in contact with Plexiglas were attacked. This is consistent with observations of other investigators (104,140) who also found that crevice corrosion did not attack the entire exposed surface.

Formation of pits within the crevice was reported by Uhlig (141) and confirmed by a number of other authors (104,142-144). Oldfield and Sutton (20) observed by scanning electron microscopy (SEM) that corrosion initiated near the centre of the crevice area and spread outward. Sharp and Laliberte (9) conducted studies of the surface morphology of stainless steel after exposure to crevice solution which showed that localized attack occurred in the form of pits that almost always attacked the alloy along lines of inclusions. Smialowski et al. (142) investigated commercial stainless steel electrodes at 500 mV SHE in 0.5 N NaCl and observed that pits evolved from MnS inclusions, and in addition, that Cl^- was required for depassivation. Subsequently studies by Janik-Czachor (143) and Karlberg (144) have confirmed that pits on stainless steels originate at sulfide inclusions.

Oldfield (145) studied the influence of Mn and S on the crevice corrosion resistance of stainless steel 316. As shown in Fig. 46, the resistance to crevice corrosion initiation is decreased with an increase in Mn and S content in the alloy. Knutsen and Ball (146) used potentiodynamic and potentiostatic tests to study the effect of sulfide inclusions on the corrosion behavior of 12 wt.% Cr steel. It is found that the MnS inclusions have a deleterious effect on the corrosion behavior. Although the dissolution

of MnS inclusions does not imply that pit propagation will occur, the general stability of the passive film and the susceptibility to crevice corrosion are affected. Therefore, an increased MnS inclusion density will lower the corrosion resistance of the steel; with a more aggressive environment, the influence of MnS inclusions will become more marked. Eklund (140) investigated crevice corrosion initiation sites on 18Cr-8Ni stainless steel in 0.1M NaCl by interrupting the corrosion process at an early stage of development and observing the metal surface by SEM and analyses in situ. He found that corrosion started at certain points on the boundary between the lacquer and the free metal surface, then spread underneath the lacquer. The starting points in all cases were sulfitic inclusions. Therefore, he proposed a mechanism that corrosion initiated at sulfide inclusions in crevice corrosion.

Thermodynamic calculations also support the idea that manganese sulfide can act as a pit initiation site. The potential-pH diagram calculated for the MnS-H_2O-Cl^- system is shown in Fig. 47 (147). The diagram is applicable only to relatively concentrated solution (e.g. 0.1 M Mn species); it may be somewhat different for more dilute solutions. However, it is useful in defining the dissolution behaviour of MnS. For example, it shows that MnS can exist between pH 4.8 and 13.8. At pH values below 4.8, MnS dissolves to form H_2S and manganese ions. However, even in the pH range of 4.8 to 13.8, the highest potential at which MnS can exist is $\sim$ -100 mV (at pH 5). At more noble potentials, MnS dissolves to yield sulfur. Therefore, the sulfide inclusions act as small local anodes in the stainless steel as they are less noble than the passivating oxide film on the stainless steel (148).

Lott and Alkire (149) made a detailed study of the role of sulfide inclusions in the initiation of crevice corrosion of stainless steel. They found that electrochemical dissolution of MnS in deaerated 0.1 N NaCl produces thiosulfate ions according to the reaction:

$$2MnS + 3H_2O \rightarrow S_2O_3^{2-} + 2Mn^{2+} + 6H^+ + 8e^- \qquad (19)$$

In addition, the presence of both chloride and thiosulfate ions above critical levels of

concentration cause rapid depassivation of 304 stainless steel in well-stirred deaerated 0.1 N NaCl solutions (Fig. 48). A mechanism was proposed based on the experimental results. As the MnS inclusions dissolve, they produce thiosulfate ions by reaction (19). If the concentration of thiosulfate and chloride ions builds up sufficiently to exceed the critical concentration indicated in Fig. 48, then breakdown of the passivity occurs at the steel surface adjoining the inclusion. Due to the potential distribution within the crevice, both the migration of chloride and the electrochemical production of thiosulfate vary with position. After breakdown of the passive film and localized activation within the crevice, metal dissolution increases by many orders of magnitude. The subsequent hydrolysis of the increased chromium ion concentration causes the localized crevice pH to drop.

Lott and Alkire also developed a mathematical model about the role of thiosulfate ions from the experimental results (150). Theoretically, buildup of dissolved metal ions, chloride ions and thiosulfate ions is expected to occur during initiation of crevice corrosion. An agreement was found with experimental data obtained for various applied potentials, crevice gaps and inclusion densities.

Ke and Alkire (151) also investigated the formation of pits near MnS inclusions on 304 stainless steel in NaCl (0.1 and 0.3 M) and $Na_2S_2O_3$ (0 and 2 mM) solutions by a combination of surface analyses (Auger electron spectroscopy, scanning electron microscopy with energy dispersive x-ray analysis and electrochemical methods). Microlithography techniques were developed to monitor a single corrosion pit initiated at a single preselected inclusion. Pits were observed to form originally from MnS inclusions.

However, in Fig. 48, we can find an interesting phenomenon that at a certain constant thiosulfate ion concentration, with an increase in chloride ion concentration, the steel surface status changes from the active state to a passive state. But as discussed in the section on the effect of chloride ion concentration on crevice corrosion, the dissolution of metals is increased with an increase of chloride ion concentration. Therefore, this phenomenon is worth more research to get a much clearer picture about the role of chloride ions in the initiation of crevice corrosion.

3. STATEMENT OF PROBLEMS AND OBJECTIVES

As discussed in the literature review, the idea of a critical pitting potential, i.e., the potential at which the passive film will break down locally, used for characterizing the susceptibility of metals and alloys to pitting corrosion may be applied to a study of crevice corrosion. Some researchers (109) also used the difference between the critical initiation potential E_{cp} for crevice corrosion and the protection potential E_{prot} for crevice corrosion as the criterion for evaluating the susceptibility of materials to crevice corrosion. However, whether the critical potential E_{cp} and the difference between E_{cp} and E_{prot} can be used to evaluate the susceptibility of metals to crevice corrosion is in argument. Some evidence (104, 108, 109) supports this idea but others (62,110, 111) found them unreliable. France and Greene (62) even claimed that the potential for crevice corrosion cannot be determined because of its definite dependence on crevice geometry.

Analysis of all these commonly used experimental methods for measuring the critical initiation potential E_{cp} and protection potential E_{prot} for crevice corrosion indicates that no experimental method exactly describes the real situation in the crevice. The applied potential is always the potential of the outer surface of the sample during the experiment. For example, in Szklarska-Smialowska's test for measuring the E_{cp} shown in Fig. 30, the reference electrode for measuring the potential is placed in the bulk solution. Therefore, the potential of the working electrode obtained is with respect to the bulk solution. As the difference between the crevice solution and the bulk solution is very great, the critical initiation potential obtained may not exactly describe the real situation for crevice corrosion. In France and Greene's test shown in Fig. 33, although they measured the potential distribution along the crevice length, they only controlled the potential of the outer surface at a constant potential with respect to the bulk solution. Therefore, the applied potential does not control the potential change inside a crevice.

In order to reflect the real situation in the crevice when the critical initiation potential and protection potential are measured during an experiment, a novel

experimental setup was constructed to measure the cyclic potentiodynamic polarization curve by controlling the potential inside a crevice.

According to the four-stage mechanism of crevice corrosion (19,20) and some results (118-120), a critical pH value exists below which the initiation of crevice corrosion occurs. As the critical pH value is another important feature characterizing the initiation of crevice corrosion, the pH variation over the cyclic anodic potentiodynamic polarization curve within the crevice was also recorded during the scan to see whether there is a relationship between the critical initiation potential E_{cp} and the critical pH value for crevice corrosion.

To evaluate the critical initiation potential E_{cp} and protection potential E_{prot} for crevice corrosion and the difference between E_{cp} and E_{prot} as criteria for characterizing the susceptibility of materials to crevice corrosion, it is necessary to choose different stainless steels at different crevice widths to measure their E_{cp} and E_{prot}.

The first objective of the study is therefore to measure the critical initiation potential E_{cp} and protection potential E_{prot} for crevice corrosion from the cyclic anodic potentiodynamic polarization curve by controlling the potential inside the crevice and to see whether E_{cp}, E_{prot} and the difference between E_{cp} and E_{prot} can be used as criteria for evaluating the susceptibility of materials to crevice corrosion. The second objective of this study is to measure the pH value within the crevice during the scan to see its change over the cyclic anodic potentiodynamic polarization curve. A mathematical model is also developed to calculate the pH change over the cyclic anodic potentiodynamic polarization curve.

4 EXPERIMENTAL MATERIALS, EQUIPMENT, SET-UP AND PROCEDURES

4.1 Experimental Materials

Type AISI 303, AISI 304 and AISI 316 stainless steel bars were chosen as the materials in the study of crevice corrosion of stainless steel. Their compositions are shown in Table 3. For the experiments, they were used in the annealed condition, as-received. Each specimen was cut in the shape of a cylinder with a height of one centimetre and a base area of one square centimetre. All the specimens were mounted in Lucite so that the working surface of a specimen was 100 mm^2. A shielded wire was used to connect the specimen to the model 342 Potentiostat/Galvanostat as shown in Fig. 49.

Chemicals used were of analytical reagent grade unless otherwise specified. Doubly deionized water was used to prepare solutions. pH adjustments were made by using sodium hydroxide and hydrochloric acid.

Parawax made by Imperial Oil Limited of Canada was used to fasten the pH electrode. Agar agar, U.S.P. made by Fisher Scientific Company and potassium chloride were used to make the salt bridge, described in section 4.3.

4.2 Experimental Equipment

To measure the pH value inside a crevice, a flat surface pH electrode made by Fisher Scientific with a Fisher Accumet pH meter (Model 610A) was used in the experiment. The diameter of the pH electrode was 1.3 cm. On the end of the electrode there is a flat glass electrode and a reference electrode with a height of about 0.1 cm. The area of the flat glass electrode tip was about 0.3 cm^2 and the area of the reference electrode tip was very small (approximately 0.1 cm^2).

A model 551 Potentiostat/Galvanostat made by ECO and a model 342 Potentiostat

/Galvanostat made by EG & G Princeton Applied Research were used to conduct the galvanostatic and cyclic potentiodynamic tests.

To examine and analyze the surface of the specimen, an optical microscope made by Zeiss and an Hitachi S-2700 Scanning Electron Microscope (SEM) were used in the experiment.

A type F thermostat made by Haake was used to control the temperature of the testing solution during the experiment. The accuracy of the thermostat was $\pm$ 1°C of the controlling temperature.

4.3 Experimental Set-up

A sample holder was constructed as shown in Fig. 49. The mounted specimen was facing upward between two pieces of Lucite which could be tightened by screws. A groove was made on the bottom of the upper Lucite block to form the crevice. The dimensions of the groove were 55 mm by 12 mm. By changing the depth of the groove, the width of crevice could be controlled. The depth of the groove was measured precisely by a Brown and Sharpe Microcal. During the experiment, grooves with depths of 12 μm, 40 μm, 96 μm, 180 μm and 330 μm were used to study crevice corrosion at different crevice widths. A hole was drilled through the upper Lucite block where a salt bridge and the flat surface pH electrode were put through and mounted by wax. Since the overall diameter of the pH electrode was larger than the diameter of the glass electrode and reference electrode, there was an empty space around the glass electrode and the reference electrode when the flat glass electrode tip and reference electrode tip formed a smooth plane with the groove. In order to prevent too much wax from contacting the crevice solution, a very thin Lucite plate covered the bottom of the electrode, with two holes to expose the tips of the glass and reference electrodes, and the salt bridge. The tips of glass electrode and reference electrode, one end of the salt bridge and the thin flat Lucite formed a smooth plane with the groove surface. The simulated crevice device was constructed as shown in Fig. 50.

A salt bridge was used to connect the research solution with the reference

electrode solution. A salt bridge has two roles: (1) to reduce the liquid junction potential; (2) to prevent or reduce the mutual pollution of the two solutions. There are many ways to make a salt bridge. In the experiment, a salt bridge with agar gel was used. To make the salt bridge with agar gel, a saturated KCl solution with 2 ~ 3% agar was heated to dissolve the agar and then filled into a glass tube. After cooling, the immobile gel formed inside the glass tube. In order to reduce the diameter of the hole in the upper Lucite block, the diameter of the glass tube close to the working electrode (the specimen) was made gradually thinner to become a Luggin capillary. Through the salt bridge, the crevice potential can be measured and controlled. A large piece of stainless steel with the same composition as the specimen was used as the counterelectrode, giving a cathode/anode area ratio of 50:1. All potentials were measured against a saturated calomel electrode. The pH electrode with a pH meter was used to monitor the acidity in the crevice during measurements, as shown in Fig. 51 with the entire apparatus.

4.4 Experimental Procedures

4.4.1 Preparation of the Specimens

The stainless steel specimens were wet ground first with 320-grit SiC paper, then wet polished with 600-grit SiC paper until previous coarse scratches were removed, and rinsed and dried. Finally they were cathodically cleaned at 100 μA for 10 minutes in the solution before forming the crevice. All the specimens were prepared under the same conditions except for those used in potentiodynamic tests studying the initiation of crevice corrosion.

In the study of initiation of crevice corrosion, as the surface of the sample was to be examined by optical microscopy and SEM, a different procedure was used to prepare the specimen. The AISI 304 stainless steel specimens were wet ground first with 320- and 600-grit SiC paper, then wet polished with 6 μm diamond and 0.05 μm alumina until all previous coarse scratches were removed, and rinsed and dried. Finally they were cathodically cleaned at 100 μA for 10 minutes in the solution before measurement.

4.4.2 Preparation of the Testing Solutions

The testing solutions were prepared by dissolving the appropriate amount of NaCl in about 800 mL double-deionized water. The solution was diluted to 1L in a volumetric flask.

4.4.3 Galvanostatic Tests

In order to compare the difference between the potential of the reference electrode inside the crevice versus the working electrode (potential inside the crevice) and the potential of the reference electrode outside the crevice against the working electrode (potential outside the crevice) under applied current, galvanostatic tests were used to provide the constant current.

Galvanostatic tests with a model 551 Potentiostat/Galvanostat were conducted at different constant current densities of the anodic current from 50 to 200 $\mu A/cm^2$ in 10% NaCl solutions open to the air at a temperature of 20°C. Under these conditions, the potential inside the crevice, as well as the potential outside the crevice, were recorded as functions of time. Crevice width was 12 μm.

4.4.4 Cyclic Potentiodynamic Tests

The cyclic potentiodynamic tests were used to measure the cyclic polarization curves with which the critical initiation potential E_{cp} for crevice corrosion and protection potential E_{prot} can be obtained. The cyclic potentiodynamic measurements were performed with a model 342 Potentiostat/Galvanostat. The tests were started from the open circuit potential at two different scan rates because the initiation potential E_{cp} depends on the scanning rate (152). When the current density reached 500 $\mu A/cm^2$, while controlling the potentials inside the crevice, the scan direction was reversed at the same scan rate until the reverse curve crossed the forward curve. After potentiodynamic measurement, the surface of the specimen was examined under an optical microscope.

The critical initiation potential E_{cp} for crevice corrosion was determined by choosing the potential at which the anodic current density reached 5 $\mu A/cm^2$. The protection potential E_{prot} for crevice corrosion was chosen as the potential at which the reverse anodic curve intersected the passive current density curve.

4.4.5 Potentiodynamic Tests Studying the Initiation of Crevice Corrosion

The potentiodynamic tests were used to study the mechanism of initiation of crevice corrosion under applied potential inside a crevice. The tests were terminated at different stages along the polarization curve to examine the process of crevice corrosion during the measurement.

The experimental set-up is shown in Fig. 51. The crevice width was 12 μm and the flat surface pH electrode was used. The anodic potentiodynamic measurements were conducted with a model 342 Potentiostat/Galvanostat while controlling the potential inside the crevice.

A series of tests was always started from the open circuit potential in 10 wt.% NaCl solution at a temperature of 20°C and scan rate of 0.2 mV/s and was terminated at different stages on the potentiodynamic polarization curve. When the current density reached 5 $\mu A/cm^2$, the test was terminated and the surface of the specimen was examined and analyzed in the optical microscope and SEM. The repolished specimen with the same polishing procedure as above was used to run other anodic cyclic potentiodynamic tests at the same conditions. When the current density reached 20, 50, 100, 200, or 500 $\mu A/cm^2$ on the potentiodynamic polarization curve, each test was terminated and the surface of the specimen was examined and analyzed in the optical microscope and SEM. One specimen was given a complete cycle, i.e. polarization in the forward direction, reversal of polarization at 500 $\mu A/cm^2$, and polarized until the reverse curve crossed the forward curve, then the specimen was also examined and analyzed in optical microscopy and the SEM.

5. EXPERIMENTAL RESULTS AND DISCUSSION

5.1 Comparison of the Method of Controlling Potential inside a Crevice with the Method of Controlling Potential outside a Crevice

As discussed in the introduction, a common electrochemical experimental method of studying crevice corrosion is to place the reference electrode outside the crevice. As the difference between the crevice solution and bulk solution is very great and the IR drop in the crevice is also very high and variable (28,31,33), the potential obtained from a reference electrode outside a crevice cannot reflect the real potential change within the crevice. Therefore, it is necessary to compare the method of controlling potential inside a crevice with that of controlling potential outside a crevice.

The potentials inside the crevice and the potential outside the crevice are shown at different currents as a function of time in Fig. 52 and 53, respectively, under galvanostatic conditions in neutral 10 wt.% NaCl solution at a temperature of 20°C with a crevice width of 12 μm. At the beginning, the potentials inside and outside the crevice changed quickly, indicating that they are in unstable conditions. After 20 minutes, the potentials increased slightly and became more stable. Fig. 54 shows the potential difference between potential inside the crevice and potential outside the crevice as a function of time. At the beginning, the potential difference also dropped quickly because of unstable conditions. After reaching a minimum, the potential difference increased slightly with time, because the resistance inside the crevice increased with time when corrosion products formed inside the crevice and reduced the conductivity of the crevice solution. This indicates that the potential differences between the potential inside the crevice and potential outside the crevice are not constant with time.

Fig. 55 shows the variation of the potential differences with current density at 30 minutes. The potential difference between the potential inside the crevice and potential outside the crevice increased with increasing current density. Therefore, the potential inside the crevice is quite different from the potential outside the crevice and the potential outside the crevice cannot be corrected by a constant value to become the potential inside

the crevice.

By controlling the potential inside the crevice, in 3.5 wt.% NaCl solution at a pH of 7.00 with a crevice width of 12 μm, the cyclic potentiodynamic anodic polarization with pH measurements at indicated potentials was obtained, as shown in Fig. 56 with a scanning rate of 0.5 mV/s. It looks like the usually typical anodic polarization curve of stainless steel. Fig. 57 shows a cyclic potentiodynamic anodic polarization curve with pH measurements at the indicated potentials obtained by controlling the potential outside the crevice in 3.5 wt.% NaCl solution at a pH of 7.00 with a crevice width of 12 μm at the scanning rate of 0.5 mV/s. When Fig. 56 and 57 are compared, the current density in Fig. 57 increased much more slowly with an increase in potential than that in Fig. 56. The difference in scans suggests that to reach a certain current density, the potential needed for a reference electrode outside the crevice is much higher than that for a reference electrode inside the crevice. The potential difference between the reference electrodes is because of the high IR drop in the crevice. The result agrees with the above results of potential differences between the potential inside and outside the crevice, shown in Fig. 54 and 55, and also agrees with other literature (28,31,33). Therefore, this again confirms that the electrochemical experimental method of controlling the potential outside the crevice does not simulate the electrochemistry of the corrosion within the crevice. In other words, the results obtained by the electrochemical method of controlling the potential inside the crevice more accurately describe real crevice corrosion.

5.2 Effect of Crevice Width on AISI 304, 303 and 316 Stainless Steels

Fig. 58 shows a cyclic potentiodynamic polarization curve for 304 stainless steel with pH measurement at indicated potentials, obtained by controlling the potential inside a 12 μm crevice in 10 wt.% NaCl solution at an initial pH of 7.25 and a temperature of 20°C. It resembles a typical anodic polarization curve for stainless steel. From the cyclic polarization curve, the critical initiation potential for crevice corrosion E_{cp} and the protection potential E_{prot} are -44 mV and -265 mV, respectively. After each experiment, the specimen surface was examined with an optical microscope which showed the

corrosion occurred around the edge of the specimen. As reported by other authors (62,104,108), they found that crevice corrosion does not attack the entire electrode surface, because current flow may be short-circuiting.

In the measurement of the cyclic potentiodynamic scan (Fig. 58), the pH first increases slightly and then gradually decreases in the passive region and at the beginning of the transpassive region. When the passive film is broken down, the pH within the crevice approximates a neutral solution (pH=6.00). The slow increase of pH at the beginning can be explained by the reduction of oxygen within the crevice as follows:

$$O_2 + 2H_2O + 4e^- \rightarrow 4OH^- \qquad (1)$$

The OH^- ions produced within the crevice increase the pH. With an increase of time, the concentration of O_2 is reduced because of restriction of diffusion, and the rate of the cathodic reaction slows down because the specimen is polarized in the anodic direction. Meanwhile, the formation of a passive film will result in the production of H^+ according to reactions (20) and (21):

$$2Cr + 3H_2O - 6e^- \rightarrow Cr_2O_3 + 6H^+ \qquad (20)$$

$$Fe + 2H_2O - 2e^- \rightarrow Fe(OH)_2 + 2H^+ \qquad (21)$$

However, the dissolution of the passive film will consume the H^+;

$$Cr_2O_3 + 6H^+ \rightarrow 2Cr^{3+} + 3H_2O \qquad (22)$$

$$Fe(OH)_2 + 2H^+ \rightarrow Fe^{2+} + 2H_2O \qquad (23)$$

In the passive region, the formation rate of passive film approximately equals the dissolution rate of passive film. It means that in the passive region the H^+ produced by reactions (20) and (21) will be consumed by reactions (22) and (23). The actual result is the production of Cr^{3+} ions and Fe^{2+} ions. The hydrolysis of Cr^{3+} and Fe^{2+} takes place to produce the H^+. Therefore, the slow decrease of pH within the crevice may be

due to the reaction of some dissolved chromium ions and iron ions with H_2O to produce H^+.

$$Cr^{3+} + 3H_2O \rightarrow Cr(OH)_3 + 3H^+ \quad (24)$$

$$Fe^{2+} + 2H_2O \rightarrow Fe(OH)_2 + 2H^+ \quad (25)$$

Since chromium has the largest hydrolysis constant of the major alloying elements in stainless steel (153), its concentration will control the pH of the crevice solution.

The pH in the crevice decreases quickly when the current density has reached about 100 $\mu A/cm^2$. This is because large amounts of chromium ions and iron ions are produced in the crevice. When the pH reaches 2, the pH begins to decrease more slowly and reaches the lowest pH of 1.91, then gradually increases to 1.96. This may be attributed to the repassivation of stainless steel inside the crevice and diffusion of hydrogen ions produced within the crevice.

Several researchers (118-120) have used a critical pH to evaluate the susceptibility of a given metal or alloy to crevice corrosion. Ulanovskii and Korovin (118) claimed that a critical pH value exists at which the potential of stainless steels shifts in the negative direction, accompanied by severe damage of a passive film. The critical pH value is usually below 3. According to Mor et al. (120), crevice corrosion occurs when the pH acquires the following values: close to 1 for austenitic and ferritic alloys with 2.5 to 3% Mo; below 2 for AISI 304 stainless steel, and below 2.5 for AISI 430. Li et al. (154) used a pH microelectrode inserted into the crevice to monitor pH variation within the crevice with time. They found that the pH of the solution in the crevice is a sensitive parameter to the onset and propagation of crevice corrosion and the critical pH at the onset of crevice corrosion is about 3.5 for AISI 304 stainless steel. Therefore, the critical pH at the onset of crevice corrosion is below 3.5, usually even lower.

However, It is clearly demonstrated from the change of pH over the cyclic polarization curve that when the initiation of crevice corrosion occurs, the pH in the crevice is about neutral. Therefore, it is not a pH decrease that causes the initiation of crevice corrosion in this situation. Fig. 58 also shows that the pH in the crevice solution

is much lower than that in the bulk solution after crevice corrosion takes place. This result is in agreement with the general results when pH is checked after crevice corrosion occurs.

The results cannot be explained by the acidification mechanism of crevice corrosion (19,20) which assumes that passivity breaks down when the crevice acidity attains a critical value. The experimental results indicate that the applied potential first breaks down the passive film so that crevice corrosion starts and then the pH decreases.

Fig. 59, 60 and 61 show the cyclic potentiodynamic anodic polarization curves of 304 stainless steel with measured pH values at the indicated potential obtained by controlling the potential inside the crevice in 10 wt.% NaCl solution at pH about 7.00 and temperature of 20°C with crevice widths of 40 μm, 96 μm and 180 μm, respectively. The critical initiation potentials for crevice corrosion E_{cp} and the protection potentials E_{prot} can also be obtained from these curves. The results are summarized in Table 4.

From Table 4, with an increase of crevice width, the critical initiation potential for crevice corrosion E_{cp} and protection potential E_{prot} become more positive. This indicates that with narrow crevice width, crevice corrosion is easier to initiate and more difficult to repassivate. In other words, the more narrow the crevice width, the more serious the crevice corrosion. This conclusion is in agreement with the visual examination. This can also be seen from the difference between E_{cp} and E_{prot} which decreases with an increase of crevice width. According to Wilde (109), the susceptibility of crevice corrosion of stainless steel may be based on the difference E_{cp} and E_{prot}. The larger the difference, the more serious the crevice corrosion. These results show that the crevice width does affect the critical potential E_{cp} and E_{prot}, as well as the difference between E_{cp} and E_{prot} for crevice corrosion. Therefore, the critical potentials for crevice corrosion seem to have a definite dependence on the geometry of the crevice. This result agrees with that of France and Greene (62).

Comparing Fig. 59, 60 and 61 with Fig. 58, the trend of pH change along the polarization curves in Fig. 59, 60 and 61 is very similar to that in Fig. 58. With an increase of crevice width, the pH within the crevice becomes higher. When the passive

film is broken down, the pH in the crevice is also close to neutral. The higher pH values in wider crevices can be easily attributed to both the increase of volume of crevice solution and the decrease of the amount of dissolved chromium ions and iron ions in the crevice. For the same amount of chromium ions, the larger the volume of the solution, the lower the H^+ concentration.

The above results can also be seen by comparing the areas of the hysteresis loops in these cyclic potentiodynamic polarization curves because the area of the hysteresis loop is proportional to the amount of electrical charge used in the experiment. With an increase of crevice width, the area of the hysteresis loop is decreased. This result can be confirmed by examination of the specimen surfaces with an optical microscope after the experiment. The corroded area of the specimen is also increased with a decrease of crevice width.

Fig. 62 shows the cyclic potentiodynamic anodic polarization curve of 304 stainless steel with measured pH values at the indicated potentials obtained by controlling the potential inside the crevice in 10% NaCl solution at an initial pH of 7.00 and temperature of 20°C with a crevice width of 330 μm. The critical initiation potential E_{cp} and the protection potential E_{prot} are shown in Table 4. After the experiment, the specimen surface was examined by optical microscopy. Pits were found on the surface and no general corrosion took place. This indicates that when the crevice width reached 330 μm, the condition of the crevice is not suitable for the occurrence of crevice corrosion and becomes a pitting condition. From the pH change over the cyclic potentiodynamic polarization curve, it can be seen that the pH value did not go down very much. This is because, with a wider crevice, the concentration of metal ions within the crevice is lower provided that the same amount of metal ions is produced within the crevice. Therefore, the amount of hydrogen ions produced by hydrolysis within the crevice is decreased. Besides, the hydrogen ions produced within the crevice more easily diffuse out from a wider crevice. However, the most important reason for this slow pH decrease is that at this crevice width of 330 μm, pitting corrosion occurs. In pitting corrosion, the hydroxide may form around the mouth of the pits to prevent metal ions produced inside pits from diffusing into the crevice. Thus, most hydrogen ions produced

by hydrolysis of metal ions will stay inside pits and the actual concentration of hydrogen ions within the crevice is very low. Therefore, the pH values obtained in the experiment are decreased only a little along the polarization curve.

Fig. 63, 64, 65 and 66 show the cyclic potentiodynamic polarization curves of 303 stainless steel obtained under the same conditions as in 304 stainless steel with crevice widths of 12 μm, 40 μm, 96 μm and 180 μm, respectively. Fig. 67, 68, 69 and 70 show the cyclic potentiodynamic polarization curves of 316 stainless steel obtained under the same conditions. Comparing these figures for both 303 stainless steel and 316 stainless steel with those for 304 stainless steel, it can be seen that the shapes of the polarization curves in these figures and the pH variation along the curves are very similar to those for 304 stainless steel. That is, the pH also first increases slightly and then gradually decreases in the passive region and at the beginning of the transpassive region. When the current density has reached about 100 $\mu A/cm^2$, the pH in the crevice begins to decrease quickly. Finally, the pH begins to slowly increase a little bit. The pH change over the cyclic potentiodynamic polarization curves for 303 and 316 stainless steels can also be explained by the same reasons for the pH variation over the cyclic polarization curve for the 304 stainless steel. It is again clearly demonstrated from the change in pH over the cyclic polarization curves that when the initiation of the crevice corrosion occurs, the pH in the crevice is about neutral in the AISI 303 and 316 stainless steels also. As discussed before, the critical pH at the onset of crevice corrosion of stainless steel is usually reported (120) to be below 3.5. Therefore, the same conclusion as in the 304 stainless steel can also be drawn that it is not a pH decrease that causes the initiation of crevice corrosion in either the 303 or the 316 stainless steels.

The results also cannot be explained by the acidification mechanism of crevice corrosion (19,20) which assumes that passivity breaks down when the crevice acidity attains a critical value. As with 304 stainless steel, the experimental results show that the applied potential first breaks down the passive film so that crevice corrosion starts and then the pH decreases.

The critical initiation potentials of crevice corrosion E_{cp} and the protection potentials E_{prot} for 303 and 316 stainless steels at different crevice widths are also

obtained from these curves. The results for 303 stainless steel and 316 stainless are summarized in Table 5 and Table 6, respectively.

From Tables 5 and 6, it can be seen that with an increase of crevice width, the critical initiation potential for crevice corrosion E_{cp} and protection potential E_{prot} also increase. This also indicates that with a narrow crevice width, crevice corrosion is easier to initiate and more difficult to repassivate. In other words, the more narrow the crevice width, the more serious the crevice corrosion. This conclusion agrees with the experimental results and is the same as for AISI 304 stainless steel. The difference between E_{cp} and E_{prot} in 316 stainless steel is also reduced with an increase in crevice width. However, the difference between E_{cp} and E_{prot} in 303 stainless steel is first decreased slightly from 12 μm to 40 μm, then keeps almost the same value for 96 μm as that for 40 μm, and finally sharply decreases for a crevice width of 180 μm. Although the changing trend of the difference between E_{cp} and E_{prot} of 303 stainless steel does not strictly go down as with 304 and 316 stainless steel with an increase of crevice width, the approximate changing trend of the difference between E_{cp} and E_{prot} in 303 stainless steel is also decreased. Therefore, the value of the difference between E_{cp} and E_{prot} can be used to evaluate the seriousness of crevice corrosion of the same material at the different crevice widths. The greater the value of the difference between E_{cp} and E_{prot}, the more serious the crevice corrosion of the material.

Fig. 71 and 72 show the cyclic potentiodynamic anodic polarization curves obtained by controlling the potential inside the crevice in 10% NaCl solution at pH of 7.00 and 20°C for a crevice width of 330 μm for 303 and 316 stainless steels, respectively. The critical initiation potential E_{cp} and the protection potential E_{prot} are -72 mV and -157 mV for 303 stainless steel and 55 mV and -54 mV for 316 stainless steel, respectively. After the experiments, the specimen surfaces were examined by optical microscope and only pits were found on the surface, as with the 304 stainless steel. This indicates that when the crevice width reaches 330 μm, the condition is not suitable for the occurrence of crevice corrosion and becomes a pitting condition for both 303 and 316 stainless steels. From the pH change over the cyclic potentiodynamic polarization curve,

it can be seen that the pH value did not go down very much for the same reason as that given in the discussion of the same phenomenon in 304 stainless steel.

5.3 Effect of Different Stainless Steels on Crevice Corrosion

In order to compare the susceptibility of crevice corrosion in different stainless steels by the critical initiation potential E_{cp} for crevice corrosion, protection potential E_{prot} and the difference between E_{cp} and E_{prot}, three kinds of stainless steel, AISI 303, AISI 304 and AISI 316, were studied by measuring the cyclic potentiodynamic polarization curves while controlling the potential inside the crevice. There is a higher sulfur content in 303 stainless steel, compared with the AISI 304 and 316 stainless steels. This higher S content reduces the corrosion resistance of 303 stainless steel because the sulfide inclusions often suffer attack first to initiate pitting and crevice corrosion. The AISI 316 stainless steel contains molybdenum which improves the pitting and crevice corrosion resistance. Many experimental results (155,156) have shown that the pitting and crevice resistance of 316 stainless steel is better than that of 304 stainless steel. Therefore, the resistance to localized corrosion increases in the following order:

$$303 < 304 < 316$$

The critical initiation potential E_{cp} for crevice corrosion, the protection potential E_{prot}, and the difference between E_{cp} and E_{prot} for 303, 304 and 316 stainless steels with crevice width 12 μm are summarized in Table 7. From Table 7, the 316 stainless steel has the highest critical initiation potential E_{cp} and protection potential E_{prot}. The 303 stainless steel has the lowest E_{cp} and E_{prot} values. This indicates that 316 stainless has the best crevice corrosion resistance and 303 stainless steel has the lowest crevice corrosion resistance among the three stainless steels. This result agrees with the general order above about corrosion resistance. This indicates that the critical initiation potential E_{cp} can be used to indicate the susceptibility of crevice corrosion. According to Wilde's result (109), the smaller the difference between E_{cp} and E_{prot}, the better the crevice corrosion resistance. However, the difference between E_{cp} and E_{prot} obtained by the method in this study does not follow the order. Therefore, the difference between E_{cp} and

E_{prot} cannot be used to indicate the susceptibility of crevice corrosion of the different materials.

The critical initiation potential E_{cp}, protection potential E_{prot} and the difference between E_{cp} and E_{prot} for 303, 304 and 316 stainless steels with crevice widths of 40 μm, 96 μm and 180 μm are summarized in Tables 8, 9 and 10 respectively. From these tables, the changing tendency of the critical potential E_{cp}, the protection potential E_{prot} and the difference between E_{cp} and E_{prot} for 303, 304 and 316 stainless steels is the same as that in Table 7. This again shows that no matter what the crevice width is, the critical initiation potential E_{cp} is a good indicator of susceptibility to crevice corrosion, but the difference between E_{cp} and E_{prot} is not.

5.4 Effect of Temperature on AISI 304 Stainless Steel

The majority of chemical and electrochemical reactions proceed more easily at higher temperature. The effect of increasing temperature on crevice corrosion, however, may not follow the general rule above, since temperature could affect various relevant factors in different and opposing ways. While transport processes and reaction kinetics would be accelerated by increased temperature, the solubility of oxygen would be decreased, and in neutral chloride solutions it is the reduction of oxygen that provides the main cathodic reaction on the surface outside the crevice. Temperature also affects the critical initiation potential E_{cp} and protection potential E_{prot} for crevice corrosion, the hydrolysis equilibrium and the composition, structure and properties of surface films. As shown in Table 11 (157), there is no simple relationship between temperature and crevice attack. Therefore, the variable of temperature was chosen to study its effect on the critical initiation potential, the protection potential for crevice corrosion and the pH change over the cyclic potentiodynamic polarization curve.

Temperature ranges only from 10°C to 35°C were chosen for study. At lower temperatures, the decrease in conductivity of the Luggin capillary filled with a gel of KCl and agar is quite great so that the measurement of the cyclic potentiodynamic polarization curve was affected and accurate results could not be obtained. At higher temperature, as

the melting point of wax is about 50°C, the melted wax used to fix the pH electrode and the Luggin capillary affected the solution composition within the crevice and poisoned it to affect the results of measurement.

Fig. 73, 74 and 75 show the cyclic potentiodynamic polarization curves with pH measurement at indicated potentials obtained by controlling the potential inside a 12 μm crevice in 10 wt.% NaCl solution at an initial pH of about 7 at temperatures of 10°C, 25°C and 35°C, respectively. They resemble the anodic polarization curve of AISI 304 stainless steel at the temperature of 20°C shown in Fig. 58. The pH changes over the cyclic potentiodynamic polarization curves in Fig. 73, 74 and 75 are also very similar to that in Fig. 58, but the pH change at a temperature of 35°C is slower. This is because at the higher temperature, the transport of H^+ from the crevice to the bulk solution is easier. This will increase the pH value a little within the crevice. When the passive film is broken down, the pH within the crevice also approximates a neutral solution (pH=6.5). This result agrees with the result at the temperature of 20°C. Therefore, it again confirms that it is not a pH decrease that causes the initiation of crevice corrosion in the studied temperature range.

The critical initiation potentials of crevice corrosion E_{cp} and the protection potentials E_{prot} can be obtained from these curves. The results are summarized in Table 12.

From Table 12, with an increase of temperature, the critical initiation potential for crevice corrosion E_{cp} is decreased. The behaviour for crevice corrosion agrees with the behaviour for pitting corrosion (155). A decrease of the critical initiation potential E_{cp} at higher temperature can be explained by a more intense agglomeration and stronger chemisorption of chloride ions on the metal surface, causing easier breakdown of passivity. At higher temperature, the weak sites are also more susceptible to attack by the corrosive environment. However, the change in the protection potential for crevice corrosion E_{prot} is uncertain with an increase in temperature, because the effect of temperature on crevice corrosion is complex. An increase in temperature also accelerates the transport of reagents and reaction products to or from an electrode. This make the repassivation of a passive film easier. On the other hand, the increase of temperature also

increases the rate of crevice corrosion according to the Arrhenius equation. The interaction of the two factors results in unpredictability of the protection potential E_{prot} change with an increase of temperature. However, with an increase in temperature, the difference between E_{cp} and E_{prot} first decreases up to 25°C and then increases at 35°C. Therefore, the difference between E_{cp} and E_{prot} cannot be used to indicate the susceptibility to crevice corrosion. The critical initiation potential E_{cp} for crevice corrosion is a quite good indicator to show the susceptibility to crevice corrosion.

When measuring the potential of pit nucleation E_{cp} and the protection potential E_{prot} by the potentiodynamic method, the values obtained depend on the rate of potential scan. Fig. 76 shows the dependence (152). With an increase in scan rate, E_{cp} is increased. The reason for this phenomenon was discussed by Schwenk (158,159), who found, as did other authors, that the more noble the potential, the shorter the time required for pit initiation. Consequently, when the potential scan rate is high, a rapid increase in current density can only be observed at potentials corresponding to a sufficiently short induction time. This means that at high scan, E_{cp} is more positive than at low scan rates.

In some cases, however, opposite results were noted; thus, Lizlovs and Bond (160) observed more noble E_{cp} values at lower scan rates. This can be explained by the development and improvement of the protective properties of a passive film within the passivation potential range, which increases the resistance of metal to pitting. Their hysteresis loop in the cyclic potentiodynamic polarization was also found to increase with increasing potential scan rate. Hence, the repassivation potential E_{prot} is also a function of scan rate. Yoshii and Hisamatsu (61) found that the protection potential in stainless steel decreased with an increase of the scan rate. Rapid potentiodynamic measurement revealed the E_{prot} to be less positive compared with those obtained in low scan rate experiments. From the above discussion, the influence of the scan rate on pitting potential and protection potential is great. In order to understand the effect of scan rate on the critical initiation potential E_{cp} and protection potential E_{prot} for crevice corrosion, a lower scan rate was employed to measure the cyclic potentiodynamic polarization curves with pH change over them.

Fig. 77-80 show the cyclic potentiodynamic polarization curves with measured pH values at the indicated potential obtained by controlling the potential inside a 12 μm crevice in 10% NaCl solution at pH of about 7 at the different temperatures with a scan rate of 0.2 mV/s. The critical initiation potential E_{cp} for crevice corrosion and the protection potential E_{prot} for crevice corrosion are summarized in Table 13. From Table 13, the critical initiation potential E_{cp} is also decreased with an increase in temperature and the change of protection potential E_{prot} with an increase of temperature is uncertain. The difference between E_{cp} and E_{prot} also first decreases with an increase of temperature from 10°C to 25°C and then increases at 35°C. Therefore, the changing tendency of E_{cp}, E_{prot} and the difference between E_{cp} and E_{prot} is same as that in Table 12. The difference is that the E_{cp} value at a scan rate of 0.2 mV/s is higher than that at the scanning rate of 0.5 mV/s.

From these four figures, it can also been seen that when the passive film is broken down, the pH within the crevice is still close to neutral. With an increase of temperature, the lowest pH value within the crevice is increased.

5.5 Effect of NaCl Concentration on AISI 304 Stainless Steel

The concentration of the chloride ion plays an important role in crevice corrosion. Lee et al. (162) found that increasing the concentration of Cl^- in the bulk electrolyte accelerates the change in pH and produces more acidic conditions in the crevice. In pitting, the pitting potential is usually decreased with an increase of Cl^- concentration. A simple relationship between the pitting potential E_{cp} and the concentration of the aggressive chloride anion C_x has been found (163-165),

$$E_{cp} = A_o - B_o \log C_x \qquad (26)$$

where B_o is a constant dependent on various factors and A_o a constant. However, there is no report about the effect of Cl^- concentration in the bulk solution on the critical initiation potential E_{cp} and protection potential E_{prot} for crevice corrosion. It is also

important to know the effect of Cl^- concentration in the bulk solution on the pH change over the cyclic potentiodynamic polarization curve. Therefore, solutions of different Cl^- concentration were used to measure the cyclic potentiodynamic polarization curves.

Fig. 81 and 82 show the cyclic potentiodynamic polarization curves of 304 stainless steel with pH measurement at indicated potentials obtained by controlling the potential inside a 12 μm crevice at an initial pH of about 7 at a temperature of 20°C in 3.5 wt.% and 15 wt.% NaCl solutions, respectively. They resemble the anodic polarization curve of AISI 304 stainless steel in 10% NaCl solution shown in Fig. 58. The pH changes over the cyclic potentiodynamic polarization curves in Fig. 81 and 82 are also very similar to that in Fig. 58. This indicates that the Cl^- concentration in the bulk solution does not greatly affect the pH change in the crevice solution. When the passive film is broken, the pH within the crevice is about neutral. Therefore, the same conclusion can be drawn that it is also not a pH decrease that causes the initiation of crevice corrosion as long as there is plenty of chloride.

From the cyclic polarization curves in Fig. 58, 81 and 82, the critical initiation potential for crevice corrosion E_{cp} and the protection potential E_{prot} can be obtained. The results are summarized in Table 14.

From Table 14, with an increase of NaCl concentration, the critical initiation potential for crevice corrosion E_{cp} is decreased. This is because with an increase of Cl^- concentration, the passive film on the steel is easier to break down. The protection potential E_{prot} is also decreased with an increase of Cl^- concentration. This is also because a higher Cl^- concentration makes it more difficult to repassivate the damaging passive film. However, the difference between E_{cp} and E_{prot} is decreased with an increase of Cl^- concentration. It is well known that the higher the Cl^- concentration, the more serious the crevice corrosion. This indicates that the critical initiation potential E_{cp} can be used to predict the crevice corrosion susceptibility of 304 stainless steel at different Cl^- concentrations and the difference between E_{cp} and E_{prot} cannot be used to predict the crevice corrosion susceptibility of stainless steel at different Cl^- concentrations.

A lower scan rate was also used to measure the cyclic potentiodynamic polarization curve and to study the pH changes over the cyclic potentiodynamic

polarization curve and critical initiation potential E_{cp} and protection potential E_{prot} for crevice corrosion. Fig. 83-85 show the cyclic potentiodynamic polarization curves of 304 stainless steel with measured pH values at the indicated potentials obtained by controlling the potential inside a 12 μm crevice at pH of about 7 at 20°C with the scan rate of 0.2 mV/s in the 3.5 wt%, 10 wt%, and 15 wt% NaCl solutions respectively. The pH changes over the cyclic potentiodynamic polarization curves in Fig. 83-85 are similar. This again confirms that the Cl^- concentration in the bulk solution does not greatly affect the pH change in the crevice solution at a low scan rate. The pH value within the crevice is also about neutral when the passive film is broken down.The critical initiation potentials E_{cp} for crevice corrosion and the protection potentials E_{prot} for crevice corrosion are summarized in Table 15.

From Table 15, the critical initiation potential E_{cp}, protection potential E_{prot} and their difference are also decreased with an increase of NaCl concentration as in the scan rate of 0.5 mV/s. Therefore, the changing tendency of E_{cp}, E_{prot} and the difference between E_{cp} and E_{prot} is the same as that in Table 14. The difference is that the E_{cp} value at the scanning rate of 0.2 mV/s is higher than that at the scanning rate of 0.5 mV/s. This again confirms that the critical initiation potential E_{cp} can be used to predict the susceptibility of 304 stainless steel at different Cl^- concentrations and the difference between E_{cp} and E_{prot} cannot be used to predict the crevice corrosion susceptibility of stainless steel at different Cl^- concentrations.

5.6 The Initiation of Crevice Corrosion by Controlling Potential inside a Crevice

In order to study the mechanism of initiation of crevice corrosion under applied potential inside a crevice, the cyclic potentiodynamic polarization measurement technique was used to create the different stages of crevice corrosion, and the SEM and optical microscope were used to study the corrosion morphology on the surface of the specimen.

As sulfide inclusions are always present in 304 stainless steel, a polished surface without corrosion was examined by SEM. Fig. 86 shows the distribution of the inclusions at a magnification of 1800X. Through x-ray analysis, they were identified as manganese

sulfide. The composition of large inclusions is a little different from that of small inclusions as shown in Fig. 87 and Fig. 88. The large inclusion contains some amount of Ti.

In the potentiodynamic polarization measurement started from the open circuit potential while controlling the potential inside a 12 μm crevice in 10 wt.% NaCl solution of pH about 7.00 at the temperature of 20°C and scan rate of 0.2 mV/s, the test was terminated when the current density reached 5 $\mu A/cm^2$. The specimen was taken from the sample holder and rinsed with distilled water and dried with alcohol. Then the surface of the specimen was examined by optical microscopy. Under the optical microscope, there was no corrosion evidence on the surface of the specimen. The repolished specimen was used to run another anodic potentiodynamic test under the same conditions as above. When the current density reached 20 $\mu A/cm^2$ on the potentiodynamic polarization curve, the test was terminated and the surface of the specimen was examined and analyzed with the optical microscope and SEM. Under optical microscopy, there was a corrosion spot on the surface of the specimen as shown in Fig. 89. Fig. 90 and Fig. 91 show the corrosion pit at high magnification under the optical microscope. From these two pictures, it is clearly indicated that the corrosion spot was initiated from a pit. Fig. 92 shows the pit as seen in the SEM. Some dimples can be observed in the picture. Fig. 93 and Fig. 94 show the deepest spot at the corrosion area under high magnification. There are some inclusions left in the dimples. The composition of these inclusions was analyzed using the x-ray detector in the SEM and is shown in Fig. 95 and Fig. 96. They are all manganese sulfide inclusions, but the large inclusions also contain some Ti. The presence of Ti in inclusions is probably due to impurities because there is no Ti in the base metal. From these pictures, it appears that the initiation of the pit is from MnS inclusions. This is in agreement with the work concluding that sulfides provide favourable sites for pitting initiation in austenitic stainless steel (142-149,166). Herbsleb (167) found that inclusion of (Fe,Mn)S, and MnS were dissolved selectively at -400 mV, i.e., at a potential value about 350 mV more negative than the open-circuit potential of stainless steel. The MnS inclusion will act as anode and stainless steel base will act as cathode when they form galvanonic cell. Therefore, MnS will corrode first. From the thermodynamic calculations

shown in Fig. 47 (147), it can be seen that in the pH range of 4.8 to 8, with an increase of anodic potential, the stable MnS can dissolve to yield Mn^{2+} and sulfur or SO_4^{2-} ions. Therefore, it is MnS in the experiment from which the initiation of the corrosion starts.

When the test was terminated at a current density of 50 $\mu A/cm^2$, there was also one corrosion spot as shown in Fig. 97. Fig. 98 shows the SEM micrograph of part of the corroded area in Fig. 97. As shown in Fig. 98, the surface of the corroded area with a current density of 50 $\mu A/cm^2$ is similar to that with a current density of 20 $\mu A/cm^2$. There are also some manganese sulfide inclusions in the dimples.

When the test was terminated at a current density of 100 $\mu A/cm^2$, there were two corrosion spots as shown in Fig. 99. One is smaller than that in Fig. 89 and the other is larger.

Fig. 100 and 101 show optical micrographs of sample surfaces when the current density reached 200 and 500 $\mu A/cm^2$ respectively. Fig. 102 shows an optical micrograph of a sample surface after the scanning direction is reversed at 500 $\mu A/cm^2$ to finish the whole cycle. Examining Fig. 89, 97, 99, 100, 101 and 102, it can be seen that with an increase of current density, the corroded area is also increased. However, the number of corrosion spots is increased slightly. In Fig 89, there is only one corrosion pit. In Fig. 102, there are four corrosion spots and the area of corrosion spots is quite large. At the other current densities, there are only two corrosion spots. This is quite different from the pitting situation. In pitting, with an increase of current density, the number of pits is also increased greatly but the area of each pit is almost the same. Therefore, the conclusion can be drawn that in crevice corrosion by controlling the potential inside the crevice during the cyclic potentiodynamic polarization measurement, crevice corrosion is initiated from pits and then spreads to a large area from pits, and the pits are initiated from manganese sulfide inclusions.

5.7 The Modification of Four Stage Mechanism of Crevice Corrosion under Applied Anodic Potential

Based on the experimental results, the discussion and Oldfield and Sutton's four

stage mechanism of crevice corrosion (19,20), some modification of four stage mechanism of crevice corrosion under applied anodic potential is proposed to account for the breakdown of the passive film by applied potential, i.e. (A) deoxygenation, (B) increase of the chloride ion and slight increase of acid concentration, (C) breakdown of the passive film, (D) propagation of crevice corrosion.

In stages (A) and (B), the process of crevice corrosion is the same as Oldfield and Sutton's four stage mechanism. During the third stage of the process the passivity of the alloy surface within the crevice is first broken down at vulnerable sites such as MnS inclusions when the applied potential reaches the critical initiation potential E_{cp} of crevice corrosion. Pits form within the crevice. This stage is different from that in the Oldfield and Sutton four stage mechanism which assumes that when local acidity attains a critical value, passivity breakdown occurs.

In the fourth stage, with the breakdown of the passive film, more metal ions are produced within the crevice and result in more Cl^- migrating into the crevice. The combined effect of increasing concentrations of chloride ions and decreasing pH in the inner solution creates an aggressive crevice solution where general attack proceeds. Therefore, the interior surface of the crevice begins to be corroded from the pits and the propagation of crevice corrosion will start. The rapid dissolution of the alloy inside the crevice is balanced by cathodic reduction outside the crevice.

5.8 Implication of the Experimental Results to Industrial Application

As the incubation period of crevice corrosion is a slow process and depends on many factors, such as crevice geometry, alloy surface conditions, etc., it is often impractical to evaluate the susceptibility of different materials to crevice corrosion by using a real crevice situation. Usually accelerated corrosion tests are used to provide faster and reproducible results. The cyclic polarization curve measurement is one of the most widely used techniques. From the polarization curve, the critical initiation potential E_{cp} and the protection potential E_{prot} can be obtained.

From the literature review (108,109), it is known that the critical initiation

potential E_{cp} for crevice corrosion and the difference between E_{cp} and E_{prot} are used to evaluate the susceptibility of materials to crevice corrosion. However, it is clearly shown from our experimental results that the difference between E_{cp} and E_{prot} obtained by controlling the potential inside a crevice cannot be used to evaluate the susceptibility of stainless steels. With an increase in NaCl concentration, temperature or change in alloy composition, the difference between E_{cp} and E_{prot} obtained at the same crevice width does not follow the change of seriousness of crevice corrosion.

With a decrease in crevice width, an increase in temperature, increasing NaCl concentration or change in alloy from 316 to 304 to 303 stainless steels, crevice corrosion becomes more serious and E_{cp} is also decreased. Therefore, the variation of E_{cp} indicates the degree of the seriousness of crevice corrosion. The lower the E_{cp} of the materials for crevice corrosion obtained at the same crevice width, the more serious the crevice corrosion of the materials. This means that the critical initiation potential E_{cp} obtained by controlling potential inside a crevice can be used to evaluate the susceptibility of materials. In industrial applications, the technique of measuring polarization curves by controlling potential inside a crevice can be used to quickly select the material with the best crevice corrosion resistance in different environments just by comparing the E_{cp} values of different materials.

6 A MATHEMATICAL MODEL FOR CALCULATION OF pH VALUES ALONG THE POLARIZATION CURVE

6.1 Introduction

Mathematical modelling, when used in conjunction with an experimental program, is useful for exploring the various mechanisms involved in crevice corrosion and determining the importance of the various parameters involved.

A number of simultaneous and interacting operations, such as mass transfer processes, production of metal ions within the crevice, hydrolysis reactions, etc., are involved in crevice corrosion. These make the processes of crevice corrosion very complex. However, a number of steady-state and transient models have been developed to simulate crevice corrosion (19,20,46-49,168-170).

In this part, a steady-state mathematical model is developed to calculate the pH values along the cyclic anodic polarization curve based on the experimental set-up and the experimental data. The major objective of this study is to compare the theoretical pH values calculated from corrosion current with the experimental pH values and to prove that it is the applied anodic potential that causes the initiation of crevice corrosion in the experimental conditions instead of attainment of a critical pH value.

6.2 Assumptions Used in the Model

6.2.1 Metal Dissolution within a Crevice

The effect of the alloy composition and the crevice environment on the relative amounts of various metal ions dissolved in the crevice solution is very complicated. Suzuki et al. (171) and Larson (172) found that the dissolved alloying elements in the anolyte were in approximately the same proportion as in the stainless steels in their pitting experiments. Lukomski (122) also found the concentration ratio of the metal ions

in the crevice solution was only approximately equivalent to the chemical composition of the stainless steel. As the pH decreased there was a marked increase in Cr/Fe ratio for which rather higher values were achieved than for the equivalent stainless steel composition. However, Bogar and Fujii (71) found the relative proportion of iron and chromium in the crevice was not directly proportional to the alloy composition. A disproportional increase in Cr^{3+} was measured as the Cr content of the alloy increased and for chromium contents > 15% the concentration of dissolved Cr^{3+} was greater than that of Fe^{2+}. However, in the proposed mathematical model, to simplify the calculation, it is quite reasonable to assume that the anodic current generates metal ions in the solution in the same molar ratio as they are present in the alloy. Other complex situations are not considered in the model.

The current used to produce Cr^{3+}, Fe^{2+}, and Ni^{2+} ions within the crevice is determined as follows based on the above assumption. If A(j) represents the molar fraction of metal j in the alloy and B(j) its charge, then the fraction of total anodic current involved in producing ions of metal j is,

$$I(j)/I_a = A(j)\times B(j)/\sum_{k=1}^{n} A(k)\times B(k) \qquad (27)$$

where n is the number of the various alloying elements present, including j; I_a is the applied anodic current; I(j) is the current used to produce metal j.

Expression (27) is based on the assumption of a uniform current density over the entire anodic area.

6.2.2 Mass Transport In and Out of a Crevice

Mass transport in and out of the crevice is an important consideration. There are three forms of mass transport: migration, diffusion and convection. The model assumes that there is no convection in the narrow crevice. To account for migration, it is assumed

that an equal amount of oppositely charged ions will move into the crevice to maintain the charge neutrality.

In order to simulate the transport processes, diffusion constants will be required. The diffusion coefficients, contained in Table 16, were calculated using the ionic radii of the species (173).

From simple diffusion theory, an estimate of diffusion distance of the species, δ_d, during the time t which it takes to diffuse, can be obtained, namely

$$\delta_d = (\pi D_o t)^{1/2} \qquad (28)$$

where D_o is the diffusion constant. Based on equation (28), the diffusion distance of oxygen or various ions in the crevice solution can be estimated at any time as long as their diffusion constants are available.

6.2.3 Reaction Equilibria

The hydrolysis of all metal ions occurs according to the equilibria shown in Table 17. All the hydrolysis reactions are mononuclear reactions (174,175) and produce an acidified environment. There is a dearth of data available in the literature to describe the rate of these reactions. However, the little amount of information that exists suggests that these hydrolysis reactions are extremely rapid (175); i.e., the reactions can be judged to be instantaneous relative to the transport process. Therefore, it can be assumed that the equilibrium among the various ions produced in the process of hydrolysis are reached immediately. All the concentration changes due to the reactions were calculated from equilibrium data in the literature with the H_2O activity held constant in the calculations.

Although all the crevice corrosion models (including this one) only consider monomer metal hydroxide reactions, significant metal-hydroxide and metal-chloro-hydroxide ligands, or oligimers, can be formed. These oligimers can be quit complex, forming a wide variety of structures (174,177).

In order to obtain the original concentration of the produced ions for the

calculation, the volume of solution in which the produced ions within the crevice are uniformly and immediately dissolved must be defined. As the sample surface within the crevice is 1 cm^2 as shown in Fig. 49 and 50, the anodic and cathodic reactions inside the crevice can only take place on the 1 cm^2 metal surface. Therefore, the volume of solution in which the produced ions within the crevice are dissolved can be defined as the metal surface area within the crevice multiplied by the crevice width, i.e. $1cm^2 \times d$ (where d is crevice width) as shown in Fig. 103. However, in the experiments, different sample holders with crevice widths of 0.0012 cm, 0.0040 cm, 0.0096 cm, 0.018 cm, and 0.033 cm are separately used to study the effect of crevice width on crevice corrosion. According to equation (28), when δ_d is 0.018 cm, the time needed for diffusion to that distance is about 17 seconds for the metal ions, while for H^+ and OH^- the times are about 1 second and 2 seconds respectively. During the experiment, the computer which controls the potentiostat takes a reading every eight seconds at a scan rate of 0.5 mV/s. Comparing the time to take a reading with the time needed for diffusion of H^+ and OH^- ions through the distance to reach the tip of the pH electrode, it is reasonable in the model to assume that the H^+ and OH^- ions generated in the crevice can almost immediately reach the tip of the pH electrode when the crevice width is equal to or less than 0.0018 cm. As for metal ions, later it will be shown that their diffusion is not an important parameter for the calculation because the rate of hydrolysis is very fast. When δ_d is 0.033 cm, for H^+ and OH^-, the times needed for diffusion to this distance are about 4 seconds and 7 seconds respectively. Comparing these times with the time for the computer to take a reading, the same assumption as above cannot be made when the crevice width is equal to 0.033 cm. Therefore, in the model it is assumed that when the crevice width is equal to or less than 0.018 cm, the volume of solution (V_r) which contains the produced ion uniformly is defined as the metal surface area inside the crevice times the crevice width, i.e.

$$V_r = 1cm^2 \times d \qquad (29)$$

where 1 cm^2 is the metal surface area inside the crevice and d is the crevice width.

When the crevice width is equal to 0.033 cm, the model assumes that the volume of solution (V_r) which contains the produced ion uniformly is defined as the metal surface area inside the crevice times 0.018 cm to make the calculation easier, i.e.

$$V_r = 1cm^2 \times 0.018\ cm \tag{30}$$

The volume of solution (V_r) in the model is called the reaction volume which is shown in Fig. 103. In the reaction volume, all produced ions are assumed to be dissolved uniformly immediately.

As the hydrolysis process is very fast, the model also assumes that no hydrolysis occurs outside the reaction volume. All produced H^+ will uniformly dissolve in the reaction volume. Therefore, the transport process of metal ions does not directly affect the pH values within the crevice. Only the diffusion of H^+ or OH^- ions out from the reaction volume can affect the pH value within the crevice. To simplify the diffusion process further, the model assumes that each species produced in the reaction volume in time t will uniformly diffuse outward to the distance δ_d from the edge of the reaction volume according to equation (28).

When the crevice width is equal to or less than 0.018 cm, the ions in the reaction volume can only diffuse outward from the sides of the reaction volume as shown in Fig. 104. In this way, each species of ions produced in time t will uniformly dissolve in the extended volume. As the radius of metal surface area inside the crevice is 0.564 cm and the diffusion distance is δ_{dL} from the edge of the reaction volume in the lateral direction in time t, the total volume (V(t)) in the time t can be calculated by equation (31),

$$V(t) = \pi(0.564+\delta_{dL})^2 \times d \tag{31}$$

where d is the crevice width and δ_{dL} is the diffusion distance in the lateral direction.

When the crevice width is 0.033 cm, in addition to diffusion outward from the edge of reaction volume in the lateral direction, the ions can also diffuse outward from the top of the reaction volume in the vertical direction as shown in Fig. 105. In this way,

the total volume V(t1) of solution for the ions in the time t can be obtained from equation (32),

$$V(t1) = \pi(0.564+\delta_{dL})^2\times(0.018+\delta_{dv}) \qquad (32)$$

where δ_{dL} is the diffusion distance in the lateral direction and δ_{dv} is the diffusion distance in the vertical direction at time t, but the maximum value of δ_{dv} is equal to crevice width 0.033 - 0.018 cm because in this case diffusion of ions reaches the top of the crevice.

From Fig. 103, the distance from the edge of the metal surface to the edge of the mounting material is 1 cm. Therefore, when the diffusion distance δ_{dL} of the ions produced in the reaction volume is greater than 1 cm, they will enter the bulk solution. As the volume of bulk solution is very large, the model assumes that the ions entering the bulk solution do not affect its composition. The only effect of this diffusion is to reduce the amount of ions inside the crevice.

6.2.4 Depletion of Oxygen within a Crevice

The average oxygen concentration in water is around 2.92×10^{-4} mol/L at 20°C (178); under diffusion controlled conditions with general agitation, say, vigorous bubbling with air, this will produce current densities in the range of 100 - 500 $\mu A/cm^2$ (179,180) depending on the exact thickness of the diffusion layer and the number of electrons per oxygen molecule involved in the oxygen reduction (180,181) (this is between 2 and 4 depending on the mechanism, which is a function of the substrate). These currents are far in excess of the values of the anodic passive current, which are of the order of microamperes or less (182,183) and therefore in practice it is the passive current which controls the rate at which oxygen is depleted from the crevice. Under gradually increasing anodic potential, the model assumes that the rate of the cathodic reaction, reduction of oxygen, is gradually decreased. At the beginning, the rate of reduction of oxygen is equal to the passive current and only oxygen dissolved in the reaction volume can take part in the reduction. With an increase in time (i.e. an increase

of anodic potential), the rate of reduction is decreased. Meanwhile, the oxygen dissolved in the volume outside the reaction volume can also diffuse into the reaction volume to participate in the reaction. From equation (28), the diffusion distance of oxygen can be obtained as long as the time is decided. Therefore, the amount of oxygen which participates in the reaction at a certain time can be calculated. If the amount of oxygen originally dissolved in the reaction volume and the amount of oxygen diffused into the reaction volume in the time t, are depleted, then after this time, the only source of oxygen to participate in the reaction comes from diffusion. From the diffusion distance, δ_d, at a certain time, t, the amount of oxygen which can diffuse into the reaction volume can be calculated. For example, at time t_1, the diffusion distance δ_{d1} is equal to $(\pi D_o t_1)^{1/2}$. At time t_2, the diffusion distance δ_{d2} is equal to $(\pi D_o t_2)^{1/2}$. When the crevice width is equal to or less than 0.018 cm, the amount of oxygen ($W(O_2)$) in moles diffused into the reaction volume from t_1 to t_2 can be found from equation (33),

$$W(O_2) = [\pi(0.564+\delta_{d2})^2 - \pi(0.564+\delta_{d1})^2]\times d\times C_o \qquad (33)$$

where C_o is the molar concentration of oxygen dissolved in the solution and d is the crevice width.

When the crevice width is 0.033 cm and t_2 is equal to or less than $(0.033-0.018)^2/\pi D_o$ seconds, the amount of oxygen ($W(O_2)$) in moles diffused into the reaction volume from t_1 to t_2 can be found from equation (34),

$$W(O_2)=\{1cm^2\times(\delta_{d2}-\delta_{d1})+[\pi(0.564+\delta_{d2})^2-\pi(0.564+\delta_{d1})^2]\times(0.018+\delta_{d1})\}\times C_o \qquad (34)$$

When the crevice width is 0.033 cm and t_2 is greater than $(0.033-0.018)^2/\pi D_o$ seconds, the amount of oxygen ($W(O_2)$) in moles diffused into the reaction volume from t_1 to t_2 can be found from equation (35),

$$W(O_2) = [\pi(0.564+\delta_{d2})^2-\pi(0.564+\delta_{d1})^2]\times 0.033\times C_o \qquad (35)$$

When the anodic potential is increased to a certain value above the open-circuit potential, i.e., the potential above the cathodic reduction potential of oxygen, the cathodic reaction cannot occur within the crevice even though oxygen exists in the reaction volume.

6.2.5 Correction of pH for Presence of Cl^- Ions

The presence of metal chlorides can affect the crevice pH, as has been documented by a number of authors in the literature (184-186). As the metal chlorides, especially chromium chloride can form various complexes with water and hydroxyl ions, this makes it very difficult to calculate the effect of Cl^- on pH in the process of hydrolysis. In order to simplify the calculation, the effect of Cl^- ions on the pH in the crevice solution was calculated separately from the hydrolysis process.

Watson (170) used the data of Mankowski and Szklarska-Smialowska (184) to derive the following empirical relationships to account for the effect of Cl^- on pH in the crevice solution in his model.

$$pH_{adj} = pH_{calculated} - 0.33(CrCl_3) - 0.22(FeCl_2+NiCl_2) \qquad (36)$$

All concentrations are expressed as normalities. In present model, equation (36) is also used to correct the effect of Cl^- ions on the pH value in the crevice solution. The $pH_{calculated}$ in the model is the pH value in the reaction volume calculated by the hydrolysis of metal ions in the reaction volume at a certain time. The normalities of $CrCl_3$, $FeCl_2$, and $NiCl_2$ in the reaction volume are obtained by calculating the amount of Cr^{3+}, Fe^{2+}, and Ni^{2+} ions produced in the reaction volume at the same time by anodic current. The pH_{adj} is the pH value in the reaction volume after considering the effect of Cl^- ions.

6.3 The Calculation of pH Values along the Polarization Curve

6.3.1 The Calculation of the Concentration of OH^- in the Reaction Volume

At the first stage of crevice corrosion, both the reduction of oxygen to hydroxyl ions and anodic dissolution of metal occur at the same time on the sample surface within the crevice. With a gradually increasing anodic potential, the rate of reduction of oxygen is decreased. Before cathodic cleaning, the open-circuit potential is about - 250 mV (vs. SCE). Therefore, when the anodic potential is about 150 mV above the open-circuit potential, it can be reasonably assumed that the reduction of oxygen on the metal surface within the crevice stops. After that, only the anodic dissolution of metal occurs within the crevice. All the cathodic reactions occur outside the crevice.

In the measurement of a cyclic anodic polarization curve, the computer which controls the potentiostat makes a reading every 4 mV, i.e. every 8 seconds at a scan rate of 0.5 mV/s. All the charge passed during the measurement between two neighbouring points can be calculated by equation (37),

$$C_h = \text{Current} \times \text{Time} \qquad (37)$$

where C_h is the charge in coulombs, current is the average current in amperes of two neighbouring points, and time is equal to 4/v seconds, where v is the scan rate in mV/s.

The amount of OH^- produced at each point can be obtained from equation (38) if all charge at each point is used to produce hydroxyl ions,

$$W(OH^-) = C_h/96500 \qquad (38)$$

where $W(OH^-)$ is the amount of OH^- in moles produced at each point and 96500 is the Faraday constant.

When the anodic potential is gradually increased, the amount of OH^- produced at each point must be decreased with the scan time. To correct the effect of increasing the

anodic potential on the decrease of cathodical reduction, a progressively decreasing equation must be used. Since the scan time (t_s) from the beginning of the scan to the potential at which the cathodic reduction of oxygen stops can be found, a linearly progressively decreasing equation (39) can be used as an approximation to reduce the rate of cathodic reduction, i.e.

$$Y = 1 - t/t_s \qquad (39)$$

where Y is the remaining percentage of the charge to produce the OH^- ions, and t is the scan time in seconds from the beginning to this point.

The actual amount of OH^- produced at each point can be obtained by equation (40) after considering the effect of increasing the anodic potential on the cathodic reduction.

$$W(OH^-) = C_h \times Y/96500 \qquad (40)$$

Therefore, the total amount of OH^- produced up to a point can be obtained from adding all the OH^- produced at each point up to the point of interest.

The molarity of a solute is the number of moles of that solute dissolved in 1 litre of solution. Here we use [ ] to indicate the molar concentration. To simplify stoichiometric calculation of reaction in the solution, normality is used to describe the solution concentration. Normality is defined as the number of equivalents per litre of solution.

The molar concentration of OH^- ($[OH^-]$) in the reaction volume at each point will be equal to the total amount of OH^- at each point divided by the reaction volume in litres,

$$[OH^-] = W(OH^-)/V_r \qquad (41)$$

However, when the total amount of OH^- produced at a certain point, (i.e. at a

certain time t) is equal to the total amount of OH^- which will be generated from oxygen originally dissolved in the reaction volume plus oxygen added in time t through diffusion into the reaction volume, all oxygen in the reaction volume is completely depleted. After this point, the produced OH^- in the reaction volume only comes from diffusion. With equations (33), (34) and (35), if the times of two neighbouring points, t_1 and t_2 are known, the amount of oxygen diffusing into the reaction volume during the scan from point 1 to point 2 can be obtained; i.e., the amount of oxygen in the reaction volume at point 2 is obtained. As the amount of oxygen added in the reaction volume through diffusion alone is very small compared with the anodic current, it is assumed that the total amount of oxygen in the reaction volume from diffusion is completely used to generate the OH^-. From equation (1), as one mole of oxygen can produce four moles of OH^-, the amount of OH^- produced in the reaction volume can be obtained by multiplying the amount of O_2 through diffusion by 4. Therefore, the molar concentrations of OH^- in the reaction volume at each point during the scan can be obtained from the following equations. When the crevice width is equal to or less than 0.018 cm,

$$[OH^-] = 4\times[\pi(0.564+\delta_{d2})^2 - \pi(0.564+\delta_{d1})^2]\times d\times C_o/V_r \qquad (42)$$

When the crevice width is greater than 0.018 cm and t_2 is equal to or less than $(0.033-0.018)^2/\pi D_o$ seconds,

$$[OH^-] = 4\times\{1cm^2\times(\delta_{d2}-\delta_{d1})+[\pi(0.564+\delta_{d2})^2 - \pi(0.564+\delta_{d1})^2]\times(0.018+\delta_{d1})\}\times C_o/V_r \qquad (43)$$

When the crevice width is greater than 0.018 cm and t_2 is greater than $(d-0.018)^2/\pi D_o$ seconds,

$$[OH^-] = 4\times[\pi(0.564+\delta_{d2})^2-\pi(0.564+\delta_{d1})^2]\times d\times C_o/V_r \qquad (44)$$

In this way, the concentration of hydroxyl ions in the reaction volume at each point can

be obtained from equations (41) to (44), depending on the crevice width and time.

6.3.2 The Calculation of the Concentration of Metal Ions in the Reaction Volume

In stainless steel, the mole fraction of metal j can be calculated from the alloy's composition. Therefore, the percentage of anodic current used to produce metal j ions can be found from equation (27). In other words, the percentage is equal to the percentage of total charges used to produce metal j ions. It is assumed that the percentage of one metal element in an alloy is f. That is, only f of total charge at each point during the scan is used to produce metal j ions. In this way, if all the charge passed between two neighbouring points during the scan is calculated from equation (37), then the charge used to produce each metal ion at each point can be obtained from equation (45),

$$C_h(j) = C_h \times f \qquad (45)$$

where $C_h(j)$ is the charge used to produce the metal j ions in the alloy, and C_h is total charge used to produce the metal ions in stainless steel.

The amount of metal j ions (W(j)) in moles produced at each point can be obtained from equation (46),

$$W(j) = C_h(j)/[96500 \times B(j)] \qquad (46)$$

where B(j) is the ion charge and 96500 is the Faraday constant.

The molar concentration of metal j, [j], in the reaction volume can be obtained from equation (47),

$$[\,j\,] = W(j)/V_r \qquad (47)$$

In this way, the concentrations of all metal ions produced in the reaction volume at each

point during the scan are obtained.

6.3.3 The Calculation of pH along the Polarization Curve

According to equilibrium (4) in Table 17, when the pH of the solution is 7, only 6×10^{-10} M of Cr^{3+} is dissolved in the solution. Therefore, it can be reasonably assumed that when the pH is greater than 7, all the chromium ions are in the form of a $Cr(OH)_3$ precipitate. When the pH is less than 7, chromium ions can exist in the forms of Cr^{3+}, $Cr(OH)^{2+}$, $Cr(OH)_2^{+}$, and $Cr(OH)_3$.

According to equilibria (7) and (10) in Table 17, when the pH of the solution is greater than 10, the iron ions and nickel ions are in the form of $Fe(OH)_2$ and $Ni(OH)_2$ precipitates. When the pH is less than 7, the iron and nickel hydroxide are far more soluble than the chromium hydroxide. Therefore, it can be assumed that it is solely the hydrolysis of chromium ions which causes the pH to fall and iron and nickel ions do not directly affect the pH change within the crevice. When the pH within the crevice is between 7 and 10, in addition to the Cr^{3+} in the form of $Cr(OH)_3$ precipitate consuming the hydroxyl ions to affect the pH in the crevice, the iron and nickel ions have also some effect on the pH change within the crevice by forming their various hydroxides.

When the normality of Cr^{3+} in the reaction volume is less than that of OH^- in the reaction volume, the pH in the solution of the reaction volume must be above 7. In this case, all chromium ions are in the form of $Cr(OH)_3$ and the iron and nickel ions will form various hydroxide ions in the solution of the reaction volume. Therefore, the effect of chromium, iron, and nickel ions generated in the reaction volume on the pH change in the solution of the reaction volume must be considered. As all chromium ions form $Cr(OH)_3$ precipitate, they must consume an OH^- normality of $3[Cr^{3+}]$. After the formation of the chromium hydroxide precipitate, the concentration of OH^- remaining in the reaction volume can be obtained from equation (48).

$$[OH^-]_r = [OH^-]_T - 3[Cr^{3+}] \qquad (48)$$

where $[OH^-]_T$ is the total concentration of OH^- produced in the reaction volume, $[OH^-]_r$ is the remaining concentration of $[OH^-]$ in the reaction volume after all the chromium ions in the reaction volume form chromium hydroxide, and $[Cr^{3+}]$ is the molar concentration of Cr^{3+} produced in the reaction volume. When equilibrium among iron ions, nickel ions and the remaining hydroxyl ions in the reaction volume is reached, suppose the molar concentration of $[Fe^{2+}] = U$, $[Fe(OH)^+] = V$, $[Fe(OH)_2] = W$, $[H^+] = X$, $[Ni^{2+}] = O$, $[Ni(OH)^+] = P$, $[Ni(OH)_2] = Q$. From the equilibria in Table 17, the following equations can be obtained:

$$\underset{U}{Fe^{2+}} + H_2O \rightleftharpoons \underset{V}{Fe(OH)^+} + \underset{X}{H^+} \qquad K_5 = 5.0\times10^{-9}$$

$$VX/U = K_5 \tag{49}$$

$$\underset{V}{Fe(OH)^+} + H_2O \rightleftharpoons \underset{W}{Fe(OH)_2(aq)} + \underset{X}{H^+} \qquad K_6 = 7.49\times10^{-12}$$

$$WX/V = K_6 \tag{50}$$

$$\underset{O}{Ni^{2+}} + H_2O \rightleftharpoons \underset{P}{Ni(OH)^+} + \underset{X}{H^+} \qquad K_8 = 3.16\times10^{-10}$$

$$PX/O = K_8 \tag{51}$$

$$\underset{P}{Ni(OH)^+} + H_2O \rightleftharpoons \underset{Q}{Ni(OH)_2(aq)} + \underset{X}{H^+} \qquad K_9 = 7.49\times10^{-10}$$

$$QX/P = K_9 \tag{52}$$

From a mass balance, the following three equations can be obtained:

$$[Fe^{2+}]_T = U + V + W \tag{53}$$

$$[Ni^{2+}]_T = O + P + Q \tag{54}$$

$$[OH^-]_r = V + 2W + P + 2Q + K_w/X \qquad (55)$$

where $[Fe^{2+}]_T$ is the total concentration of $[Fe^{2+}]$ produced in the reaction volume, $[Ni^{2+}]_T$ is the total concentration of $[Ni^{2+}]$ produced in the reaction volume, and Kw/X is the concentration of OH^- in the reaction volume at equilibrium.

$[OH^-]_r$, $[Fe^{2+}]_T$ and $[Ni^{2+}]_T$ can be calculated from the above procedures. Since there are seven unknown variables and seven equations from (49) to (55), using Newton's method in Mathematica (see Appendix A), the concentration of hydrogen ions in the reaction volume can be found by solving the set of non-linear equations, i.e., the pH value in the reaction volume can be obtained.

When the concentration of chromium ions in the solution exceeds the concentration of $[OH^-]_T$, the pH value in the reaction volume must be less than 7. In this case, the effect of iron and nickel ions on pH change can be neglected and only chromium ions and hydroxyl ions are considered. It can be assumed that at equilibrium, the concentration of $[Cr^{3+}]$ = G, $[Cr(OH)^{2+}]$ = H, $[Cr(OH)_2^+]$ = J, $[Cr(OH)_3]$ = L, and $[H^+]$ = S. According to equilibria in Table 17, the following equations can be obtained:

$$\underset{G}{Cr^{3+}} + H_2O \rightleftharpoons \underset{H}{Cr(OH)^{2+}} + \underset{S}{H^+} \qquad K_1 = 1.58\times10^{-4}$$

$$HS/G = K_1 \qquad (56)$$

$$\underset{H}{Cr(OH)^{2+}} + H_2O \rightleftharpoons \underset{J}{Cr(OH)_2^+} + \underset{S}{H^+} \qquad K_2 = 6.31\times10^{-7}$$

$$JS/H = K_2 \qquad (57)$$

$$\underset{J}{Cr(OH)_2^+} + H_2O \rightleftharpoons \underset{L}{Cr(OH)_3(aq)} + \underset{S}{H^+} \quad K_3 = 6.31\times10^{-7}$$

$$LS/J = K_3 \qquad (58)$$

From a mass balance, the following equation can be obtained:

$$[Cr^{3+}]_T = G + H + J + L \qquad (59)$$

As all hydrogen ions are produced from the hydrolysis of chromium ions, every hydrogen ion produced from hydrolysis must correspond to an hydroxyl ion produced from the process. However, as the amount of $[OH^-]_T$ in the reaction volume is not from the hydrolysis, the total amount of hydrogen ions produced from the hydrolysis in the reaction volume must be equal to the total amount of $[OH^-]$ ions in the solution minus the $[OH^-]_T$. Therefore, the following equation can be obtained.

$$[OH^-]_T = H + 2J + 3L - S \qquad (60)$$

Since we have five unknown variables and five equations from (55) to (60), using Newton's method in Mathematica (see Appendix A), the concentration of hydrogen ions in the reaction volume can be calculated by solving the set of non-linear equations. Therefore, the pH value in the reaction volume can be obtained.

From the above equations, if the concentrations of OH^-, Cr^{3+}, Fe^{2+} and Ni^{2+} produced in the reaction volume at each point during the scan are known, the pH value in the reaction volume at each point can be calculated.

Depending on the concentration of chromium, iron, nickel ions and hydroxyl ions in the solution of the reaction volume at each point, the pH value in the reaction volume can be calculated from the set of equation (49) to (55) and the set of equations (56) to (60). Using equation (36), the adjusted pH value in the reaction volume can be obtained by considering the effect of chloride ions. Therefore, the total hydrogen ions produced in the reaction volume at each point during the scan can be obtained.

Now consider diffusion of hydrogen ions and hydroxyl ions from the reaction volume. When the pH is greater than 7, the concentration of hydroxyl ions in the reaction volume is higher than that outside the reaction volume. According to Fick's diffusion law, the hydroxyl ions in the reaction volume have to diffuse outward from the

reaction volume. When pH is less than 7, the concentration of hydrogen ions in the reaction volume is higher than that outside the reaction volume. In the same way, the hydrogen ions in the reaction volume have to diffuse outward from the reaction volume.

According to the above assumption about the diffusion process, when the crevice width is equal to or less than 0.0018 cm, the total volume (V(t)) in which the hydroxyl ions and hydrogen ions are uniformly dissolved in the time t can be obtained from equation (31). Therefore, when the pH in the reaction volume is above 7, from the scan time t up to a certain point, the total volume (V(t)) for the hydroxyl ions can calculated from equation (31). The final concentration of hydroxyl ions in the crevice at that point during the scan can be calculated by equation (61),

$$[OH^-]_f = W(OH^-)/V(t) \qquad (61)$$

where $[OH^-]_f$ is the final concentration of hydroxyl ions in the crevice and $W(OH^-)$ is the moles of hydroxyl ions in the reaction volume at time t after considering the effect of chloride ions. From the values of $[OH^-]_f$ at each point, the corresponding final pH value at each point can also be calculated.

When the pH in the reaction volume is less than 7, the total volume (V(t)) for hydrogen ions can also be calculated from equation (31). However, the time t in equation (31) is not the scan time from the beginning of the scan up to the point of interest because at the beginning, it is diffusion of hydroxyl ions instead of hydrogen ions. The time t in equation (31) for diffusion of hydroxyl ions is the time from the first point at which the pH in the crevice is less than 7 up to the calculated point. Therefore, the final concentration of hydrogen ions in the crevice (i.e., the extended volume) can be obtained by equation (62).

$$[H^+]_f = [H^+]/V(t) \qquad (62)$$

where $[H^+]_f$ is the final molar concentration of hydrogen ions in the crevice and $[H^+]$ is the concentration of hydrogen ions in the reaction volume after considering the effect

of chloride ions. From the values of $[H^+]_f$ at each point, the corresponding final pH value can be obtained.

When the crevice width is 0.033 cm, the total volume (V(t1)) in which the hydroxyl ions and hydrogen ions are uniformly dissolved in the time t can be obtained from equation (32). Therefore, using the same procedure as in the above-mentioned method, the final hydroxyl ion and hydrogen ion concentration in the crevice at each point during the scan can also be calculated as long as equation (32) is used to calculate the total volume of solution (V(t1)) for the hydroxyl ions or hydrogen ions instead of equation (31). From the value of $[OH^-]_f$ or $[H^+]_f$ at each point of interest, depending on the pH value in the reaction volume, the final corresponding pH value at each point in the crevice can be obtained.

6.4 Comparison of Simulation Results with Experimental Values

Using data in Fig. 58, for 304 stainless steel obtained by controlling potential inside a 12 μm crevice at a scan rate of 0.5 mV/s in 10% NaCl solution of pH about 7.25 at a temperature of 20°C, the pH value at each point on the polarization curve can be calculated according to the above procedure. The results are shown in Table 18 and Fig. 106.

From Table 18, it can seen that although the pH values in the theoretical calculation do not perfectly match the experimental values, the pH change trend in the theoretical calculation is very similar to that in the experiment, i.e., the pH first increases slightly, then gradually decreases, and finally the pH slightly increases again. The differences between the theoretical value and experimental value are within a reasonable range. This indicates that the proposed model for the calculation of pH values inside a crevice is quite reasonable. From Fig. 106, when the passive film is broken down, the pH in theoretical calculation is about 4.5. The pH value is also much higher than the critical pH (2.00) for 304 stainless steel. Therefore, from theoretical calculation of pH at a crevice width of 12 μm, the conclusion can also be obtained that it is not a pH decrease which causes the initiation of crevice corrosion.

Using data in Fig. 59, 60, and 61 for 304 stainless steel obtained by controlling potential inside crevices of different widths at the scan rate of 0.5 mV/s in 10% NaCl solution of pH about 7.25 at a temperature of 20°C, the pH value at each point on the polarization curve can be calculated according to the above procedure. The results are shown in Table 19 and Fig. 107, Table 20 and Fig. 108, Table 21 and Fig. 109 for crevice widths of 40 μm, 96 μm and 180 μm, respectively. As in Table 18, it can also be seen from these tables that the pH values in theoretical calculation at the different crevice widths also do not perfectly match the experimental values, but the pH change trend in the theoretical calculation is also very similar to that in the experiment, i.e., the pH first increases slightly, then gradually decreases, and finally the pH slightly increases again. Again, the differences between the theoretical values and experimental values are within a reasonable range.

From Fig. 107, 108 and 109, when the passive film is broken down, the pH in theoretical calculation is above 4.5. Therefore, from theoretical calculation of pH at different crevice widths, the conclusion can also be obtained that it is not a pH decrease that causes the initiation of crevice corrosion.

From Tables 18, 19, 20 and 21, it can be seen that with an increase in crevice width, the pH change becomes slower and the final pH inside the crevice is increased. These change trends can be explained from the model itself. From the calculation of ion concentration in the reaction volume, it is known that with an increase of crevice width, the reaction volume is increased so that the concentration of produced ions in the reaction volume is decreased. However, with an increase in the reaction volume, the total amount of hydroxyl ions produced at each point in the reaction volume is increased because more oxygen can participate in the reaction to produce OH^-. The smaller the reaction volume, the faster the consumption of oxygen. Relatively, the amount of oxygen that diffuses into the reaction volume to participate in the reaction at each point is much smaller. However, the total amount of metal ions produced at each point during the scan in the reaction volume changes very little if the passed current and the time are about the same. Therefore, with an increase of the crevice width, the decrease in concentration of metal ions produced at each point during the scan in the reaction volume is greater than the

decrease of OH^- concentration produced at the same point during the scan in the reaction volume. This makes the pH change slower with an increase of crevice width.

When the effect of chloride ions on the pH change is considered, from equation (36) it can be seen that with an increase in the metal ion concentration in the reaction volume, the adjusted pH is decreased. This also makes the pH change slower at greater crevice width.

Using data in Fig. 62 for 304 stainless steel obtained by controlling potential inside a 330 μm crevice at the scan rate of 0.5 mV/s in 10% NaCl solution of pH about 7.00 at a temperature of 20°C, the pH values calculated at each point on the polarization curve, using the same calculation method described earlier, are shown in Table 22 and Fig. 110. From Table 22 and Fig. 110, it can be seen that before the current begins to increase greatly, i.e. at a pH about 7, the theoretical values are very close to the experimental values. However, when the current begins to increase greatly, the difference between the experimental values and the theoretical values is apparently larger than those in Tables 18 to 21. From the experimental results, it is known that at this crevice width, the condition of the crevice is not suitable for the occurrence of crevice corrosion, but for pitting corrosion. In the pitting situation, the produced metal ions do not easily diffuse into the reaction volume, and find it even more difficult to reach the tip of the pH electrode, because in pitting corrosion, hydroxide may form around the mouth of the pits to prevent the diffusion of metal ions. Therefore, the actual concentration of metal ions produced at each point during the scan in the reaction volume is much less than the calculated values which are based on the assumption that the produced metal ions are uniformly dissolved in the reaction volume. That is why the calculated pH values are much lower than the experimental values. Therefore, the proposed mathematical model for the calculation of pH value within the crevice is not suitable for the calculation of pH with a crevice width of 330 μm or larger because in this situation, pitting corrosion occurs.

6.5 A Sensitivity Analysis of the Assumption about Uniform Dissolution

In this model, the assumption is made that the anodic current generates metal ions in the solution in the same molar ratio as they are present in the alloy. However, as the dissolution of metal ions may not follow uniform dissolution, an analysis of preferential dissolution on the sensitivity of the numerical solution for the set of non-linear equations is necessary.

In uniform dissolution, the mole ratio of Cr/Fe is 0.277 for 304 stainless steel. If the Cr/Fe ratio becomes 1 and the percentage of Ni dissolved in the reaction volume keeps the same fraction as in the alloy, the new molar concentrations of Cr^{3+}, Fe^{2+}, and Ni^{2+} at the first point in Fig. 58 are 1.029×10^{-5}, 1.029×10^{-5}, and 1.97×10^{-6} respectively. Introducing the data and concentration of hydroxyl ions into equations (5a), (6a) and (7a) and solving the set of non-linear equations from (1a) to (7a) (in Appendix A), the value of X is 1.03×10^{-9}. The variation of starting point does not affect the results.

For the point of experimental pH 7.50 in Fig. 58, the new concentrations of Cr^{3+}, Fe^{2+}, and Ni^{2+} at the first point in Fig. 58 are 1.1×10^{-3}, 1.1×10^{-3}, and 2.59×10^{-4} respectively. Solving the set of equations from (8a) to (12a) (in Appendix A) at the new concentration, the value of S is 1.53×10^{-7}. The variation of starting point also does not affect the results.

When the Cr/Fe ratio is 2, the new molar concentrations of Cr^{3+}, Fe^{2+}, and Ni^{2+} at the first point in Fig. 58 are 1.317×10^{-5}, 1.833×10^{-5}, and 1.97×10^{-6}, respectively. Solving the set of equations from (1a) to (7a), the value of X is 1.92×10^{-3}.

For the point of experimental pH 7.50 in Fig. 58, the new molar concentrations of Cr^{3+}, Fe^{2+}, and Ni^{2+} at the first point in Fig. 58 are 1.467×10^{-3}, 7.33×10^{-4}, and 2.59×10^{-4} respectively. Solving the set of equations from (8a) to (12a), the value of S is 5.16×10^{-6}.

The calculated results show that the pH value will change depending on the ratio of Cr/Fe dissolved in the solution. However, the change in the Cr/Fe ratio does not affect the sensitivity of the sets of non-linear equations. Therefore, Newton's method can

be used to solve the sets of non-linear equations.

6.6 Discussions of Other Factors Affecting the pH Values within the Crevice

From Tables 18 to 21, it can also be seen that the calculated pH values for the last two or three points within the crevice are greater than those from the experiment except those in Table 18. However, based on the assumptions that the equilibria among the various ions produced in the reaction volume are reached immediately after they are produced, the calculated pH values in the last two or three points within the crevice should be less than the experimental values because the kinetical parameter has been ignored. Therefore, there must be some other factors which are ignored in the model to affect the pH value within the crevice. Here, some factors affecting the pH values within the crevice will be simply discussed in order to better understand the mechanism of crevice corrosion and improve the model later.

6.6.1 Effect of Chromium Ions within a Crevice on the pH Value

In part 6.2.1, it is assumed in the model that the dissolved alloying elements in the crevice were in the same proportion as in the steel and no selective dissolution of metal ions may occur. However, this assumption is only based on approximation (122,171,172). Some researchers (71,122) also reported that preferential dissolution takes place in the stainless steel. Lukomski and Bohnenkamp (122) found the concentration ratio of metal ions in the crevice solution is only approximately equivalent to the chemical composition of the stainless steel. As the pH decreases the ratio of Cr/Fe in the crevice solution is much higher than that of Cr/Fe in the stainless steel. Bogar and Fujii (71) also reported that the relative proportion of iron and chromium in the crevice was not directly proportional to the alloy composition. A disproportional increase in Cr^{3+} was measured at Cr contents > 15%; the concentration of dissolved Cr^{3+} was greater than that of Fe^{2+}. Therefore, if preferential dissolution of Cr in the stainless steel occurs in the experiment, the pH values in the experiment will be smaller than those obtained from

the calculation according to the model.

Based on the above discussion, a model is assumed that with an increase of acidity in crevice solution, the mole ratio of Cr/Fe in the crevice solution is increased. At the end of the scan, the Cr/Fe ratio within the crevice reaches 1.2 from the original mole ratio 0.277 for 304 stainless steel and the percentage of nickel dissolved within the crevice maintains the same ratio as in the stainless steel. In order to estimate the effect of the preferential dissolution on the pH, it is further assumed that the ratio of Cr/Fe increases linearly with decreasing pH values within the crevice and the experimental pH values are used to estimate the ratio of Cr/Fe produced in the reaction volume. Based on the above assumptions, the following equation can be used to calculate the ratio of Cr/Fe at any given point along the polarization curve:

$$Cr/Fe = R_{ori} \times [\, 1 + (pH_{ori} - pH_{Ecal})/(pH_{ori} - pH_f)] \times (1.2 - R_{ori}) \qquad (63)$$

where R_{ori} is the mole ratio of Cr/Fe in the stainless steel, pH_{ori} is the pH value at the first point on the polarization curve, pH_{Ecal} is the pH value obtained from the experiment at the calculated point and pH_f is the pH value at the last point on the polarization curve.

As the amount of chromium, iron and nickel ions in the reaction volume at each point can be calculated using the method in part 6.3.2, the total amount of chromium and nickel ions can also be obtained at each point. When the new ratio of Cr/Fe is obtained from equation (63), the corrected concentration of chromium and iron ions in the reaction volume can be calculated. Solving equations (56) to (60) according to the new concentration of chromium, iron and nickel ions in the reaction volume as in the before-mentioned method, the calculated pH values at the crevice widths of 12 μm, 40 μm, 96 μm and 180 μm are shown in Tables 18, 19, 20 and 21.

From Tables 18, 19, 20 and 21, it can be seen that under the assumption of the preferential dissolution of chromium in the alloy, except for those in Table 18, the calculated pH values in Tables 19, 20 and 21 are closer to the experimental pH values than those under the assumption of the uniform dissolution in the alloy. However, this is not enough to account for the lower pH values obtained from the experiment. The

reason for much lower pH-values obtained in the crevice width of 12 μm is the relative error in the crevice width because there is no way to put two pieces of Lucite together without any space between them. Suppose that there is an additional space between the two pieces of Lucite except for the groove. The actual reaction volumes are larger than those used in the calculation. If the additional space is constant in all different crevice widths, the actual reaction volume in the crevice width of 12 μm will be increased most relative to its reaction volume used in the calculation. Therefore, the actual pH values should be higher than those obtained in the calculation.

The second reason for higher pH values in the calculation is that in the model it is assumed that all the reactions are mononuclear reactions. However, with an increase in concentration of chromium ions in the solution, Cr(III) hydroxide has a strong tendency to polymerize. Baes and Wesmer (174) and Rollinson (177) described those reactions quite extensively. This gives rise to bridged complexes, from dimer to colloidal compounds. For example:

$$[Cr(H_2O)_6]^{3+} \rightleftharpoons [Cr(H_2O)_5OH]^{2+} + H^+ \qquad (64)$$

then olation:

$$[Cr(H_2O)_6]^{3+} + [Cr(H_2O)_5OH]^{2+} \longrightarrow [(H_2O)_5Cr\ \underset{\displaystyle H}{\overset{\displaystyle O}{\diagup\diagdown}}\ Cr(H_2O)_5]^{5+} + H_2O \qquad (65)$$

The dial and any complex containing H_2O may act as an acid. It means that H^+ is released and a new -OH bridge may be created leading to growing molecules.
From there oxalation may occur:

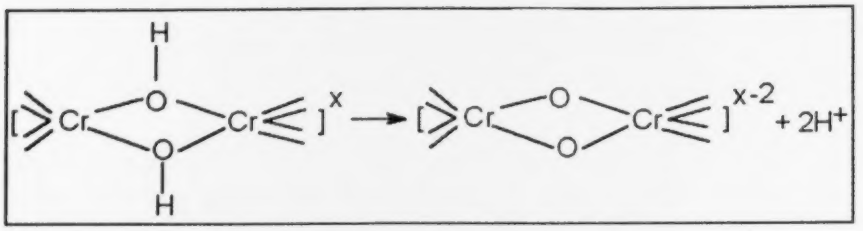

(66)

With chlorides, equilibria between oxychlorocomplexes are present:

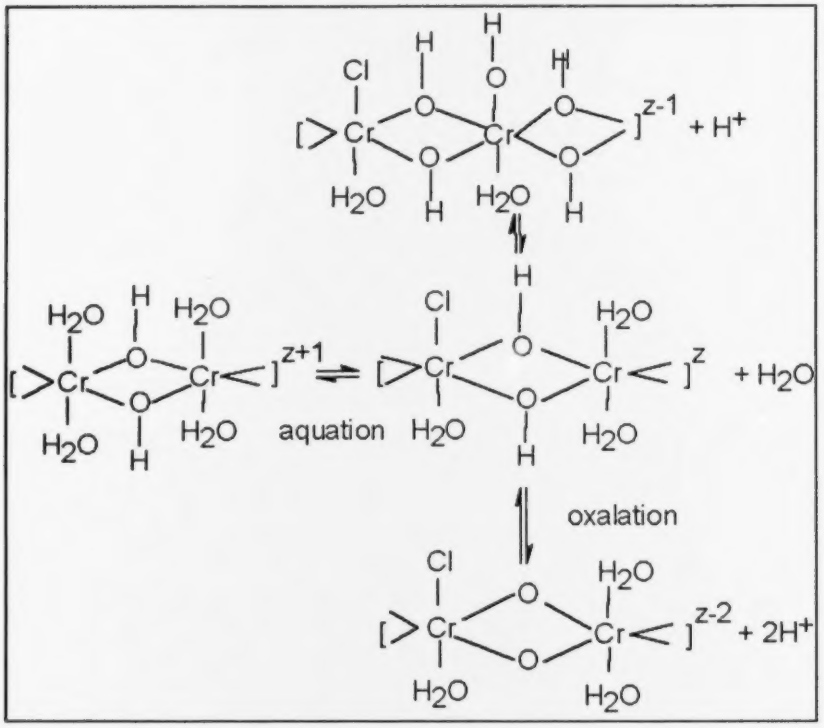

(67)

Hydrogen ions are released from the -OH ions, leaving the -O- as a bridge between the chromium ions. Therefore, more hydrogen ions can be produced by the complexing of chromium ions within the crevice which leads to lower pH values within the crevice. This may explain why pH values obtained in the experiment were lower than those calculated in the mathematical model.

6.6.2 Effect of Iron Ions within a Crevice on the pH Value

In the model, it is assumed that all produced iron ions are in form of Fe^{2+}. However, in the condition of the applied anodic potential, some of the Fe(II) may become Fe(III). Kho et al. (187) studied the anodic behavior of iron in ammoniacal carbonate solution and found that the thickness of the passive layer and the Fe(III)/Fe(II) ratio increase with noble potentials in the passive region. Peterson et al. (83) carried out crevice tests using Type 304 stainless steel in the form of three-inch O-ring, flange seals. The tests were conducted in seawater for a period of 393 days. The analysis of the solution chemistry indicated that there is a strong indication of Fe^{2+} ions but only a trace of Fe^{3+} in the active cell or under cathodic protection from mild steel anodes. But under cathodic protection from zinc anodes, there is no trace indication of Fe^{3+} in the solution. Therefore, it can be reasonably assumed that under the applied anodic potential, there must be a certain amount of Fe^{3+} produced in measurement of the polarization curve.

In order to approximately estimate the effect of Fe^{3+} ions on the pH value within the crevice, the pH values for the last point in each crevice width are simply calculated by considering hydrolysis of Fe^{3+} ions within the crevice using the same method as for hydrolysis of Cr^{3+} ions. To simply the calculation, it is assumed that all Fe(II) ions produced within the crevice finally become Fe(III) ions. Assume at equilibrium, the concentration of $[Fe^{3+}] = G_1$, $[Fe(OH)^{2+}] = H_1$, $[Fe(OH)_2^{+}] = J_1$, $[Fe(OH)_3] = L_1$, $[H^+] = S_1$. According to equilibria in Table 17, the following equations can be obtained:

$$\begin{array}{lll} Fe^{3+} + H_2O \rightleftharpoons Fe(OH)^{2+} + H^+ & & K_{11} = 3.71\times10^{-3} \\ G_1 \qquad\qquad\qquad H_1 \quad S_1 & & \end{array}$$

$$H_1S_1/G_1 = K_{11} \tag{67}$$

$$\begin{array}{lll} Fe(OH)^{2+} + H_2O \rightleftharpoons Fe(OH)_2^{+} + H^+ & & K_{12} = 2.04\times10^{-5} \\ H_1 \qquad\qquad\qquad J_1 \quad S_1 & & \end{array}$$

$$J_1S_1/H_1 = K_{12} \tag{68}$$

$$Fe(OH)_2^+ + H_2O \rightleftharpoons Fe(OH)_3(aq) + H^+ \qquad K_{13} = 4.60\times10^{-8}$$

$$J_1 \qquad\qquad L_1 \qquad S_1$$

$$L_1S_1/J_1 = K_{13} \tag{69}$$

From the mass balance, the following two equations can be got:

$$[Fe^{3+}]_T = G_1 + H_1 + J_1 + L_1 \tag{70}$$

$$[OH^-]_T = H_1 + 2J_1 + 3L_1 - S_1 \tag{71}$$

where $[Fe^{3+}]_T$ is equal to the total amount of Fe^{2+} produced in the reaction volume up to the last point and $[OH^-]_T$ is the total amount of OH^- produced in the reaction volume by reduction of oxygen. Since there are five equations and five unknown variables, the concentration of hydrogen ions in the reaction volume can be calculated from these equations as was done for chromium ions. The results are shown in Table 23.

From Table 23, it can been seen that after assuming that all Fe^{2+} ions become Fe^{3+} ions within the crevice, the calculated pH values are very close to the experimental values except for the calculated pH value at the crevice width of 12 μm. Of course, in practice, it is impossible that all Fe^{2+} ions become Fe^{3+} ions within the crevice, but from the rough calculation, it is shown that when some of the Fe^{2+} ions become Fe^{3+} ions, the pH values are affected within the crevice.

6.6.3 Effect of Diffusion of Hydrogen Ions on the pH Values

In the calculation of pH values along the potentiodynamic polarization curve, it is assumed that all produced hydrogen ions are uniformly dissolved in the extended solution volume by ignoring the diffusion gradient of hydrogen ions. However, in practice, a concentration gradient of hydrogen ions will form during the diffusion. Therefore, the real concentration of hydrogen ions in the reaction volume would be higher than that if the concentration gradient is ignored during the diffusion process and

lower pH values within the crevice will be expected than those obtained from the theoretical calculation.

From the above discussion, it can be seen that after considering the effect of chromium ions, iron ions and diffusion gradient on the pH values within the crevice, the reason that the calculated pH values for the last two or three points within the crevice are greater than those from the experiment, except those in the narrowest crevice (12 μm), can be quite reasonably explained. This also indicates that the proposed mathematical model needs further improvement in order to better understand the mechanism of crevice corrosion.

6.7 Implication of the Mathematical Model to Crevice Corrosion

The pH change along the polarization curve, calculated in the model, shows that under applied potential conditions, the pH value at the point of breakdown of the passive film is much higher than the critical pH necessary for initiation of crevice corrosion. This indicates that from a thermodynamic point of view, the crevice solution at the point of passive film breakdown does not become so aggressive as to cause the breakdown of passive film. It is the applied potential that initiates crevice corrosion. Therefore, this means that the mechanism of crevice corrosion under applied potential is different from Oldfield and Sutton's four-stage mechanism of crevice corrosion in natural crevice corrosion conditions.

In the present model, the effect of applied potential on the process of crevice corrosion is not considered and the calculation of pH within the crevice is based on the thermodynamic equilibrium. As the applied potential, instead of the critical pH value, plays the dominant role in breaking down the passive film during the measurement of the polarization curve, it is impossible to predict the condition for passive film breakdown from pH calculations alone. However, as the calculated pH from the model is in good agreement with the experimental results, this indicates that the assumptions made in the model are quite reasonable. Therefore, under natural crevice corrosion conditions, it is possible to apply the model for calculation of pH within a crevice as long as the passive

current, geometry of crevice, etc., are obtained in order to find out the critical pH for initiation of crevice corrosion.

7. CONCLUSIONS

A novel system has been constructed to measure the cyclic potentiodynamic polarization curves of AISI 303, 304 and 316 stainless steels by controlling potential inside a crevice, with the pH variations within the crevice being recorded during the scan. The effects of different crevice widths, temperatures and concentrations of sodium chloride on the cyclic potentiodynamic polarization curves have also been studied. Based on the passed charge during the scan and the four-stage mechanism of crevice corrosion, a mathematical model is developed to calculate the pH values along the polarization curve. From the experimental and theoretical results and discussion above, the following conclusions can be drawn:

1. A significant difference was found between electrodes controlling potential inside or outside a crevice. The method controlling potential inside a crevice simulates better the electrochemical characteristics in crevice corrosion.
2. In the situation of applied potential, it is not a pH decrease to a certain critical value that causes the initiation of crevice corrosion of AISI 304, 303, or 316 stainless steels. Even at different temperatures and different NaCl concentrations, when the passive film is broken down, the pH within the crevice is not low enough to come close to a critical pH value. It is the applied potential that first breaks down the passive film on a few vulnerable sites, such as MnS inclusions, and then pits spread to become general corrosion.
3. With an increase of crevice width, the pH within the crevice becomes higher and crevice corrosion becomes less serious. When a crevice width reaches 330 μm, crevice corrosion in 303, 304 and 316 stainless steels is no longer in existence. Pitting corrosion takes place.
4. The critical initiation potential E_{cp} obtained by controlling the potential inside a crevice can be used to evaluate the susceptibility of stainless steel. With a decrease

of crevice widths, and an increase of temperature and NaCl concentrations, crevice corrosion becomes more serious and the critical initiation potential E_{cp} is also decreased. The critical initiation potential E_{cp} of crevice corrosion in 316 stainless steel is the highest and the critical initiation potential E_{cp} of crevice corrosion in 303 stainless steel is lowest at the same crevice width among the three stainless steels of 303, 304 and 316. This indicates that the lower the critical initiation potential E_{cp}, the more serious the crevice corrosion. The conclusion agrees with other authors' conclusions obtained by using the method of controlling the potential outside a crevice (108,155,156).

5. The difference between E_{cp} and E_{prot} obtained by controlling the potential inside a crevice is not a good indicator to be used to evaluate the susceptibility of stainless steels to crevice corrosion. With an increase of crevice widths, the difference between E_{cp} and E_{prot} is decreased. However, with an increase of NaCl concentration, temperature or change in alloy composition, the differences between E_{cp} and E_{prot} do not follow the change of the seriousness of crevice corrosion.
6. The critical initiation potential E_{cp} and protection potential E_{prot} obtained under the condition of controlling the potential inside a crevice have a definite dependence on the crevice width and scan rate. With an increase of scan rate, the critical potential E_{cp} and E_{prot} are decreased slightly. This conclusion also agrees with some authors' conclusions obtained by controlling potential outside a crevice (62, 152).
7. Based on corrosion current from the crevice and assuming immediate thermodynamic equilibrium, a mathematical model is developed to calculate the pH change within the crevice, with theoretical results in good agreement with the experimental results. This indicates that the assumptions made on the processes of crevice corrosion are reasonably correct.

8. SUGGESTIONS FOR FURTHER WORK

Using the novel experimental set-up of controlling the potential inside a crevice many good results have been obtained and a very important conclusion has been drawn that it is the applied potential that caused the initiation of crevice corrosion in electrochemical tests instead of a critical pH value. However, in Fig. 33 (53), when the outer surface is controlled at a constant potential, the potential inside the crevice is not constant. According to the potential-shift mechanism of crevice corrosion (29,34), the potential inside a crevice shifts to a more negative potential into the active region. Therefore, if the experimental set-up can been improved later to measure the potential distribution along the crevice length and also to measure the Cl^- concentration within the crevice when the potential at a point inside a crevice is controlled, then one could see whether the potential inside a crevice is the same value as the applied potential or not. This would further the present study.

Some aspects in the proposed mathematical model also need to be further improved because, for example, in this model the diffusion process of metal and hydrogen ions within the crevice is too simply dealt with, and preferential dissolution of metal ions is not considered. If a more strict way is developed to account for the diffusion process and the preferential dissolution of the alloy, a better simulation of results could be obtained. On the other hand, if the Cl^- concentration within the crevice can be recorded along with the pH value, then the Cl^- concentration could also be calculated from the assumption of charge neutrality in the reaction volume. By comparing the calculated Cl^- concentration with experimental results, perhaps the role of Cl^- in crevice corrosion could be better understood.

Table 1 Critical pH Value and Corrosion Rates in Crevices for Various Stainless Steels Exposed in Natural Seawater for Two Years (Ref. 118)

Critical pH Range	Corrosion Rate in Crevice, $g/cm^2 \cdot y$	Types of Stainless Steels
2.7 to 2.2	0.030 to 0.015	13Cr, 13Cr-Mo, 13Cr-2Mo, 13Cr-Cu, 13Cr-B, 14Cr-18Mn, 17Cr 25Cr, 17Cr-2Ni-Al
2.2 to 1.4	0.015 to 0.005	17Cr-2Ni, 17Cr-2Ni-Mo, 17Cr-2Ni-B, 14Cr-14Mn, 14Cr-14Mn-Ti, 14Cr-14Mn-N, 14Cr-14Mn-Ni, 14Cr-14Mn-Cu, 18Cr-6Ni-N
1.4 to 0.4	0.005 to 0.003	18Cr-9Ni, 23Cr-18Ni, 16Cr-6Ni-Cu-N, 16Cr-10Ni-Cu, 17Cr-2Ni-2Mo 17Cr-Ti, 18Cr-6Ni-Cu-Nb-N, 18Cr-11Ni-Nb
0.4 to −0.1	0.003 to 0.001	18Cr-9Ni-Ti, 21Cr-3Ni-Ti, 21Cr-5Ni-Ti, 28Cr, 18Cr-9Ni-Ti-B, 21Cr-5Ni-Ti, 21Cr-6Ni-2Mo-Ti, 17Cr-12Ni-3Mo-Ti

Table 2 Crevice Corrosion of Various Metals in Contact with Red Medical Rubber (Free Exposed Area to Crevice Area = 3:1; Crevice Area = 15 cm^2; Exposure Time = 100 Days; 0.5M NaCl) (Ref. 130)

Material	Attacked Area (cm^2)	Average Pit Depth (mm/y)
13Cr	1.12	1.67
17Cr	0.25	1.52
28Cr	0.01	0.22
18Cr-9Ni	0.20	1.30
18Cr-9Ni-Ti	0.17	0.85
13Cr-4Ni-9Mn	0.90	0.67
18Cr-9Ni-3Mo-Ti	0.00	0.00
18Cr-15Ni-2Mo-Nb	0.15	0.74
18Cr-12Ni-3Mo-Ti	0.00	0.00
18Cr-11Ni-Nb	0.13	0.67
18Cr-12Ni-2Mo-Ti	0.00	0.00
Chromium	0.00	0.00
Nickel	Dark Spots	0.00
Molybdenum	0.00	0.00
Titanium	0.00	0.00

Table 3 Chemical Composition of the Test Stainless Steels

	C	Cr	Mn	Ni	S	Si	Mo	Fe
AISI 303	0.10	17.80	1.70	8.68	0.15	1.30		Bal.
AISI 304	0.08	18.04	1.40	9.27	0.03	1.40		Bal.
AISI 316	0.08	18.30	1.20	11.58	0.03	1.10	2.35	Bal.

Table 4 The Critical Potentials E_{cp} and E_{prot} for AISI 304 Stainless Steel at Different Crevice Widths in 10% NaCl Solution at a Temperature of 20°C and Scan Rate of 0.5 mV/s

	12 μm	40 μm	96 μm	180 μm	330 μm
E_{cp}(mV)	-44	-38	-29	0	6
E_{prot}(mV)	-265	-235	-218	-161	-127
E_{cp}-E_{prot}(mV)	221	197	189	161	133

Table 5 The Critical Potentials E_{cp} and E_{prot} for AISI 303 Stainless Steel at Different Crevice Widths in 10% NaCl Solution at a Temperature of 20°C and Scan Rate of 0.5 mV/s

	12 μm	40 μm	96 μm	180 μm	330 μm
E_{cp}(mV)	-137	-106	-99	-86	-72
E_{prot}(mV)	-382	-342	-336	-247	-157
E_{cp}-E_{prot}(mV)	245	236	237	161	85

Table 6 **The Critical Potentials E_{cp} and E_{prot} for AISI 316 Stainless Steel at Different Crevice Widths in 10% NaCl Solution at a Temperature of 20°C and Scan Rate of 0.5 mV/s**

	12 μm	40 μm	96 μm	180 μm	330 μm
E_{cp}(mV)	25	34	45	54	55
E_{prot}(mV)	-223	-199	-160	-95	-54
E_{cp}-E_{prot}(mV)	248	233	205	149	99

Table 7 **The Critical Potentials E_{cp} and E_{prot} for Different Stainless Steels at Crevice Width of 12 μm in 10% NaCl Solution at a Temperature of 20°C and Scan Rate of 0.5 mV/s**

	AISI 303	AISI 304	AISI 316
E_{cp}(mV)	-137	-44	25
E_{prot}(mV)	-382	-265	-223
E_{cp}-E_{prot}(mV)	245	221	248

Table 8 **The Critical Potentials E_{cp} and E_{prot} for Different Stainless Steels at Crevice Width of 40 μm in 10% NaCl Solution at a Temperature of 20°C and Scan Rate of 0.5 mV/s**

	AISI 303	AISI 304	AISI 316
E_{cp}(mV)	-106	-38	34
E_{prot}(mV)	-342	-235	-199
E_{cp}-E_{prot}(mV)	236	197	233

Table 9 The Critical Potentials E_{cp} and E_{prot} for Different Stainless Steels at Crevice Width of 96 μm in 10% NaCl Solution at a Temperature of 20°C and Scan Rate of 0.5 mV/s

	AISI 303	AISI 304	AISI 316
E_{cp}(mV)	-99	-29	45
E_{prot}(mV)	-336	-218	-160
E_{cp}-E_{prot}(mV)	237	189	205

Table 10 The Critical Potentials E_{cp} and E_{prot} for Different Stainless Steels at Crevice Width of 180 μm in 10% NaCl Solution at a Temperature of 20°C and Scan Rate of 0.5 mV/s

	AISI 303	AISI 304	AISI 316
E_{cp}(mV)	-86	0	54
E_{prot}(mV)	-247	-161	-159
E_{cp}-E_{prot}(mV)	161	161	213

Table 11 Effect of Seawater Temperature on the Probability of Crevice Corrosion Initiation. Multiple Crevice Test, 30 Day Exposure (Ref. 157)

Stainless Steel	Probability of Crevice Corrosion Initiation, %			
	5°C	15°C	25°C	50°C
Type 304	2	13	70	90
Type 316	0	2	51	21
Type 317	0	0	1.4	4
Type 430	0.8	52	98	98
Type 446	0	7	43	19
E-BRITE 26-1	0	0	0	4

Table 12 The Critical Potentials E_{cp} and E_{prot} for AISI 304 Stainless Steel at Different Temperatures (°C) for a Crevice Width of 12 μm in 10% NaCl Solution with a Scan Rate of 0.5 mV/s

Temperature	10°C	20°C	25°C	35°C
E_{cp}(mV)	49	-44	-47	-69
E_{prot}(mV)	-216	-265	-228	270
E_{cp}-E_{prot}(mV)	265	221	181	201

Table 13 The Critical Potentials E_{cp} and E_{prot} for AISI 304 Stainless Steel at Different Temperatures (°C) for a Crevice Width of 12 μm in 10% NaCl Solution with a Scan Rate of 0.2 mV/s

Temperature	10°C	20°C	25°C	35°C
E_{cp}(mV)	65	-16	-24	-69
E_{prot}(mV)	-220	-257	-205	-314
E_{cp}-E_{prot}(mV)	285	241	181	245

Table 14 The Critical Potentials E_{cp} and E_{prot} for AISI 304 Stainless Steel at Different NaCl Concentrations for a Crevice Width of 12 μm at a Temperature of 20°C and Scan Rate of 0.5 mV/s

Concentrations(wt.%)	3.5	10	15
E_{cp}(mV)	-4	-44	-74
E_{prot}(mV)	-237	-265	-283
E_{cp}-E_{prot}(mV)	233	221	209

Table 15 The Critical Potentials E_{cp} and E_{prot} for AISI 304 Stainless Steel at Different NaCl Concentrations for a Crevice Width of 12 μm at a Temperature of 20°C and Scan Rate of 0.2 mV/s

Concentrations(wt.%)	3.5	10	15
E_{cp}(mV)	7	-16	-66
E_{prot}(mV)	-246	-257	-291
E_{cp}-E_{prot}(mV)	253	241	225

Table 16 Diffusion Coefficients of Ions (25°C) (Ref. 169)

Chemical Species	Diffusion Coefficient (10^{-5} cm^2/s)
H^+	9.31
OH^-	5.31
Na^+	1.33
Cl^-	2.03
O_2	1.40
Cr^{3+}	0.59
Fe^{2+}	0.71
Ni^{2+}	0.72

Table 17 Hydrolysis Equilibria

1 $Cr^{3+} + H_2O \rightleftharpoons Cr(OH)^{2+} + H^+$	$K_1 = 1.58\times10^{-4}$ (Ref. 169)
2 $Cr(OH)^{2+} + H_2O \rightleftharpoons Cr(OH)_2^{+} + H^+$	$K_2 = 6.31\times10^{-7}$ (Ref. 169)
3 $Cr(OH)_2^{+} + H_2O \rightleftharpoons Cr(OH)_3(aq) + H^+$	$K_3 = 6.31\times10^{-7}$ (Ref. 169)
4 $Cr(OH)_3(s) \rightleftharpoons Cr^{3+} + 3(OH)^-$	$K_4 = 6\times10^{-31}$ (Ref. 169)
5 $Fe^{2+} + H_2O \rightleftharpoons Fe(OH)^+ + H^+$	$K_5 = 5.0\times10^{-9}$ (Ref. 169)
6 $Fe(OH)^+ + H_2O \rightleftharpoons Fe(OH)_2(aq) + H^+$	$K_6 = 7.49\times10^{-12}$ (Ref. 169)
7 $Fe(OH)_2(s) \rightleftharpoons Fe^{2+} + 2(OH)^-$	$K_7 = 7.49\times10^{-16}$ (Ref. 169)
8 $Ni^{2+} + H_2O \rightleftharpoons Ni(OH)^+ + H^+$	$K_8 = 3.16\times10^{-10}$ (Ref. 169)
9 $Ni(OH)^+ + H_2O \rightleftharpoons Ni(OH)_2(aq) + H^+$	$K_9 = 7.49\times10^{-10}$ (Ref. 169)
10 $Ni(OH)_2(s) \rightleftharpoons Ni^{2+} + 2(OH)^-$	$K_{10} = 1.35\times10^{-15}$ (Ref. 169)
11 $Fe^{3+} + H_2O \rightleftharpoons Fe(OH)^{2+} + H^+$	$K_{11} = 3.71\times10^{-3}$ (Ref. 172)
12 $Fe(OH)^{2+} + H_2O \rightleftharpoons Fe(OH)_2^{+} + H^+$	$K_{12} = 2.04\times10^{-5}$ (Ref. 172)
13 $Fe(OH)_2^{+} + H_2O \rightleftharpoons Fe(OH)_3(aq) + H^+$	$K_{13} = 4.60\times10^{-8}$ (Ref. 173)
14 $Fe(OH)_3(s) \rightleftharpoons Fe^{3+} + 3(OH)^-$	$K_{14} = 4\times10^{-38}$ (Ref. 175)
15 $H_2O \rightleftharpoons H^+ + OH^-$	$K_w = 1\times10^{-14}$ (Ref. 175)

Table 18 pH Values from Experiment and Theoretical Calculation Obtained by Controlling Potential inside a 12 μm Crevice at the Scan Rate of 0.5 mV/s in 10% NaCl Solution of pH about 7.25 at a Temperature of 20°C

Experimental pH Values	Theoretical pH Values for Uniform Dissolution	Theoretical pH Values for Preferential Dissolution
7.60	9.29	9.29
7.73	9.71	9.84
7.50	6.95	6.82
7.00	5.59	4.91
6.00	4.52	4.18
5.00	3.39	3.17
4.00	2.73	2.45
3.00	2.00	1.53
2.00	1.61	1.01
1.91	1.51	0.87
1.96	1.52	0.88

Table 19 pH Values from Experiment and Theoretical Calculation Obtained by Controlling Potential inside a 40 μm Crevice at the Scan Rate of 0.5 mV/s in 10% NaCl Solution of pH about 7.15 at a Temperature of 20°C

Experimental pH Values	Theoretical pH Values for Uniform Dissolution	Theoretical pH Values for Preferential Dissolution
7.54	9.00	9.00
7.69	9.58	9.65
7.00	6.66	6.36
6.00	6.17	4.96
5.00	3.74	3.48
4.00	3.21	2.96
3.00	2.82	2.52
1.98	2.70	2.34
2.03	2.71	2.36

Table 20 pH Values from Experiment and Theoretical Calculation Obtained by Controlling Potential inside a 96 μm Crevice at the Scan Rate of 0.5 mV/s in 10% NaCl Solution of pH about 6.89 at a Temperature of 20°C

Experimental pH Values	Theoretical pH Values for Uniform Dissolution	Theoretical pH Values for Preferential Dissolution
7.11	8.07	8.07
7.15	9.43	9.44
7.00	9.71	9.68
6.50	9.11	8.82
6.00	7.80	6.47
5.75	7.03	5.92
5.00	4.27	3.86
4.00	3.45	3.20
3.00	3.30	3.03
2.23	3.28	3.01
2.25	3.32	3.05

Table 21 pH Values from Experiment and Theoretical Calculation Obtained by Controlling Potential inside a 180 μm Crevice at the Scan Rate of 0.5 mV/s in 10% NaCl Solution of pH about 7.05 at a Temperature of 20°C

Experimental pH Values	Theoretical pH Values for Uniform Dissolution	Theoretical pH Values for Preferential Dissolution
7.34	8.35	8.35
7.61	9.62	9.66
7.00	9.51	9.38
6.00	8.08	7.17
5.50	7.33	5.82
5.00	5.54	4.25
4.00	3.36	3.29
3.00	3.47	3.20
2.63	3.51	3.24

Table 22 pH Values from Experiment and Theoretical Calculation Obtained by Controlling Potential inside a 330 μm Crevice at the Scan Rate of 0.5 mV/s in 10% NaCl Solution of pH about 7.00 at a Temperature of 20°C

Experimental pH Values	Theoretical pH Values
7.35	7.93
7.65	8.77
7.00	8.19
6.50	4.02
6.00	3.70
5.93	3.71
5.97	3.74

Table 23 Comparison of the Theoretical pH Values When Iron Dissolves as Fe^{2+} with the Theoretical pH Values When Iron dissolves as Fe^{3+} for the Last Point on the Polarization Curves

Crevice Width	Experimental pH Values	Theoretical pH Value in the Form of Fe^{2+}	Theoretical pH Values in the Form of Fe^{3+}
12 μm	1.96	1.52	0.50
40 μm	2.03	2.71	1.65
96 μm	2.25	3.32	2.35
188 μm	2.63	3.51	2.42

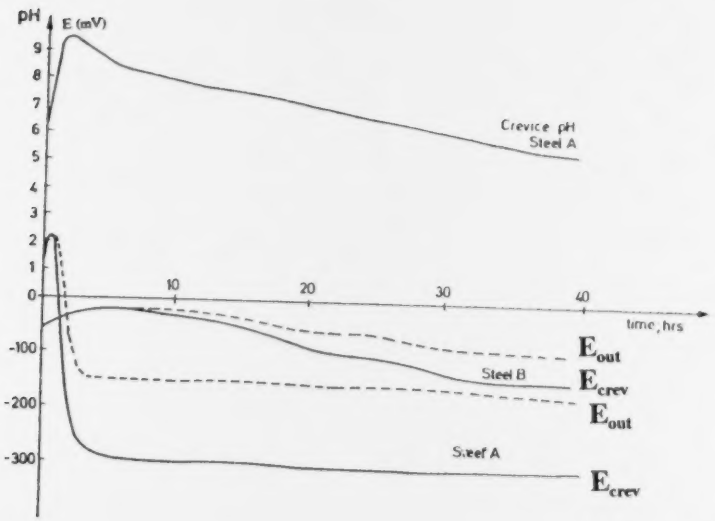

Fig. 1 Potential and pH change for Steel A (13% Cr) and potential change for Steel B (17% Cr) during crevice corrosion. Width of crevice = 0.15mm. $E_{crev.}$ is potential of specimen within crevice. $E_{out.}$ is potential of outer surface (Ref. 18).

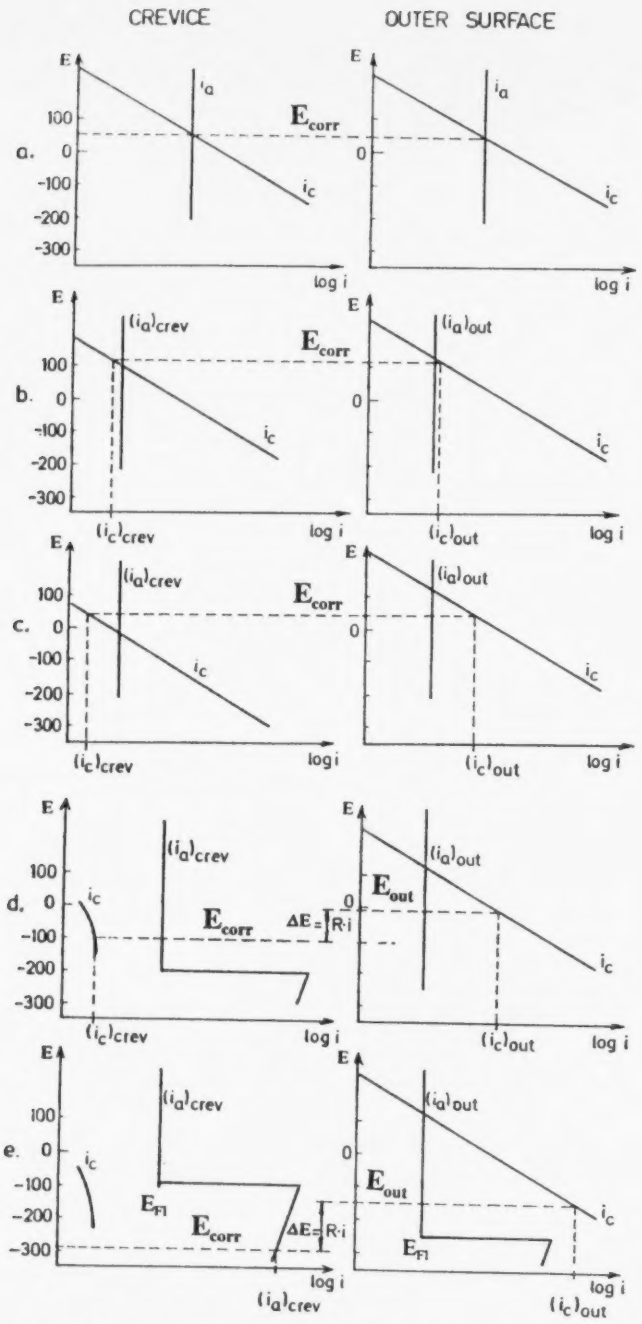

Fig. 2 Mechanism of crevice corrosion initiation stage. I_c and I_a denote cathodic and anodic current on polarization curves. The subscripts crev and out refer to crevice and outer surface respectively. Diagram e shows propagation stage. R = internal (electrolyte) resistance in crevice corrosion cell. E_{Fl} = Flade potential (Ref. 18).

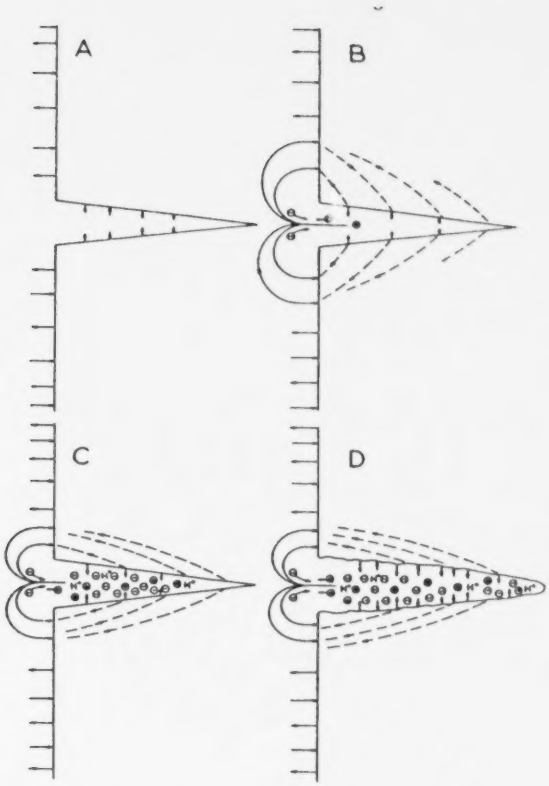

Fig. 3 Schematic representation of the four stages which can be distinguished in the mechanism of the crevice corrosion process on stainless steel. (Ref. 19)
A. Start: general corrosion; B. Differential aeration: local current, migration of ions; C. Increasing concentration of ions, including H^+; D. Depassivation, active/passive cell, propagation.

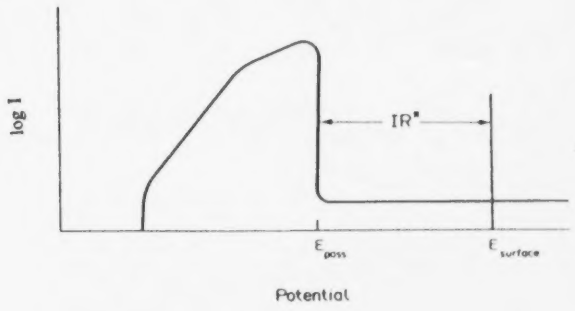

Fig. 4 Schematic polarization curve of the electrolyte within a pit, crevice or crack for the potential shift mechanism (Ref. 31).

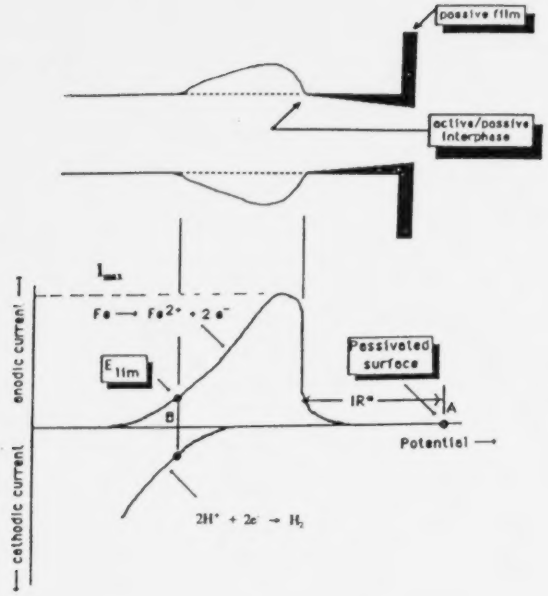

Fig.5 Schematic illustrating the relation between the local cell site in the crevice and the polarization curve of the crevice solution for a sample polarized to potential A in the passive region (Ref.31).

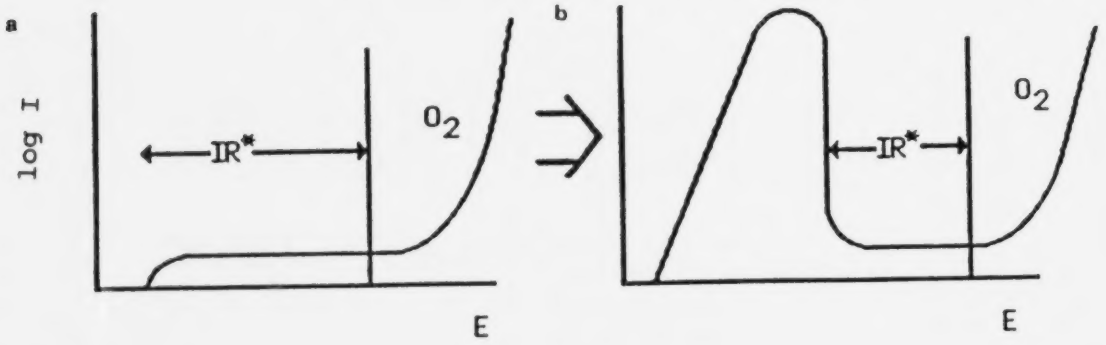

Fig.6 Schematic illustrating a decrease in IR* resulting from development and enlargement of the active region by change in concentration of the cavity solution
(a) no active region appearing for the solution composition in the cavity.
(b) acidification and /or aggressive ion buildup decreasing IR*. (Ref.34).

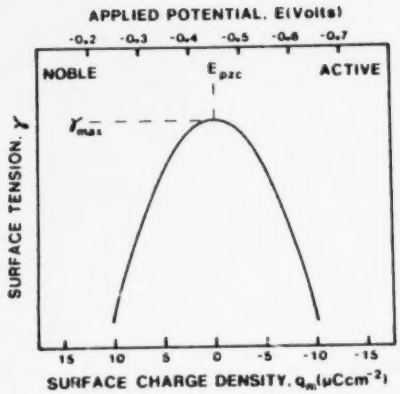

Fig. 7 Schematic representation of $\gamma=\gamma max-2\pi dq_m^2/\epsilon$ with nominal values of E and q_m for illustrative purposes (Ref. 43).

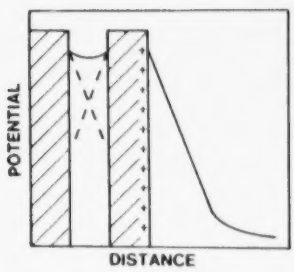

Fig. 8 Model of initial (dashed) and final potential gradients and surface charge densities of parallel metallic plates forming a crevice in which the mirror double layer interacts strongly (Ref. 43).

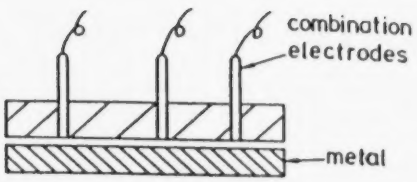

Fig. 9 Crevice set-up (Ref. 53).

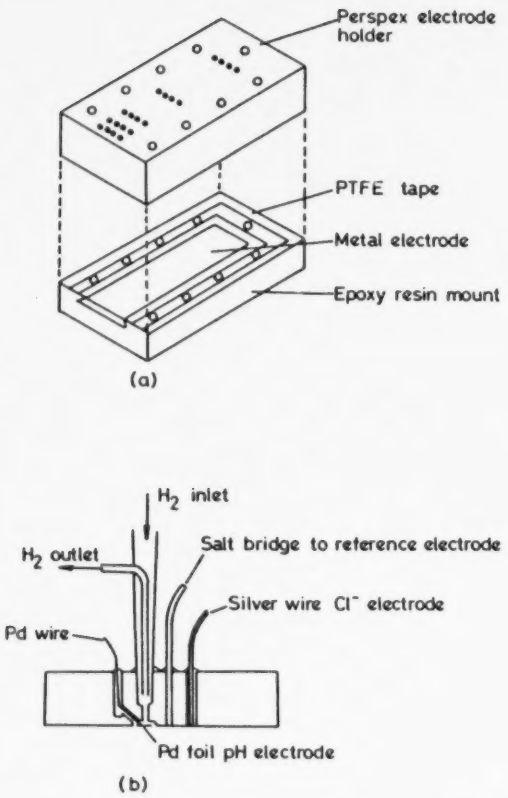

Fig. 10 The metal-Perspex artificial crevice assembly (Ref 66).

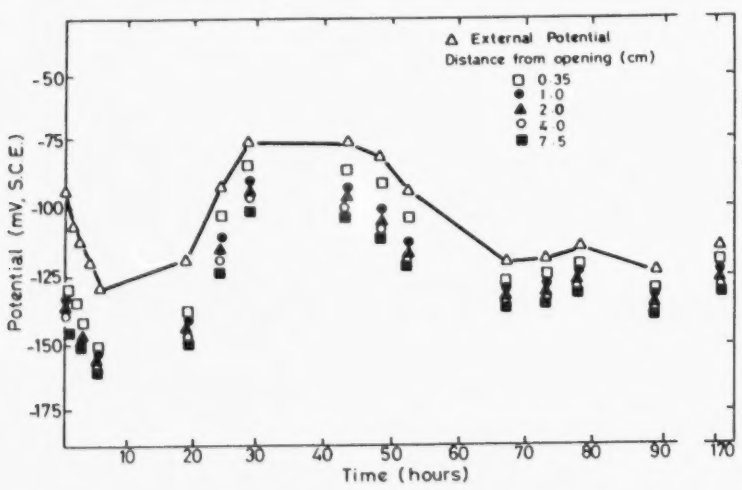

Fig. 11 The variation of potential along the artificial crevice of type 304 stainless steel with time in free corrosion (Ref. 66).

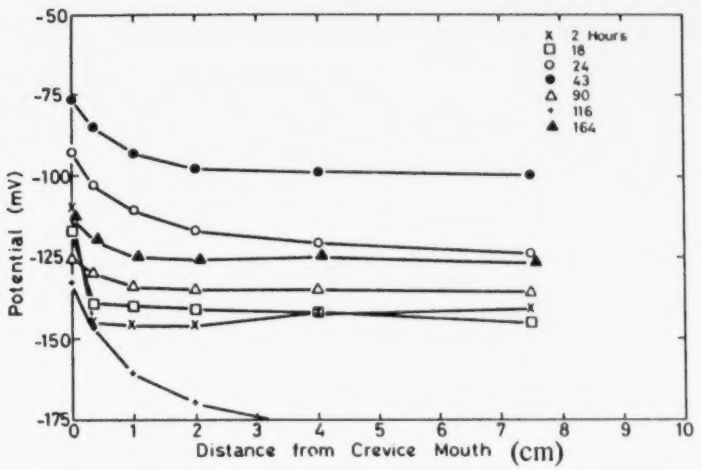

Fig. 12 The variation of potential with distance from crevice mouth measured on the stainless steel (Ref. 66).

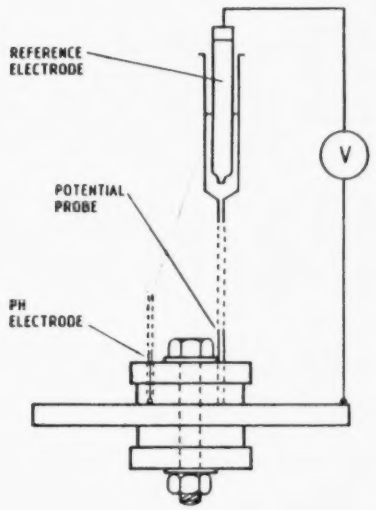

Fig. 13a General arrangement of the artificial crevice (Ref. 67).

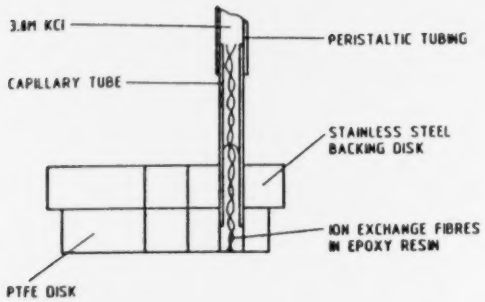

Fig. 13b Detailed construction of the resin fibre potential probe (Ref. 67).

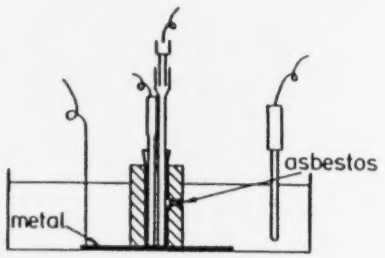

Fig. 14 Crevice corrosion apparatus of two compartment cell (Ref. 53).

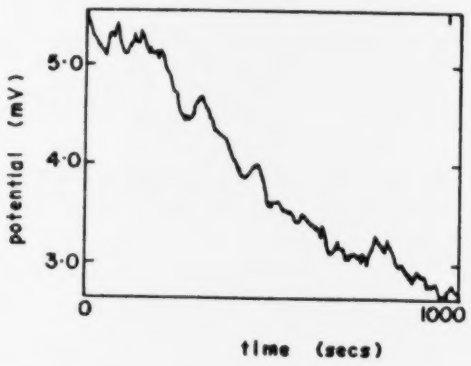

Fig. 15 Time record for mild steel electrode in 0.5 N H_2SO_4
20 min after immersion (sampling rate = 10s) (Ref. 94).

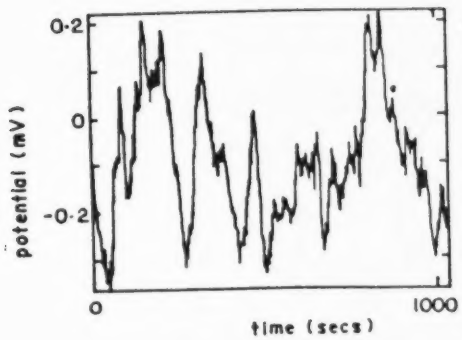

Fig. 16 Time record from Fig. 15 after dc tread removal (Ref. 94).

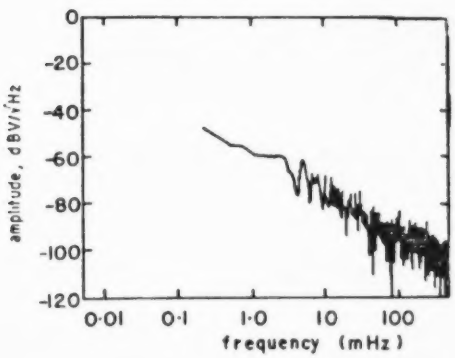

Fig. 17 FFT spectrum for time record shown in Fig. 15 (Ref. 94).

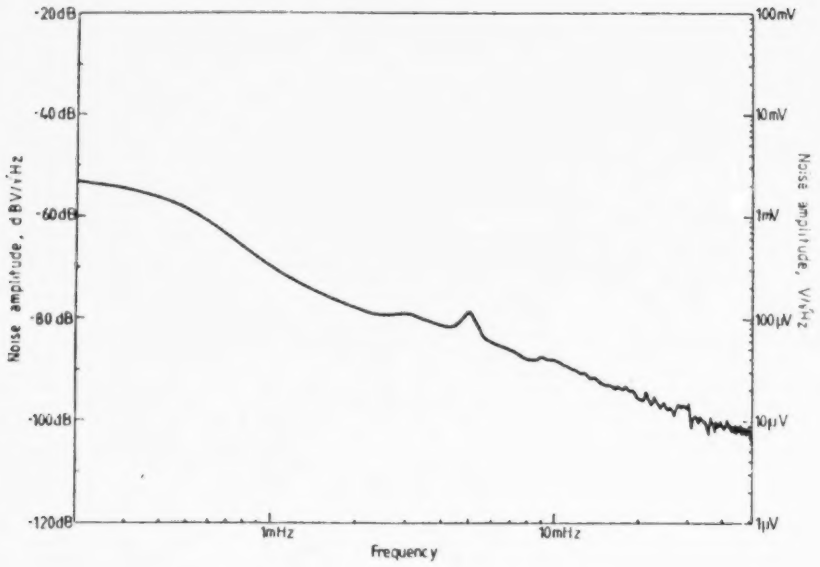

Fig. 18 Memory alloy (Ti-Ni) in 0.3 M HCl. Electrochemical noise amplitude spectrum showing effects of crevice attack (Ref. 95).

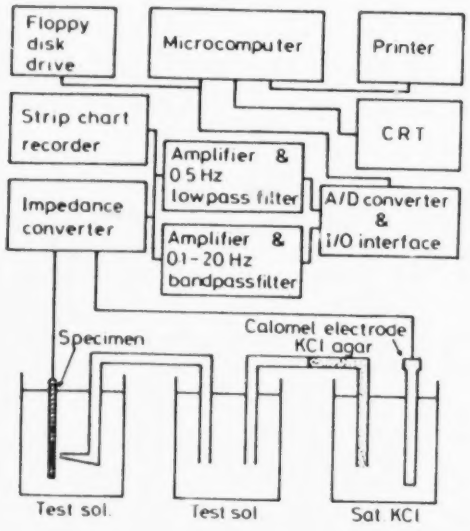

Fig. 19 Schematic diagram of the apparatus for the measurement of corrosion potential fluctuations (Ref. 96).

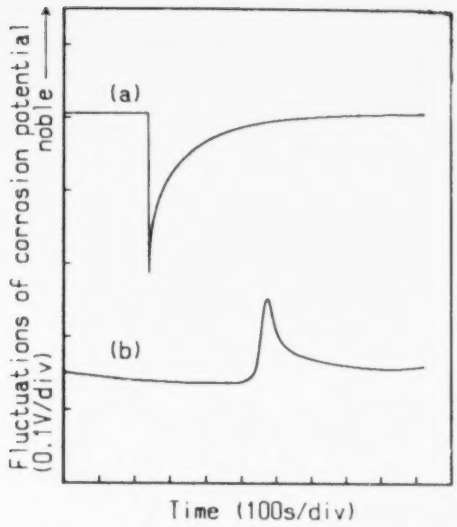

Fig. 20 Typical wave forms of the corrosion potential fluctuations obtained when micropits were formed and when crevice corrosion was proceeding:
(a) 4M NaCl + 0.1M NaClO (pH=11.2), with micropits; (b) 1M NaCl + 0.1M NaClO (pH=11.6), with crevice corrosion (Ref. 96).

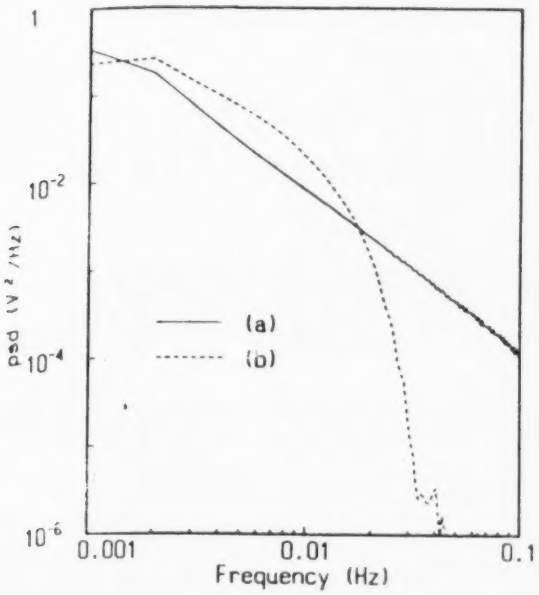

Fig. 21 Power spectral density (psd) of the corrosion potential fluctuation shown in Fig. 20 (Ref. 96).

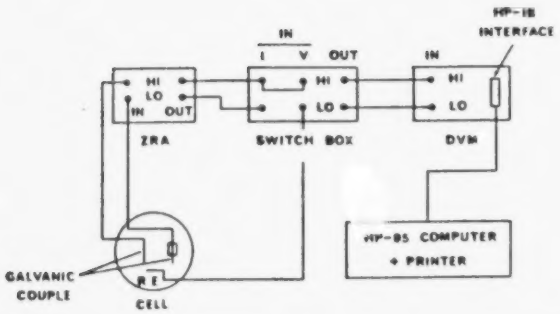

Fig. 22 Electrical setup for simultaneous potential and current noise measurements (Ref. 97).

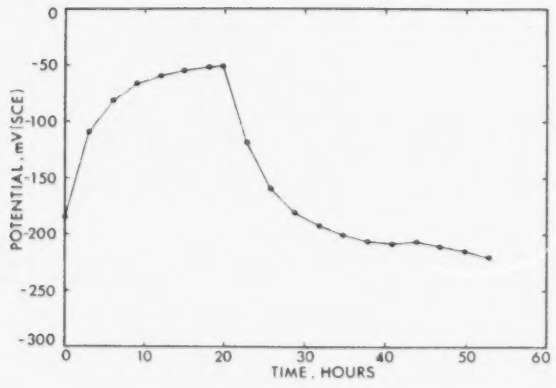

Fig. 23 Potential-time plot for typical galvanic couple (Ref. 97).

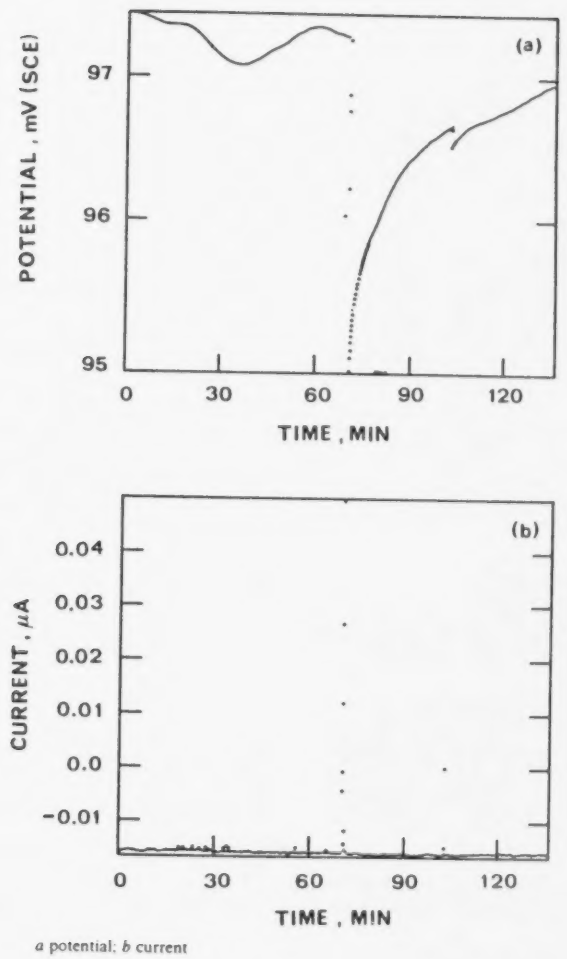

a potential; *b* current

Fig. 24 Potential and current records showing potential and current transients typical of stage 2 of potential evolution (linear treads not removed) Sampling interval 8 s and the ratio of bare electrode area (A_c) to covered electrode area (A_a), $A_c/A_a = 13.8$ and $A_a = 1450$ mm^2 (Ref. 97).

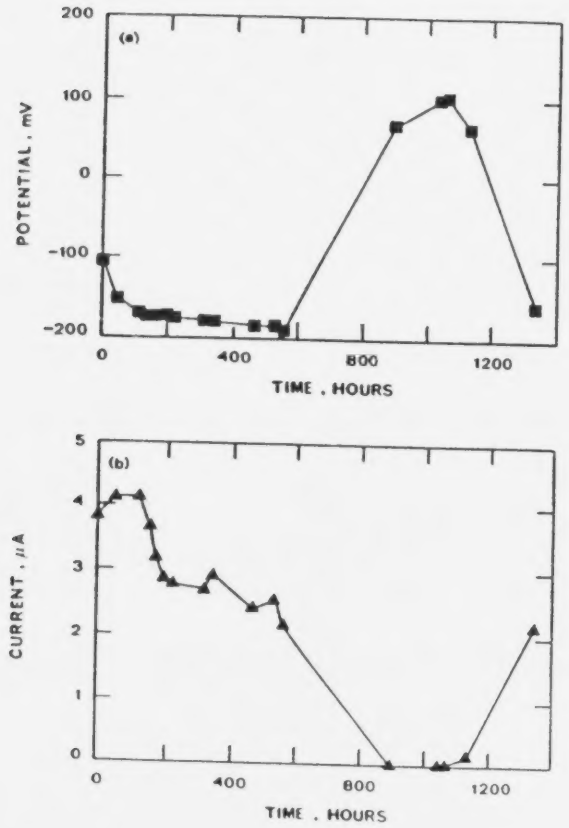

Fig. 25 Variation of potential and current with time for long term experiment (values obtained as in Fig. 23): $A_c/A_a = 13.8$, $A_a = 1450\ mm^2$ (Ref. 97).

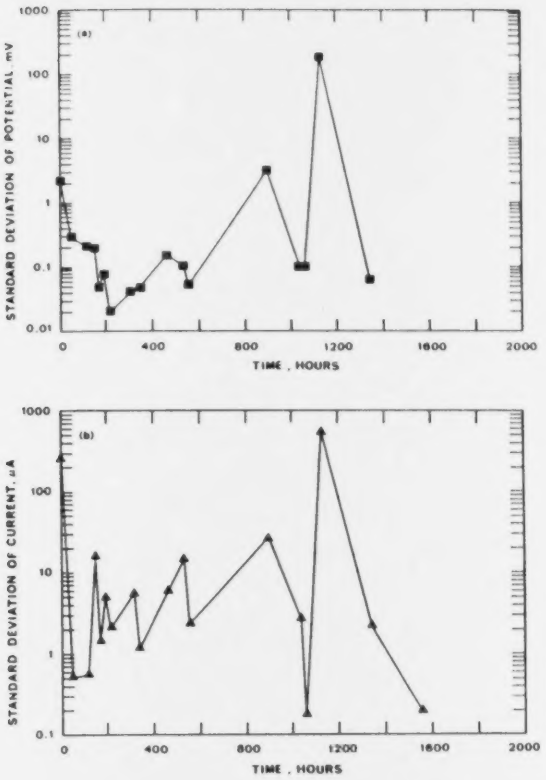

Fig. 26 Variation of standard deviation of potential and current records with time for data in Fig. 25 (Ref. 97).

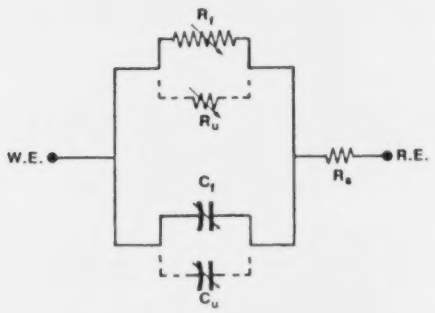

Fig. 27 Hypothetical equivalent circuit for breakdown or repair of air-passivated AA6061 in aqueous chloride solutions. R_u is the charge transfer resistance of the uncovered area; R_f is the passive film resistance; R_s is the solution resistance; C_u is the capacitance of the uncovered area; C_f is the capacitance of the passive film area. (Ref. 101).

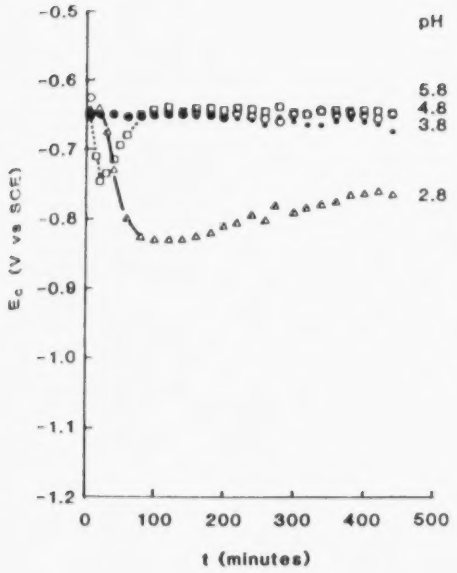

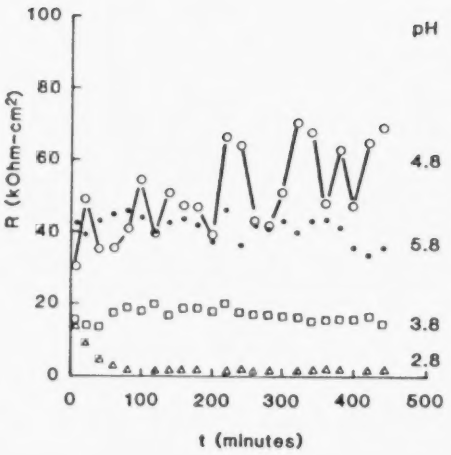

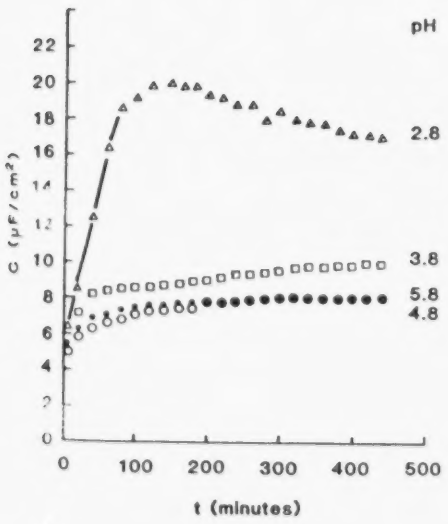

Fig. 28 (a, top left) Corrosion potential as a function of time for AA6061 in air-sparged 0.05N sodium chloride solution and solutions acidified to pH 5.8, 4.8, 3.8 and 2.8. (b, above) Charge transfer resistance as a function of time. (c, left) Double layer capacitance as a function of time (Ref. 101).

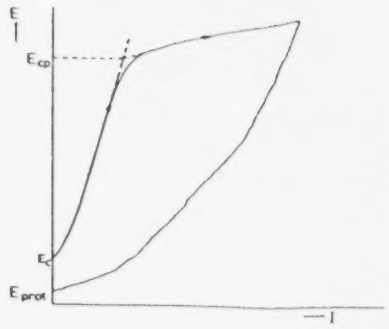

Fig. 29 Polarization diagram obtained with cyclic anodic polarization of stainless steel in chloride solution, showing open-circuit critical pitting potential (E_{cp}) and protection potential (E_{prot}) (Ref. 105).

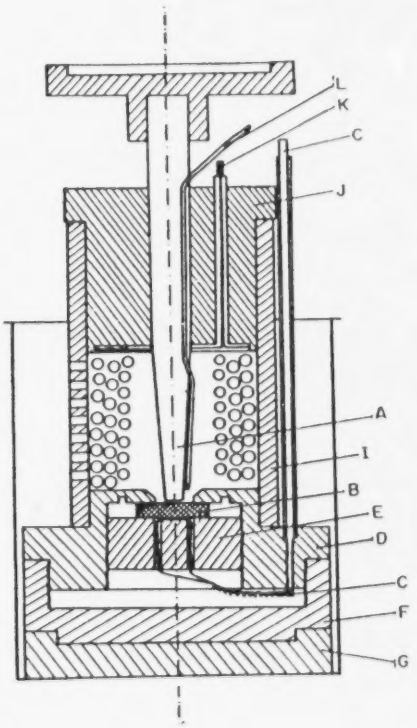

Fig. 30 Assembly used for measurements of the critical potential for crevice corrosion. A-Plexiglas rod; B-specimen; C-specimen lead; D,E-specimen holder; F,G-support; L-Luggin capillary; I-perforated Plexiglas tube; K-lead to the cathode (Ref. 108).

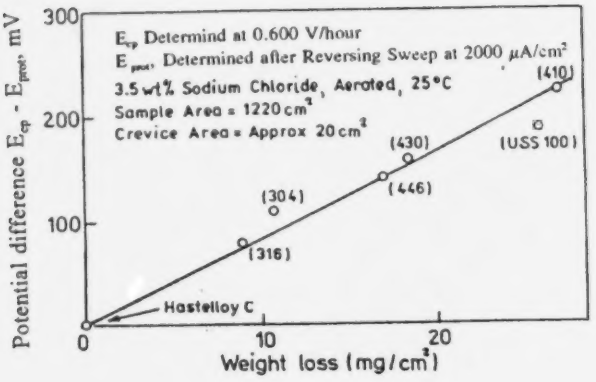

Fig. 31 Correlation of the potential difference E_{cp}-E_{prot} and corrosion weight loss of stainless steels exposed to seawater for 4.25 years (Ref. 109).

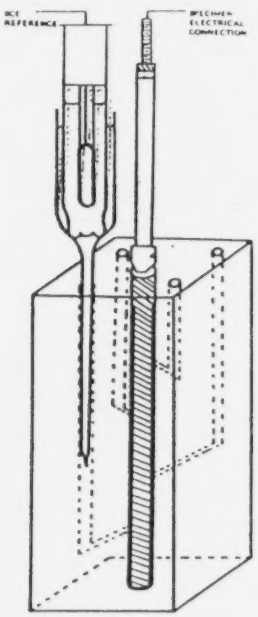

Fig. 32 Electrode assembly fabricated from Plexiglas block for crevice studies. Orifice dimensions: 0.75 cm by 6.25 cm. Internal probe openings spaced at 1.25 cm intervals (Ref. 62).

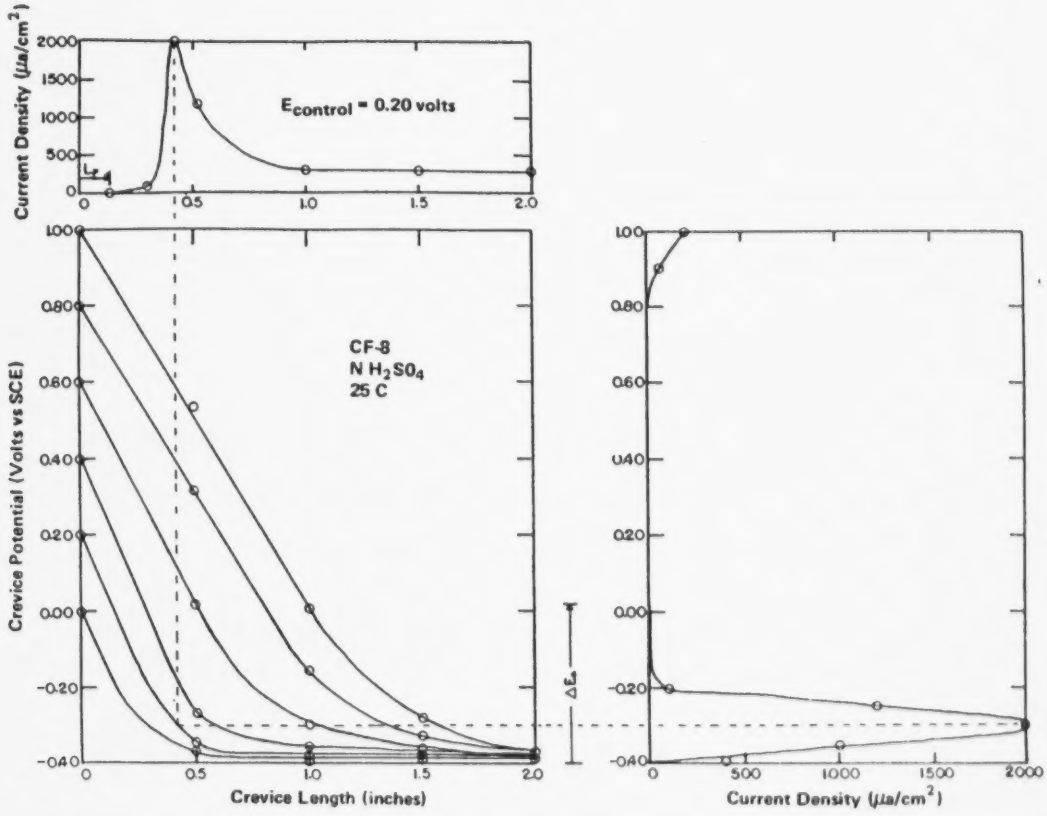

Fig. 33 Crevice potential variation of CF-8 stainless steel together with anodic polarization curve and calculated current distribution. Hydrogen-saturated N H_2SO_4 at 25°C. Crevice width: 0.0225 cm (Ref. 62).

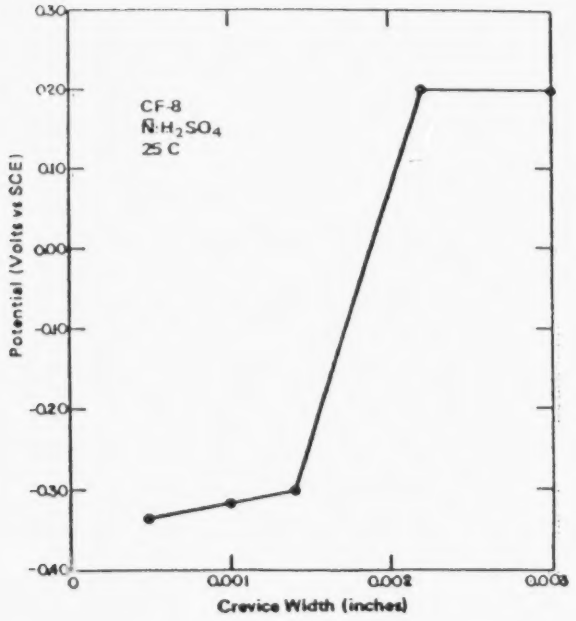

Fig. 34 Crevice potential variation at a depth of 0.625 cm as a function of crevice width. Material: CF-8; control potential: 0.20 V(vs. SCE); N H_2SO_4 at 25°C (Ref. 62).

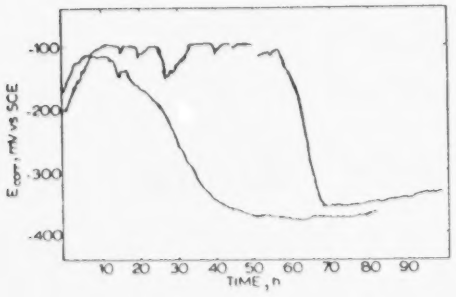

Fig. 35 E_{corr} vs. time: Type 316 crevice with approximately 10 μm gap in 1M NaCl, pH 6, crevice area ratio 1:1 (Ref. 20).

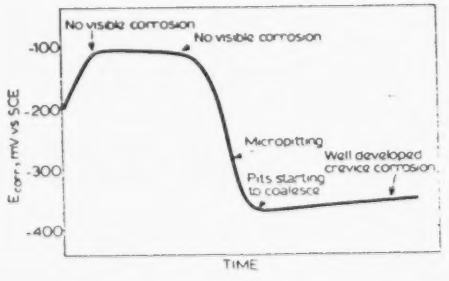

Fig. 36 Schematic composite E_{corr}/time curve showing the development of corrosion in Type 316 crevices (Ref. 20).

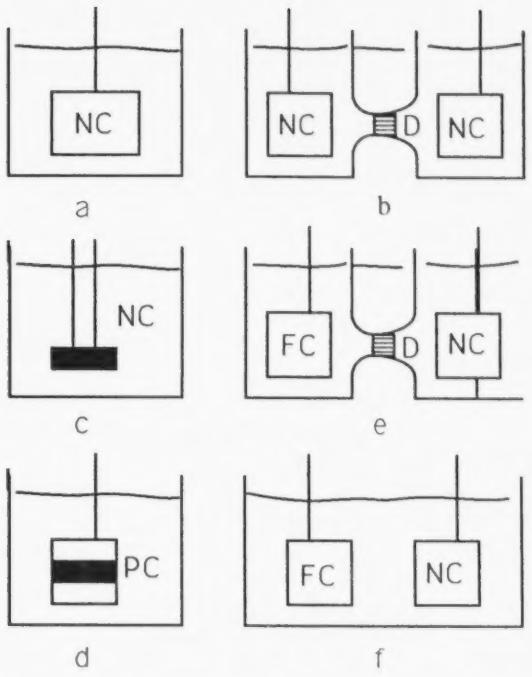

Fig. 37 Schematic representation of different types of experimental possibilities for electrochemical cells to be used in crevice corrosion testing; NC Non-creviced test electrode, PC Partially-creviced electrode FC Fully-creviced electrode, D Diaphragm (Ref. 112).

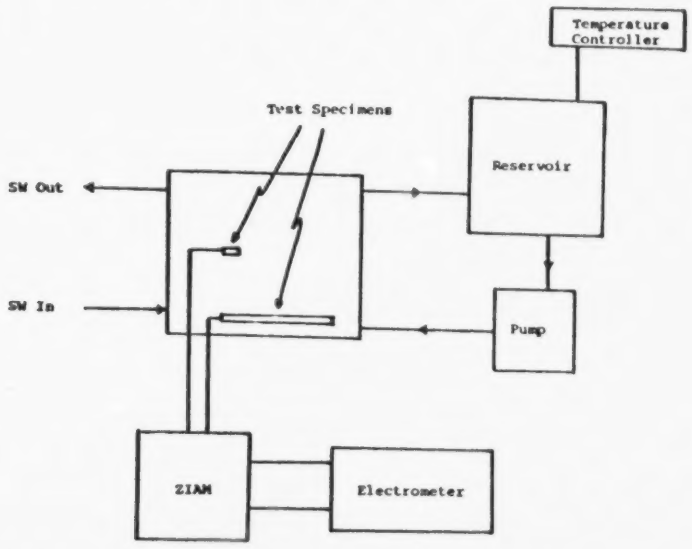

Fig. 38 Schematic of test loop utilized for remote crevice evaluation (Ref. 112).

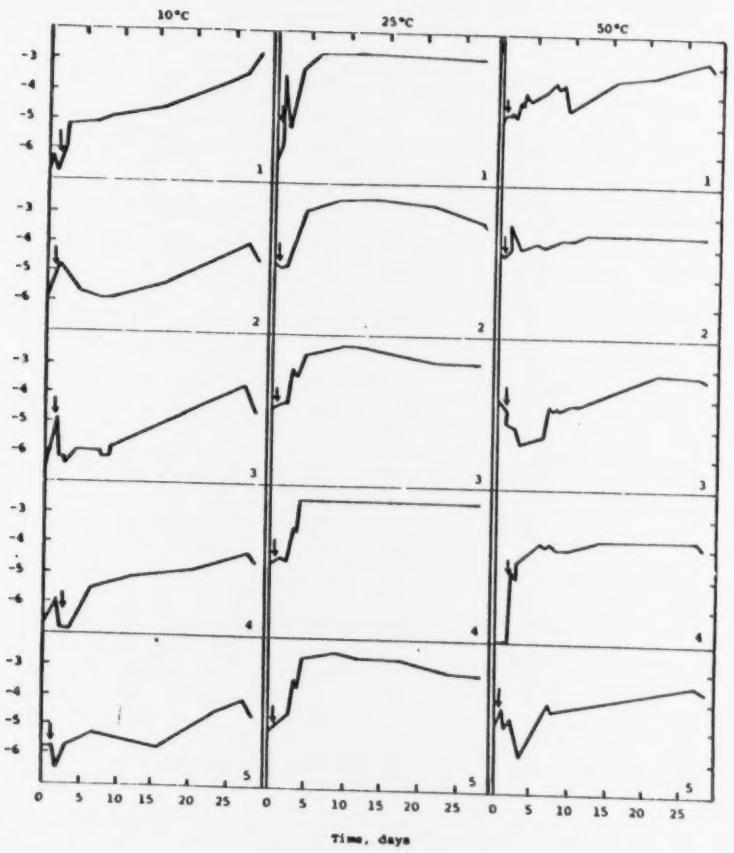

Fig. 39 Current (logarithmic) to remote crevices as a function of time for Type 304 stainless steel during a 28-day exposure in seawater at 10, 25 and 50°C. (Ref. 112).

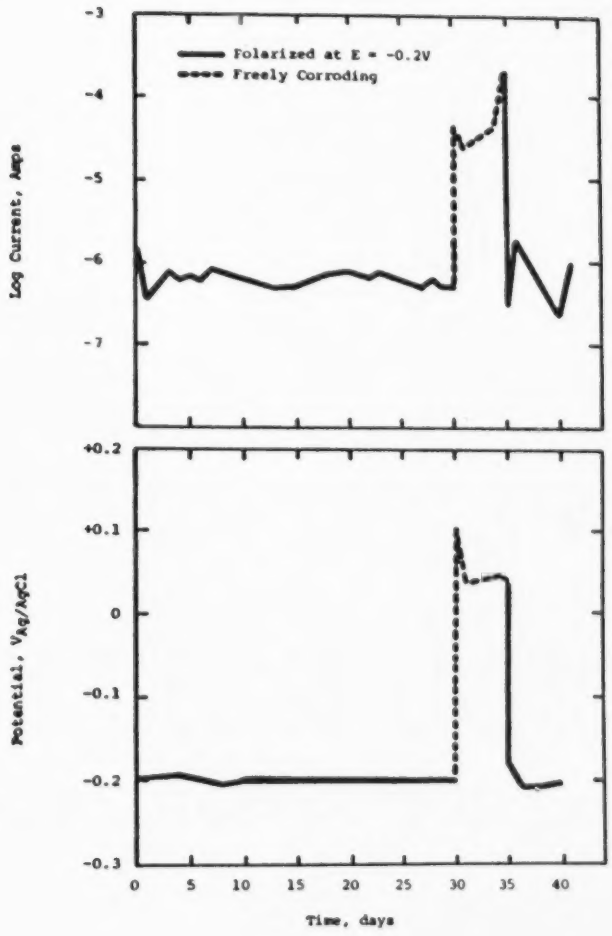

Fig. 40 Typical current (logarithmic) and potential values versus time for Type 304 stainless steel in seawater at 25°C. Specimen was polarized at -0.2 V(Ag/AgCl) between days 0 and 30 and between days 35 and 40. Specimen was freely corroding between days 30 and 35 (Ref. 112).

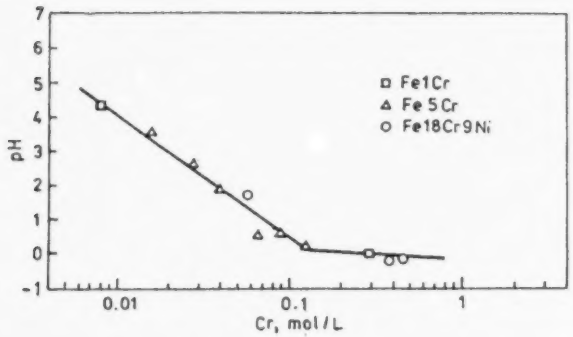

Fig. 41 Relationship between pH and chromium ion concentration in the crevice solution (Ref. 122).

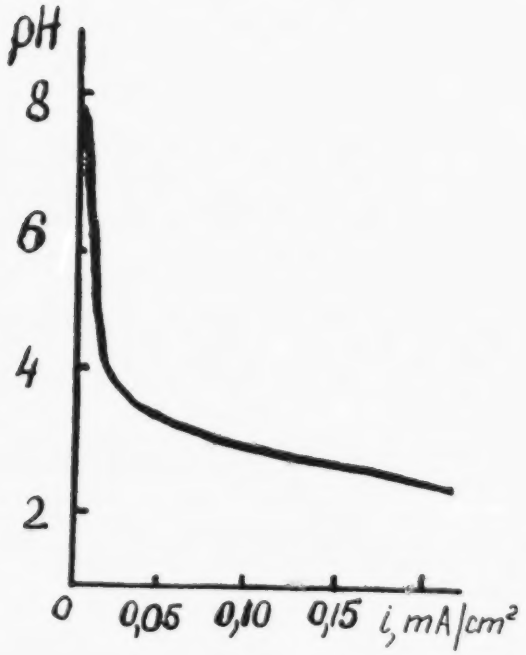

Fig. 42 Influence of anodic current density on change in pH (0.5N NaCl), volume 5 cm^3. Time of polarization, 24 hours (Ref. 128).

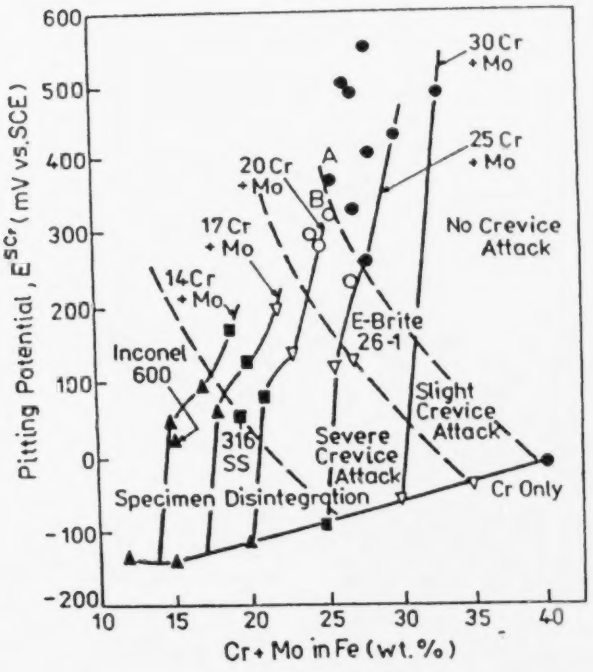

Fig. 43 Relationship between scratch pitting potential and composition of Fe-Cr-Mo alloys by scratch method in deaerated synthetic seawater at 90°C, pH 7.2 ± 0.2, and their resistance to crevice corrosion after 6 days of exposure to aerated 10% $FeCl_3$ at 21 ± 1°C (Ref. 132).

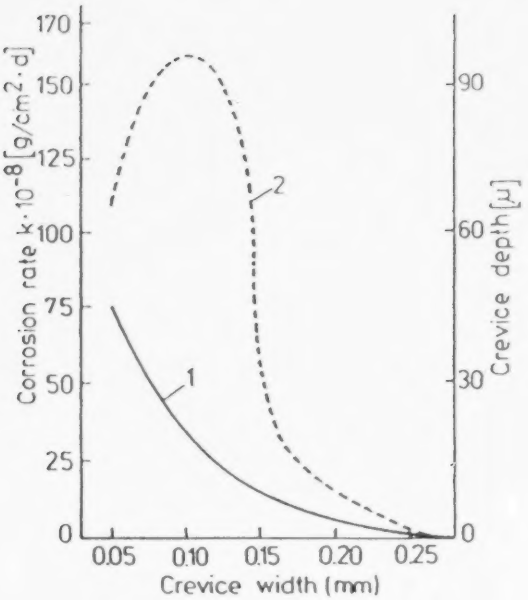

Fig. 44 Effect of crevice width on corrosion rate (1) and distance into the crevice where attack occurs (2) for 13% Cr stainless steel exposed to 5M NaCl solution for 52 days (Ref. 130).

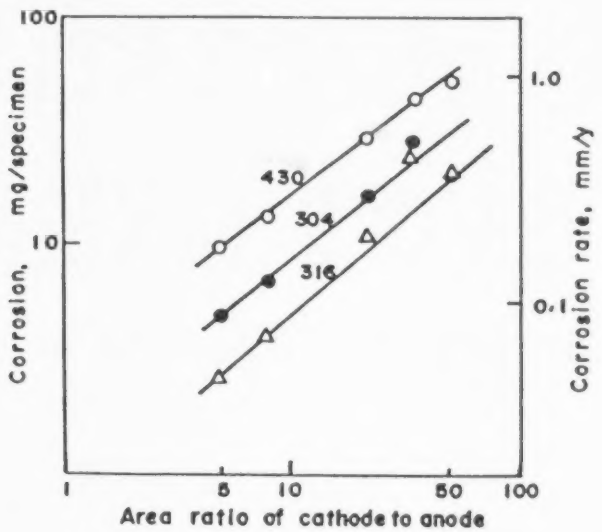

Fig. 45 Effect of cathode to anode area ratio on crevice corrosion in 3% NaCl, 50°C. Crevice was made between a Bakelite bolt and nut and stainless steel plate. (Ref. 24).

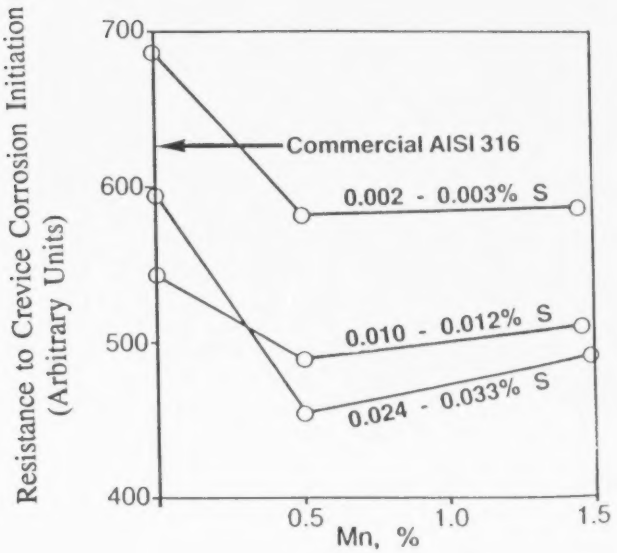

Fig. 46 Alloy rankings for experimental high-purity equivalents of alloy 316 with various Mn and S levels. (Ref. 145).

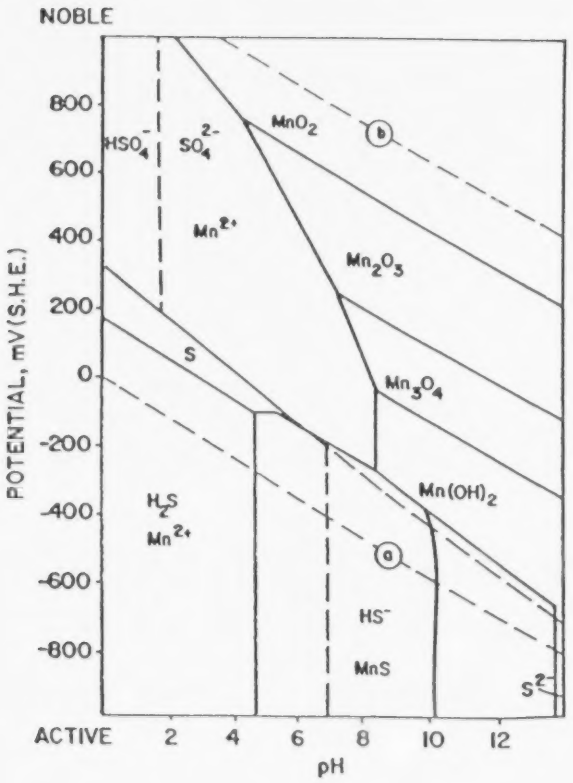

Fig. 47 Potential-pH diagram for MnS-H_2O-Cl^- system calculated on the basis of 0.1 M for SO_4^{2-}, Cl^- and Mn^{2+} (Ref. 147).

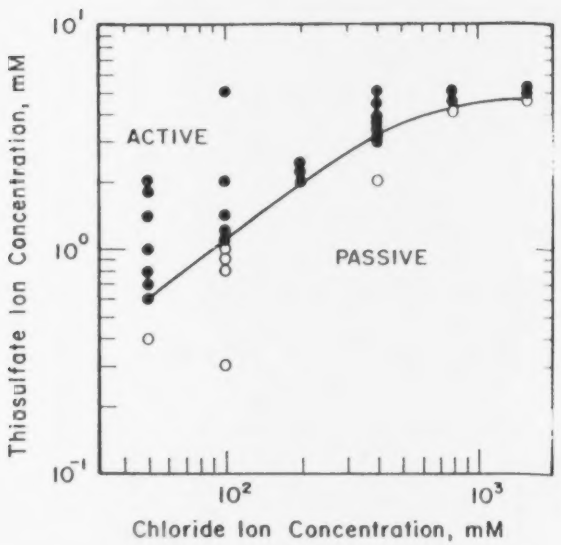

Fig. 48 Conditions under which 304 stainless steel remains active or becomes active during dissolution at 25 $\mu A/cm^2$ in deaerated sodium chloride/sodium thiosulfate electrolytes (Ref. 149).

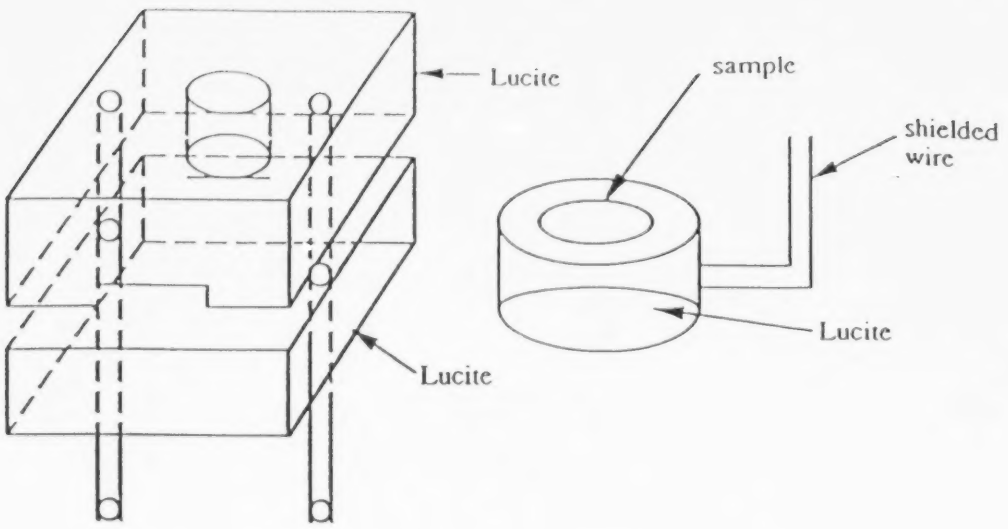

Fig. 49 Sample holder and sample.

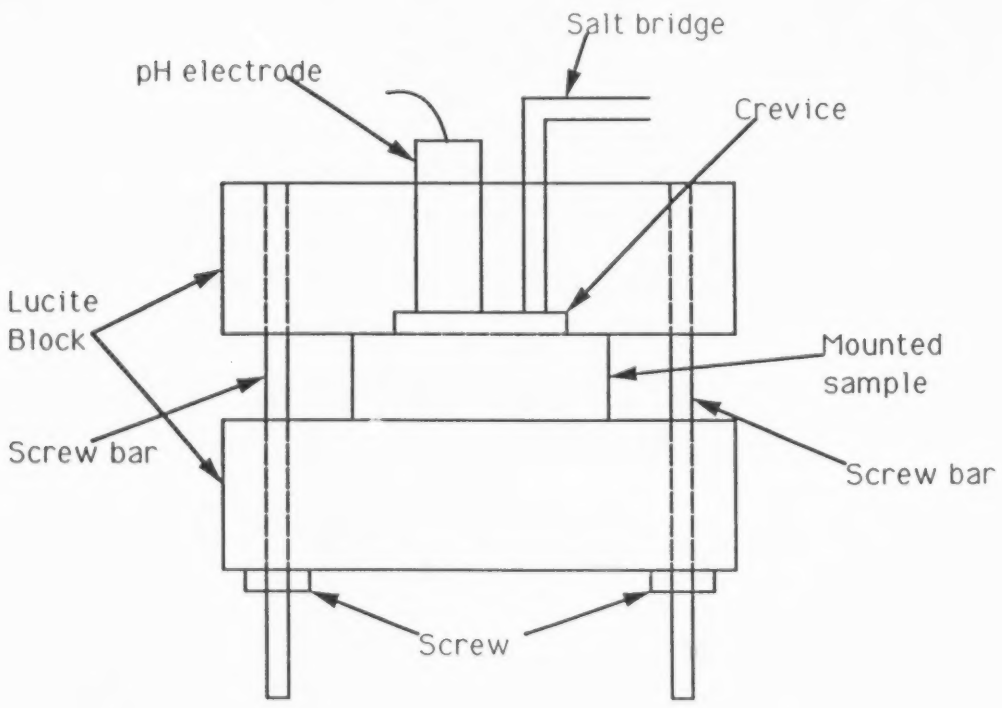

Fig. 50 Crevice assembly.

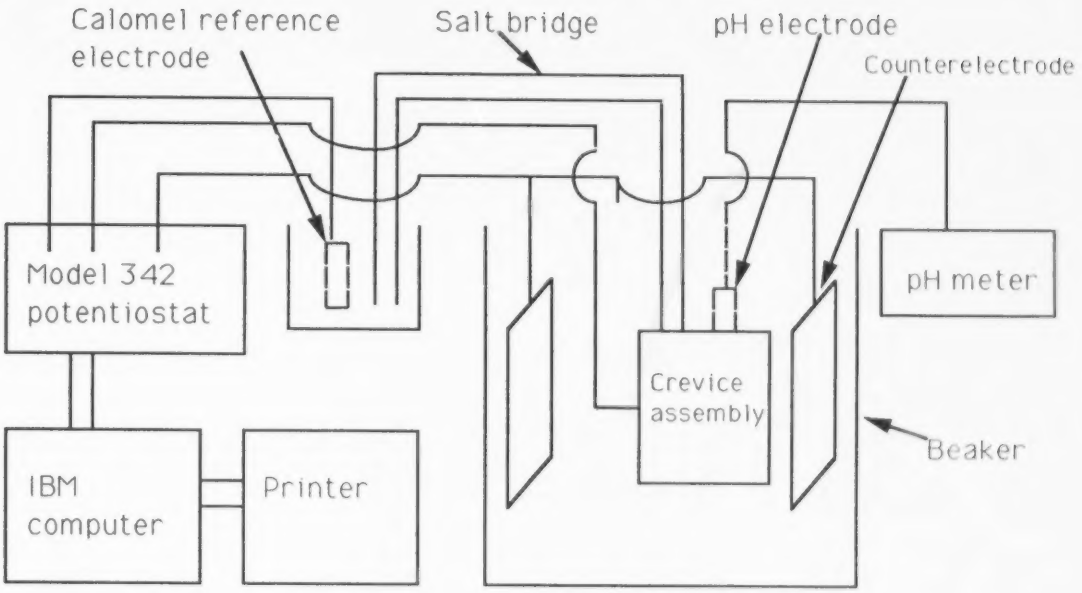

Fig. 51 Experimental set-up for controlling the potential inside a crevice.

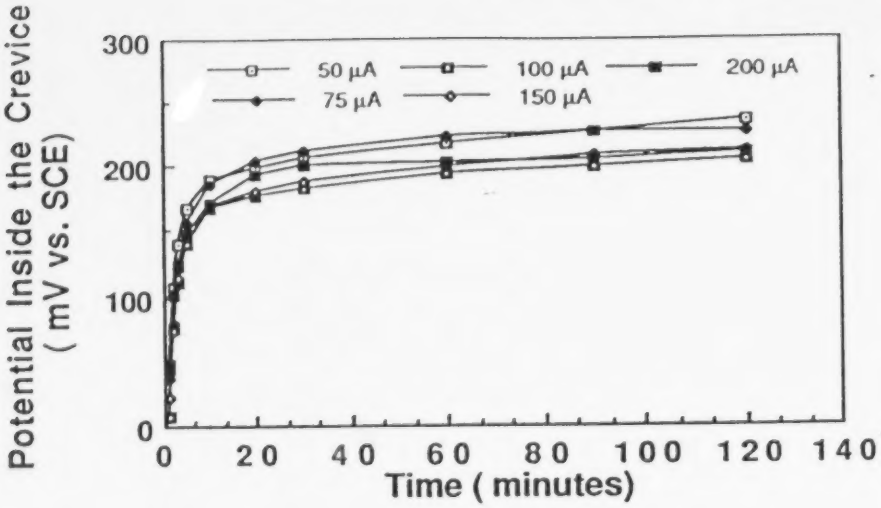

Fig. 52 Variation of potential inside the crevice with time at constant current density in 10 wt.% NaCl solution.

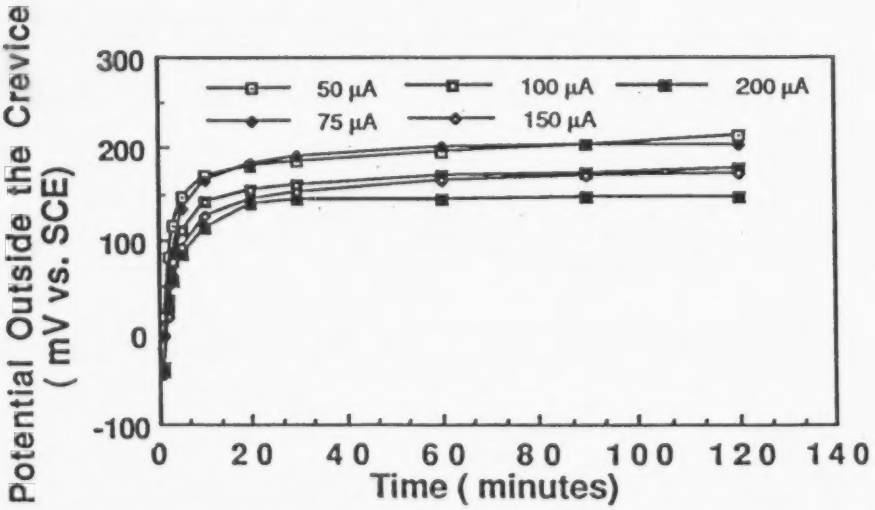

Fig. 53 Variation of potential outside the crevice with time at constant current density in 10 wt.% NaCl solution.

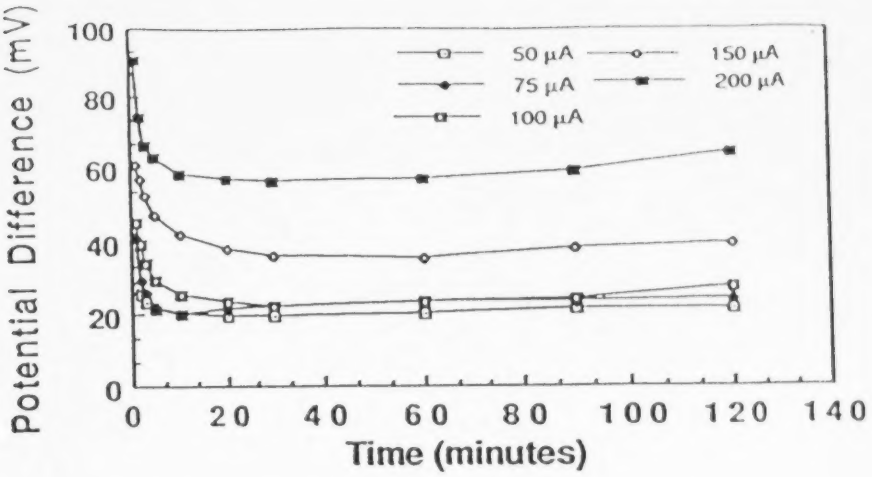

Fig. 54 Variation of potential difference with time for potential inside a crevice and potential outside a crevice at constant current density in 10 wt.% NaCl solution.

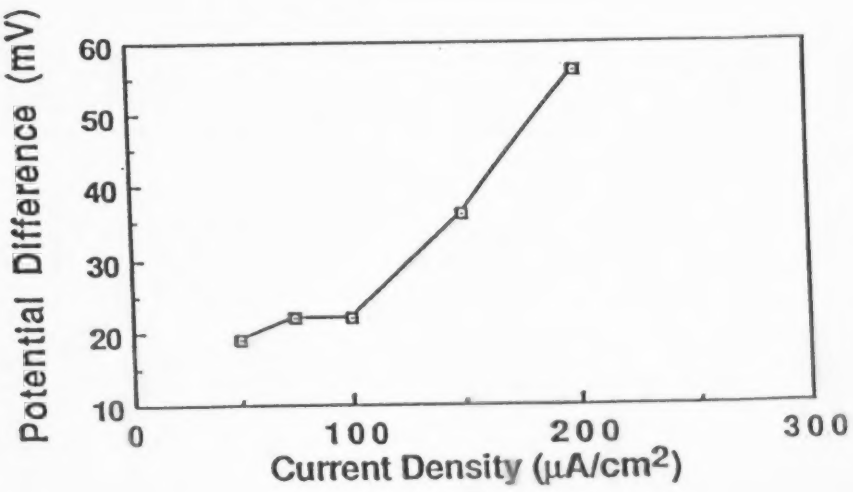

Fig. 55 Effect of current density on potential difference between potential inside a crevice and potential outside a crevice at 30 minutes.

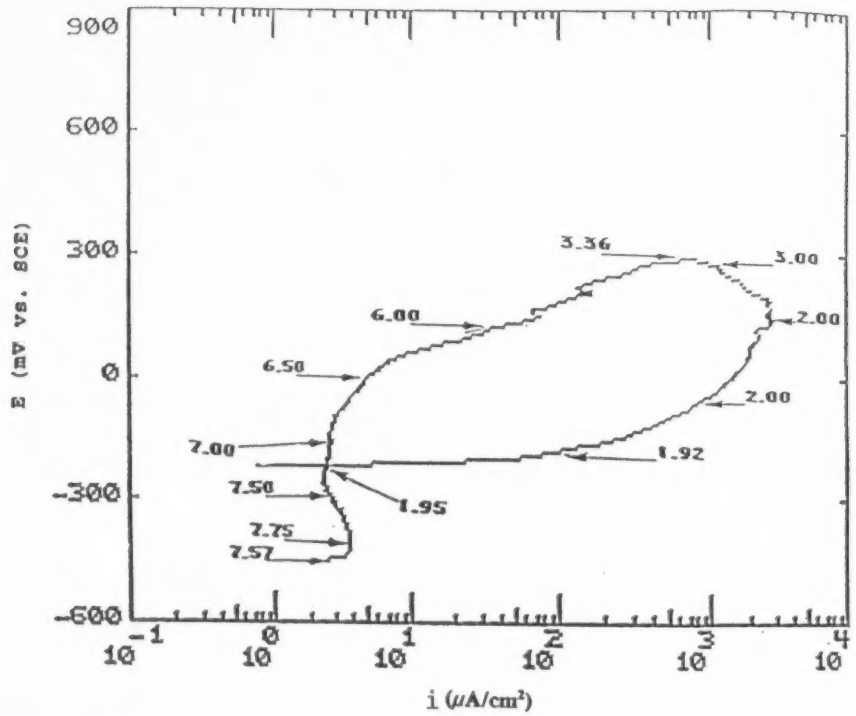

Fig. 56 The cyclic potentiodynamic polarization curve for 304 stainless steel in 3.5% NaCl solution, pH 7.00 and 20°C, obtained by controlling potential inside a 12 μm crevice. Scan rate was 0.5 mV/s. Measured pH values within the crevice are shown on the curve.

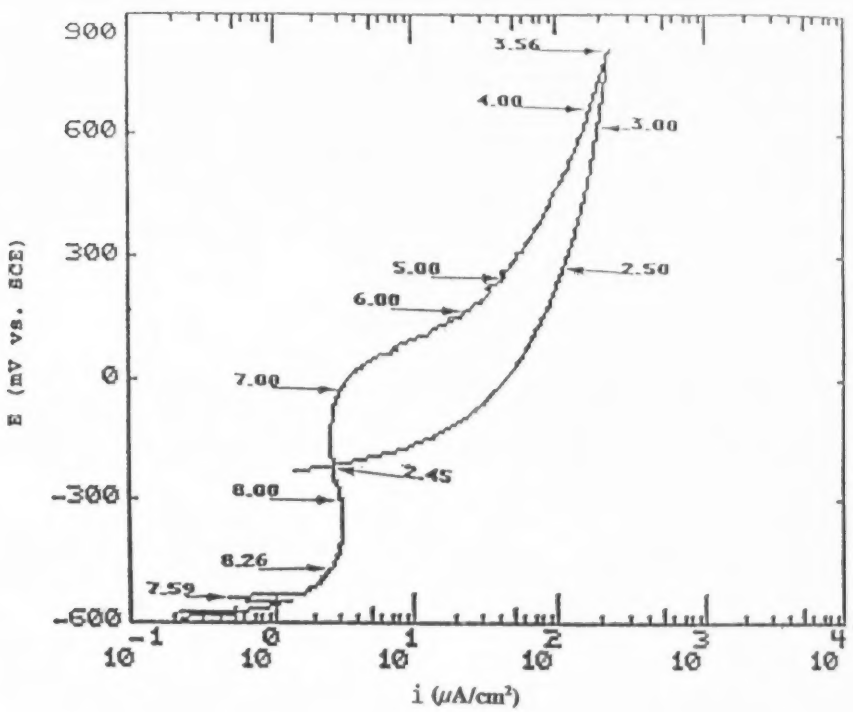

Fig. 57 The cyclic potentiodynamic polarization curve for 304 stainless steel in 3.5% NaCl solution, pH 7.00 and 20°C, obtained by controlling potential outside a 12 μm crevice. Scan rate was 0.5 mV/s. Measured pH values within the crevice are shown on the curve..

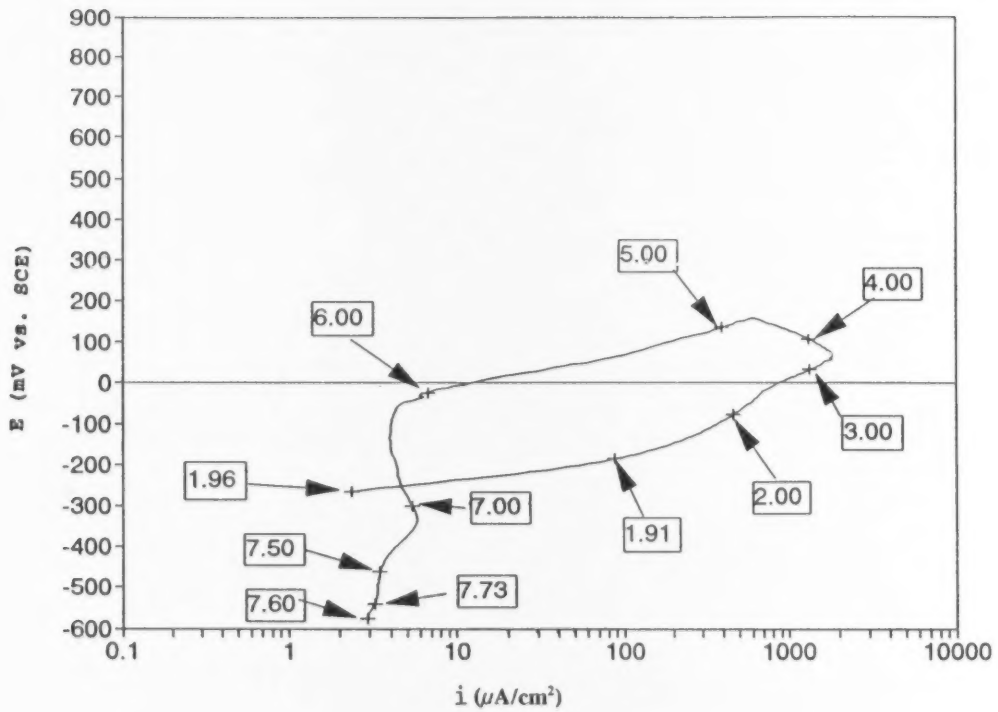

Fig. 58 The cyclic potentiodynamic polarization curve for 304 stainless steel in 10% NaCl solution, pH 7.25 and 20°C, obtained by controlling potential inside a 12 μm crevice. Scan rate was 0.5 mV/s. Measured pH values within the crevice are shown on the curve.

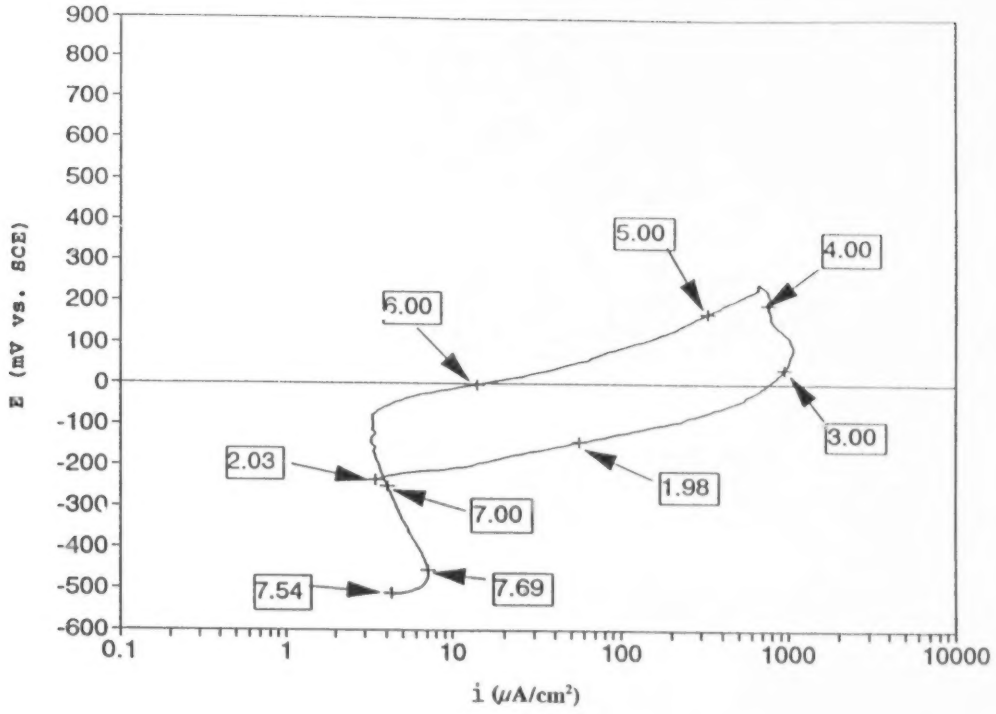

Fig. 59 The cyclic potentiodynamic polarization curve for 304 stainless steel in 10% NaCl solution, pH 7.15 and 20°C, obtained by controlling potential inside a 40 μm crevice. Scan rate was 0.5 mV/s. Measured pH values within the crevice are shown on the curve.

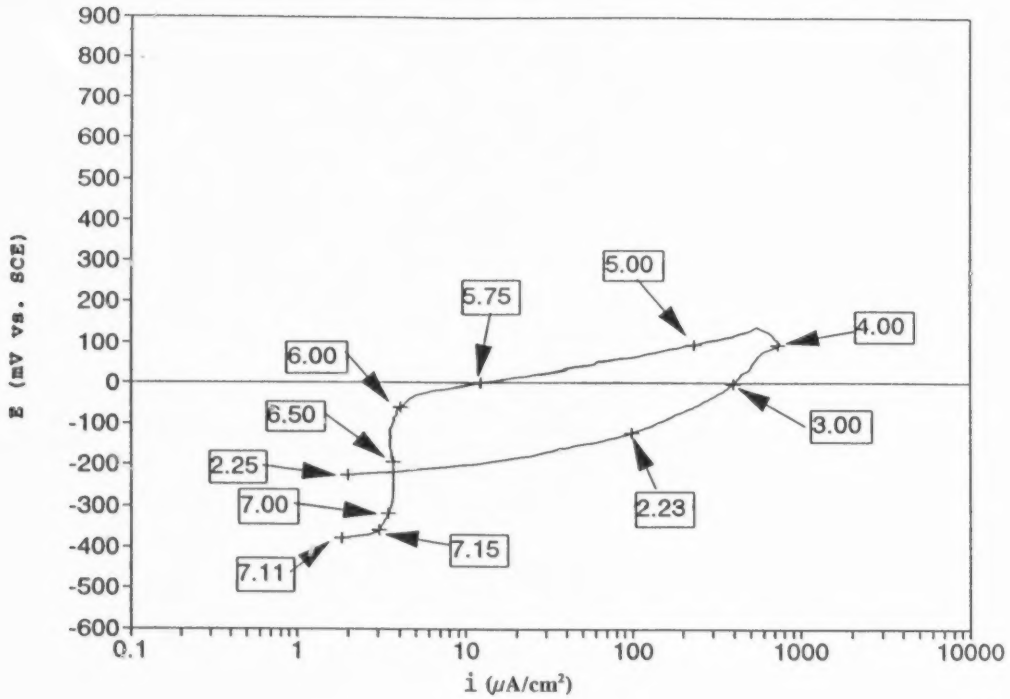

Fig. 60 The cyclic potentiodynamic polarization curve for 304 stainless steel in 10% NaCl solution, pH 6.89 and 20°C, obtained by controlling potential inside a 96 μm crevice. Scan rate was 0.5 mV/s. Measured pH values within the crevice are shown on the curve.

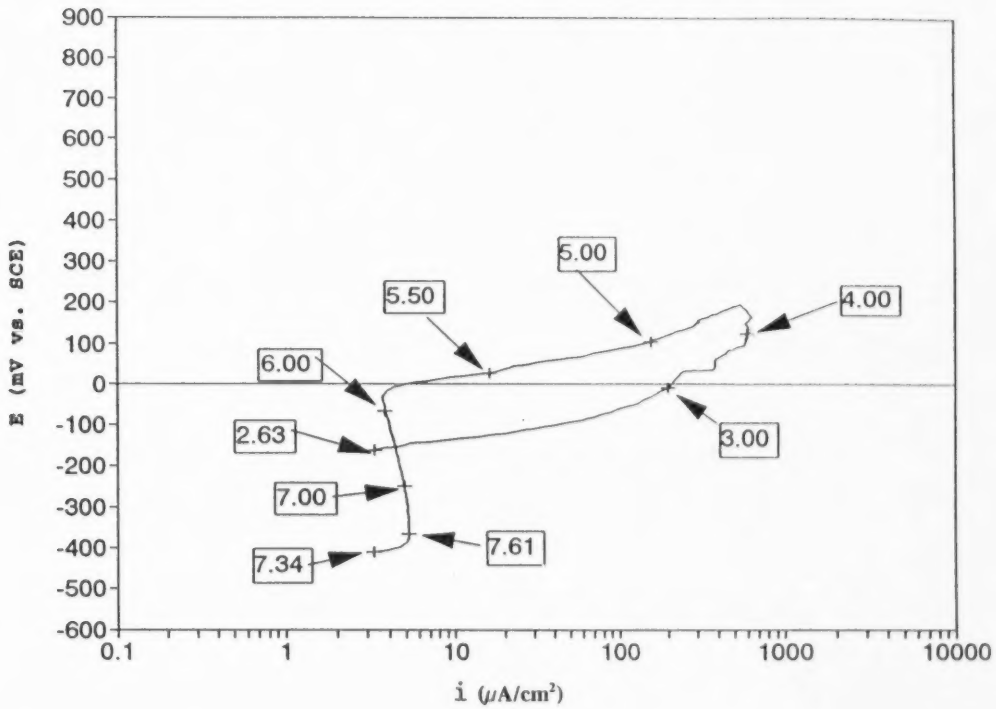

Fig. 61 The cyclic potentiodynamic polarization curve for 304 stainless steel in 10% NaCl solution, pH 7.05 and 20°C, obtained by controlling potential inside a 180 μm crevice. Scan rate was 0.5 mV/s. Measured pH values within the crevice are shown on the curve.

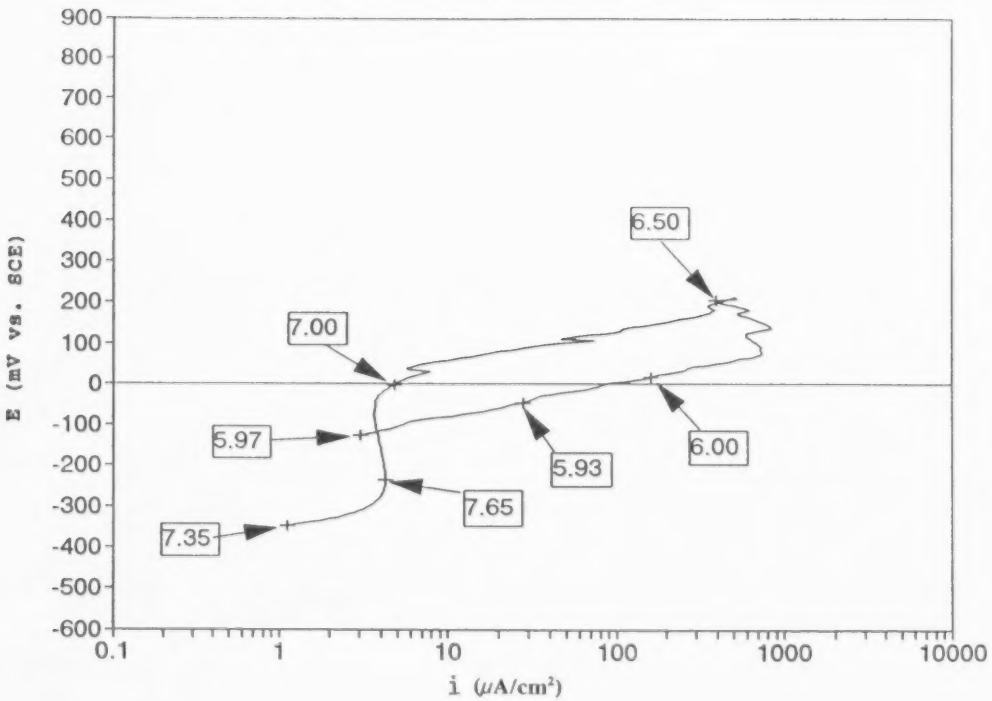

Fig. 62 The cyclic potentiodynamic polarization curve for 304 stainless steel in 10% NaCl solution, pH 7.00 and 20°C, obtained by controlling potential inside a 330 μm crevice. Scan rate was 0.5 mV/s. Measured pH values within the crevice are shown on the curve.

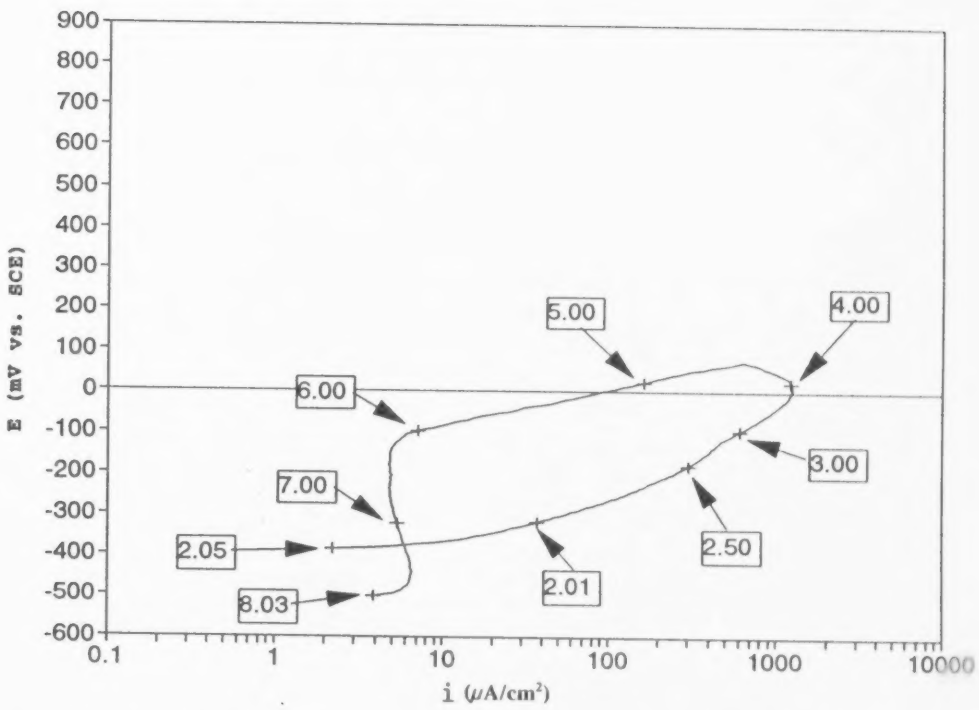

Fig. 63 The cyclic potentiodynamic polarization curve for 303 stainless steel in 10% NaCl solution, pH 7.25 and 20°C, obtained by controlling potential inside a 12 μm crevice. Scan rate was 0.5 mV/s. Measured pH values within the crevice are shown on the curve.

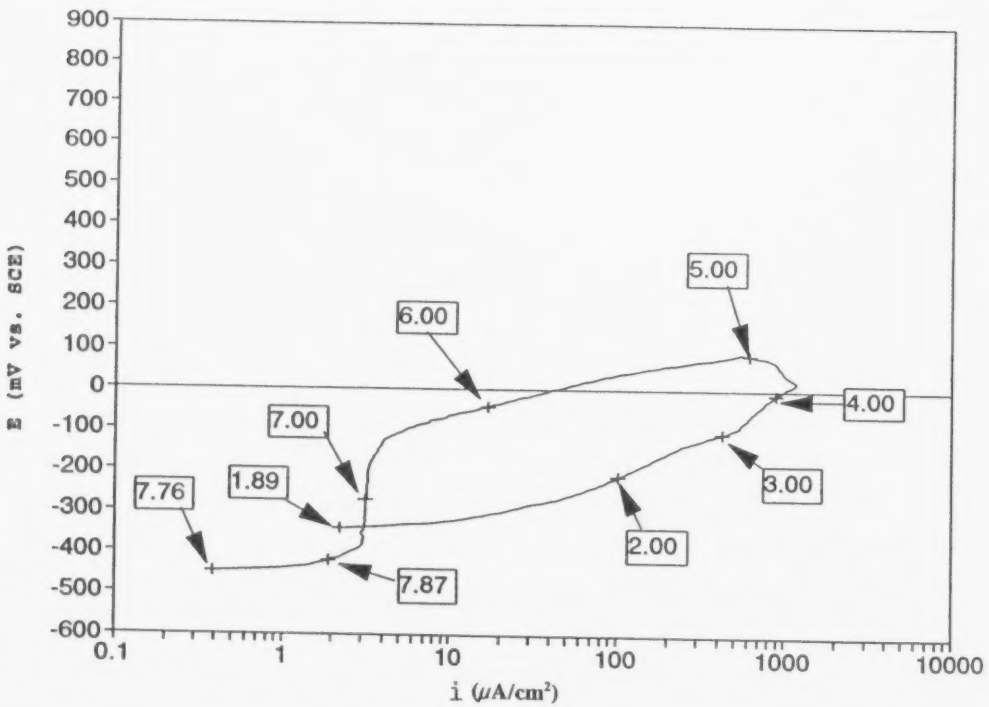

Fig. 64 The cyclic potentiodynamic polarization curve for 303 stainless steel in 10% NaCl solution, pH 7.25 and 20°C, obtained by controlling potential inside a 40 μm crevice. Scan rate was 0.5 mV/s. Measured pH values within the crevice are shown on the curve.

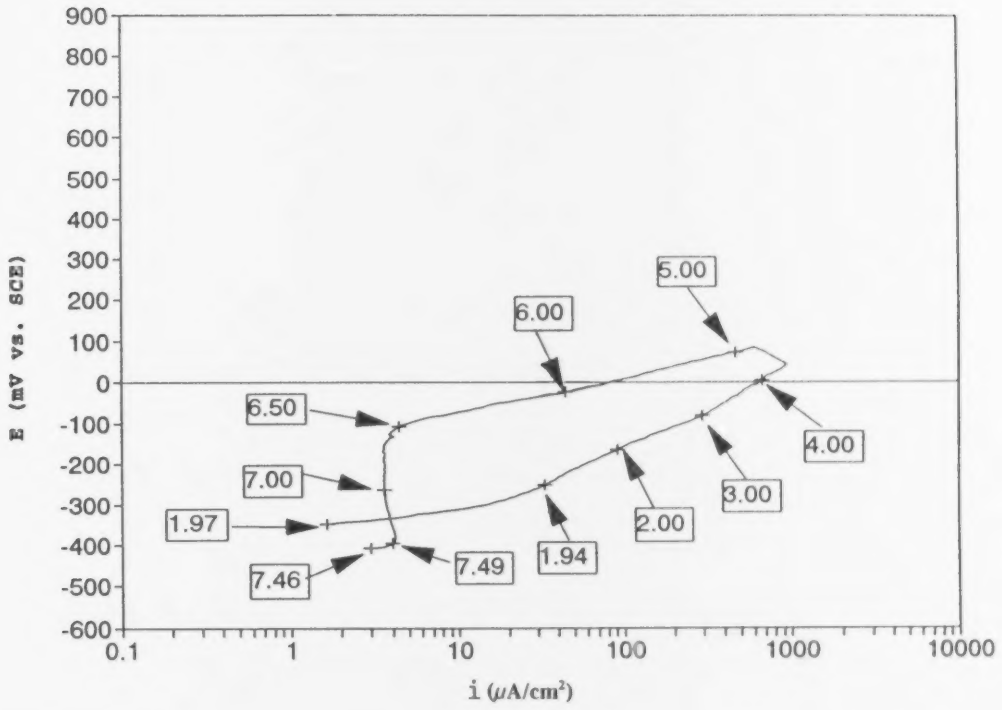

Fig. 65 The cyclic potentiodynamic polarization curve for 303 stainless steel in 10% NaCl solution, pH 7.00 and 20°C, obtained by controlling potential inside a 96 μm crevice. Scan rate was 0.5 mV/s. Measured pH values within the crevice are shown on the curve.

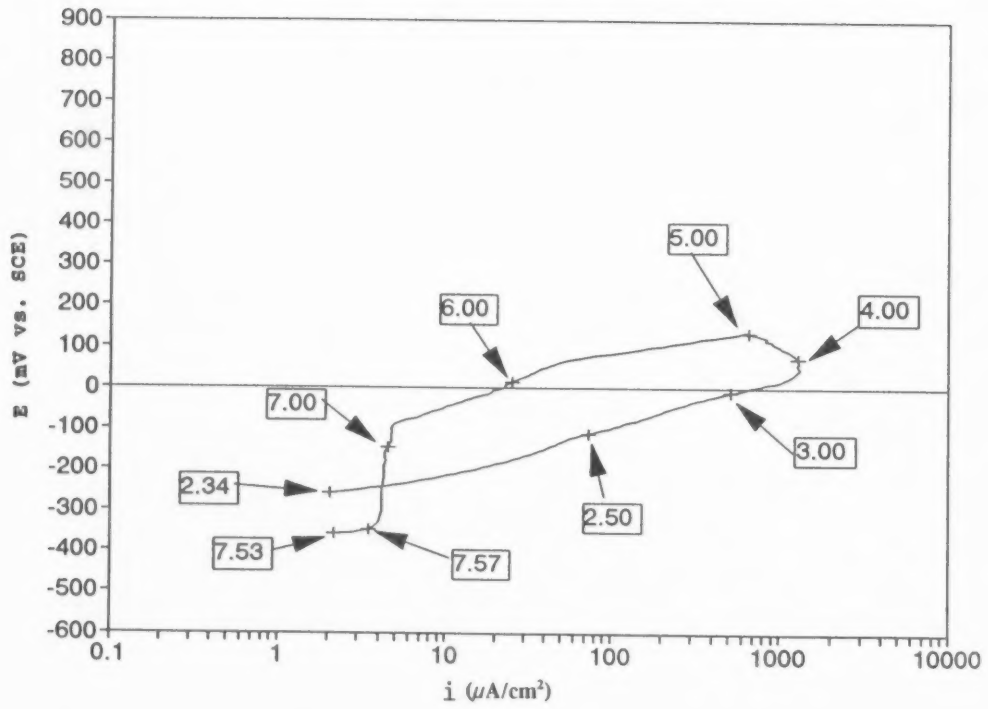

Fig. 66 The cyclic potentiodynamic polarization curve for 303 stainless steel in 10% NaCl solution, pH 7.00 and 20°C, obtained by controlling potential inside a 180 μm crevice. Scan rate was 0.5 mV/s. Measured pH values within the crevice are shown on the curve.

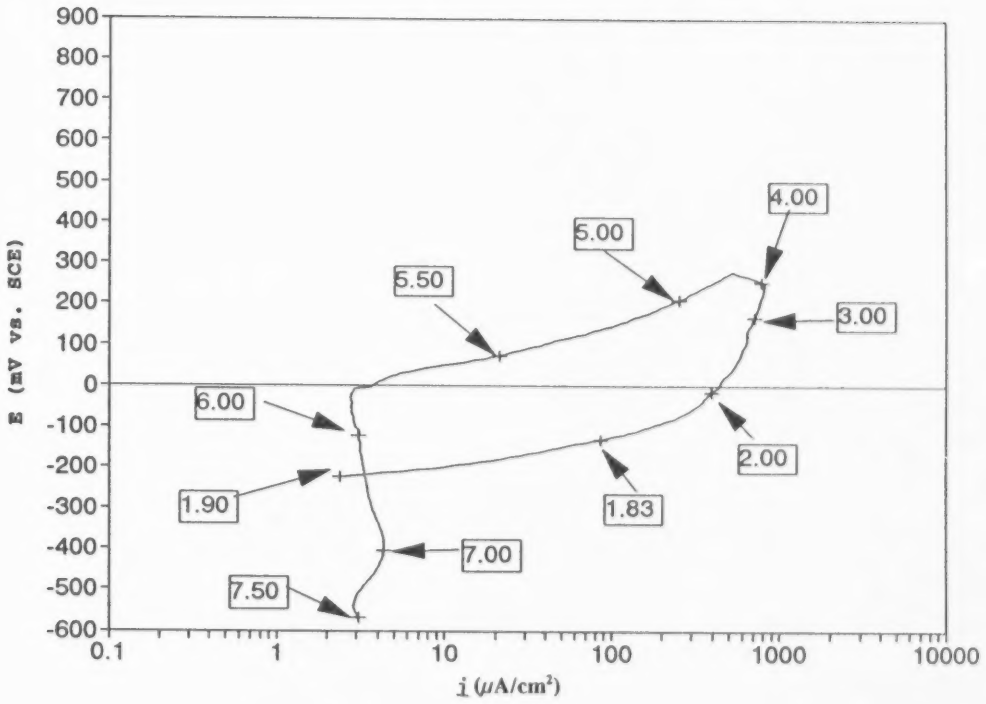

Fig. 67 The cyclic potentiodynamic polarization curve for 316 stainless steel in 10% NaCl solution, pH 7.13 and 20°C, obtained by controlling potential inside a 12 μm crevice. Scan rate was 0.5 mV/s. Measured pH values within the crevice are shown on the curve.

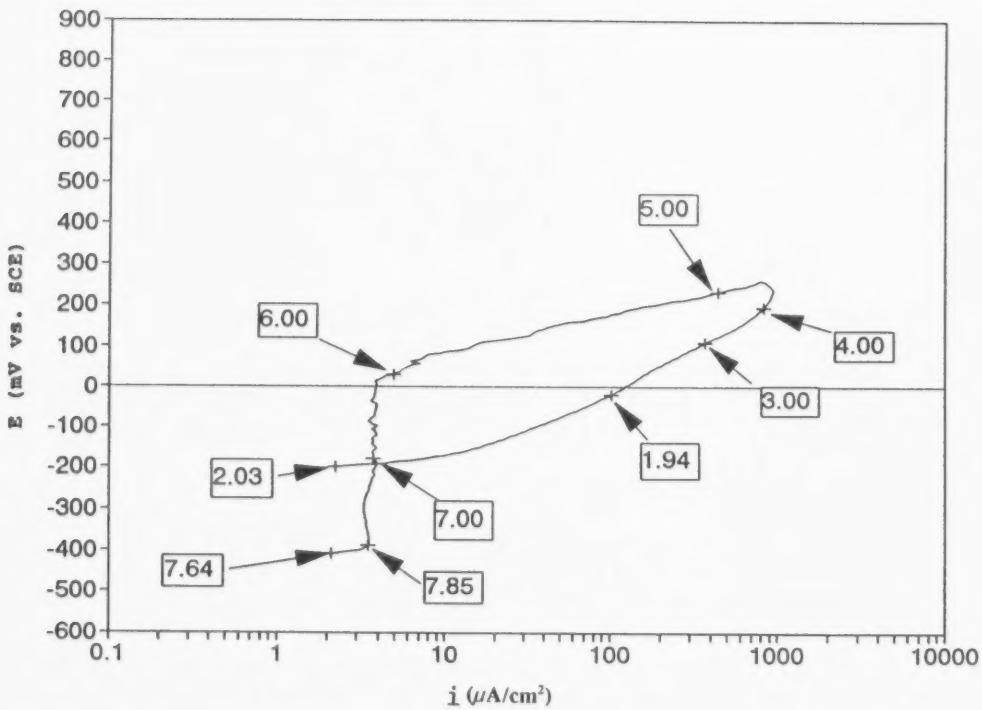

Fig. 68 The cyclic potentiodynamic polarization curve for 316 stainless steel in 10% NaCl solution, pH 7.20 and 20°C, obtained by controlling potential inside a 40 μm crevice. Scan rate was 0.5 mV/s. Measured pH values within the crevice are shown on the curve.

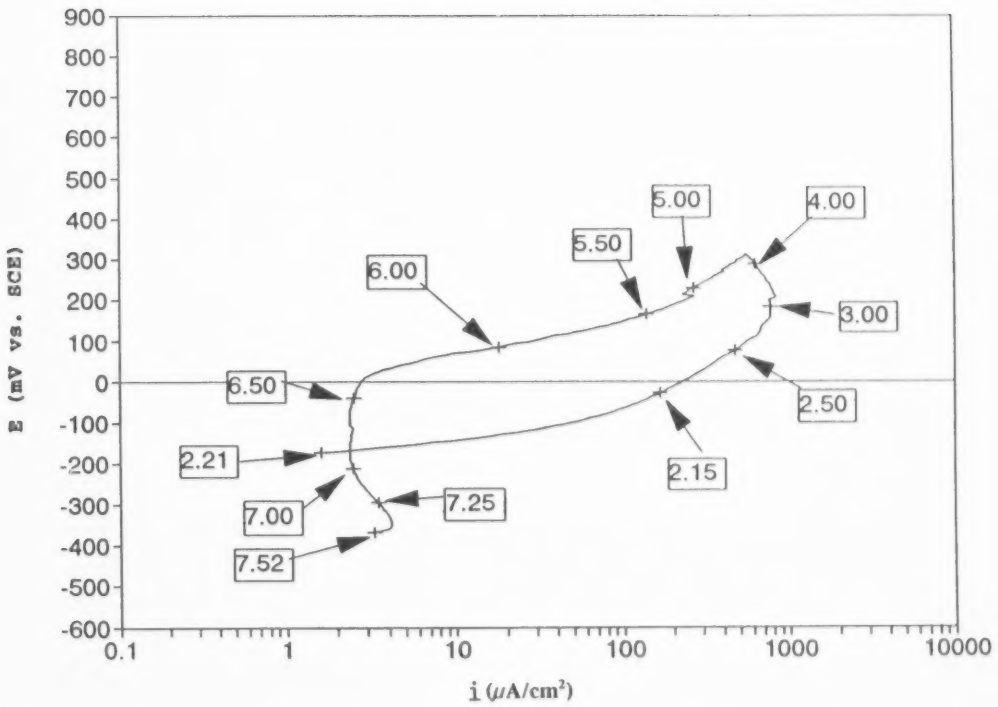

Fig. 69 The cyclic potentiodynamic polarization curve for 316 stainless steel in 10% NaCl solution, pH 7.25 and 20°C, obtained by controlling potential inside a 96 μm crevice. Scan rate was 0.5 mV/s. Measured pH values within the crevice are shown on the curve.

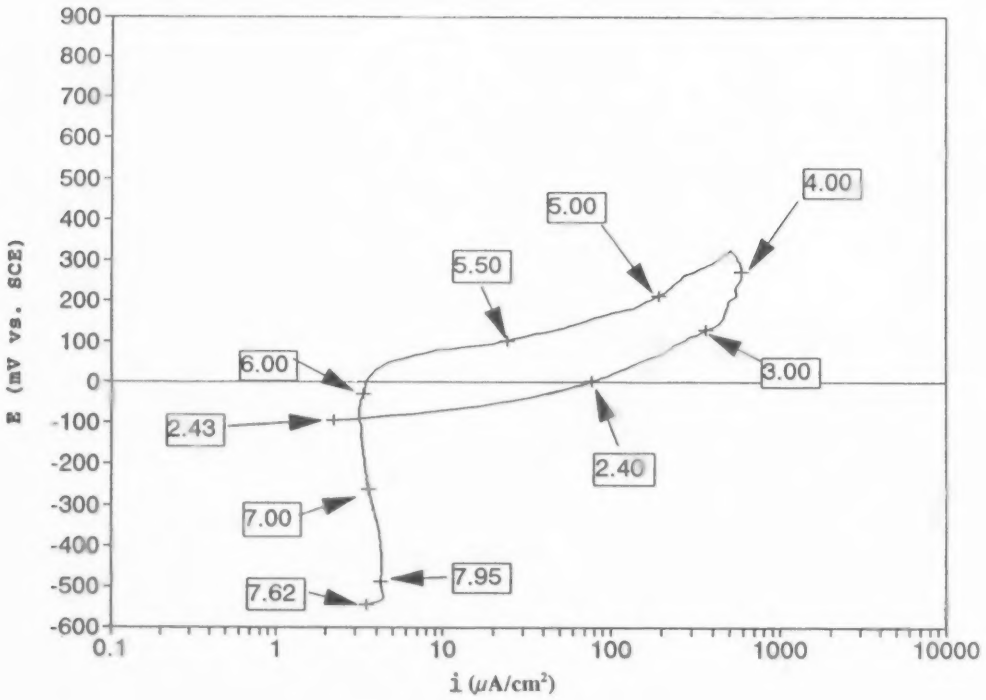

Fig. 70 The cyclic potentiodynamic polarization curve for 316 stainless steel in 10% NaCl solution, pH 7.15 and 20°C, obtained by controlling potential inside a 180 μm crevice. Scan rate was 0.5 mV/s. Measured pH values within the crevice are shown on the curve.

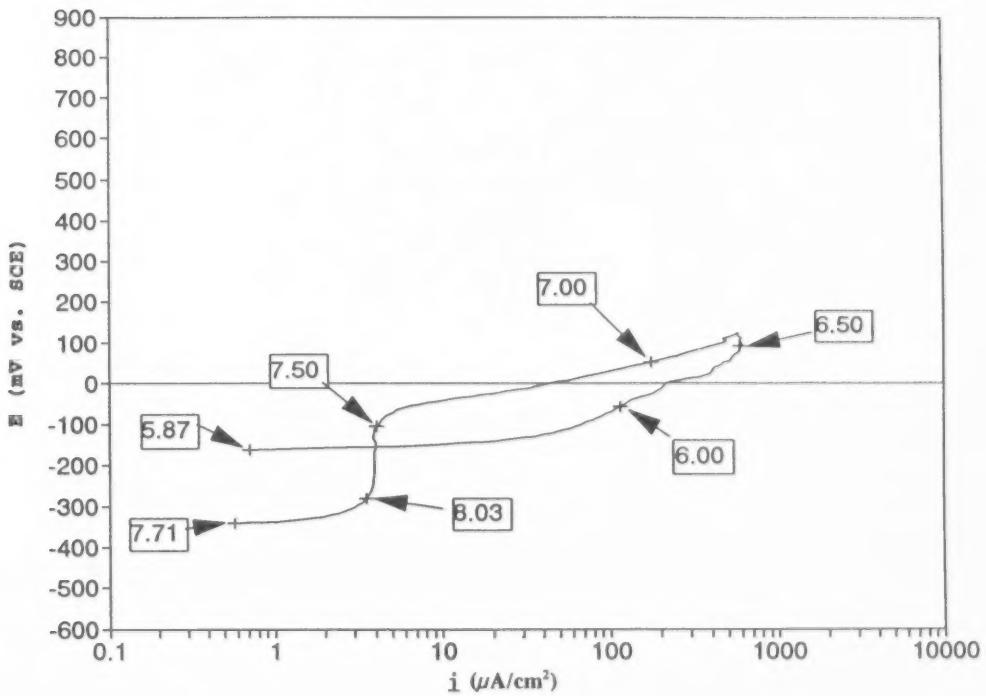

Fig. 71 The cyclic potentiodynamic polarization curve for 303 stainless steel in 10% NaCl solution, pH 7.50 and 20°C, obtained by controlling potential inside a 330 μm crevice. Scan rate was 0.5 mV/s. Measured pH values within the crevice are shown on the curve.

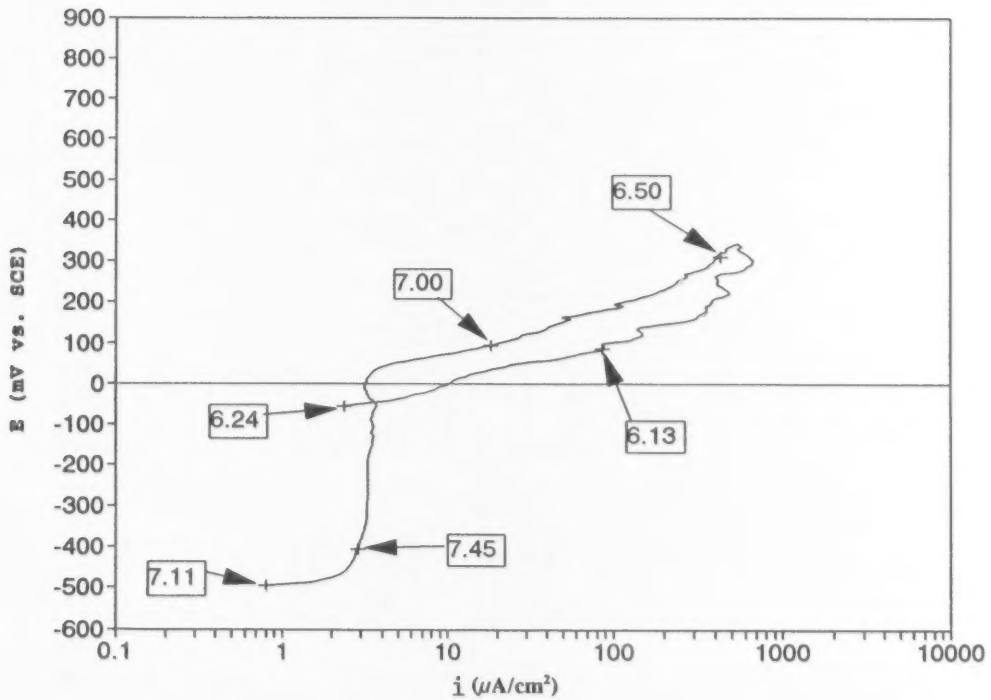

Fig. 72 The cyclic potentiodynamic polarization curve for 316 stainless steel in 10% NaCl solution, pH 7.00 and 20°C, obtained by controlling potential inside a 330 μm crevice. Scan rate was 0.5 mV/s. Measured pH values within the crevice are shown on the curve.

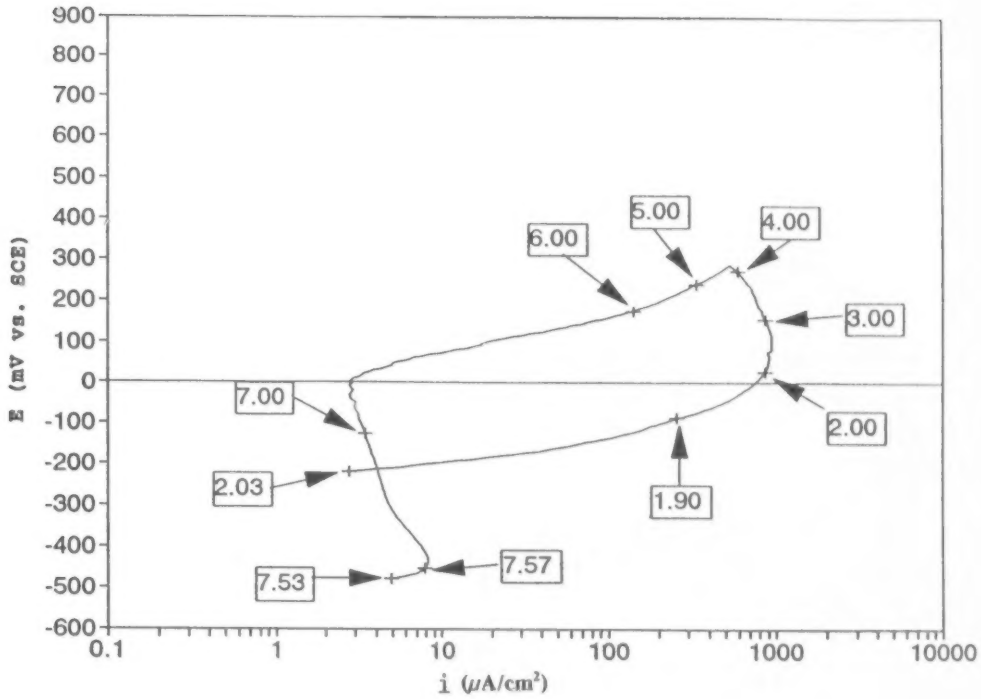

Fig. 73 The cyclic potentiodynamic polarization curve for 304 stainless steel in 10% NaCl solution, pH 7.25 and 10°C, obtained by controlling potential inside a 12 μm crevice. Scan rate was 0.5 mV/s. Measured pH values within the crevice are shown on the curve.

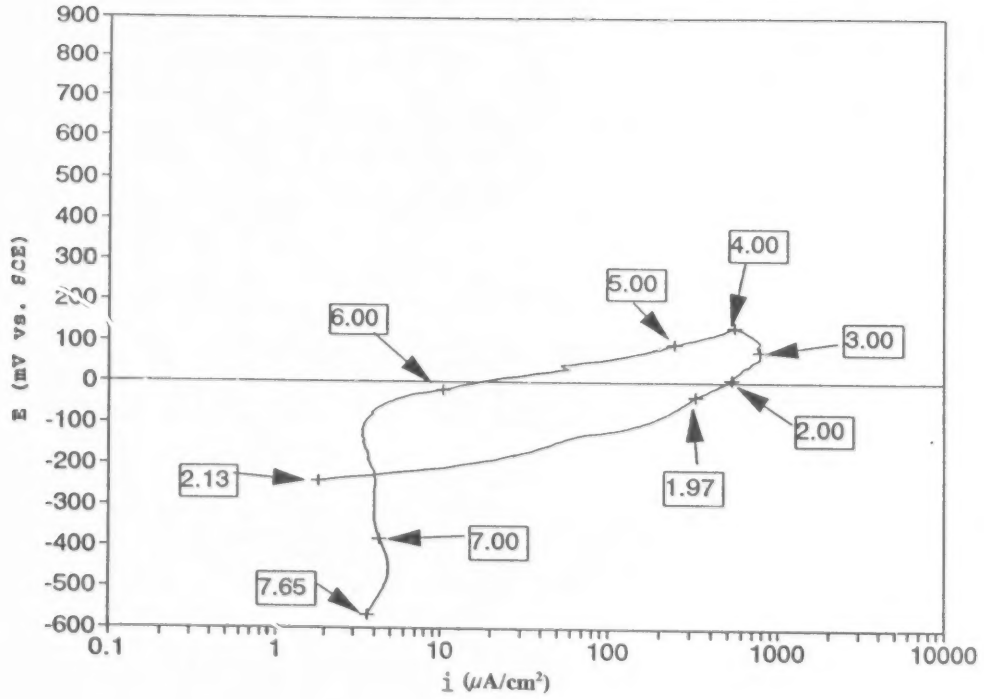

Fig. 74 The cyclic potentiodynamic polarization curve for 304 stainless steel in 10% NaCl solution, pH 7.25 and 25°C, obtained by controlling potential inside a 12 μm crevice. Scan rate was 0.5 mV/s. Measured pH values within the crevice are shown on the curve.

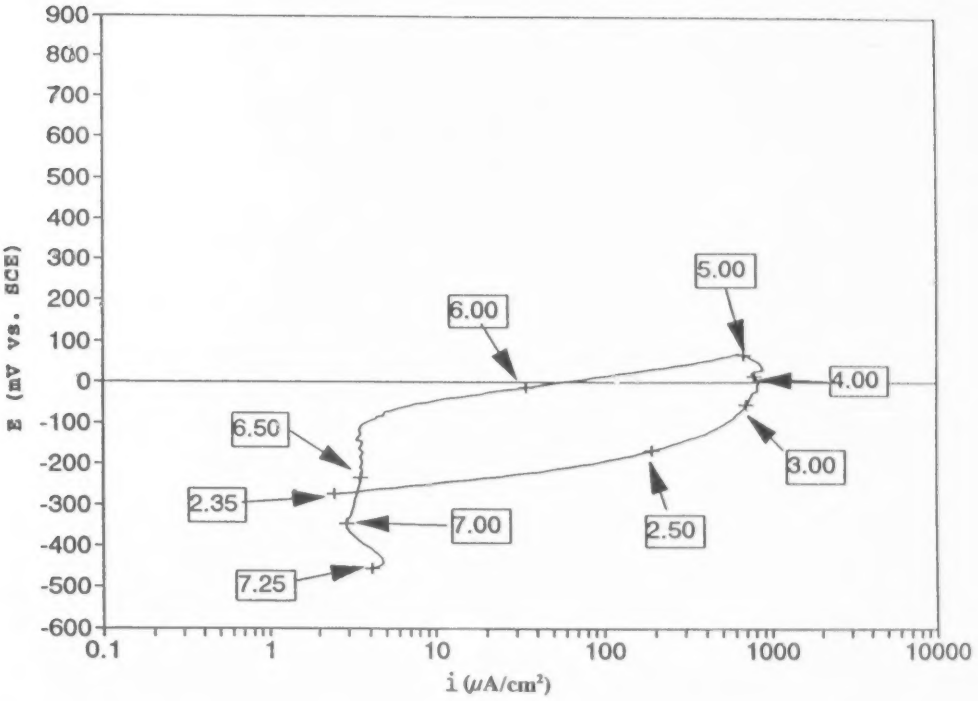

Fig. 75 The cyclic potentiodynamic polarization curve for 304 stainless steel in 10% NaCl solution, pH 7.00 and 35°C, obtained by controlling potential inside a 12 μm crevice. Scan rate was 0.5 mV/s. Measured pH values within the crevice are shown on the curve.

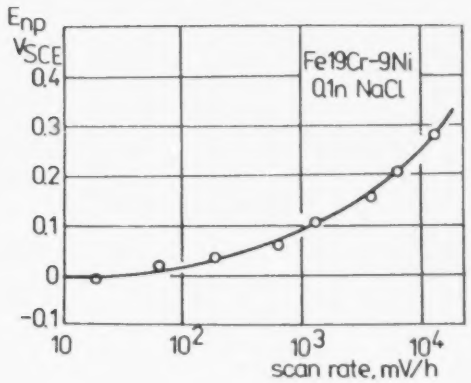

Fig. 76 Pit nucleation potential vs. rate of potential change for 19Cr-9Ni stainless steel (Ref. 152).

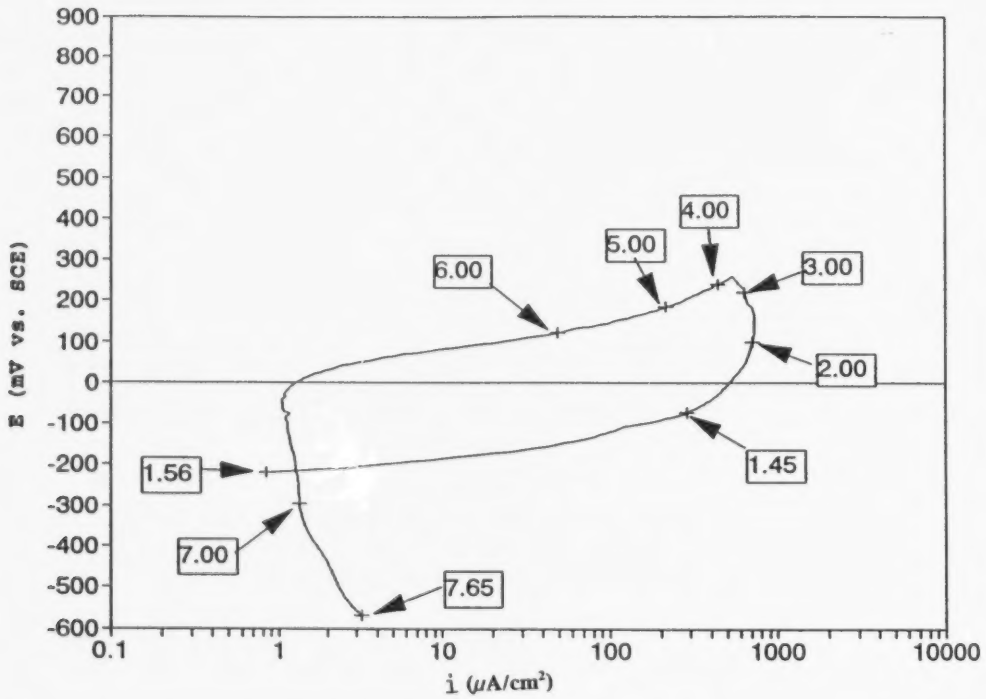

Fig. 77 The cyclic potentiodynamic polarization curve for 304 stainless steel in 10% NaCl solution, pH 7.00 and 10°C, obtained by controlling potential inside a 12 μm crevice. Scan rate was 0.2 mV/s. Measured pH values within the crevice are shown on the curve.

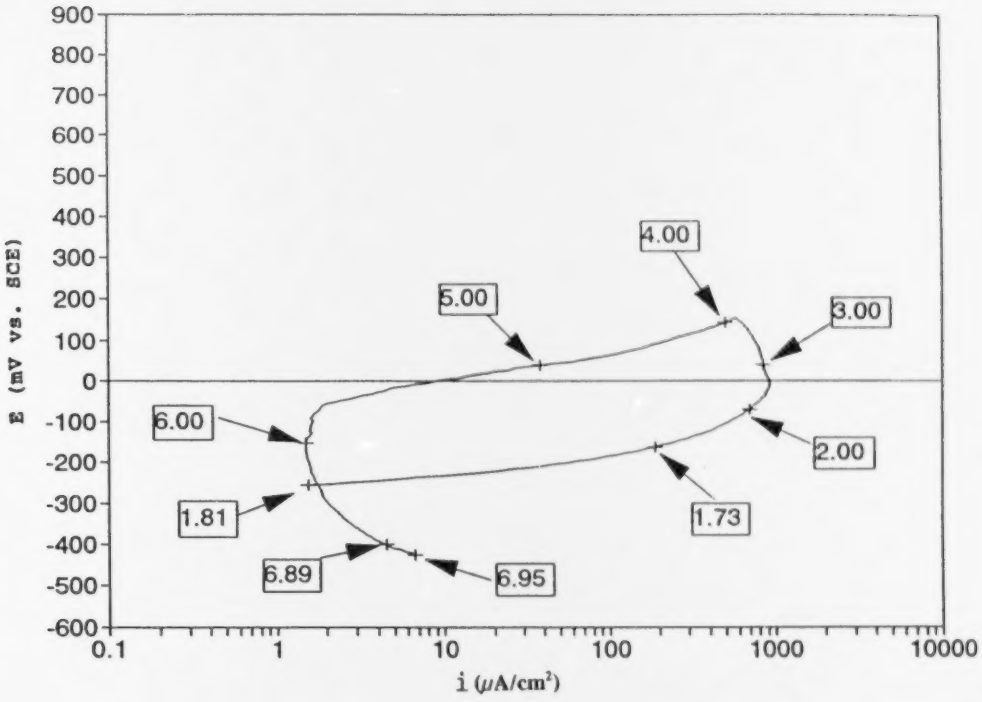

Fig. 78 The cyclic potentiodynamic polarization curve for 304 stainless steel in 10% NaCl solution, pH 6.80 and 20°C, obtained by controlling potential inside a 12 μm crevice. Scan rate was 0.2 mV/s. Measured pH values within the crevice are shown on the curve.

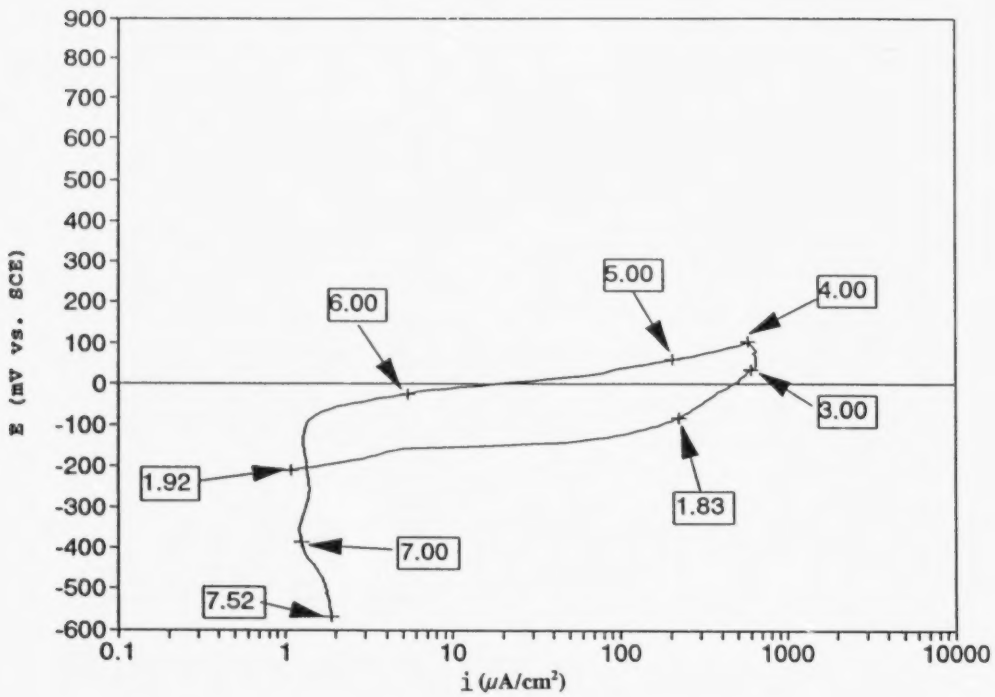

Fig. 79 The cyclic potentiodynamic polarization curve for 304 stainless steel in 10% NaCl solution, pH 7.19 and 25°C, obtained by controlling potential inside a 12 μm crevice. Scan rate was 0.2 mV/s. Measured pH values within the crevice are shown on the curve.

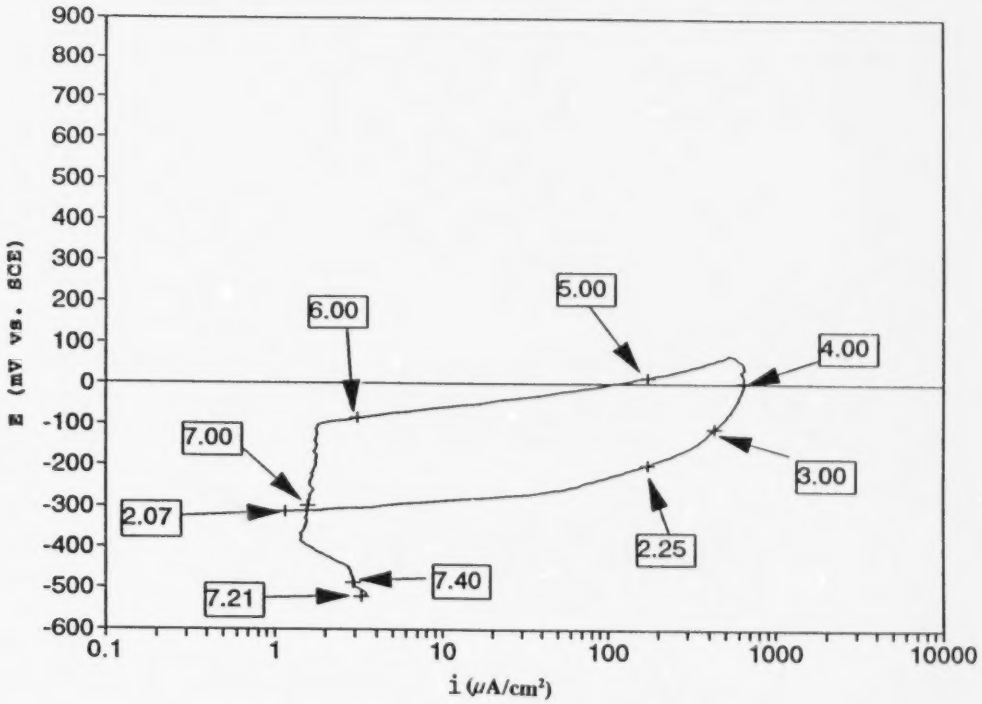

Fig. 80 The cyclic potentiodynamic polarization curve for 304 stainless steel in 10% NaCl solution, pH 6.91 and 35°C, obtained by controlling potential inside a 12 μm crevice. Scan rate was 0.2 mV/s. Measured pH values within the crevice are shown on the curve.

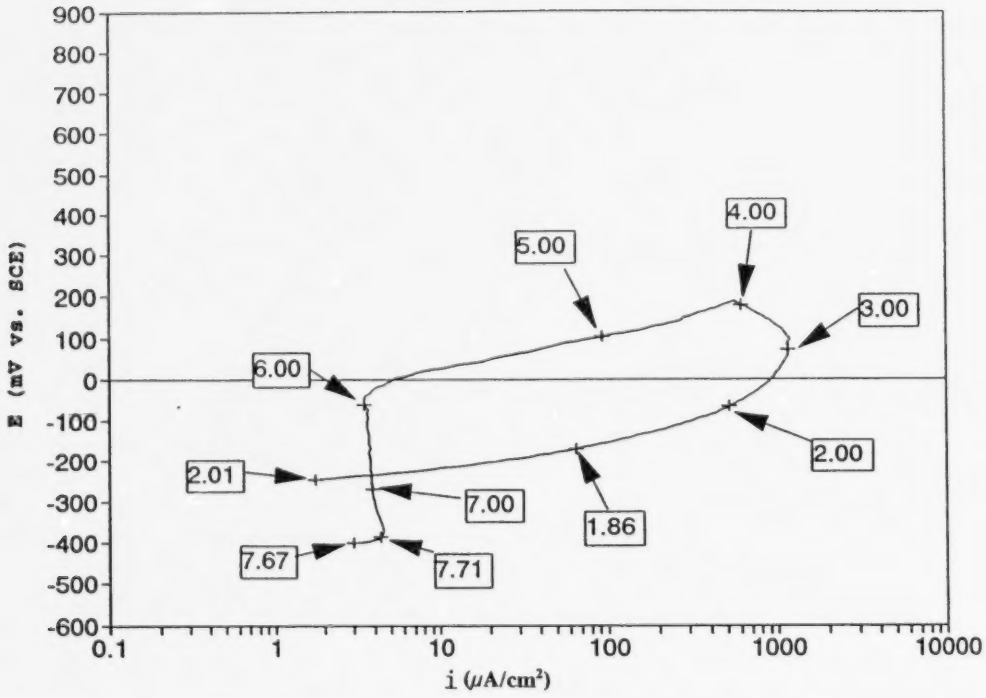

Fig. 81 The cyclic potentiodynamic polarization curve for 304 stainless steel in 3.5% NaCl solution, pH 7.25 and 20°C, obtained by controlling potential inside a 12 μm crevice. Scan rate was 0.5 mV/s. Measured pH values within the crevice are shown on the curve.

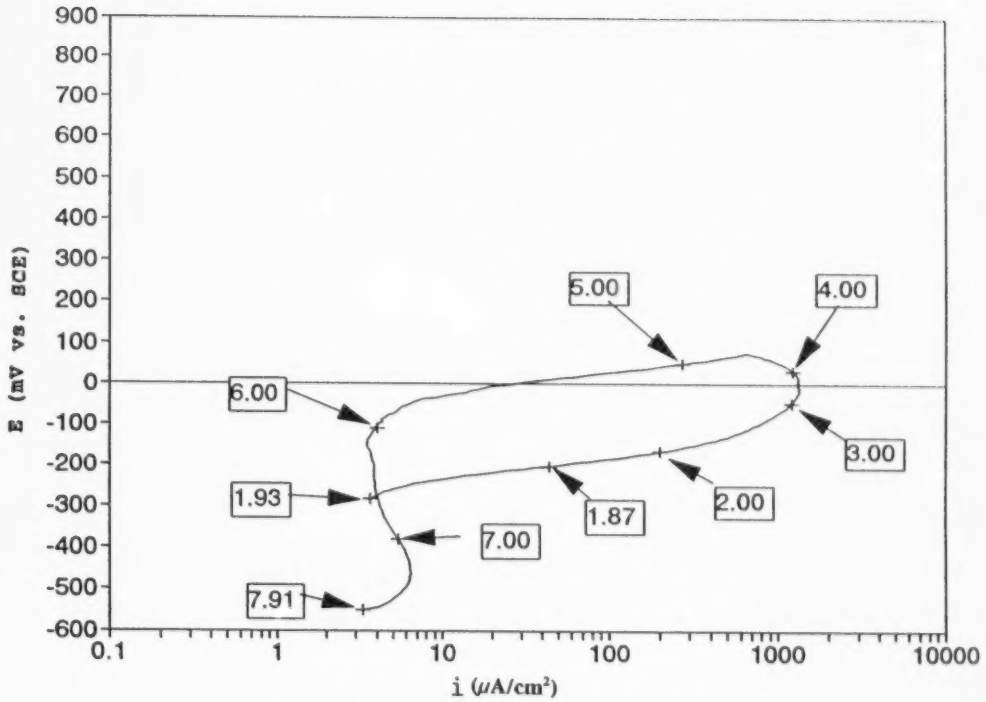

Fig. 82 The cyclic potentiodynamic polarization curve for 304 stainless steel in 15% NaCl solution, pH 7.50 and 20°C, obtained by controlling potential inside a 12 μm crevice. Scan rate was 0.5 mV/s. Measured pH values within the crevice are shown on the curve.

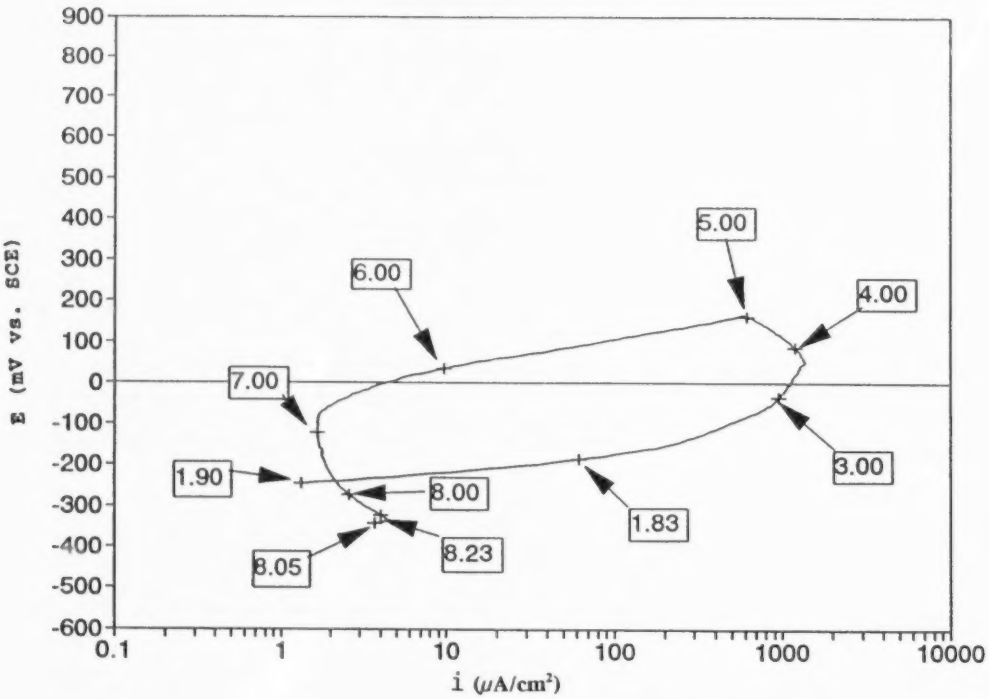

Fig. 83 The cyclic potentiodynamic polarization curve for 304 stainless steel in 3.5% NaCl solution, pH 7.53 and 20°C, obtained by controlling potential inside a 12 μm crevice. Scan rate was 0.2 mV/s. Measured pH values within the crevice are shown on the curve.

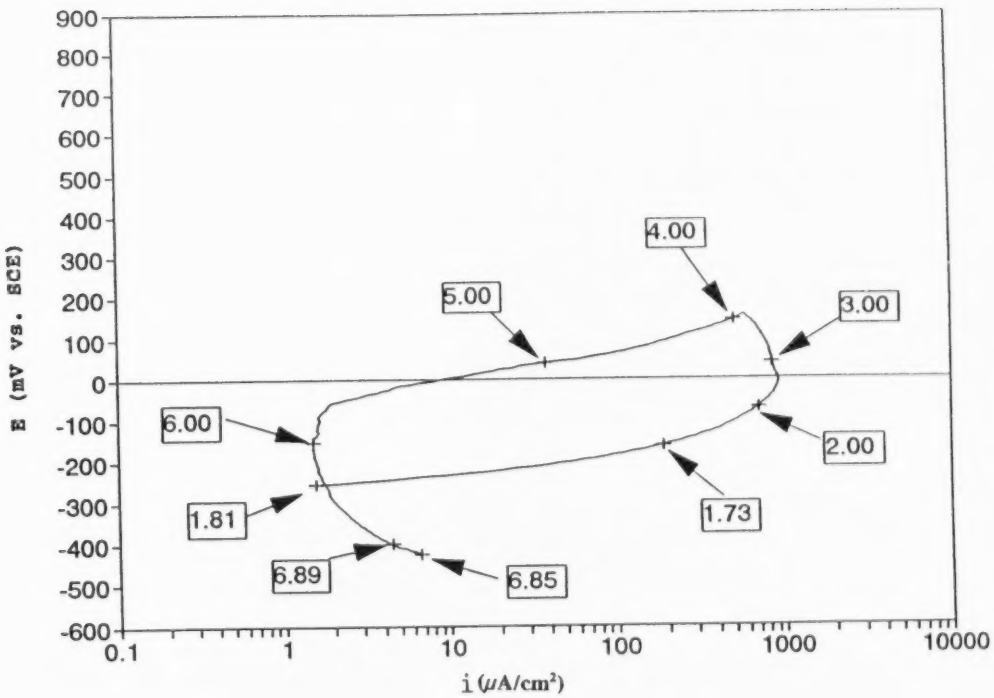

Fig. 84 The cyclic potentiodynamic polarization curve for 304 stainless steel in 10% NaCl solution, pH 6.80 and 20°C, obtained by controlling potential inside a 12 μm crevice. Scan rate was 0.2 mV/s. Measured pH values within the crevice are shown on the curve.

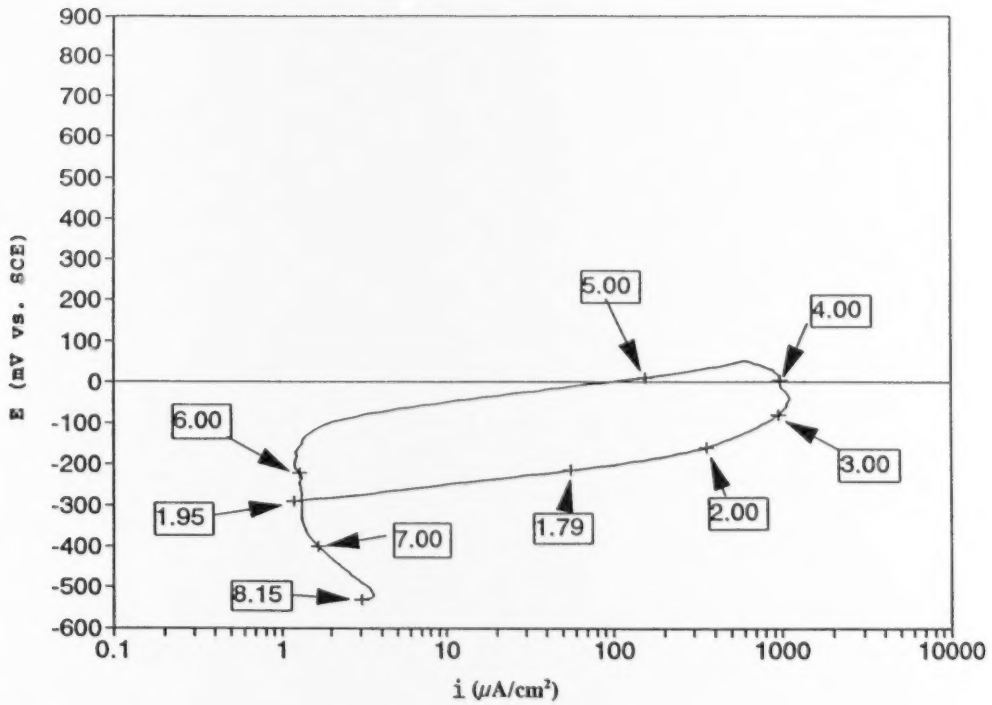

Fig. 85 The cyclic potentiodynamic polarization curve for 304 stainless steel in 15% NaCl solution, pH 7.37 and 20°C, obtained by controlling potential inside a 12 μm crevice. Scan rate was 0.2 mV/s. Measured pH values within the crevice are shown on the curve.

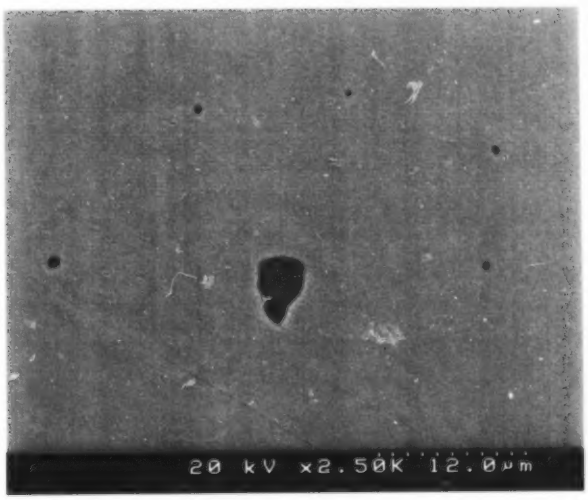

Fig. 86 SEM micrograph of a polished surface of AISI 304 stainless steel without corrosion (1800X).

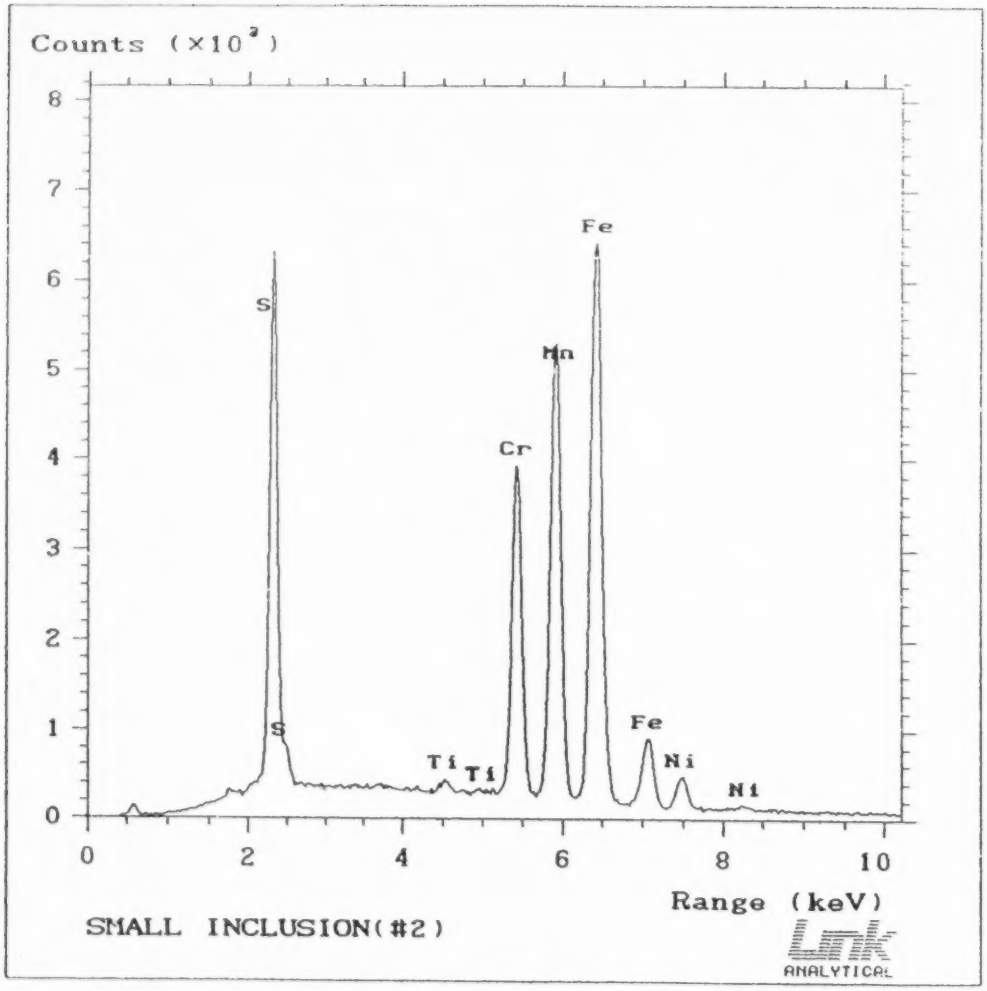

Fig. 87 X-ray analysis of small inclusion in SEM on the polished surface of AISI 304 stainless steel without corrosion in Fig. 86.

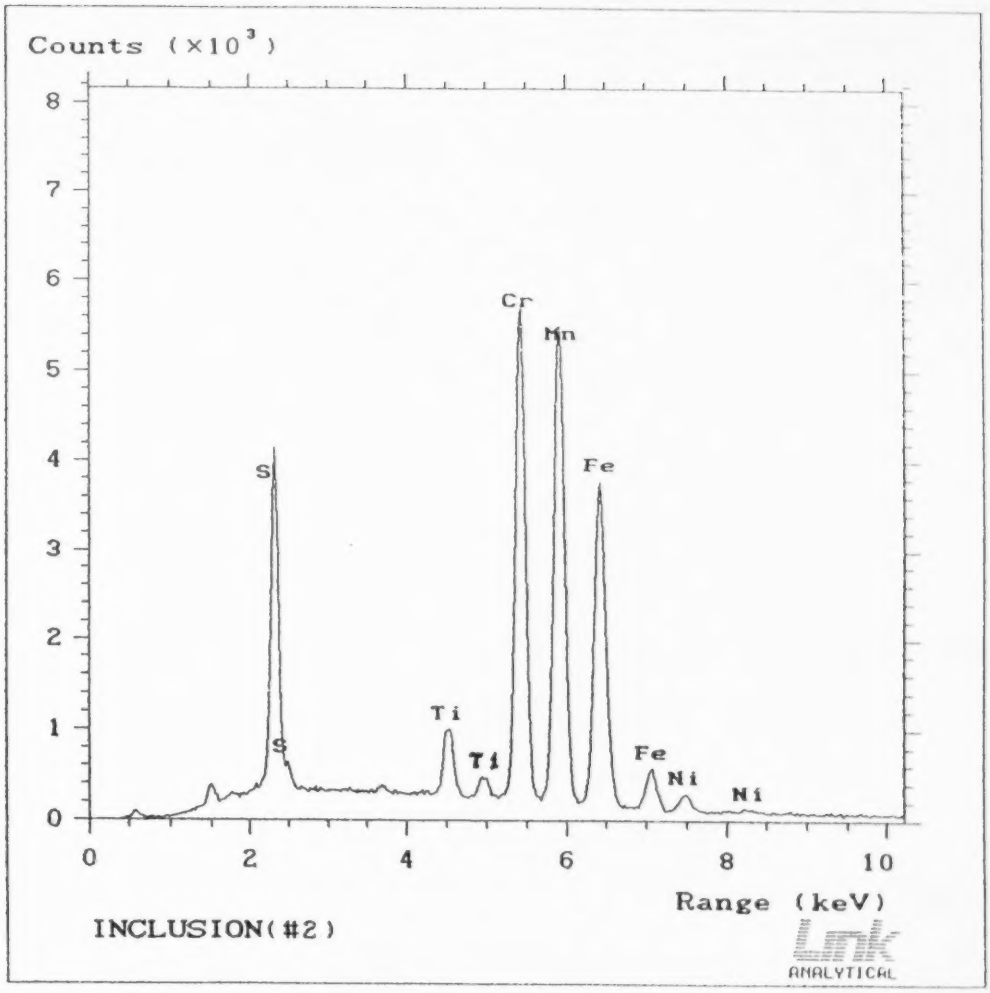

Fig. 88 X-ray analysis of large inclusion in SEM on the polished surface of AISI 304 stainless steel without corrosion in Fig. 86.

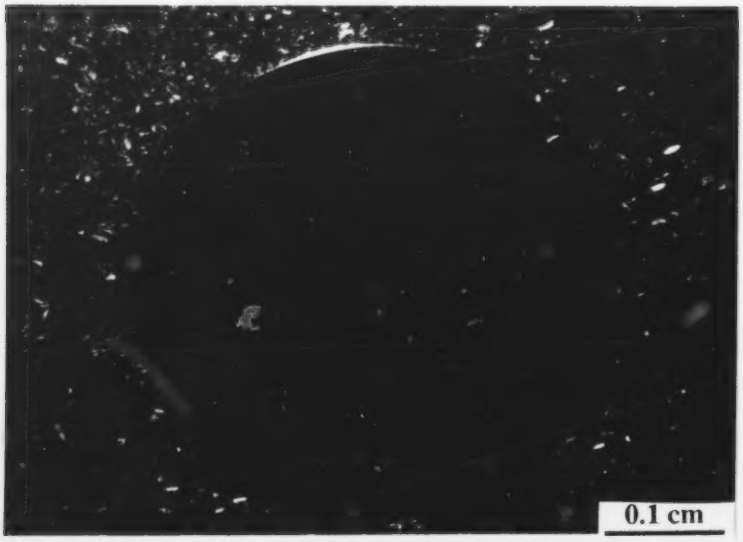

Fig. 89 Corroded surface of AISI 304 stainless steel in optical microscopy at a current density of 20 $\mu A/cm^2$ during potentiodynamic polarization at a scan rate of 0.2 mV/s in 10% NaCl solution at temperature of 20°C (6.4X).

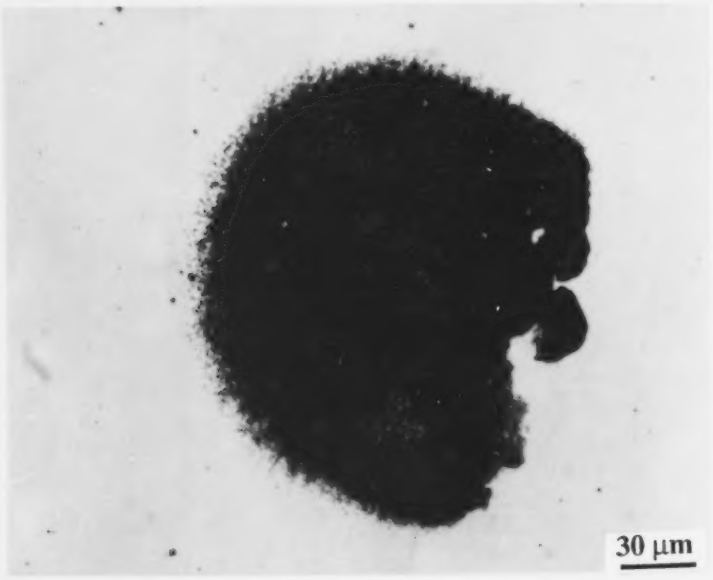

Fig. 90 The corroded spot in Fig. 89 under optical microscopy (320X).

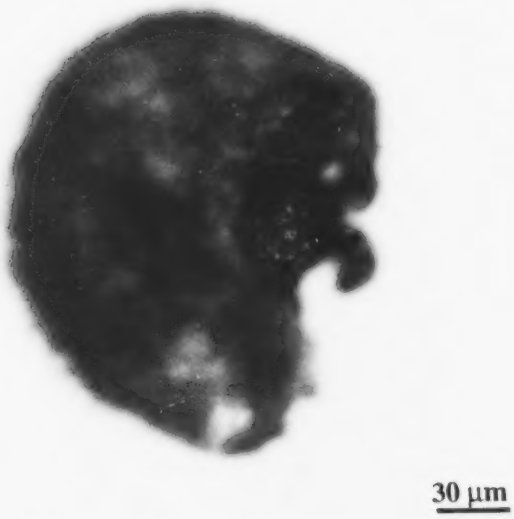

Fig. 91 The corroded spot in Fig. 89 under optical microscopy (320X).

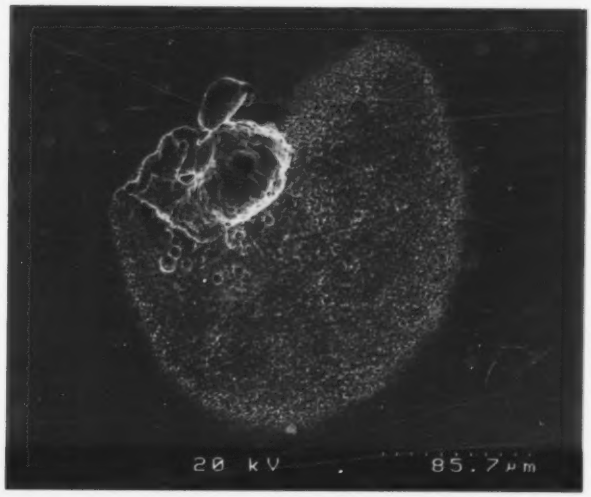

Fig. 92 SEM micrograph of the corroded spot in Fig. 89 (260X).

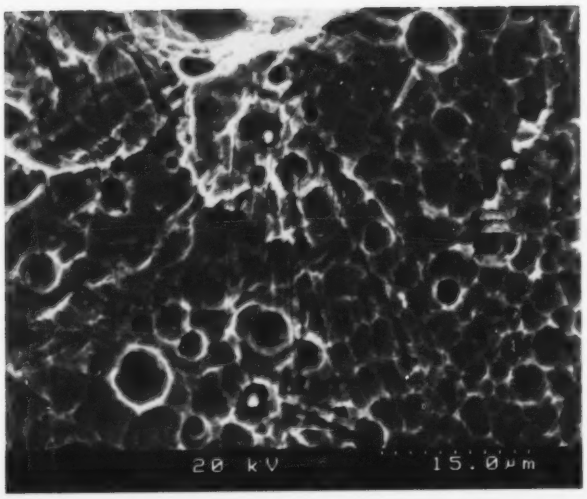

Fig. 93 SEM micrograph of part of the corroded spot in Fig. 89 (1500X).

Fig. 94 SEM micrograph of part of the corroded spot in Fig. 89 (1800X).

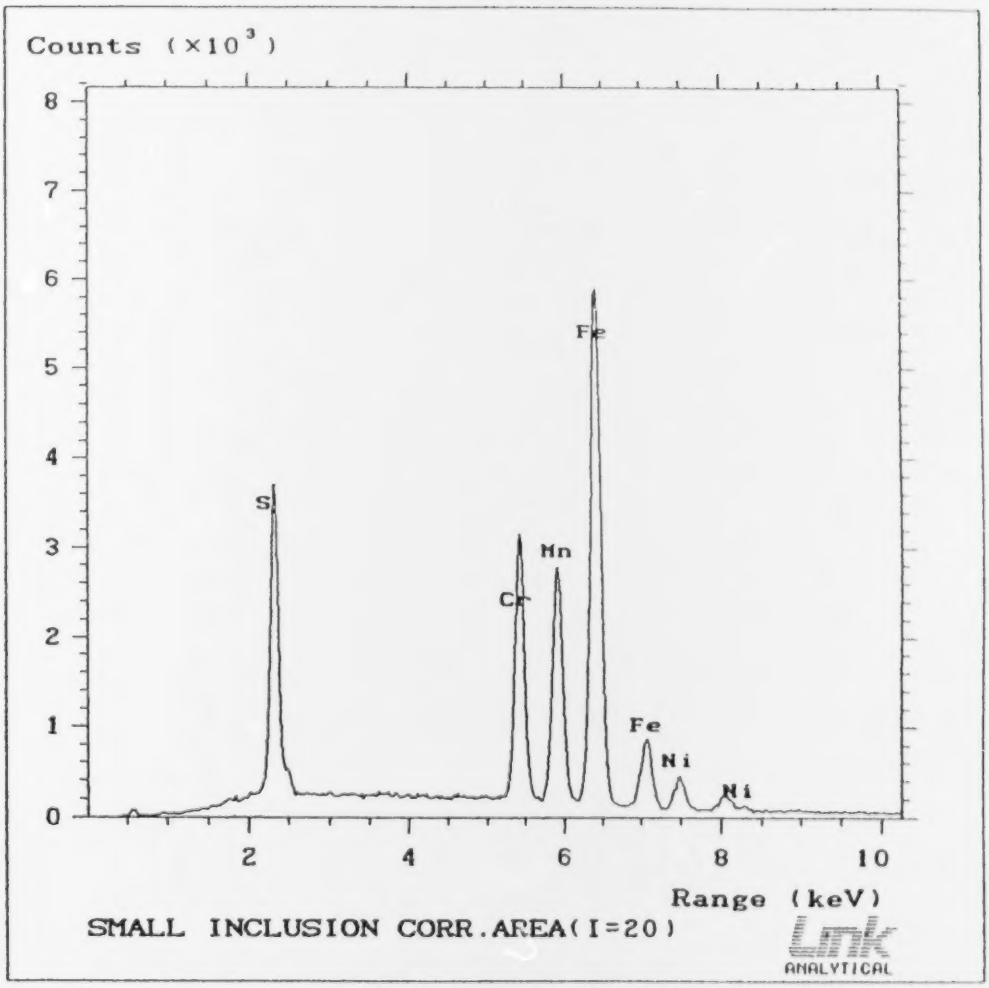

Fig. 95 X-ray analysis of small inclusion in SEM on the corroded spot of AISI 304 stainless steel in Fig. 93 at i=20 $\mu A/cm^2$ during cyclic potentiodynamic polarization at a scan rate of 0.2 mV/s in 10% NaCl solution at a temperature of 20°C.

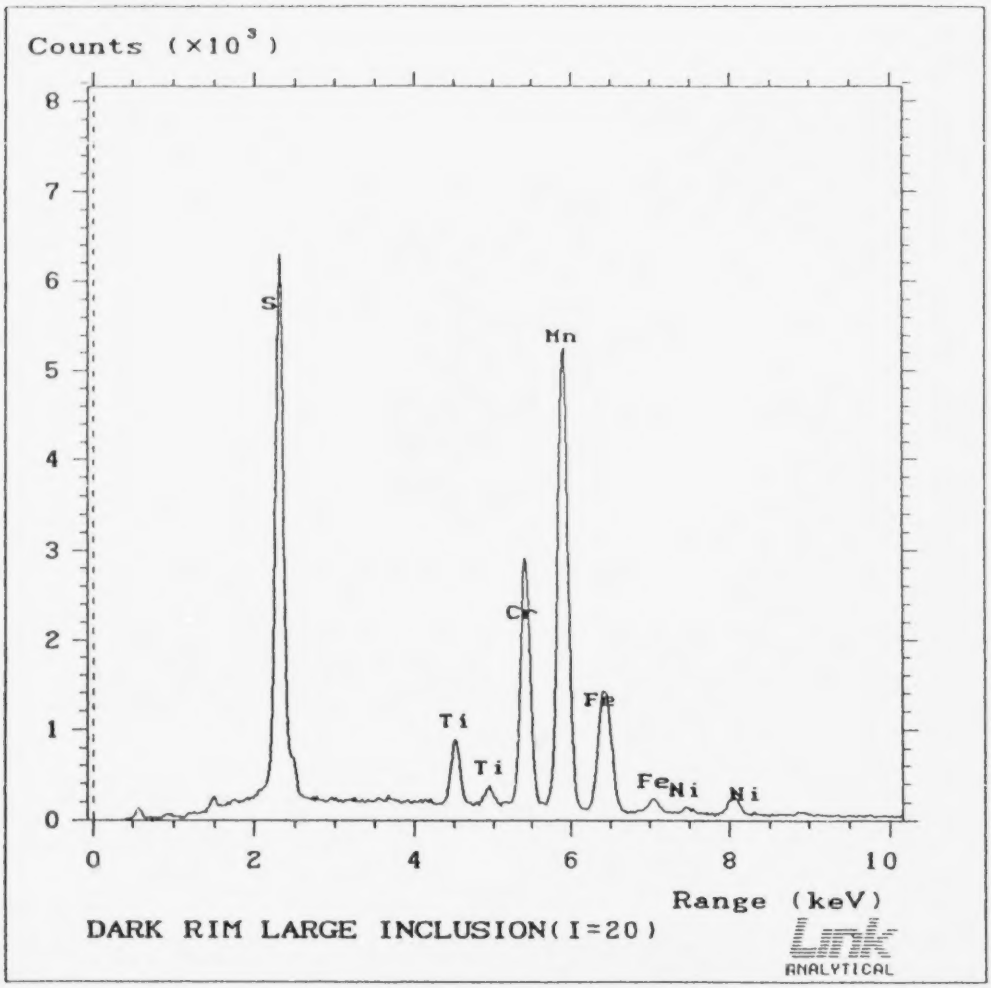

Fig. 96 X-ray analysis of large inclusion in SEM on the corroded spot of AISI 304 stainless steel in Fig. 93 at i=20 $\mu A/cm^2$ during cyclic potentiodynamic polarization at a scan rate of 0.2 mV/s in 10% NaCl solution at a temperature of 20°C.

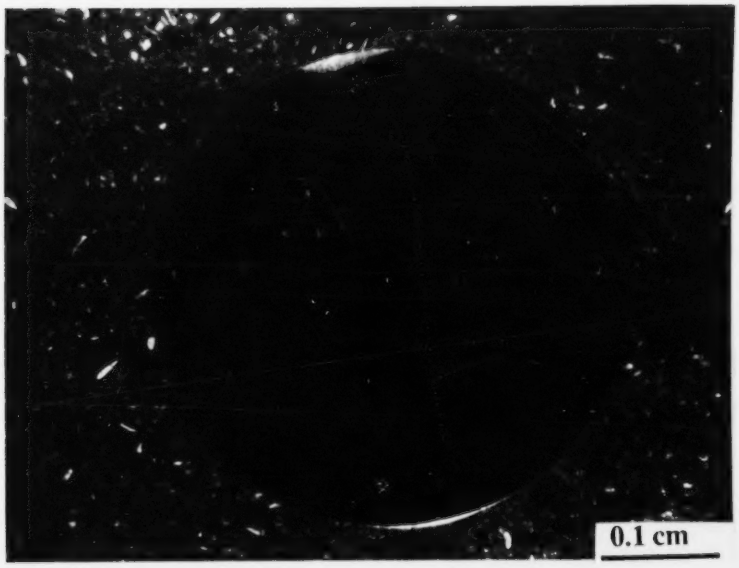

Fig. 97 Corroded surface of AISI 304 stainless steel in optical microscopy at a current density of 50 $\mu A/cm^2$ during potentiodynamic polarization at a scan rate of 0.2 mV/s in 10% NaCl solution at temperature of 20°C (6.4X).

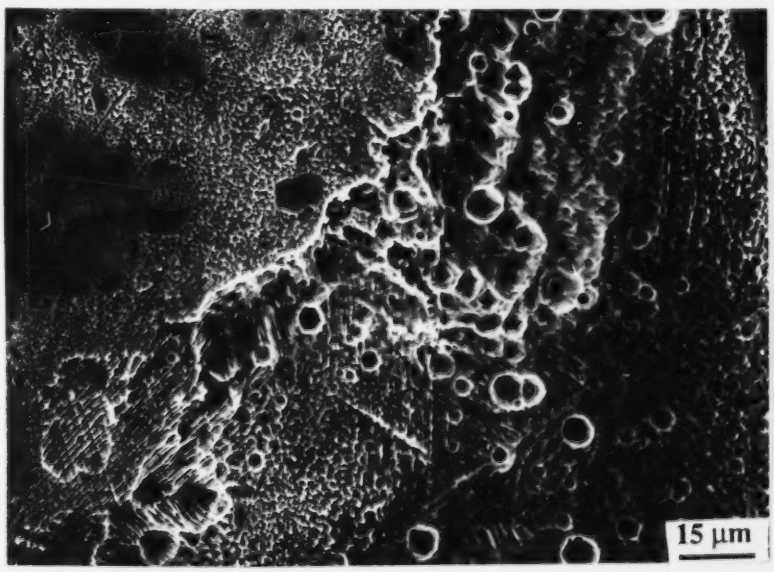

Fig. 98 SEM micrograph of part of the corroded spot in Fig. 89 (700X).

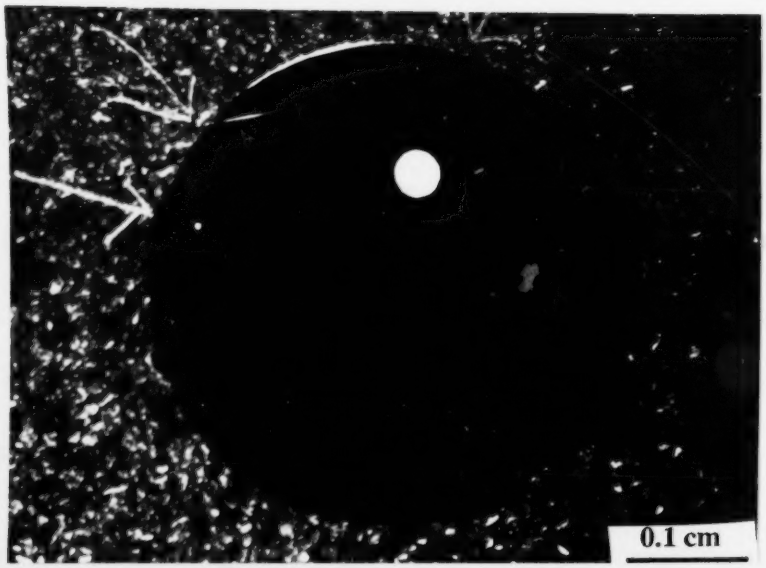

Fig. 99 Corroded surface of AISI 304 stainless steel in optical microscopy at a current density of 100 $\mu A/cm^2$ during potentiodynamic polarization at a scan rate of 0.2 mV/s in 10% NaCl solution at temperature of 20°C (6.4X).

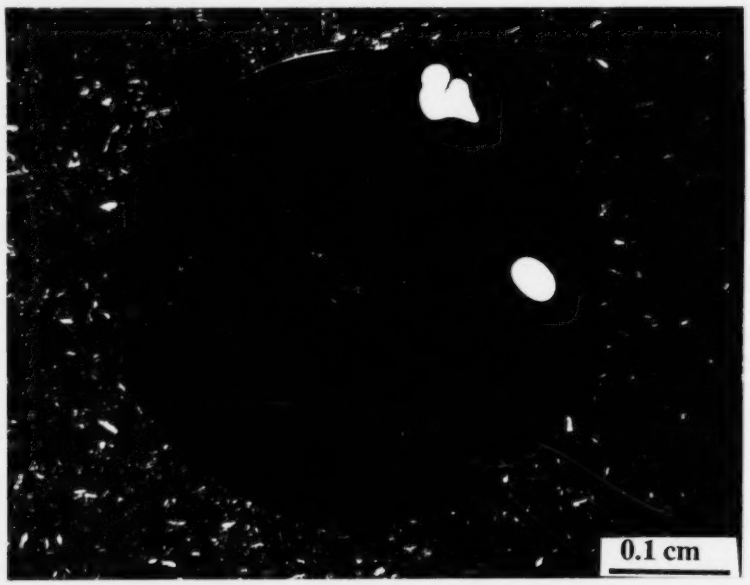

Fig. 100 Corroded surface of AISI 304 stainless steel in optical microscopy at a current density of 200 $\mu A/cm^2$ during potentiodynamic polarization at a scan rate of 0.2 mV/s in 10% NaCl solution at temperature of 20°C (6.4X).

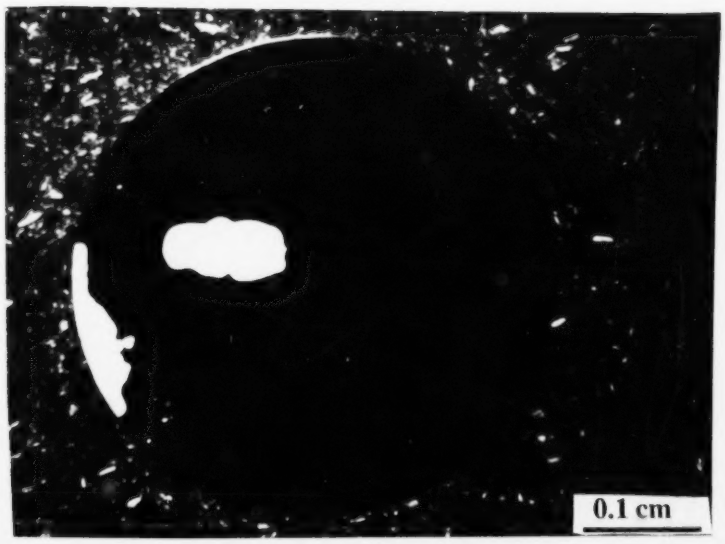

Fig. 101 Corroded surface of AISI 304 stainless steel in optical microscopy at a current density of 500 $\mu A/cm^2$ during potentiodynamic polarization at a scan rate of 0.2 mV/s in 10% NaCl solution at temperature of 20°C (6.4X).

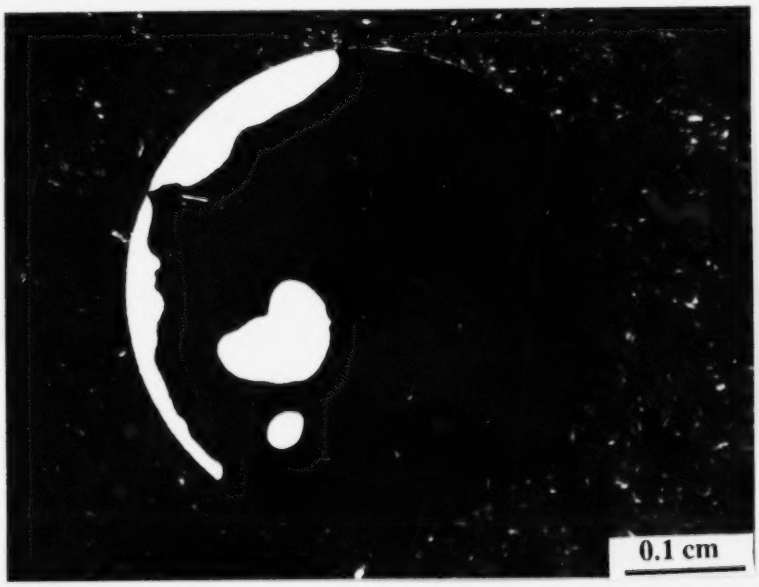

Fig. 102 Corroded surface of AISI 304 stainless steel in optical microscopy after the scanning direction was reversed at 500 $\mu A/cm^2$ to finish the whole cycle during cyclic potentiodynamic polarization at a scan rate of 0.2 mV/s in 10% NaCl solution at temperature of 20°C (6.4X).

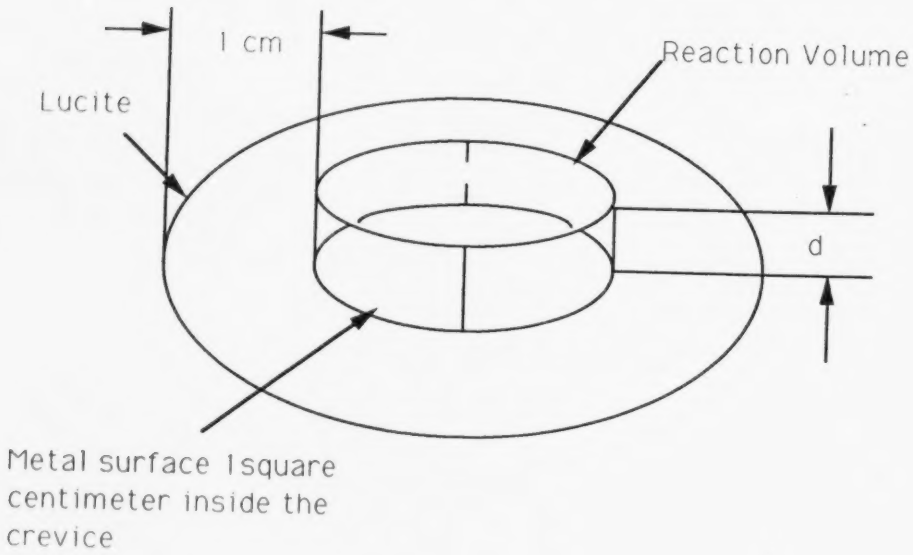

Fig. 103 Reaction volume inside a crevice.

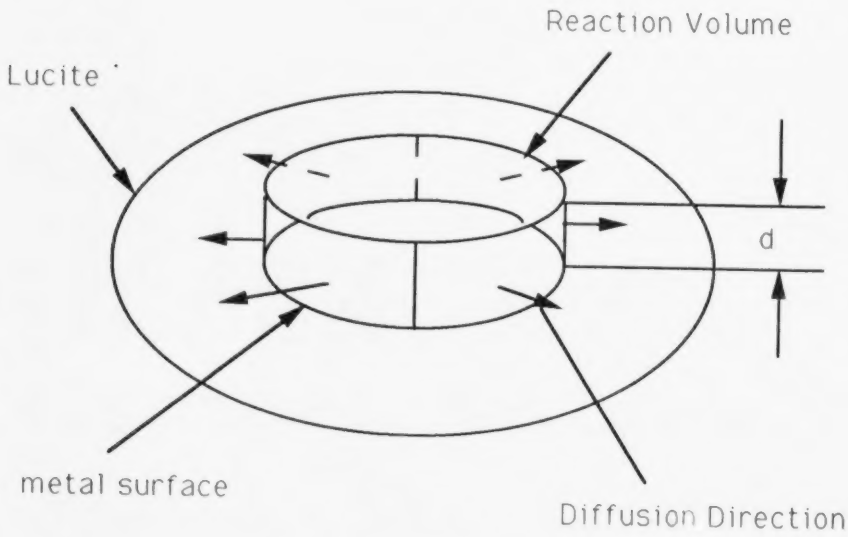

Fig. 104 Diffusion direction of ions in the reaction volume when the crevice width is equal to or less than 0.018 cm.

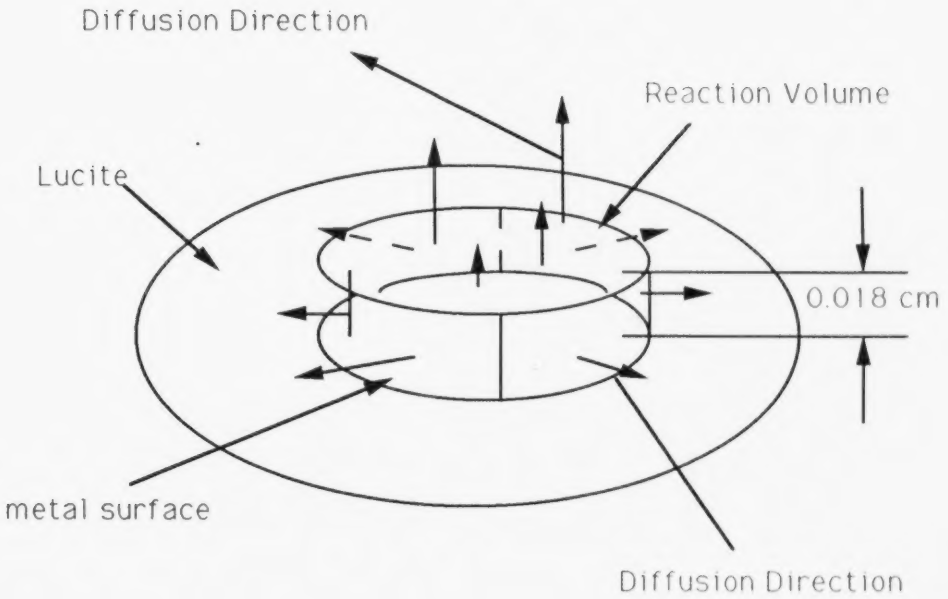

Fig. 105 Diffusion direction of ions in the reaction volume when the crevice width is greater than 0.018 cm.

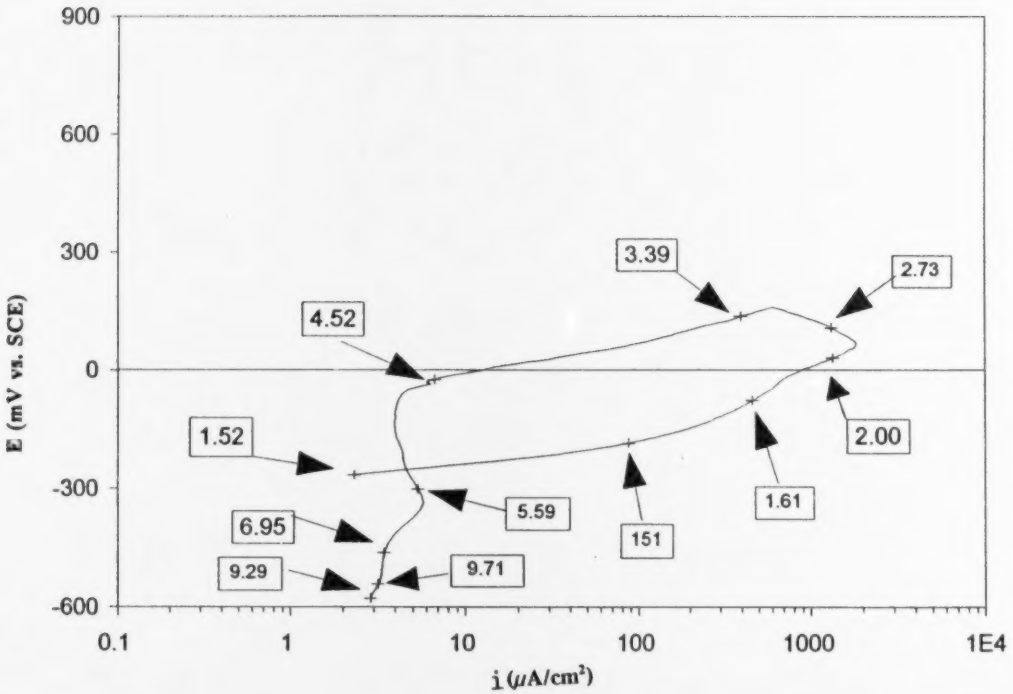

Fig. 106 The cyclic potentiodynamic polarization curve for 304 stainless steel in 10% NaCl solution, pH 7.25 and 20°C, obtained by controlling potential inside a 12 μm crevice. Scan rate was 0.5 mV/s. Calculated pH values within the crevice are shown on the curve.

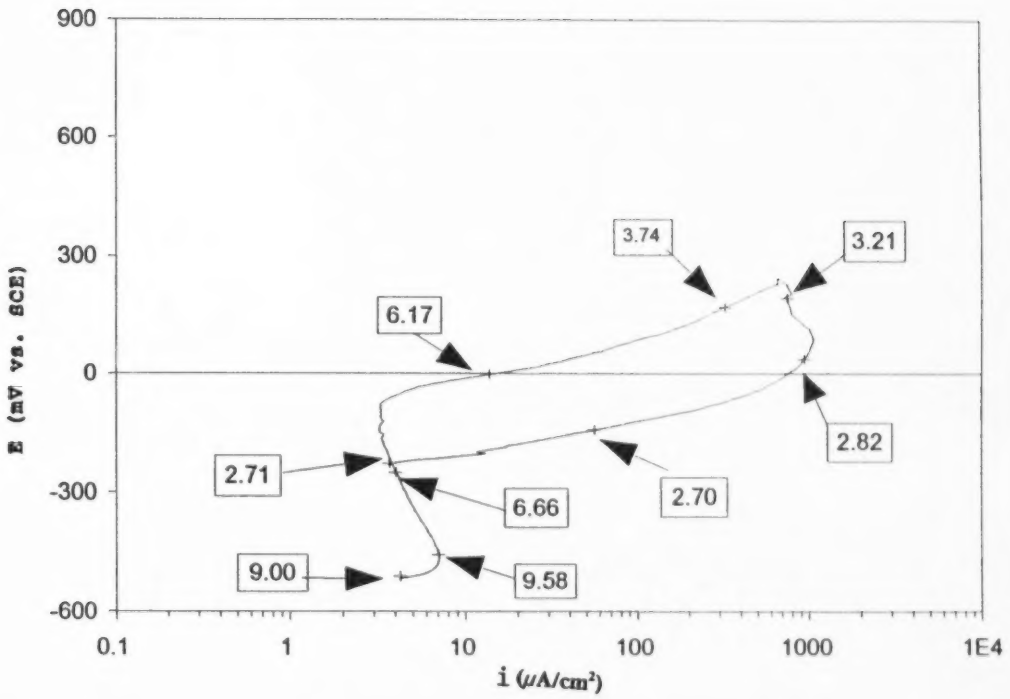

Fig. 107 The cyclic potentiodynamic polarization curve for 304 stainless steel in 10% NaCl solution, pH 7.15 and 20°C, obtained by controlling potential inside a 40 μm crevice. Scan rate was 0.5 mV/s. Calculated pH values within the crevice are shown on the curve.

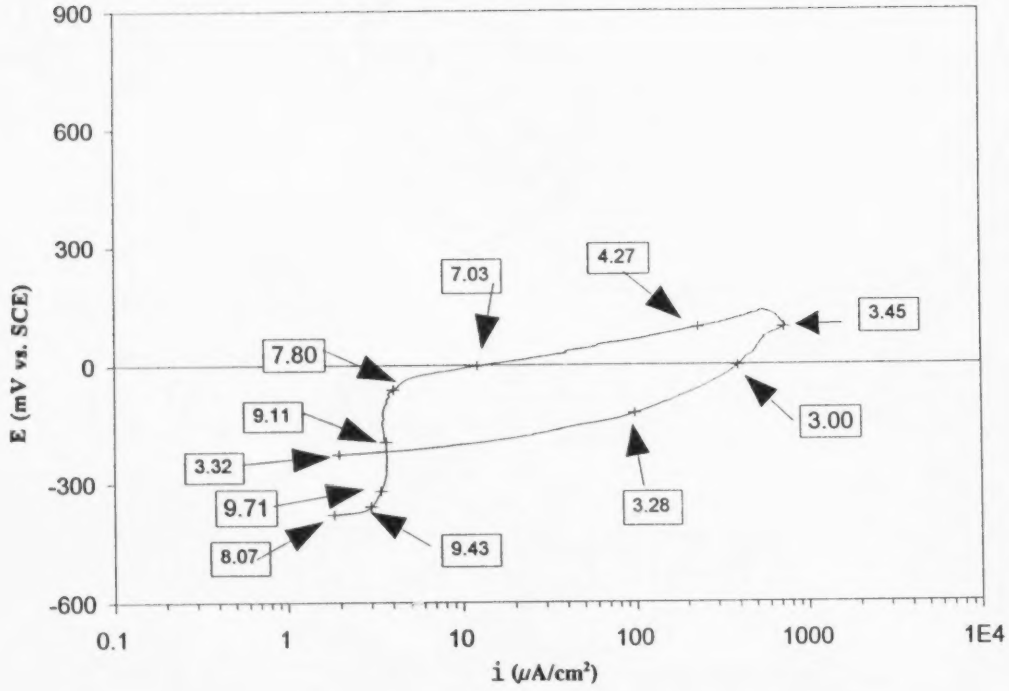

Fig. 108 The cyclic potentiodynamic polarization curve for 304 stainless steel in 10% NaCl solution, pH 6.89 and 20°C, obtained by controlling potential inside a 96 μm crevice. Scan rate was 0.5 mV/s. Calculated pH values within the crevice are shown on the curve.

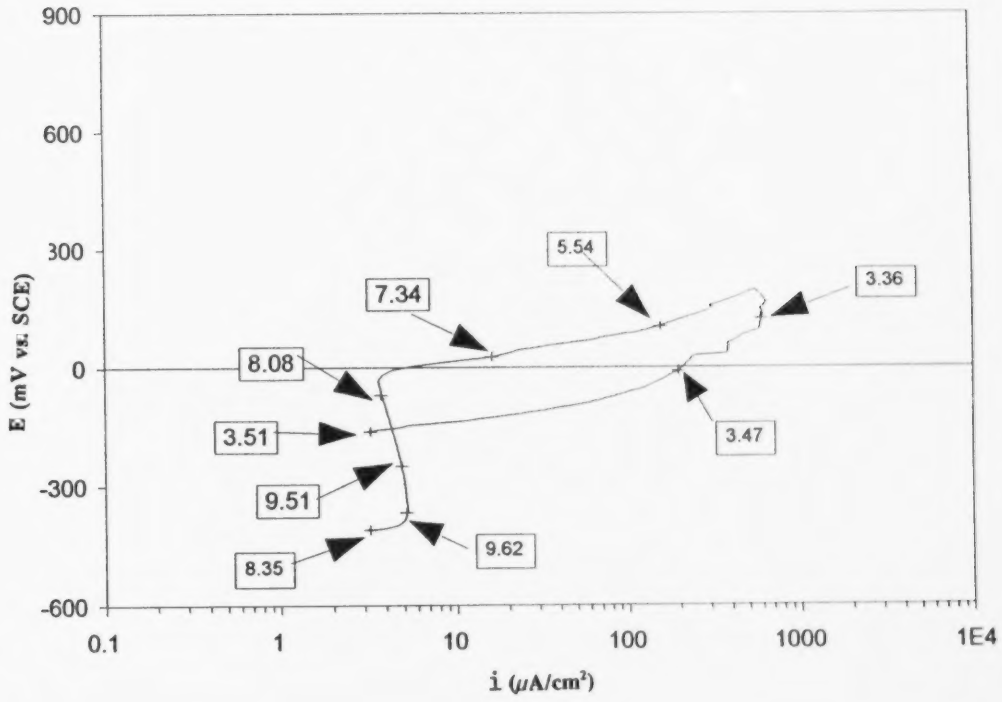

Fig. 109 The cyclic potentiodynamic polarization curve for 304 stainless steel in 10% NaCl solution, pH 7.05 and 20°C, obtained by controlling potential inside a 180 μm crevice. Scan rate was 0.5 mV/s. Calculated pH values within the crevice are shown on the curve.

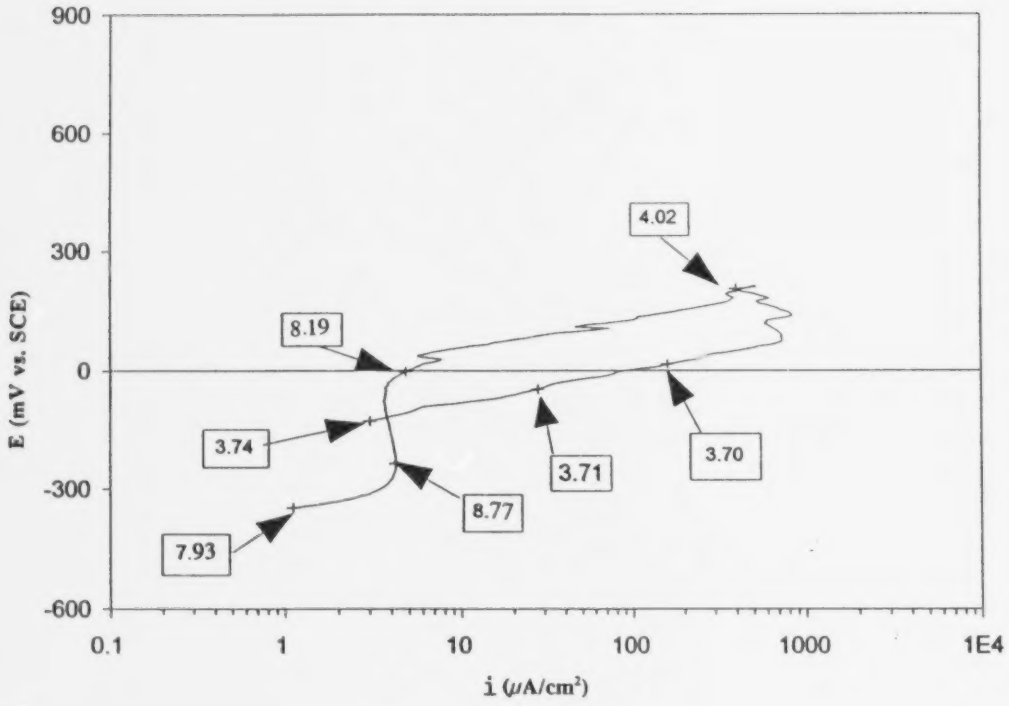

Fig. 110 The cyclic potentiodynamic polarization curve for 304 stainless steel in 10% NaCl solution, pH 7.00 and 20°C, obtained by controlling potential inside a 330 μm crevice. Scan rate was 0.5 mV/s. Calculated pH values within the crevice are shown on the curve.

REFERENCES

1. G.V. Akimov, Bases of Studies on Corrosion and Metal Protection, Metallurgia, p. 54, 1940
2. U.R. Evans, The Corrosion and Oxidation of Metals, Edward Arnold Ltd. London, 1960
3. M.P. Klushin, Corrosion and Combatting It, Vol. 3, No. 3, 1937
4. R.B. Mears and U.R. Evans, Trans. Faraday Soc., Vol. 30, p. 417, 1934
5. E.V. Kunkel, Corrosion, Vol. 10, No. 8, p. 260, 1954
6. G.I. Schafer, J.R. Gabriel and P.K. Faster, J. Electrochem. Soc., Vol. 107, p. 1002, 1960
7. I.B. Ulanovskii and U.M. Korovin, Zh. Prikl. Khim., Vol. 35, No. 8, p. 1753, 1962
8. O.B. Ellis and F.L. LaQue, Corrosion, Vol. 7, No. 11, p. 362, 1951
9. W.B.A. Sharp and L.H. Laliberte, "The Propagation of Crevice Corrosion in Alloys Being Considered for Bleach Plant Service," CORROSION/78, Preprint No. 16, NACE, Houston, TX, 1978
10. E.D. Mor, V. Scotto and A. Mollica, Werkst. Korros., Vol. 31, p. 281, 1980
11. D.A. Vermilyea and C.S. Tedmon, Jr., J. Electrochem. Soc., Vol. 117, p. 437, 1970
12. G. Bombara, Corros. Sci., Vol. 9, p. 519, 1969
13. H.S. Isaacs, J. Electrochem. Soc., Vol. 120, p. 1456, 1973
14. J.L Crolet and J.M. Defranoux, Corros. Sci., Vol. 13, p. 575, 1973
15. J.M Defranoux and R. Tricot, Mem. Sci. Dev. Met., Vol. 69, p. 317, 1972
16. J.L Crolet, L. Serphin and R. Tricot, Mem. Sci. Dev. Met., Vol. 73, p. 1, 1976
17. R. Doling, H. Holtan, A. Steren and R. Tunold, Werkst. Korros., Vol. 31, p. 470, 1980

18. G. Karlberg and G. Wranglen, Corros. Sci., Vol. 11, p. 499, 1971
19. J.W. Oldfield and W.H. Sutton, Brit. Corros. J., Vol. 13, p. 13, 1978
20. J.W. Oldfield and W.H. Sutton, Brit. Corros. J., Vol. 13, p. 104, 1978
21. A.B. Ijzermans, Corros. Sci., Vol. 10, p. 627, 1970
22. I.L. Rosenfeld, Proc. 5th Int. Congr. Metall. Corros., p. 53, Tokyo, 1972
23. I.B. Ulanovskii and Yu.M. Korovin, Zashchita Metallov, Vol. 10, p. 433, 1974
24. I. Matsushima, J. Saka and K. Masdamura, Proc. 7th Int. Congr. Metall. Corros., Vol. 2, p. 507, Rio de Janeiro, 1978
25. J.W. Oldfield and W.H. Sutton, Brit. Corros. J., Vol. 15, No. 1, p. 31, 1980
26. J.C. Rowlands, Innovation and Technology Transfer for Corrosion Control, 11th Int. Congr. Metall. Corros., Vol. 4, p. 265, Florence, Italy, 1991
27. A. Valdes, PhD Thesis, Pennsylvania State University, University Park, PA, 1978, as cited by H.W. Pickering in reference 34.
28. A. Valdes and H.W. Pickering, "IR Drops in the Absence of Gas Constrictions During Crevicing of Iron," in Advances in Localized Corrosion, NACE-9 (Ed. H. Isaacs), NACE, Houston, TX, p. 393, 1989
29. A. Valdes and H.W. Pickering, "El Potential Local De Electrode En Caridades, Y Grietas Y Su Papel Como Cause Del Detrioro De Materials Estructurales, " II Congr. Iberoamericano De Corros. Y Protection, Maracaibo, Venezuela, NACE, Houston, TX, 1986
30. B.G. Ateya and H.W. Pickering, J. Electrochem. Soc., Vol. 122, p. 1018, 1975
31. H.W. Pickering, Corrosion Sci., Vol. 29, p. 325, 1989
32. K. Cho and H.W. Pickering, J. Electrochem. Soc., Vol. 137, p. 3313, 1990
33. A. Valdes and H.W. Pickering, "The Local Electrode Potential in Cavities, Crevices and Its Role in Causing Degradation of Structural Materials, " in Environmental Degradation of Engineering Materials III, (Eds. M.R. Louthan Jr., R.P. McNitt and R.D. Sisson Jr.), p. 227, The Pennsylvania State University, University Park, PA, 1987

34. H.W. Pickering, "A Critical Review of IR Drops and Electrode Potentials Within Pits, Crevices, and Cracks," in Advances in Localized Corrosion (ed. H. Isaacs), NACE, Houston, TX, p. 77, 1989
35. B.A. Shaw, D.J. Moran and P.O. Gartland, Corros. Sci. Vol. 32, p. 707, 1991
36. H.W. Pickering and R.P. Frankenthal, J. Electrochem. Soc., Vol. 119, p. 1297, 1972
37. H.W. Pickering and R.P. Frankenthal, J. Electrochem. Soc., Vol. 119, p. 1304, 1972
38. H.W. Pickering and A. Valdes, "A Review of the Effect of Gas Bubbles and Cavity Dimension on the Local Electrode Potential within Pits, Crevices and Cracks, " in Embrittlement by the Localized Crack Environment (Ed. R.P. Gangloff), p. 33, Metallurgical Soc. of AIME, Warrendale, PA, 1984
39. H.W. Pickering, Corrosion, Vol. 42, p. 125, 1986
40. M.G. Fontana and N.D. Greene, Corrosion Engineering, McGraw-Hill Book Company, New York, Second Edition, p. 323, 1978
41. K. Cho and H.W. Pickering, J. Electrochem. Soc., Vol. 138, p. 256, 1991
42. Y. Xu and H.W. Pickering, J. Electrochem. Soc., Vol. 140. p. 658, 1993
43. R.J Brigham, Corros. Sci., Vol. 28, No. 1, p. 57, 1988
44. R.J. Brigham, Corros. Sci. Vol. 29, p. 995, 1989
45. R.J. Brigham, Corros. Sci. Vol. 33, p. 799, 1992
46. D.W. Siitari and R.C. Alkire, J. Electrochem. Soc., Vol. 129, No. 3, p. 481, 1982
47. D.W. Siitari and R.C. Alkire, J. Electrochem. Soc., Vol. 129, No. 3, p. 488, 1982
48. K. Hebert and R.C. Alkire, J. Electrochem. Soc., Vol. 130, No. 5, p. 1001, 1982
49. K. Hebert and R.C. Alkire, J. Electrochem. Soc., Vol. 130, No. 5, p. 1007, 1982
50. D.E. Williams, C. Westcott and M. Fleischmann, AERE Reports, AERE-R11146 and AERE-R11147, 1984

51. M. Feinherg, Chemical Reactor Theory, A Review (Eds. L. Lapidus and N.R. Amundson,), Ch. 1, Prentice-Hall, Englewood Cliffs, N.J., 1980
52. S.M. Sharland, Corros. Sci., Vol. 27, No. 3, p. 289, 1987
53. A. Turnbull, Corros. Sci., Vol. 23, p. 833-870, 1983
54. T.J. Lennox, Jr. and M.H. Peterson, Localized Corrosion, p. 173, NACE, Houston, TX, 1974
55. N. Lukomski and K. Bohnenkamp, Werkstoffe Korros., Vol. 30, p. 482, 1979
56. A. Turnbull and M.K. Gardner, Brit. Corros. J., Vol. 16, p. 140, 1981
57. T. Turnbull and A.T. May, NPL Report DMA(A), p. 45, 1982
58. E. McCafferty, J. Electrochem. Soc., Vol. 121, p. 1007, 1974
59. A.C. Toncre and N. Ahmad, Mat. Perf., Vol. 19, No. 6, p. 39, 1980
60. I. Matsushima and J. Sakai, Tetsu-to-Hagane, Vol. 63, p. 598, 1977
61. J.F. Bates, Corrosion, Vol. 29, p. 28, 1973
62. W.D. France and N.D. Greene, Corrosion, Vol. 24, p. 247, 1968
63. C.M. Chen, F.H. Beck and M.G. Fontana, Corrosion, Vol. 27, p. 234, 1971
64. B. Vicentini, D. Sinigaglia and G. Taccani, Corros. Sci., Vol. 15, p. 479, 1975
65. K. Shiobara and S. Moriaka, Nipon Kinzoku Gakhaislii, Vol. 35, No. 8, p. 812, 1971
66. A. Alavi and R.H. Cottis, Corros. Sci., Vol. 27, No. 5, p. 443, 1987
67. B.H. Haltman and M.J. Robinson, Corros. Sci., Vol. 27, No. 8, p. 879, 1987
68. J.A. Smith, M.H. Peterson and B.F. Brown, Corrosion, Vol. 26, p. 539, 1970
69. D.A. Meyn, Metals Trans., Vol. 2, p. 853, 1971
70. T. Hodgekiess, Mechanisms of Environment Sensitive Fracture of Materials, (American Society for Metals), Metals Park, Ohio, p. 348, 1977
71. F.D. Bogar and C.T. Fujii, NRL Rept. 7690, AD 778 002, 1974
72. J.C. Greiss, Corrosion, Vol. 24, p. 96, 1968
73. D.F. Taylor and Silverman, Corrosion, Vol. 36, p. 447, 1980
74. C.T. Fujii, Localized Corrosion, NACE, Houston, TX, p. 140, 1974
75. M. Pourbaix, Localized Corrosion, NACE, Houston, TX, p.12, 1974
76. A. Pourbaix, Corrosion, Vol. 27, p. 449, 1971

77. N. Stolica, Corros. Sci., Vol. 9, p. 205, 1969
78. Y.H. Lee, Z. Takehara and S. Yoshizawa, Corros. Sci., Vol. 21, p. 391, 1981
79. E.D. Verink, K.K. Starr and J.M. Bowers, Corrosion, Vol. 32, p. 60, 1976
80. C. Edeleanu and U.R. Evans, Trans. Faraday Soc., Vol. 47, p. 1121, 1951
81. C.M. Chen, M.H. Froning and E.D. Verink, Stress Corrosion-New Approaches, ASTM STP 610, Philadelphia, PA, p. 289, 1975
82. O.V. Kurov, A.M. Krutsan and R.K. Melekhov, Zedal., Vol. 14, p. 123, 1978
83. M.H. Peterson, T.J. Lennox and R.E. Groover, Mater. Prot., Vol. 9, No. 1, p.23, 1970
84. N.J.H. Holroyd, G.M. Scamans and R. Hermaan, in Embrittlement by the Localized Crack Environment (Ed. R.P. Gangloff), p. 327, Metall. Soc. AIME, Warrendale, PA, 1984
85. L. Sathler and J. Van Muylder, Cebelcor, RT 224, 1974
86. L. Sathler, J. Van Muylder, R. Winand and M. Pourbaix, 7th Int. Cong. Metallic Corros., Rio de Janeiro, Vol. 2, p. 705, 1978
87. C.T. Fujii, Cebelcor, RT 213, 1973, as cited by A. Turnbull in ref. 53.
88. J.E. Euvrard, P. Combrade and H. Pages, Innovation and Technology Transfer for Corrosion Control, 11th Int. Congr. Metall. Corros., Vol. 1, p. 599, Florence, Italy, 1991
89. G.C. Barker, J. Electroanal. Chem. Interfacial Electrochem., Vol. 21, p. 127, 1969
90. G. Blanc, I. Epelboin, C. Gabbille and M. Keddam, J. Electroanal. Chem. Interfacial Electrochem., Vol. 75, p. 97, 1977
91. D.E. Williams, C. Westcott and M. Fleischmann, Passivity of Metals and Semiconductors, Elsevier, Amsterdam, p. 217-228, 1983
92. U. Bertocci, NBS Spec. Publ., Vol. 572, p. 92-94, 1980
93. K. Hladky and J.L. Dawson, Corros. Sci., Vol. 21, p. 317, 1981
94. P.C. Searson and J.L. Dawson, J. Electrochem. Soc., Vol. 135, p. 1008, 1988
95. K. Hladky and J.L. Dawson, Corros. Sci., Vol. 22, p. 231, 1982

96. S. Magaino, A. Kawaguchi, A. Hirata and T. Osaka, J. Electrochem. Soc., Vol. 134, p. 2993, 1987

97. A.M.P. Simes and M.G.S. Ferreira, Brit. Corros. J., Vol. 22, No. 1, p. 21, 1987

98. J.W. Dawson and M.G.S. Ferreira, Corros. Sci., Vol. 26, p. 1009, 1986

99. K. Hladky, L. Callow and J.L. Dawson, Brit. Corros. J., Vol. 15, p. 20, 1981

100. L. Callow J. Richardson and J.L. Dawson, Brit. Corros. J., Vol. 11, p. 123, 1976

101. R.F. Reising, J. Electrochem. Soc., Vol. 134, No. 6, p. 1366, 1987

102. M.G.S. Ferreira and J.L. Dawson, Proc. 9th Int. Congr. Metall. Corros., Vol. 4, p 378, Toronto, 1984

103. M.G.S. Ferreira and J.L. Dawson, Passsivity of Metals and Semiconductors, (Ed. M. Froment), Elsevier, Amsterdam, p. 349, 1983

104. I.B. Ulanovskii, Zhurn. Prikl. Khim., Vol. 39, p. 814, 1966

105. M. Pourbaix, Corros. Sci., Vol. 3, p. 239, 1966

106. M. Pourbaix, Corros. Sci., Vol. 26, p. 431, 1979

107. M. Pourbaix, Proc. U.R. Evans Conf. Localized Corrosion, Williamsburg, VA, p. 12, 1971

108. Z. Szklarska-Smialowska and J. Mankowski, Corrosion Sci., Vol. 18, No. 8, p. 953, 1978

109. B.E. Wilde, Corrosion, Vol. 28, No. 8, p. 283, 1972

110. J.C. Rowlands, Brit. Corros. J., Vol. 11, p. 195, 1976

111. I.L. Rozenfeld, "Crevice Corrosion of Metals and Alloys," Localized Corrosion, NACE, Houston, TX, p. 373, 1974

112. T.S. Lee, "A Method for Quantifying the Initiation and Propagation Stages of Crevice Corrosion," in Electrochemical Corrosion Testing, ASTM STP 727, Eds. F. Mansfeld and U. Bertocci, ASTM, Philadephia, PA, p. 43, 1981

113. K.E. Scheidegger and R.D. Muller, Werks. Korros., Vol. 31, p. 387, 1980

114. E. McCafferty, J. Electrochem. Soc., Vol. 126, p. 383, 1979

115. G. Bambara, D. Sinigaglia and G. Taccani, Electrochim. Met., Vol. 3, p. 81, 1968
116. Y.H. Lee, Z. Takehara, S. Yoshizawa, Corros. Sci., Vol. 21, p. 391, 1981
117. E.D. Verink, Jr., K.K. Starr and J.M. Bowers, Corros., Vol. 32, No. 2, p. 60, 1976
118. I.B. Ulanovskii and Yu.M. Korovin, Zashchita Metallov, Vol. 10, p. 433, 1974
119. M.M. Kurtepov, M.J. Fokin, V.K. Zhuraulev and V.J. Oreshkin, Korroziya i Zachchita Konstrukcyionnykh Salavov, Nauka, Moscow, p. 28, 1966
120. E.D. Mor, V. Scott and A. Mollica, Werkst. Korros., Vol. 31, p. 281, 1980
121. R.M. Kain and T.S. Lee, Corrosion 84/27, NACE, Houston, TX, 1984
122. N. Lukomski and K. Bohnenkamp, Werkst. Korros., Vol. 30, No. 6, p. 482, 1979
123. M. Marek and R.F. Hochman, Corrosion, Vol. 30, No. 6, p. 208, 1974
124. R.J. Brigham, Corrosion, Vol. 30, No. 11, p. 396, 1974
125. R.J. Brigham and E.W. Tozer, Corrosion, Vol. 32, No. 7, p. 174, 1976
126. R.J. Brigham, Mater. Performance, Vol. 24, No. 12, p. 44, 1985
127. K.H. Yashiro, K. Tanna, H. Hanayama and A. Miura, Corrosion, Vol. 46, p. 727, 1990
128. I.B. Ulanovskii, Doctor's Thesis, Institute of Physical Chemistry, USSR Academic of Science, Moscow, 1968
129. M.M. Kurtepov, M.J. Fokin, V.K. Zhuraulev and V.J. Oreshkin, Korroziya i Zachchita Konstrukcyionnykh Salavov, Nauka, Moscow, p. 28, 1966
130. J.L. Rozenfeld, Korroziyz i Zashchita Metallov, Lokalniye Korrozinniye Processy Izd, Metallurgia, 1970
131. H.J. Dundas, Corrosion 81/222, NACE, Houston, TX, 1981
132. N. Pessal and J.I. Nurminen, Corrosion, Vol. 30, No. 11, p. 381, 1974
133. M.A. Streicher, Corrosion, Vol. 32, No. 3, p. 79, 1976
134. A.J. Asphahani, Mater. Performance, Vol. 19, No. 8, p. 9, 1980
135. R.M. Kain, Mater. Performance, Vol. 23, No. 2, p. 24, 1984
136. Yu.M. Korovin and I.B. Ulanovskii, Zashchita Metallov, Vol. 8, p 245, 1972

137. J. Pleva, Nyby Uddeholm Corros. Control. Inf., No. 1, p. 11-18, 1984
138. J.W. Oldfield, Mater. Performance, Vol. 27, No. 7, p. 57, 1988
139. R.J. Brigham, Corrosion, Vol. 37, No. 10, p. 608, 1981
140. G.S. Eklund, J. Electrochem. Soc., Vol. 123, p. 170, 1976
141. H.H. Uhlig, Corrosion and Corrosion Control, John Wiley and Sons, New York, p. 272, 1963
142. M. Smialowski, Z. Szklarska-Smialowska, M. Rychik and A. Szummer, Corros. Sci., Vol. 9, p. 123, 1969
143. M. Janik-Czachor, Bull. Acad. Pol. Sci., Vol. 25, p. 561, 1977
144. G. Karlberg, Scand. J. Metall., Vol. 3, p. 46, 1977
145. J.W. Oldfield, Corrosion, Vol. 46, No. 7, p. 574, 1990
146. R.D. Knutsen and A. Ball, Corrosion, Vol. 47, p. 359, 1991
147. G.S. Eklund, J. Electrochem. Soc., Vol. 121, p. 467, 1974
148. A.J. Sedriks, Int. Corros. Conf. Ser., NACE-9 (Advanced Localized Corrosion), Houston, TX, p. 253, 1990
149. S.E. Lott and R.C. Alkire, J. Electrochem. Soc., Vol. 136, No. 4, p. 973, 1989
150. S.E. Lott and R.C. Alkire, J. Electrochem. Soc., Vol. 136, No. 7, p. 3256, 1989
151. R. Ke and R. Alkire, J. Electrochem. Soc., Vol., 139, p. 1573, 1992
152. P. Leckie, J. Electrochem. Soc., Vol. 117, p. 1152, 1970
153. A.J. Sedriks, Corrosion of Stainless Steels, Wiley-Interscience, New York, p. 90, 1979
154. L. Li, K. Wang, Q. Kong and S. Wang, 10th Int. Cong. Metall. Corros., p. 3119, Madras, India, 1987
155. K.D Efird, The Effect of Temperature on Crevice Corrosion of Stainless Steel in Seawater, Paper presented at the 6th International Congress on Metallic Corrosion, December 1975, Sydney, Australia
156. E.C. Hoxie, "Some Considerations in the Selection of Stainless Steel for Pressure Vessels and Piping," in Pressure Vessels and Piping: Decade of

Progress, Vol. 3, The American Society of Mechanical Engineers, New York, 1977

157. A.J. Sedriks, Corrosion of Stainless Steels, Wiley-Interscience, New York, p. 108, 1979
158. W. Schwenk, Corrosion, Vol. 20, No. 4, p. 129t, 1964
159. W. Schwenk, Corros. Sci., Vol. 5, p. 245, 1965
160. E.A. Lizlovs, A.P. Bond, J. Electrochem. Soc., Vol. 117, p. 1130, 1968
161. T. Yoshii, Y. Hisamatsu, J. Japan Inst. Metals, Vol. 36, p. 750, 1972
162. Y.H. Lee, Z. Takehara, S. Yoshizawa, Corros. Sci., Vol. 21, p. 391, 1981
163. K.E. Heusler, L. Fischer, Werkst. Korros., Vol. 27, p. 551, 1976
164. H.H. Strehblow, B. Titze, Corros. Sci., Vol. 17, p. 461, 1977
165. G. Sussek, M. Kesten, Corros. Sci., Vol. 15, p. 225, 1975
166. A.J. Sedriks, Int. Met. Rev., Vol. 28, No. 5, p. 295, 1983
167. G. Herbsleb, Arch. Eisenbuettenw., Vol. 4, p. 747, 1973
168. A Turnbull and D.H. Ferriss, Corros. Sci. Vol. 26, p. 601, 1986
169. S.M. Sharland and P.W. Tasher, Corros. Sci. Vol. 24, p. 517, 1984
170. M. Watson and J. Postlethwaite, Corrosion, Vol. 46, p. 523, 1990
171. T. Suzuki, M. Yamahe and Y. Kitamara, Corrosion, Vol. 29. p. 18, 1973
172. W.A. Larson, Ph.D Thesis, University of Minnesota, Minnesota, 1974, as cited by A. Turnbull in ref. 53.
173. M. Pourbaix, Atlas of Electrochemical Equilibria in Aqueous Solutions, Pergamon Press, New York, 1976
174. J. Baes and W. Wesmer, The Hydrolysis of Cations, New York, John Wiley and Sons, 1976
175. S. Bernhardsson, L. Eriksson, J. Oppelstrup, I.Puigdomenech and T.Wallin, Proceedings of 8th Int. Congr. Metall. Corros., Vol. 1, p. 193, (Frankfurt/Main, FRG: DECHEMA, 1981)
176. R.S. Boikess and E. Edelson, Chemical Principles, Harper International Edition, Harper & Row Publishers, New York, p. 433, 1978

177. C.L. Rollinson, Comprehensive Inorganic Chemistry, Pergamon Press, Oxford, 1973

178. D.R. Lide, Editor-in-Chief, Handbook of Chemistry and Physics, 72nd edition, CRL Press Inc., 1991-1992, p. 6-3

179. F.M. Donahue, and K. Nobe, 2nd Int. Congr. Metall. Corros., New York, p. 916, 1963 (Houston, NACE)

180. G. Bianch, F. Mazza and T. Mussini, 2nd Int. Congr. Metall. Corros., New York, p. 893, 1963 (Houston, NACE)

181. A.N. Frumkin, Uspekhi Khimii, Vol. 34, p. 717, 1965

182. F. Franz, V. Barte and J. Korilta, 4th Int. Congr. Metall. Corros., Amsterdam,, p. 705, 1969 (Houston, NACE)

183. I.G. Murgulescu and V. Radovici, 1st Int. Congr. Metall. Corros., New York, p. 109, 1961 (London, Butterworths)

184. J. Mankowski and Z. Szklarska-Smialowska, Corros. Sci., Vol. 15, p. 493, 1975

185. W. Batista, A.M.T. Louvisse, O. Mattos and L. Sathler, Corros. Sci., Vol. 28, No. 8, p. 759, 1988

186. W. Yang, R.Ni, H. Hua and A. Pourbaix, Corros. Sci., Vol. 24, No. 8, p. 691, 1984

187. Y.T. Kho, K. Osseo-Asave and H.W. Pickering, J. Electrochem. Soc., Vol. 139, No. 1, p. 32, 1992

188. S. Wolfram, Mathematica : A System for Doing Mathematics by Computer, Addison-Wesley Publishing Company, New York, 1988

APPENDIX

Appendix A The Method Used for Numerical Calculation in Obtaining pH Values on the Polarization Curve

As equations from (49) to (55) and from (56) to (60) are two sets of non-linear equations, a numerical method must be used to do the calculation. A program of numerical root finding, FindRoot, in the first version of Mathematica (a system for doing mathematics by computer) (188) was used to search for a numerical solution to the sets of non-linear equations in a Next workstation. FindRoot uses Newton's method.

Since there are some limitations to Newton's method which affect the results, the following error analysis, including consideration of accuracy, starting points and sensitivity, has been made.

In order to show the validation of the numerical results, only one data point on a polarization curve is chosen in the discussion of results for each set of non-linear equations.

From the data in Fig. 58, the molar concentrations of Cr^{3+}, Fe^{2+}, Ni^{2+} and OH_T^- at the first point of the polarization curve are 4.47×10^{-6}, 1.61×10^{-5}, 1.97×10^{-6} and 5.0×10^{-5}, respectively. As the normality of Cr^{3+} is less than that of OH^-, the equations from (49) to (55) are used. Introducing the data and the equilibrium constants into equations from (49) to (55), the following equations are obtained.

$$VX - 5.0\times10^{-9}U = 0 \qquad (1a)$$

$$WX - 7.47\times10^{-12}V = 0 \qquad (2a)$$

$$PX - 3.16\times10^{-10}O = 0 \qquad (3a)$$

$$QX - 7.49\times10^{-10}P = 0 \quad (4a)$$

$$U + V + W = 1.61\times10^{-5} \quad (5a)$$

$$O + P + Q = 1.97\times10^{-6} \quad (6a)$$

$$VX + 2WX + PX + 2QX + K_w - 3.66\times10^{-5}X = 0 \quad (7a)$$

The molar concentrations of Cr^{3+}, Fe^{2+}, Ni^{2+} and OH_T^- at the point of experimental pH 7.50 in Fig. 58 are 5.88×10^{-4}, 2.12×10^{-3}, 2.59×10^{-4} and 1.61×10^{-3}, respectively. As the normality of Cr^{3+} is greater than that of OH^-, the set of equations from (56) to (60) are used. Introducing the data and equilibrium constants into the equations from (56) to (60), the following equations are obtained.

$$HS - 1.58\times10^{-4}G = 0 \quad (8a)$$

$$JS - 6.31\times10^{-7}H = 0 \quad (9a)$$

$$LS - 6.31\times10^{-7}J = 0 \quad (10a)$$

$$G + H + J + L = 5.88\times10^{-4} \quad (11a)$$

$$H + 2J + 3L - S = 1.61\times10^{-3} \quad (12a)$$

1. Accuracy Analysis

There are several options to control the operation of FindRoot. First, MaxIterations can be used to specify the maximum number of steps that Findroot should use in attempting to find a solution. To work out whether it has found an acceptable root, FindRoot evaluates the function and sees whether the result is zero to within the accuracy

specified by setting the option AccuracyGoal --> n. The setting for AccuracyGoal gives the number of digits to the right of the decimal point that FindRoot tries to get for the function, i.e., the difference between the left side and right side in each equation is at least within the 10^{-n} order.

To test the accuracy of the set of equations from (1a) to (7a), the starting points must be chosen for the calculation. As the pH is above 7, the molar concentration of hydrogen ions ($[H^+]$) must be less than 10^{-7}. Therefore, a reasonable starting concentration of $[H^+]$ is chosen as 10^{-9}. From equation (5a), the values of U, V and W cannot exceed 1.61×10^{-6}. The starting points of U, V and W are chosen as 10^{-8}, 10^{-7} and 10^{-7}, respectively. In the same way, from equation (6a), the starting points of O, P and Q are set at 10^{-8}, 10^{-9} and 10^{-8}, respectively. By changing the variable of AccuracyGoal while fixing MaxIterations at 50, the calculated results obtained from equations (1a) to (7a) are shown in Table 1A.

Table 1A The Hydrogen Ion Concentrations Calculated by FindRoot Method for Different AccuracyGoals at MaxIterations 50

AccuracyGoal	Hydrogen Ion Concentration X
6	6.68843×10^{-10}
10	6.68843×10^{-10}
15	5.1319×10^{-10}
20	5.04409×10^{-10}
25	5.04409×10^{-10}
30	5.04409×10^{-10}

From Table 1A, when AccuracyGoal is equal to or greater than 20, the calculated results are the same. Therefore, AccuracyGoal in the calculation is always chosen as 20.

Fixing AccuracyGoal at 20, when MaxIterations is 5, Newton's method failed to converge to the prescribed accuracy after 5 iterations. When MaxIterations is 10, the

value of X is 5.04409×10^{-10} which is equal to the value of X at MaxIterations 50. Therefore, the rate of convergence of the set of equations is quite fast. In order to make sure there is enough iteration for convergence, MaxIterations is always chosen as 50.

When the MaxIterations and AccuracyGoal are 50 and 20, respectively, the complete solutions of U, V, W, O, P, Q and X at the first point of the polarization curve are 1.45572×10^{-6}, 1.443×10^{-5}, 2.14272×10^{-7}, 7.70514×10^{-7}, 4.82709×10^{-7}, 7.16777×10^{-7} and 5.04409×10^{-10}, respectively. Introducing these answers into the equations from (1a) to (7a) to check the accuracy, the results obtained are summarized in Table 2A.

Table 2A The Results of the Left Side and Right Side in Each Equation Obtained by Solving Equations (1a) to (7a) after Introducing the Roots into the Original Equations (1a) to (7a)

Equations	Left Side	Right Side
1a	2.19×10^{-20}	0
2a	3×10^{-23}	0
3a	7.6×10^{-22}	0
4a	-2.7×10^{-22}	0
5a	1.61×10^{-3}	1.61×10^{-3}
6a	1.97×10^{-6}	1.97×10^{-6}
7a	5.5×10^{-21}	0

The above results clearly indicate that the accuracy is very good when AccuracyGoal is chosen as 20 and MaxIterations is chosen as 50.

To test the accuracy of the set of equations from (8a) to (12a), the starting points are chosen as follows. As the pH is below 7, the concentration of hydrogen ions must be greater than 10^{-7}. Therefore, the starting point of S is set at 10^{-6}. From equation (11a), G, H, J and L must be less than 5.88×10^{-4}. The starting points of G, H, J and L are chosen as 10^{-5}, 10^{-6}, 10^{-7}, and 10^{-8}, respectively.

By changing the variable of AccuracyGoal while fixing MaxIterations at 50, the calculated results are obtained from equations (8a) to (12a) as shown in Table 3A.

Table 3A The Hydrogen Ion Concentrations Calculated by FindRoot Method for Different AccuracyGoals at MaxIterations 50

AccuracyGoal	Hydrogen Ion Concentration S
6	-5.3989×10^{-4}
10	9.23543×10^{-9}
16	1.4324×10^{-7}
20	1.4324×10^{-7}
25	1.4324×10^{-7}
30	1.4324×10^{-7}

From Table 3A, when the AccuracyGoal is 6, the calculated result is negative. As the hydrogen ion concentration cannot be negative, the result is not correct. When AccuracyGoal is equal to or greater than 20, the calculated results are the same. Therefore, AccuracyGoal in the calculations is always chosen as 20.

Fixing AccuracyGoal at 20, when MaxIterations is 10, Newton's method fails to converge to the prescribed accuracy after 10 iterations. When MaxIterations is 15, the value of S is 1.4324×10^{-7}. Therefore, when MaxIterations is 15, the number of iterations is enough for convergence. To make sure of enough iteration for a calculation, the MaxIterations is always chosen as 50.

When MaxIterations and AccuracyGoal are 50 and 20, respectively, the complete solutions of G, H, J, L and S at the point of experimental pH 7.50 in the polarization curve are 2.14844×10^{-8}, 2.36983×10^{-5}, 1.04396×10^{-4}, 4.59884×10^{-4}, and 1.4324×10^{-7}, respectively. Introducing these answers into the equations from (1a) to (7a) to check the accuracy, the results obtained are summarized in Table 4A.

Table 4A The Results of the Left Side and Right Side in Each Equation Obtained by Solving Equations (1a) to (7a) after Introducing the Roots into the Original Equations (1a) to (7a)

Equations	Left Side	Right Side
8a	9.3×10^{-20}	0
9a	5.6×10^{-20}	0
10a	-9.2×10^{-21}	0
11a	5.88×10^{-4}	5.88×10^{-4}
12a	1.61×10^{-3}	1.61×10^{-3}

The above results clearly indicate that the accuracy is very good when AccuracyGoal is chosen as 20 and MaxIterations is chosen as 50.

2. Analysis of Starting Point

As the starting point is crucial in getting useful answers from FindRoot, the starting point must be tested to see whether there is only one convergence point at different starting points.

For the set of equations from (1a) to (7a), according to the experimental conditions, only a certain range of starting points of X, U, V, W, O, P and Q can be chosen as meaningful. As the molar concentration of hydrogen ion must be less than 10^{-7}, the starting point of X must also be less than 10^{-7}. The starting points of U, V and W must be less than 1.61×10^{-5} from equation (5a) and the starting points of O, P and Q must be less than 1.97×10^{-6} from equation (6a). Therefore, it is reasonable to assume starting points of U, V, W, O, P and Q to be 10^{-8}, 10^{-7}, 10^{-7}, 10^{-8}, 10^{-8}, and 10^{-8}, respectively. When the starting point of X is 10^{-7}, the value of X is 5.04409×10^{-10}. When the starting point of X is 10^{-8}, the value of X is also 5.04409×10^{-10}. Assuming that the starting points of U, V, W, O, P, and Q are 10^{-10}, 10^{-6}, 10^{-8}, 10^{-6}, 10^{-8}, and 10^{-10}, respectively, when the starting point of X is 10^{-9}, the value of X is still 5.04409×10^{-10}.

Therefore, the starting points do not affect the final results in the set of non-linear equations from (1a) to (7a).

For the set of equations from (8a) to (12a), according to the experimental conditions, only a certain range of starting points of S, U, V, W, O, P and Q can be chosen as meaningful. As the molar concentration of hydrogen ions must be greater than 10^{-7}, the starting point of S must also be greater than 10^{-7}. The starting points of G, H, J, and L must be less than 5.88×10^{-4} from equation (11a). Therefore, it is reasonable to assume starting points of G, H, J and L to be 10^{-5}, 10^{-6}, 10^{-7}, and 10^{-8}, respectively. When the starting point of S is 10^{-7}, the value of S is 1.4324×10^{-7}. When the starting point of S is 10^{-5}, the value of S is -0.00167326. As the concentration cannot be negative, the result can be ignored. Assuming that the starting points of G, H, J, and L are 10^{-8}, 10^{-7}, 10^{-5}, and 10^{-6}, respectively, when the starting point of S is 10^{-6}, the value of X remains 1.4324×10^{-7}. Therefore, the starting points of G, H, J, and K do not affect the final results in the set of non-linear equations from (8a) to (12a). When the starting point of S is greater than 10^{-5}, a negative value for $[H^+]$ is obtained. Since at this point on the polarization curve, the normality of Cr^{3+} is just above the normality of OH^-, the pH in the solution should be very close to 7. This indicates that the results obtained in the calculation are reasonable.

3. Sensitivity Analysis

As the equilibrium constants obtained from the experiment have a certain range of error, they may affect the sensitivity of the numerical solution of the two sets of non-linear equations. To test the effect of equilibrium constant on the sensitivity of equations, it is reasonable to assume that there is 10% error in these equilibrium constants.

For the set of equations from (1a) to (7a), when K_5, K_6, K_8 and K_9 are increased 10%, the value of X is 5.10853×10^{-10}. When K_5, K_6, K_8 and K_9 is decreased 10%, the value of X is 5.00498×10^{-10}. The values are very close to the 5.04409×10^{-10} previously calculated. Therefore, the variations of equilibrium constants affect the results only

slightly and the stability of the set of non-linear equations is very good.

For the set of equations from (8a) to (12a), when K_1, K_2 and K_3 are increased 10%, the value of X is 1.5755×10^{-7}. When K_1, K_2 and K_3 are decreased 10%, the value of X is 1.28927×10^{-7}. The error with 10% increase or 10% decrease in equilibrium constants is about 10%. Therefore, the variation of K_1, K_2 and K_3 has some effect on the results. However, as the pH within the crevice corresponding to 10% increase in equilibrium constants is 6.90 and the pH within the crevice corresponding to 10% decrease in equilibrium is 7.00, the difference between the these two pH values is much smaller than the difference between the experimental pH 7.50 and the originally calculated pH 6.95 in Table 18. Therefore, the variations of equilibrium constants also only slightly affect the final results and the stability of the set of non-linear equations is good.